Estimation and Prediction of Fouling Behaviour in a Shell-and-Tube Heat Exchanger

THESIS

Submitted in partial fulfilment
of the requirements for the degree of
DOCTOR OF PHILOSOPHY

by

DILLIP KUMAR MOHANTY

Under the Supervision of
Dr. Pravin M. Singru

BIRLA INSTITUTE OF TECHNOLOGY AND SCIENCE
PILANI (RAJASTHAN) INDIA

2012

BIRLA INSTITUTE OF TECHNOLOGY AND SCIENCE
PILANI (RAJASTHAN)

CERTIFICATE

This is to certify that the thesis entitled **"Estimation and Prediction of Fouling Behaviour in a Shell-and-Tube Heat exchanger"** submitted by **Dillip Kumar Mohanty,** ID No. **2007PHXF410G** for award of Ph. D. Degree of the Institute embodies original work done by him/her under my supervision.

Signature in full of the Supervisor: _____

Name in capital block letters: **Dr. PRAVIN M. SINGRU**
Designation: **Assistant Professor**
(Mechanical Engineering)

Date:

Abstract

Heat exchangers are essential components in complex engineering systems related to energy generation and energy transformation in industrial scenarios. Fouling is the deposition of unwanted materials onto the heat transfer surfaces of a heat exchanger causing an increase in thermal resistance and subsequent reduction in thermal efficiency. It acts as an added thermal resistance and therefore affects adversely the value of the overall heat transfer coefficient. The deposit has a considerable impact on the overall heat transfer coefficient as the thermal conductivity of a solid foulant deposited on a heat exchanger surface is invariably smaller than that of the metal on which it resides. In this research work, a system approach for investigation of fouling effects on the heat transfer performances of a shell-and-tube heat exchanger is developed using statistical analysis, Wilson plot method and C-factor method. Subsequently the neural network approach is applied to predict the performance of the exchanger so that a proper cleaning schedule can be developed without hindering the exchanger performance.

The heat transfer performance parameters such as overall heat transfer coefficient and fouling resistance have been estimated taking into account the geometrical and operational parameters. The analysis is based on the Bell-Delaware method which can incorporate the entire range of geometric parameters of practical interest to describe the shell-side flow. A fouling growth model has been developed for the shell-and-tube heat exchanger using statistical approach. The statistical analysis is considered for normal, log-normal, exponential and weibull distributions. However the fouling model is developed taking into account the log-normal distribution as it is found to be the most suitable. The statistical analysis is found to be very effective in detecting critical fouling in a heat exchanger which can be utilized for predicting the optimal maintenance schedule. This can be used for optimal cleaning schedule in chemical process industries so that the idle time can be reduced to possible minimum and simultaneously the heat exchanger running with poor performance can be avoided. The uncertainty in the measurements of temperature and mass flow rate has been taken into consideration for determination of thermal performances of the heat exchanger. The unsteadiness of each working regime has taken into account the dispersion both about the mean heat duty and overall heat transfer coefficient.

The estimation of convection coefficients constitutes a crucial issue in designing and sizing any type of heat exchange devices. The Wilson plot method and its different modifications have been used as a tool for the analysis of convection heat transfer processes. The correlations between the overall heat transfer coefficient and Nusselt Number have been developed both for the tube side and shell side flow based on the Wilson plot method and modified versions of Wilson plot.

In this work, a very sensitive methodology has been introduced for performance evaluation of a heat exchanger by using C-factor which eliminates the application of idealized assumptions. The C-factor is a parameter which gives the indication of fouling growth on heat transfer surfaces and its effects on the heat transfer performances of a heat exchanger. As the C-factor takes into account the pressure drop and volume flow rate, it brings out the complete information of the fouling effects including the overall heat transfer coefficient, overall thermal resistance and the pressure drop. This tool can find wide applications in chemical process industries involving heat exchangers to provide cost and performance effective operations.

The artificial neural network approach has also been taken up to predict the fouling behavior of the exchanger under operating conditions. The efficiency based on C-factor and the temperature differences both for the shell and tube side have been predicted with a local linear wavelet neural network that uses back-propagation gradient descent approach. The trained network is tested and found to be a suitable tool for prediction of heat transfer efficiency of a heat exchanger subjected to fouling.

Acknowledgement

I wish to record my sincere gratitude to Dr. Pravin M. Singru, my research supervisor, for his role in shaping my thought process. His knowledge, keen interest, constant encouragement, help, constructive criticism, endless patience and unstinting encouragement have contributed greatly to making this doctoral study a successful and enjoyable journey. Any word would not be sufficient to express my deep gratitude and respect to Dr. Singru for his guidance on the thesis as well as career-related aspects. Working with him has been enlightening and pleasant. I hold close to my heart several of his statements and analogies which I will cherish forever.

I am grateful to Prof. B. N. Jain, Vice Chancellor, Prof. L.K. Maheswari, Ex-Vice Chancellor and Advisor to Chancellor and Prof. A. K. Das, Dean, Research and Consultancy Division, BITS Pilani, for granting me an opportunity to conduct research at this renowned institute and also for assuring the availability of necessary infrastructure and facilities to carry out my work. I wish to offer my sincere thanks to Prof. K.E. Raman, Director, BITS Pilani- K. K. Birla Goa Campus, for his constant encouragement and support. Sincere thanks are also due to Late Prof. T. C. Goel, former Director, BITS Pilani- K. K. Birla Goa Campus, for his valuable motivation and inspiration to the work towards my Ph.D degree.

I would like to extend my sincere gratitude to Dr. S.D. Manjare, Faculty In-charge, Research and Consultancy and Education Development Division, BITS PIlani- K. K. Birla Goa Campus, for helping me through out with his valuable inputs on this research and dissertation.

Special thanks are due to Dr. Shibu Clement for his encouragement and for sharing with me thoughts on matters beyond my imagination. I would like to specially thank Dr Sachin D. Waigaonkar for his constant motivation in shaping this work. My special thanks to Prof. B.J.C. Babu and Prof. D.M. Kulkarni for having contributed in one way or another towards successful completion of this work. I would also like to fondly acknowledge their generosity in sharing with me their inspiring inputs on issues beyond the academic world and for their company during several occasions, all of which have gone a long way in forging a great working relationship.

I would like to thank my colleagues from the Mechanical Engineering Department who have made my journey cheerful, happy and memorable. My sincere gratitude goes to Kiran,

Raghavendra, Abhishek, Hemanth, Sreedhar, Varinder, A C Kulkarni, Ramkumar, C P Kiran, Vikash, Saroj and Rajendra for their share of emotional and inspirational support.

I would like to thank my father and mother for their love and endless praying. I am so deeply indebted to my parents, they are indeed my true teachers. Special thanks go to my brother and sister for their continuous support and help. I also would like to thank my parents in law for their support and help during the difficult times.

Finally, a very special appreciation is due to my wife, Sanuja, not only for her constant encouragement and unreserved support in every circumstance but also for her love and sacrifice, without which completing of this thesis would not have been possible. I would like to thank my son Swapnil, who not only filled my life with joy and happiness, but also provided an unseen inspiration for carrying out this work.

Dillip Kumar Mohanty

Table of Contents

List of Figures

List of Tables

List of Abbreviations

A	heat transfer surface area (m^2)
A_c	heat transfer area under clean operating conditions (m^2)
A_f	heat transfer area under fouled conditions (m^2)
A^e	the experimental output data
A^p	the predicted output of ANN
a_1, a_2, a_3, a_4	correlational coefficients for the estimation of the heat transfer factor j_i
b_1, b_2, b_3, b_4	correlation coefficients for the estimation of the friction factor f_s
C	C-Factor
c_p	specific heat of both fluids (J/kg.^{o}C)
C_{ps}	specific heat of shell-side fluid (kJ/kg.^{o}C)
C_{pt}	specific heat of tube-side fluid (kJ/kg.^{o}C)
d_c	inner diameter of the tube under clean condition (mm)
D_{ctl}	diameter of the circle through the centers of the outermost tubes of a bundle (mm)
d_f	inner diameter of the tube under fouled condition (mm)
d_i	inner tube diameter (mm)
D_{otl}	diameter of the circle through the centers of the outermost tubes of a bundle (mm)
F(t)	Cumulative distribution function.
F_c	fraction of total tubes in cross-flow
F_{sbp}	fraction of cross-flow area available for bypass flow
F_t	temperature correction factor.
G_t	mass velocity of the tube side fluid (kg/m^2.sec)
H(t)	Cumulative hazard function.
$h_{i,c}$	heat transfer coefficient of fluid inside the tube under clean condition (W/m^2.K)
$h_{i,c}$	heat transfer coefficient of fluid inside the tube under clean condition (W/m^2.K)
$h_{i,c}$	heat transfer coefficient of fluid inside the tube under clean condition (W/m^2.K)
$h_{i,f}$	heat transfer coefficient of fluid inside the tube under fouled condition (W/m^2.K)
$h_{o,c}$	heat transfer coefficient of fluid outside the tube under clean condition (W/m^2.K)
$h_{o,f}$	heat transfer coefficient of fluid outside the tube under fouled condition (W/m^2.K)
J_h	Colburn factor for tube side heat transfer.

J_i Colburn factor for shell side heat transfer

K the number of free model parameters

k_f thermal conductivity of foulant layer (W/m.^{0}C)

k_t thermal conductivity of tube-side fluid (W/m^2.^{o}C)

k_w thermal conductivity of tube wall (W/m.K.)

L_{bb} inside shell-to-bundle bypass clearance (diametral) (mm)

L_{bc} central baffle spacing (mm)

L_{bi} inlet baffle spacing (mm)

L_{bo} outlet baffle spacing (mm)

LMTD Logarithmic Mean Temperature Difference (^{o}C)

LPH Liter per hour

L_{ta} effective tube length for heat transfer area calculations (mm)

L_{ts} tubesheet thickness (mm)

L_{tt} total tube length (mm)

M mass deposit rate of foulant per unit heat transfer area. (kg/m^2.sec)

m net mass fouling rate (kg/sec)

m_1 mass flow rate of hot fluid (kg/sec)

m_2 mass flow rate of cold fluid. (kg/sec)

m_d mass deposit rate of foulant (kg/sec)

M_d mass deposit rate of foulant per unit heat transfer area (kg/m^2.sec)

m_r mass removal rate of foulant (kg/sec)

M_r mass removal rate of foulant per unit heat transfer area (kg/m^2.sec)

N the number of observations

N_b number of baffles

N_c number of tube rows crossed in one cross flow section

N_{cw} number of tube rows crossed in one baffle window

N_s number of shells in series required for multipass flow heat exchangers

N_t Number of tubes

Nu Nusselt number

Pr Prandtle number

Pr_s shell-side Prandtle number

Pr_t Tube-side Prandtle number

p_t tube pitch (mm)

Q heat duty (W)

Q_1 heat duty of hot fluid (W)

Q_2 heat duty of cold fluid.(W)

Q_c heat transfer rate for clean surface (W)

Q_f heat transfer rate for fouled surface (W)

Q_m mean heat duty (W)

R(t) Reliability function.

R^2 Coefficient of determination.

R_B pressure drop correction factor for bundle-bypassing effects

R_c clean overall heat transfer resistance (m^2.K/W)

R_d rate of fouling deposition (m^2.K/J)

Re Reynolds Number

R_f total fouling resistance (m^2.K/W)

R_{fs} shell-side fouling factor, m^2 .K/W.

R_{ft} tube side fouling factor, m^2.K/W.

R_i thermal resistance due to internal convection, m^2.K/W

R_L pressure drop correction factor for baffle-leakage effects.

R_o thermal resistance due to external convection, m^2.K/W

R_{ov} Overall thermal resistance, m^2.K/W

R_r rate fouling removal rate (m^2.K/J)

Rs baffle end zones correction factor for pressure drop.

R_w thermal resistance due to tube wall (m^2.K/W)

S_m reference normal area for shell-side flow, mm^2.

S_{sb} shell-to-baffle leakage area, mm^2.

S_{tb} tube-to-baffle leakage area for one baffle, mm^2.

S_w area flow through the window, mm^2.

t local temperature of the cold fluid at any instant (^oC)

T local temperature of the hot fluid at any instant (^oC)

T_1 hot fluid inlet temperature (^oC)

T_2 hot fluid exit temperature. (^oC)

T_3 cold fluid inlet temperature (^oC)

T_4 cold fluid exit temperature. (^oC)

T_f Bulk temperature of fluid flowing through the tube (^oC)

T_i shell inlet temperature (^0C)

t_i tube inlet temperature (^0C)

T_s Temperature of tube wall, ^oC

U overall heat transfer coefficient ($W/m^2.K$)

U_c overall heat transfer coefficient for clean surface ($W/m^2.K$)

U_f overall heat transfer coefficient for fouled surface ($W/m^2.K$)

U_m mean overall heat transfer coefficient ($W/m^2.K$)

V volume flow rate of fluid (LPH)

v_s velocity of shell-side fluid

v_t velocity of tube-side fluid, m/sec

Greek symbols

δ_f thickness of foulant layer (m)

δ_{sb} shell-baffle clearance, mm.

δ_{tb} tube-baffle clearance, mm

θ mean time between failures

η Efficiency of heat exchanger in terms of C-factor

ξ Evaluation factor for scatter accuracy

Ψ Evaluation factor for average accuracy

λ constant rate in failure per cycle

σ standard deviation of the times to failure

σ^2 the variance.

μ mean of the normal time to failure

μ_s dynamic viscosity of shell-side fluid ($N.sec/m^2$)

μ_t dynamic viscosity of tube-side fluid ($N.sec/m^2$)

ρ_f foulant mass density (kg/m^3)

ρ_s density of shell-side fluid ($kg/m^{3)}$

ρ_t density of tube-side fluid (kg/m$^{3)}$

Δm uncertainty in mass measurement

ΔP pressure drop (kPa)

ΔP_{bi} shell-side pressure drop for ideal cross-flow for a single baffle (kPa.)

ΔP_c pressure drop under clean condition (kPa)

ΔP_{cf} shell –side cross flow pressure drop (kPa)

ΔP_e pressure drop at the end baffle compartments (kPa)

ΔP_f pressure drop under fouled condition (kPa)

ΔP_w pressure drop in the window of a segmentally baffled heat exchanger (kPa)

Δ_Q dispersion factor about mean heat duty

ΔT uncertainty in temperature measurement.

ΔT_{lm} Logarithmic Mean Temperature Difference (^oC)

Subscripts:

c clean

d deposit

f fouled

max maximum

min minimum

r removal

s shell side

t tube side

CHAPTER 1

Introduction

The process of heat exchange between two fluids at different temperatures and separated by a solid wall is found in many engineering applications. The equipment used to implement such heat exchange process is termed as a heat exchanger. A heat exchanger is a device in which two fluid streams, one hot and one cold, are brought into thermal contact with each other in order to transfer heat from the hot fluid stream to the cold one. It provides a relatively large surface area of heat transfer for given volume of the equipment. The specific applications of heat exchangers are most frequently found in chemical process industries as well as power production, waste heat recovery, cryogenic, air conditioning, petrochemical industries, etc.

Heat exchangers may be classified on the basis of contacting techniques, construction, flow arrangement or surface compactness. A shell and tube heat exchanger is most widely used in process plants. Shell and tube heat exchangers contribute more than 65% of the exchangers in chemical process industries (Shah and Sekulic, 2003). This is due to the fact that they provide area density greater than 700 m^2/m^3 for gases and greater than 300 m^2/m^3 for liquids (Kakac and Liu, 2002). Besides higher efficiency, reduced volume, weight and cost for specific heat duty justify shell and tube heat exchangers to be the best among all other kinds of heat exchange equipments. This exchanger is generally built of a bundle of round tubes mounted in a cylindrical shell with the tube axis parallel to that of the shell. The major components of this exchanger are tubes, shell, front end head, rear end head, baffles and tube sheet. Figure 1.1 (Incropera and Dewitt, 2010) shows the schematic diagram of a typical single pass heat exchanger. The fluid flowing through the inner tubes is referred to as ‘tube-side fluid’ while the fluid flowing through the annulus is referred to as shell-side fluid. The scope of application of this exchanger includes a pressure range of 300 bar on shell side and 1400 bar on the tube side. The temperature that can be handled ranges within -100^o C and 600^o C.

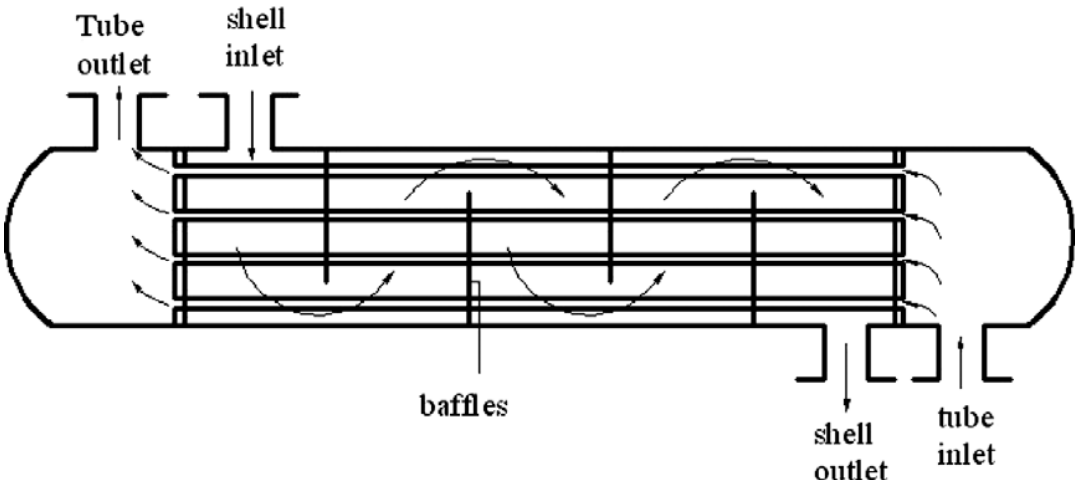

Figure 1.1 : Shell and Tube Heat Exchanger with one shell pass and one tube pass

1.1 Heat Exchanger Fouling

The accumulation of unwanted deposits on the heat transfer surfaces of a heat exchanger is usually referred to as fouling. Undesirable materials may be crystals, sediments, polymers, coking products, inorganic salts, biological growth, corrosion products, and so on. The presence of these deposits represents a resistance to the transfer of heat and consequently reduces the efficiency of the particular heat exchanger. Fouling is a synergistic consequence of transient mass, momentum and heat transfer phenomena involved with exchanger fluids and surfaces which significantly affects the heat exchanger operating performances. Thermal fouling in the presence of temperature gradient means accumulation of undesirable deposits of a thermally insulating material which provides added thermal resistance to heat flow on heat transfer surfaces over a period of time. This solid layer not only adds thermal resistance to heat flow, but also increases hydraulic resistance to fluid flow along the tubes. It is an extremely complex phenomenon characterized by combined heat, mass and momentum transfer under transient conditions. Fouling can occur as a result of the fluids being handled and their constituents in combination with operating conditions such as temperature and velocity. Though any solid or semisolid can become a heat exchanger foulant, but commonly encountered foulants in industrial operations include inorganic material such as air borne dusts and grit, waterborne mud and slits, calcium and magnesium salts, iron oxide and organic materials such as biological substances, bacteria, fungi, algae, heavy organic deposits, polymers, tars and carbon.

The thermal fouling in the presence of a temperature gradient influences the heat transfer and flow conditions in a heat exchanger by providing an additional resistance to heat flow process. The effect of the presence of fouling layer on temperature distribution is illustrated in Figure1.2 (Bott,1995). T_1 and T_6 represent the bulk temperatures of hot and cold fluids respectively. Under turbulent flow conditions, these temperatures extend almost to the boundary layer in respective fluids since there is a good mixing and the heat is carried physically. In general, the thermal conductivity of foulants is extremely low as compared to that of the tube material. The thermal resistances offered by both the deposit layers require a large temperature gradient to drive the heat through the foulants. But in actual operating conditions, the temperature difference across the tube wall is comparatively low (Bott, 1995).

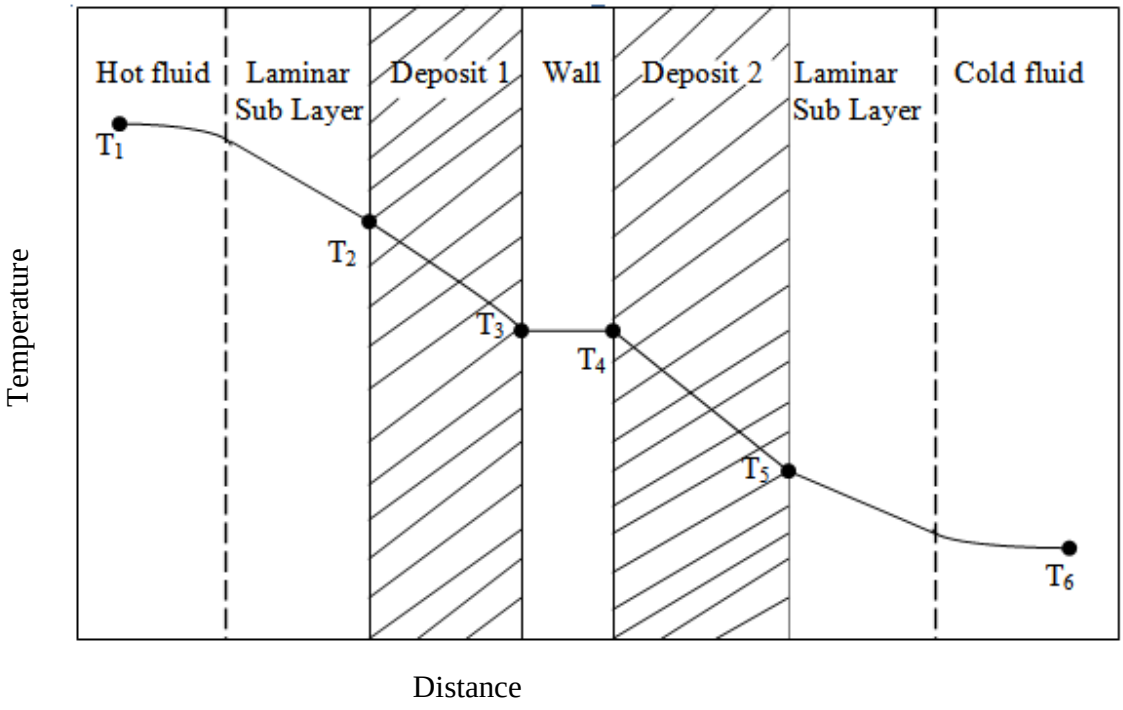

Figure 1.2 : Temperature distribution across fouled heat exchanger surfaces

The problem of heat exchanger fouling therefore represents a challenge to designers, technologists and scientists in terms of heat transfer technology. In most commonly observed fouling phenomenon, three basic stages can be visualized in relation to deposition on surfaces from a moving fluid (Steinhagen, 2000).

(i) The diffusional transport of the foulant or its precursors across the boundary layers adjascent to the solid surface within the flowing fluid.

(ii) The adhesion of the deposit to the surface and itself.

(iii) The removal of the material from the exchanger surface.

The rate of fouling growth is the difference between the rates of deposition and removal. Figure 1.3 (Bott, 1995) indicates an idealized asymptotic growth rate of a deposit on a heat transfer surface. The region A indicates the initiation of adhesion which is most commonly known as induction period. The duration of induction period depends on the fluids involved and the operating conditions of the exchanger. But it is quite significant in case of crystallization fouling as compared to other fouling mechanisms. Second phase represented by region B is the steady growth of fouling deposits on the surface. During this phase, removal of foulants exists along with deposit. Initially the rate of removal is quite low as compared to deposit rate. But afterwards the deposit rate gradually decreases while the removal rate increases leading to a saturation state. Finally the steady state is reached when removal rate becomes equal to deposit rate so that deposit thickness remains virtually constant.

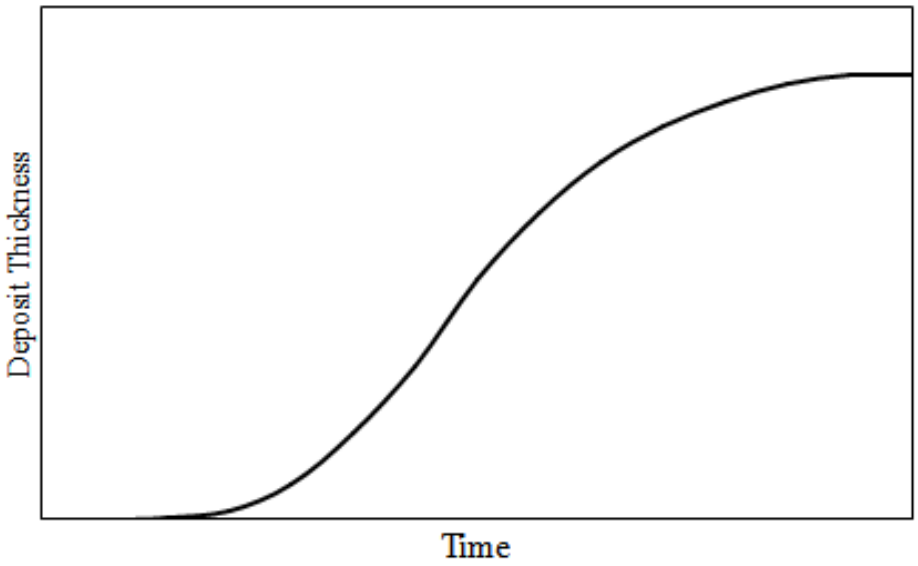

Figure 1.3 : Variation of deposit thickness with time

1.2 Types of Fouling

Depending on the mechanism of fouling formation on heat transfer surfaces, fouling can be broadly classified into six categories.

- **Crystallization Fouling**

  Crystallization or precipitation fouling involves crystallization of solid salts, oxides and hydroxides from solutions. Such kind of fouling contributes around 35% of fouling problems in industrial heat exchange equipments (Shah and Sekulic, 2003). These are most often water solutions commonly occurring in boilers and heat exchangers operating with hard water. Through changes in temperature, the concentration of salts may exceed the saturation, leading to precipitation of solids or crystals. In general, the dependence of the salt solubility on temperature or presence of evaporation will often be the driving force for precipitation fouling. The salts with the normal solubility increase their solubility with increasing temperature and thus will foul the cooling surfaces. The salts with inverse or retrograde solubility will foul the heating surfaces. Some of the industrially common phases of precipitation fouling deposits observed in practice to form from aqueous solutions include Calcium Carbonate, Calcium Sulfate, Calcium Oxalate, Magnesium Oxide, Magnesium Hydroxide, Serpentine and amorphous silica etc. A detailed review of the mechanism of crystallization fouling is illustrated in Appendix A.

- **Particulate fouling**

  Fouling by particles suspended in water or gas is referred to as particulate fouling. This process is usually most important for colloidal particles smaller than about 1 μm in at least one dimension. Particles are transported to the surface by a number of mechanisms and there they can attach themselves by flocculation or coagulation. Being essentially a surface chemistry phenomenon, this fouling mechanism can be very sensitive to factors that affect colloidal stability. A maximum fouling rate is usually observed when the fouling particles and the substrate exhibit opposite electrical charge. With time, the resulting surface deposit may harden through processes collectively known as deposit consolidation or aging. The common particulate fouling deposits formed from aqueous suspensions include iron oxides and iron hydroxides.

- **Corrosion fouling**

  When a metallic heat transfer surface is exposed to a corrosive liquid medium, the products of corrosion may foul the surfaces. The corrosion fouling of a heat transfer

surface involves two simultaneous electrochemical reactions. These occur at the anodic and cathodic portions of the surface which can be visualized as an array of very small area with areas of different polarity mixed in random manner (Melo et. al., 1988). Corrosion deposits are created by the corrosion of the substrate. Corrosion deposits will normally have composition related to the composition of the substrate. Also, the geometry of the metal-oxide and oxide-fluid interfaces may allow practical distinction between the corrosion and fouling deposits. An example of corrosion fouling can be formation of an iron oxide or oxyhydroxide deposit from corrosion of the carbon steel underneath.

- **Chemical reaction fouling**

Chemical reactions may occur on contact of the chemical species in the process fluid with heat transfer surfaces. In such cases, the metallic surface sometimes acts as a catalyst. For example, corrosion and polymerization occurs in cooling water for the chemical industry which has a minor content of hydrocarbons. Systems in petroleum processing are prone to polymerization of olefins or deposition of heavy fractions of asphaltenes and waxes. High tube wall temperatures may lead to carbonizing of organic matters. Food industries such as milk processing industries experience fouling problems by chemical reactions.

- **Solidification fouling**

Solidification fouling occurs when a component of the flowing fluid "freezes" onto a surface forming a solid fouling deposit. Examples may include solidification of wax with a high melting point from a hydrocarbon solution or solidification of molten ash carried in a furnace exhaust gas onto a heat exchanger surface. The surface needs to have a temperature below a certain threshold in order to avoid the solidification point of the foulant.

- **Biofouling**

  Biofouling or biological fouling is the undesirable accumulation of micro-organisms, algae and diatoms, plants, and animals on heat transfer surfaces involving untreated water. This can be accompanied by microbiologically influenced corrosion. Bacteria can form biofilms or slimes which is very complex. The organisms can aggregate on surfaces using colloidal hydrogels of water and extracellular polymeric substances such as polysaccharides, lipids, nucleic acids, etc. Bacterial fouling can occur under either aerobic conditions with oxygen dissolved in water or anaerobic conditions with no oxygen. In practice, aerobic bacteria prefer open systems, when both oxygen and nutrients are constantly delivered, often in warm and sunlit environments. Anaerobic fouling more often occurs in closed systems when sufficient nutrients are present. Examples may include sulfate-reducing bacteria which produce sulfide and often cause corrosion of ferrous metals and other alloys. Sulfide-oxidizing bacteria like Acidithiobacillus can produce sulfuric acid, and can be involved in corrosion of concrete.

- **Composite fouling**

  Composite fouling is the most commonly occurring fouling process in heat transfer surfaces of a heat exchanger. This type of fouling involves more than one foulant or more than one fouling mechanism working simultaneously. The multiple foulants or mechanisms may interact with each other resulting in a synergistic fouling which is too much complex rather than a simple arithmetic sum of the individual components. Also, one mechanism may be a fouling precursor for another mechanism.

1.3 Fouling Fluids

The development of fouling greatly depends on the nature of fluids being involved in the heat transfer process. Fluids may be categorized into three groups according to their potential for fouling (Nesta and Bennet, 2005).

- **Asymptotic fouling Fluids**

Asymptotic fouling fluids reach a maximum constant fouling resistance after a short run time. The fluid velocity imparts a shear stress at the fouling layer that removes some of the deposit. As the fouling layer thickens, flow area is reduced and velocity increases, thereby increasing the removal rate. When the rate of removal equals the rate of deposition, fouling reaches an asymptotic limit. The thickness of the final asymptotic fouling layer is inversely proportional to the original velocity. Cooling tower water is an example of an asymptotic fouling fluid.

- **Linear fouling Fluids**

  Linear fouling fluids have a fouling layer that is too tenacious to shear off at economic design velocities. The fouling layer continues to build as a roughly linear function of time. The rate of fouling over time is dependent on velocity. At low velocity, fouling is controlled by mass diffusion to the surface. Increasing velocity in this range increases mass diffusion, and thus promotes fouling. At high velocity, fouling is controlled by deposit shearing, residence time, and decreases with increasing velocity. Linear fouling mechanisms are also strongly dependant on surface temperature. Crude oils and polymerizing hydrocarbons are examples of linear fouling fluids.

- **Non-fouling Fluids**

  This kind of fluids has lowest affinity for fouling on heat exchanging surfaces. Non-fouling fluids do not require regular cleaning. Most commonly used non-fouling fluids in chemical process industries include non-polymerizing light hydrocarbons, steam and sub-cooled boiler feed water.

1.4 Fouling Progress

Fouling is a dynamic phenomenon which progresses with time. However the deposit on a surface does not always develop steadily with time. The fouling deposition rate can be either constant or decreasing with time corresponding to process parameters and the dominant fouling mechanism. Depending on the nature of the system, the fluids involved and the local thermohydraulic conditions at the heat transfer surface, fouling grows in a number of phases. Figure 1.4 (Kuppan, 2000) illustrates the time dependent characteristic scenario of fouling resistance for various kinds of fouling growth.

- **Induction Period**

  At the initial stage of operation of a heat exchanger, a near-nil fouling rate is observed on the heat transfer surfaces. This is considered to be the initiation of fouling growth. This is often observed in biofouling and precipitation fouling. After the induction period, the fouling rate increases.

- **Negative Fouling**

  Negative fouling occurs when fouling rate is quantified by monitoring heat transfer. Relatively small amounts of deposit can improve heat transfer relative to a clean surface, and give an appearance of negative fouling. Negative fouling is often observed under nucleate-boiling heat-transfer conditions where deposit improves bubble nucleation or forced-convection if the deposit increases the surface roughness and the surface no longer remains hydraulically smooth. After the initial period of surface roughness control, the fouling rate usually becomes strongly positive.

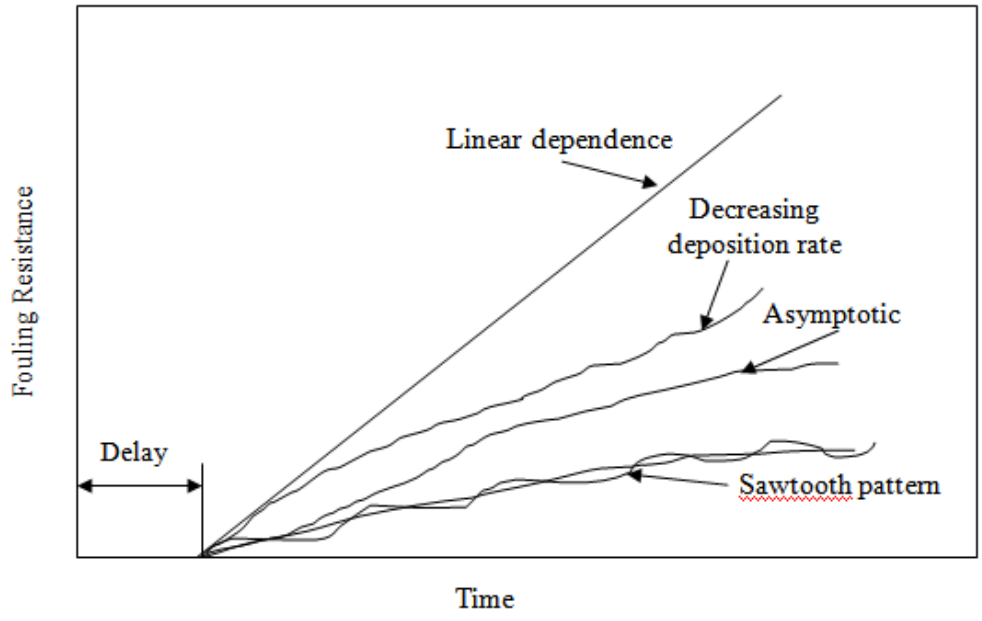

Figure 1.4 : Time dependence of fouling resistance

- **Linear fouling**

If the deposition rate is constant and the removal rate is negligible or if the difference between deposit and removal rate is constant, the fouling-time curve is a straight line indicating linear fouling. The linear fouling is generally represented by tough, hard, adherent deposits due to crystallization fouling. In this case, the fouling rate can be steady with time.

- **Falling fouling**

The falling rate fouling results from a falling deposition rate or increasing removal rate as compared to deposit rate. However the falling rate fouling kinetics is regarded as the early stage of asymptotic fouling. During this stage, the fouling rate decreases with time, but never drops to zero. The progress of fouling can be described by the initial fouling rate represented by a tangent to the fouling curve at zero deposit loading and the fouling rate after a long period of time represented by an oblique asymptote to the fouling curve.

- **Asymptotic fouling**

For weaker deposits, the fouling resistance approaches a constant or asymptotic value which may not allow acceptable operation of the process. In this case, the fouling rate decreases with time, until it finally reaches zero. At this point, the deposit thickness remains constant with time which can be represented by a horizontal asymptote. The asymptote is usually interpreted as the deposit loading at which the deposition rate equals the deposit removal rate.

- **Seesaw fouling**

Fouling generally increases with time assuming a linear or falling rate. But in actual practice, the fouling progress is periodically interrupted and takes the form of sawtooth curve depending on the deposit and removal rate. The periodic sharp variations in the apparent fouling amount often correspond to the moments of system shutdowns, startups or other transients in operation.

1.5 Sequential Events of Fouling

The growth of fouling is a transient mechanism that commonly occurs in five consecutive stages (Shah and sekulic, 2003).

(i) Initiation Period or Delay Period :

When the new or clean heat exchanger has been taken into operation, the initially high heat transfer coefficients may remain unchanged for a certain period of time. During this period, nuclei for crystallization are formed or nutrients for biological growth are deposited. This delay period may last any time from few seconds to several days. Almost no delay period is observed for particulate fouling. For crystallization fouling and chemical reaction fouling, initiation period decreases with increasing surface temperature as supersaturation and reaction rate increases. Generally before the start of deposition, delay time decreases with increasing roughness of heat transfer surface.

(ii) Mass Transport :

To form a deposit at the heat transfer surface, it is necessary that at least one component is transported from the bulk fluid to the heat transfer surface. In most cases, it occurs by diffusion. For the transport of particles to the wall, inertia forces and thermophoretic forces have to be considered.

(iii)Formation of Deposit :

After the foulant has been transported to the heat transfer surface, it must stick to the surface as in case of particulate fouling or react to the deposit forming substance.

(iv)Removal or Auto-Retardation :

Depending on the strength of the deposit, erosion occurs immediately after the first deposit has been laid down. Furthermore several mechanisms exist which cause auto retardation of the deposition process. For the thermal boundary condition of constant temperature difference between hot and cold fluid, the growth of deposit causes a reduction of the driving temperature difference between heat transfer surface and the fluid.

(v) Ageing :

Every deposit is subjected to ageing. Ageing may increase the strength of the deposit by polymerization, re-crystallization or de-hydration. Biological deposits get poisoned by metal ions and may be washed away by the bulk flow. Ageing is the least investigated and understood step and is usually ignored in modeling attempts.

1.6 Cost of fouling

Fouling is ubiquitous and generates tremendous operational losses. Garrett-Price et. al.(1985) estimated the energy and economic penalties associated with heat exchanger fouling for the US refineries, as more than $2 billion per year. According to investigations of Garrett-Price, the total heat exchanger fouling costs for highly industrialised countries such as the US and the UK are about 0.25% of the countries' gross national product (GNP). The overall cost of fouling to industries in the UK is in the range of £ 8 – 14x 10^8 per annum while that of the US is in the range of 8- 10 x 10^9 per annum. According to Pritchard et. al. (1988) about 15% of the maintenance costs of a process plant can be attributed to heat exchangers and boilers, and of this, more than half is caused by fouling. Pilavachi and Isdale (1992) concluded over the European community as a whole that the cost of heat exchanger fouling is of the order of 10 x 10^9 ECU and of this total 20 – 30% cost is due to additional energy. A detailed study by Chaudgane figures overall cost of fouling in the industries of France around 1 x 10^{10} French Francs per annum (Chaudgane, 1992). Steinhagen et. al. (1993) found that the fouling costs for New Zealand are 0.15% of the New Zealand GNP. Another analysis by Xu Zhi-Ming et. al. (2007) estimated the economical loss due to boiler and turbine fouling in China about 4.68 billion dollars, which is about 0.169% the country GDP.

The losses resulting from impaired heat transfer, corrosion damage, increased pressure drop, flow instabilities, induced vibrations and premature failure of heating elements due to fouling include the following.

- Increases capital costs due to the need of oversurface the heat exchanger and for cleaning.
- Increases the maintenance cost resulting from cleaning, trouble shooting and chemical additives.
- Results in loss of production due to shut down or reduced capacity
- Increases energy losses due to reduced heat transfer and increased pressure drop.

It is clear from the limited data that fouling costs are substantial and any reduction in these costs plays a vital role in industries involved with heat exchangers. However frequent dismantling and cleaning of the exchanger can affect the continued integrity of the equipment. Especially in shell and tube heat exchangers, the tubes and baffles may be damaged due to

frequent cleaning which may aggravate the fouling problems by causing restrictions to fluid flow and upsetting the required temperature distribution.

1.7 Research objectives and the scope of the thesis

In this work, the fouling growth characteristics and its effect on the thermo hydraulic performances in a shell and tube heat exchanger subjected to fouling is investigated. The main aim of the work described in this thesis is to develop a new methodology in order to gain an insight into the effect of fouling on heat transfer efficiency and pressure drop of a shell and tube heat exchanger. The overall objectives of the present work are summarized as follows.

1. Estimation of the overall heat transfer coefficient and fouling resistance of a shell and tube heat exchanger under specific operating conditions.
2. To develop a numerical model for finding out the time required to attain critical fouling conditions under specific operating conditions taking into account the uncertainties in measurements.
3. To develop a methodology using Wilson plot method and its modification by which heat transfer and flow parameters can be correlated to obtain time required for attaining critical fouling condition.
4. To develop a new methodology which eliminates the use of empirical correlations and takes into account the minimum number of thermo-hydraulic parameters for quantification of fouling and its effects so that the performance evaluation is not affected by the uncertainties involved in the experimental measurements of all parameters. Development of this method using C-factor is the major contribution of this thesis.
5. To perform the accurate prediction of heat transfer performances by using neural network approach so that online adaptation and control of heat exchanger system can be achieved.

In the present work, four different methodologies/tools namely thermal analysis, statistical method, Wilson plot method and C-factor method are used. In addition to the above mentioned methods, a neural network approach is proposed for prediction of fouling at any point of time. The applicability of the developed approaches and methodologies has been

elaborately discussed in the respective chapters with reference to a laboratory scale shell and tube heat exchanger system.

1.8 Organization of the Thesis

To represent the subject matter in a logical sequence, the thesis work is organized in 8 chapters.

Chapter 1 gives an introduction to the process of fouling in heat exchangers. A brief summary of the different types of fouling based on mechanism of fouling growth, the sequential events during fouling formation and the costs associated with fouling is presented. The motive of this thesis is highlighted for which this research work has been carried out.

Chapter 2 reviews the principles, operational parameters, significant developments of fouling process in heat exchangers. This chapter discusses the various models and methodologies along with their limitations for investigation of fouling and its effects on heat exchanger performance. Literatures regarding the heat exchanger design methods are also referred to obtain the film coefficients both on the tube and shell side. An overview the conventional thermal analysis and statistical approach in the area of heat transfer analysis is presented. Furthermore a general review of the Wilson plot method for convective heat transfer and neural network methodology for prediction of fouling behaviour has been discussed in brief. Based on the literature survey, the existing gaps in literature were identified.

Chapter 3 introduces a comprehensive calculation procedure of fouling taking into account the constructional geometry and operational constraints. The Bell-Delaware method has been used in this work to estimate the heat transfer performances such as overall heat

transfer coefficient, overall thermal resistance and fouling resistance. The sample results of thermal analysis obtained by applying the Bell-Delaware method are presented in Appendix A.

Chapter 4 proposes a theoretical framework by the application of statistical methodology and thermal analysis for fouling growth. The materials and methods for the experimental work along with the application of statistical approach for development of fouling growth model are introduced in chapter 4. Simultaneously the uncertainty in measurement of flow rate and temperature has been taken into consideration for carrying out the thermal analysis.

Chapter 5 introduces the application of Wilson plot method and the modified version of Wilson plot method in the fouling analysis. The original Wilson plot and its modifications have been used to develop the correlations among the Nusselt number and overall heat transfer coefficient for the heat exchanger under fouled condition.

Chapter 6 introduces a new factor known as C-factor for quantification of fouling and its effects on heat transfer performances of a heat exchanger. The development of the C-factor is the major contribution of this thesis work towards study of fouling in heat exchangers. The C-factor provides an indirect measure of fouling by correlating the flow rate and pressure drop. The methodology eliminates all the assumptions involved in empirical correlations for calculation of thermal performances like overall heat transfer coefficient and thermal resistance. Simultaneously the accuracy is high as only two parameters are involved in this method and the uncertainties associated with other experimental parameters have no role in the quantification of fouling. Thus this method proves to offer the most accurate, reproducible and consistent results while being easy to be implemented.

Chapter 7 deals with the future prediction of fouling behavior of a heat exchanger under steady operating conditions. It emphasizes the development of a model based on neural network approach for further prediction of the performance parameters of a heat exchanger with experimental data. The processes of data reduction and network configuration of a feed-forward back-propagation based neural network have been discussed elaborately in this chapter. The behavior of the heat exchanger under fouled condition has been highlighted in terms of the shell side temperature difference, tube side temperature difference and the efficiency.

Chapter 8 presents an overview of the salient features, the outcome and the future scope of the present work. This chapter contains the most significant conclusions drawn from the experiments as well as some perspectives for further investigation in this field of research.

Chapter 2

Literature Review

Fouling is a major unresolved problem in heat exchangers since their invention. The serious financial and performance consequences of these problems have raised the profile of heat exchanger fouling as an important area of study. Several studies have been conducted in this regard and many techniques have been developed and evaluated to reduce fouling. This chapter gives an overview of the studies carried out on fouling of heat exchangers.

2.1 Introduction

Taborek et. al., (1972) published an article entitled "Heat Transfer Fouling: The Major Unresolved Problem in Heat Transfer". The article outlines ideas on the fouling problem through analyzing its stages and suggesting various predictive models. Afterwards many researchers such as Somerscales (1981), Watkinson (1988), Hewitt et al.,(1994) and Zubair et al., (1999) categorized thermal fouling into six categories based on the dominant mechanism of fouling evolution. These are crystallization, solidification, particulate, corrosion, chemical reaction and biofouling. The classification of various aspects of fouling can be broken down according to the physical and chemical processes that occur.

2.1.1 A Basic Description of Fouling

Fouling induces an increase in the thermal resistance and the subsequent decrease in thermal efficiency. For a clean surface that has not experienced fouling, the heat is transferred from the bulk of the liquid of the hot side by convection to the heat transfer surface and then is transmitted through the surface by conduction. The overall resistance is quantified in the form of the overall heat transfer Coefficient (U_c).

$$\frac{1}{U_c} = \frac{1}{h_s} + \frac{1}{k_t} + \frac{1}{h_t} \tag{2.1}$$

The variables Uc, h_s, h_t and k_t represent the clean overall heat transfer coefficient, heat transfer coefficient of the shell side, tube side and the thermal conductivity of the heat transfer surface, respectively. The occurrence of fouling adds an extra obstacle to the transfer of heat and the mode of transfer is conduction since the foulant deposit is solid. The deposit has a considerable impact on the overall heat transfer coefficient because the thermal conductivity of a foulant

deposited on a heat exchanger surface is invariably smaller than that of the metal on which it resides. This impact causes the thermal resistance to increase and the thermal efficiency to significantly fall by adding another resistance to heat transfer. This can be described by calculating the new fouled value of the overall heat transfer coefficient (U_f) where R_f represents the foulant resistance on the tube side of the heat transfer surface (Bott, 1995).

$$\frac{1}{U_c} = \frac{1}{h_s} + \frac{1}{k_t} + R_f + \frac{1}{h_t} \tag{2.2}$$

The results from calculating the overall heat transfer coefficient in the above equations for both clean and fouled surfaces can be used to obtain the total heat transferred and the fouling resistance. The total heat transferred is calculated using the total heat transfer surface area and the logarithmic mean temperature difference.

$$Q = UA\Delta T_{lm} \tag{2.3}$$

The fouling resistance is difference between the inverse value of the overall heat transfer coefficient for the clean and fouled surface.

$$R_f = \frac{1}{U_f} - \frac{1}{U_c} \tag{2.4}$$

2.1.2 Influential Aspects of Fouling

The classification of various aspects of fouling can be broken down according to the physical and chemical processes involved in the process of fouling growth and propagation. Epstein (1983) suggested a novel approach to this by stating that there were five primary fouling categories, known as mechanisms, and for each there are five successive events, processes. The five mechanisms include crystallization fouling, particulate fouling, corrosion fouling, chemical reaction fouling and biofouling. The solidification fouling was considered as a specific type of crystallization fouling. The five processes include initiation, transport, attachment, removal and ageing. Epstein referred to the combination of the five mechanisms and five processes as the 5×5 matrix. The aim of formulating this matrix was initially to break the overall fouling problem down into simpler elements that could be progressively solved. However fouling is distinctly transient in nature and the processes involved in fouling can occur simultaneously within a unit experiencing fouling. These points emphasize the complexity involved in the analysis of fouling phenomenon.

However fouling is a complex phenomenon and its accurate prediction based on current knowledge is quite a difficult task. The current knowledge is either based on practical experience or application of fouling factors at the design stage. At the design stage fouling of the outer surface of the tubes is accounted for by making allowances for the added thermal resistance that the deposited layers introduce to the heat transfer surface. This is essentially achieved by increasing the heat transfer surface area in the heat exchanger. According to Garret-Price et al., (1985) the general practice is to design heat exchangers with an average oversize of about 35% in terms of surface area. While this strategy is widely accepted, it has some economic penalties associated with it. Heat exchangers designed with excess surface area tend to be larger and heavier, which evidently results in extra costs to cover additional material, transportation, and installation.

Kakac et al., (1998) proposed another approach by implementation of the percentage over surface index (OS) described by

$$OS = \frac{R_f}{R_c} \times 100 = (\frac{A_f}{A_c} - 1) \times 100 \tag{2.5}$$

where (R_c) is the clean overall heat transfer resistance and (R_f) is the total fouling resistance. The total fouling resistance represents the insulating effect of the deposits on the heat transfer surfaces. The heat transfer surface area under clean operating conditions is (A_c), while the required surface area under fouled conditions is (A_f).

A critical review of chemical reaction fouling by Watkinson and Wilson (2002) summarized the state of knowledge in the field of chemical reaction fouling and identified a number of key technical areas. Watkinson developed a fouling model on the premise that the chemical reaction for generation of precursor can take place in the bulk fluid, in the thermal boundary layer or at the fluid-wall interface. It depends upon the interactive effects of fluid dynamics, heat and mass transfer and the controlling chemical reaction. The mathematical model followed a generalized approach commonly used for tubular chemical reactors to describe the interactive effects of the controlling chemical reaction and transport processes. The analysis was used to examine the experimental data for fouling deposition of poly-peroxides produced by autoxidation of indene in kerosene. The effects of fluid and wall temperatures for different flow geometries were analyzed and the results indicated that the relative effects of

physical parameters on the fouling rate would differ for different fouling mechanisms. Therefore, it is important to identify the controlling mechanism in applying the closed-flow-loop data to industrial conditions. This analytical fouling model, even though an approximate model, served as a useful tool for analysis of the experimental data. Such an analytical tool was helpful for identifying the controlling mechanisms in the overall fouling process, determining the effects of physical conditions, and applying the experimental data to industrial conditions.

Poley et. al. (2002) investigated the operating variables on fouling rate and the effect of fouling on thermo hydraulic performances of a 10MW heat exchanger in a crude oil refinery. The two variables which significantly controlled the fouling rate were identified to be velocity of crude oil through the tubes and tube wall temperature. The heat transfer coefficient on tube side dropped from 3680 to 1965 $W/m^2.K$ as the fouling factor increased to 0.7×10^{-3} $m^2.K/W$ from clean operating condition. For same fouling factor, the shell side heat transfer coefficient dropped from 4090 to 2350 $W/m^2.K$. This indicates the cost of fouling on the efficiency of a heat exchanger.

The impact of heat exchanger fouling on the optimum operation and maintenance of stirling engine has been reported by Kuosa et. al. (2007). Conventionally the fouling in heat exchanger was estimated using overall heat transfer coefficient and additional thermal resistances as fouling factors. With a variation of fouling factor from 0 to 40 $m^2.K/kW$, the heater power declined by 24% from 13kW to 9.8 kW while the cooler power declined by 15% from 9kW to 7.6 kW. Correspondingly the brake efficiency reduced from 30% to 22%. In feed-water heaters, the outlet shell-side fluid temperature increases by around 7% due to decrease in heat duty as a result of fouling (Antar and Zubair, 2007). During this period, the fouling resistance increased from 3.52×10^{-5} $m^2.K/w$ to 8.8×10^{-5} $m^2.K/W$ and the overall heat transfer coefficient decreased by 44% from $160 W/m^2.K$ to $90 W/m^2.K$.

Wright et. al. (2009) presented a focused literature review to understand the common problem of fouling of air-conditioning heat exchangers in aircraft applications. The paper additionally estimated the deposition fraction and the factors that influence it. The primary focus was a mathematical model of deposition in a fin- and tube-heat exchanger that accounted for inertial impaction, gravitation settling, air turbulence and Brownian diffusion. The phenomenon of fouling has a significant effect in the operational efficiency of a process plant involving heat exchangers. Coletti and Macchietto (2011) investigated the energy losses due to

heat exchanger fouling in oil refineries. The estimated loss was around 250000GBP in a refinery of 200000 billion barrels per day capacity when the coil inlet temperature reduced by 1^{o}C due to fouling.

Heat exchangers are the workhorse of most chemical, petrochemical, food-processing, and power-generating processes. The global heat exchanger market is estimated to top a total of $12.7 billion by 2012, with an increase of 3–5% per annum (Stein-Hagen et. al., 2011). Conservative studies estimated that heat exchanger fouling leads to additional costs in the order of 0.25% of the gross domestic product (GDP) of industrialized countries, and that it is responsible for 2.5% of the total equivalent anthropogenic emissions of carbon dioxide. While significant progress has been made in the mitigation of heat exchanger fouling, the challenge to reduce its impact on heat exchanger performance is still enormous. Many mitigation and cleaning techniques that have found their way into regular plant operation have been developed by an empirical trial-and-error approach.

2.2 Fouling Models

Fouling in heat exchangers has been the subject of intensive research by several groups of investigators. Therefore many mathematical models to represent fouling have been developed to predict the fouling rates as a function of key design and operational parameters.

The first model was suggested by Kern and Seaton (1959) which is based on the approach that the net fouling rate is the difference between the rates of deposition and removal. The basic differences between various models reported in literature are in the description of the deposition and removal terms. The rate of deposition is described by either a transport-reaction model or reaction model while the rate of removal is described either by shear-related or mass-transfer related expressions. In general, transport-reaction models are more rigorous than the reaction models. The general model of fouling growth is described in Appendix B. Although the general models have many attractions for study of fouling growth, but with the present state of knowledge, specific models have been developed for particular mechanisms.

Watkinson and Epstein (1969) attempted to quantify the fouling results from experiments in gas oil fouling and developed a model for gas oil fouling. The model focused on the deposition of particles onto the heat transfer surface in the usual two-step process namely transport then adhesion. It was found that the deposition rate was proportional to both the mass flux and the sticking probability. However, they made a modification by defining the mass flux as a mass convection equation taking into consideration the concentration of foulant on the surface of deposit.

In 1973, Ruckenstein and Prieve (1973) developed a model that separates the resistance of the transport and attachment for deposition of particles in turbulent flow due to both momentum and molecular diffusionstep . The object of their work was to develop a model that could predict the deposition rate of colloidal particles by considering the effects of diffusion, convection, and interaction forces. The attachment model by Ruckstein and Prieve considered the surface particle interactions and the requirement for the particle to overcome the resultant forces acting on it to attach. The expression for this was defined in equation (2.6) with the constant k_R having an Arrhenius relationship to temperature.

$$\phi_d = k_R C_S \tag{2.6}$$

The result of this model was two separated resistances, one for each process. This model attempted to quantify the actual forces rather than just expressing the resulting interactions as a probability term.

A transport-reaction model was developed by Crittenden and Kolaczkowski (1979) considering chemical reaction as well as the transport of fouling precursor to and from the heated surface. They also proposed a modified model that includes a back-diffusion term (Crittenden et al., 1987). The modified model described the transport of precursor mass flux to the heat transfer surface as

$$N_r = \rho_f \lambda_f \frac{dR_f}{dt} + C_3 \frac{\tau}{\chi} R_f \tag{2.7}$$

where ρ_f and λ_f are the deposit constant and thermal conductivity respectively, τ is the shear stress, χ is the deposit strength and C_3 is a constant. Tests were performed in a circulation system in which the crude oil is circulated through an annular test section at velocities ranging from 0.91 to 3.1 m sec^{-1} and at two bulk temperatures of 149 and 204°C. The experiments have been carried out at surface temperatures ranging from 177 to 329°C and the experimental data

were reported. But this model could not justify the finite concentration of foulant at the surface which would be required for back diffusion to occur.

Epstein (1994) developed a model for the initial chemical reaction fouling rates at the surface in which the surface attachment is proportional to residence time of the fluid at the surface. The greater the residence time, the greater would be the opportunity for the chemical reaction to occur. The relationship between the initial fouling rate and the mass flux is given as

$$\left[\frac{dR_f}{dt}\right]_{t=0} = \frac{m\phi}{k_f \rho_f} \tag{2.8}$$

where, m is the stoichiometric factor, ρ_f the foulant density, k_f the thermal conductivity of foulant and ϕ is the deposition mass flux. The driving force for the mass transfer from the bulk fluid to the heater surface of foulant precursor was expressed as the difference between its bulk and surface concentrations, C_b and C_s, respectively. The deposition mass flux (ϕ) is given by

$$\phi = \frac{C_b}{\frac{kSe^{2/3}}{uf^{1/2}} + \frac{k' \rho u^2 f}{\mu \exp(-E / RT_s) C_s^{n-1}}} \tag{2.9}$$

where, k and k' are constants, S_c is Schmidt number, f is the friction factor, ρ is the fluid density, u is fluid velocity, E is activation energy, T_s is the bulk temperature, R is universal gas constant μ is dynamic viscosity of fluid and n is the order of the reaction plus attachment process. The first term in the denominator represents the mass transfer of foulant or precursor to the heated surface and the second term represents the reaction and attachment aspects. Epstein's model showed an excellent fit to Crittenden's data for initial fouling rates of polymerization of styrene (Crittenden et. al., 1987). It was also able to explain the effects of temperature and velocity. However the order of the reaction term n and S_c are unknown for the crude oil fouling. It is also quite difficult to isolate the key precursors of fouling as the crude oil has complex compositions and this creates difficulty in finding out the concentration of exact precursor and its role in fouling. Therefore this model was not able to be used for describing the crude oil fouling.

Ebert and Panchal (1995) introduced the concept of threshold fouling models for quantifying and mitigating fouling in crude oil processing. By modeling the fouling process as a rate equation, the theoretical concept of fouling and the threshold temperature were introduced. The threshold temperature is the temperature below which fouling is minimum. The numerical model allowed users to estimate operating conditions where the fouling rate would be close to zero termed as fouling threshold. The emphasis on rates steered attention away from oversizing exchangers based on anticipated worst case design scenarios suggested by the use of asymptotic fouling resistances. This model was based on certain assumptions.

- The foulant forming reactions occur in the thermal boundary layer at a mean film temperature, T_f,
- The foulant is transported by diffusion and turbulence eddies from the boundary layer to the bulk flow
- The net rate of deposition is the difference between the rate of formation and rate of removal.

The semi-empirical model by Ebert and Panchal (1995) for predicting the linear rate of fouling as a function of film temperature and fluid velocity is given as:

$$\frac{dR_f}{dt} = \alpha \,\mathrm{Re}^{\beta} \exp\left(-\frac{E}{RT_f}\right) - \gamma\tau_w \qquad (2.10)$$

where α, β, E and γ are constants to be determined from the experimental data. For crude oil fouling, the constants were found to be $\beta = -0.88$, $E = 68 kJ/mol$, $\alpha = 8.39 m^2 K/J$ and $\gamma = 4.03\times10^{-11} m^2 K/J$. This model allowed users to estimate operating conditions where the fouling rate would be close to zero which is termed as the threshold fouling conditions. This model also ignored the effect of crude oil thermal conductivity, specific heat and only considered the effect of crude oil density, viscosity through Reynolds number.

Panchal et al. (1997) modified the Ebert and Panchal (Ebert and Panchal, 1995) model by incorporating the Prandtl number. The revised model is given as

$$\frac{dR_f}{dt} = \mathrm{Re}^{\beta}\,\mathrm{Pr}^{-0.33}\exp\left(-\frac{E}{RT_f}\right) - \gamma\tau_w$$

(2.11)

The value of β was assumed to be -0.66 and the film temperature $T_{f,}$ was determined in terms of surface temperature (T_s) and bulk temperature (T_b) as

$$T_f = T_b + 0.55(T_s - T_b)$$

(2.12)

Threshold models for crude oil fouling developed by Polley et. al. (2002) presented a logical framework for analyzing chronic fouling problems in refinery pre-heat trains. This model measured physical parameters that actually resulted in no observable fouling. The model incorporated simple modifications to the Ebert and Panchal model by considering wall temperature instead of film temperature in the reaction term and retained the dependency of velocity in form of Reynolds number in the generation term. This model considered the removal term based on the wall shear stress and suggested a physical mechanism to remove deposit from the tube wall. It was also suggested that prior to deposit formation, the mechanism opposing fouling is associated with a mass transfer process rather than one associated with wall shear stress. The presented model was given as

$$\frac{dR_f}{dt} = \alpha\,\mathrm{Re}^{-0.8}\,\mathrm{Pr}^{-0.33}\exp\left(\frac{-E}{RT_w}\right) - \gamma\,\mathrm{Re}^{0.8}$$

(2.13)

Based on laboratory crude oil fouling data of a refinery preheat train, the constants of this model were found out to be $\alpha = 10^6 m^2K/Wh$, $\gamma = 1.5\times10^9 m^2K/Wh$ and $E = 48kJ/mol$.

Saleh et. al. (2005) studied the effect of fluid properties and operating conditions, with the intention of using the results to guide a fouling mitigation strategy. The observations of fouling rates showed a relatively strong effect of surface temperature, bulk temperature, a small effect of pressure and a decrease in fouling rate with increase in velocity. Experiments were carried out to examine the effect of operating conditions on the fouling of the light crude oil of an Australlian refinery. The following ranges of conditions were covered: velocity of 0.25–0.65 m/s, surface temperature of 180–260◦C, bulk temperature of 80–120◦C, and pressure from 379–655 kPa. Fouling rates ranged from 1.94E-07 m^2K/kJ at surface temperature of 180^{o}C to 5.89E-

07 m^2K/kJ at surface temperature of 260°C. Similarly by increasing the bulk temperature from 80 to 120°C, and the film temperature from 163 to 183°C, the fouling rate was increased from 3.06E−07 to 5.28E−07 m^2K/kJ. At a velocity of 0.25 m/s, the heat transfer coefficient decreased around 20% from 2.17 to 1.74 kW/m^2K, while at a velocity of 0.4 m/s, the heat transfer coefficient decreased by 12%. These observations suggested that the deposition of the precursors that may be present increases with bulk temperature, and that both adhesion and the transport of foulants may be important for growth of fouling. Fouling was investigated to be caused by fine solids from the feed material. Physical examination of the fouling probe showed that attachment of these solids was limited to the heated parts of the unit, which is consistent with the surface temperature effect. An Arrhenius-type equation was used to determine the activation energy based on the film and surface temperatures.

Nasr and Givi (2006) proposed a threshold fouling model which is independent of Prandtl number as

$$\frac{dR_f}{dt} = \alpha \mathrm{Re}^{-\beta} \exp\left(-\frac{E}{RT_f}\right) - \gamma \mathrm{Re}^{0.4} \quad (2.14)$$

This model was investigated with the above mentioned experimental data presented by Saleh et. al., (2005) and the empirical constants were found to be $\alpha = 10.98 m^2K/kJ, \beta = -1.547$, $\gamma = 0.96\times10^{-10} m^2K/kJ$ and $E = 22.618 kJ/mol$ The model included a term for fouling formation and a term for fouling removal due to chemical reaction and tube wall shear stress. It may be noted that Nasr and Givi model has become more empirical than the earlier models since a numerical value for β has no physical significance as compared to the other models. The disadvantage with this model was that it cannot be used for extrapolation at other operating conditions.

The Tubular Exchanger Manufacturers' Association (TEMA) (2007) produces the most widely known standard for shell-and-tube heat exchangers. For tubular exchangers, it is common practice in industry to use fixed values of fouling resistances in design. These values are most usually those listed by the Tubular Exchangers Manufacturers Association (TEMA). According to the original TEMA reference in 1947, these values allow heat exchangers designed using these fouling resistances to operate for an acceptable period of time. However,

the “fouling factors” given in TEMA tables, though based on the experience of people in industry, were not in general the result of systematic research. Resistances for tubular exchangers range from 0.088×10^{-3} to $0.53\times10^{-3} m^2K/W$ for different types of fresh water. However, the value of the fouling resistance that applies depends critically on operating conditions. One of the many weaknesses of the TEMA Tables is the fact that they differentiate approximately for the effect of water quality, flow velocity and surface temperature.

A comprehensive review of fouling in heat exchange systems considering scaling, corrosion, biofouling and particulate deposition has been presented in the ESDU (Engineering Sciences Data Unit) report. ESDU 07006 (2007) is a practical User Guide to the occurrence, mitigation and removal of fouling in fresh water systems and on the design of such systems to minimize the consequences of fouling. It introduces fresh water fouling as it affects heat transfer in various types of heat exchanger. It provides suggestions on the design and subsequent operational management of a plant to minimize fouling. It also discusses the importance of various parameters that affect fouling and indicates appropriate methods for dealing with fouling in all stages from design through to operation of heat exchanger equipment

A new heat mass transfer model was developed by Zhen Hua et. al., (2008) to predict the fouling process of calcium carbonate on heat transfer surface. The model takes into account not only the crystallization fouling but also the particle fouling which was formed on the heat transfer surface by the suspension particles of calcium carbonate in the supersaturated solution. Based on experimental results of the fouling process, the deposition and removal rates of the mixing fouling were expressed. Furthermore, the coupling effect of temperature with the fouling process was considered in the physics of the model. As a result the fouling resistance varying with time was obtained to describe the fouling process and the prediction was compared with experimental data under same conditions. The results showed that the present model could give a good prediction of fouling process, and the deviation was less than 15% of the experimental data in most cases.

Crittenden et. al. (2009) reported findings on the mass transfer and chemical kinetics in hydrocarbon fouling. A transport-reaction model was developed considering chemical reaction as well as the transport of fouling precursor to and from the heated surface. Based on the findings, a modified model was proposed that includes a back-diffusion term. This model

demonstrated the practical benefits of using a parallel tube test apparatus to obtain initial rate data on the fouling surface at constant heat flux. But at time $t = 0$, it is difficult to justify the finite concentration of foulant at the surface which would be required for back diffusion to occur. The modified model investigated the complex effect of velocity and identified apparent activation energy for each velocity.

The importance of reviewing the models in this section was to examine the information that needs to be considered for developing a new model. In addition, in various models emphasis was placed on the idea of breaking down the deposition into a number of consecutive resistances that enables one to determine the controlling process. These models assist in the development of an understanding into the interaction of the consecutive processes that occur during deposition.

2.3 Statistical Methods Used in Fouling Analysis

Statistical analysis has been used as an effective tool for evaluation of heat exchanger fouling and maintenance strategy of fouling by several users. Sheikh et. al. (1996) developed maintenance strategy for heat transfer equipments subjected to fouling by applying statistical methodology. A reliability-based maintenance strategy by incorporating the risk and scatter parameters of the linear random fouling growth model was highlighted in this work. In addition, the dimensionless cost-objective function was formulated by considering various cost elements for a heat exchanger used in a crude oil preheat train. The variation in the dimensionless cost with reduced time was presented for different values of unit cost parameters representing additional fuel cost, antifoulant cost, and other miscellaneous costs. In the further development in this regard, Zubair et. al. (1997) presented a stochastic approach to the analysis of fouling models. In view of the performance indicator of the heat exchangers, a maintenance strategy for planned maintenance schedules was presented and various scenarios of reliability based maintenance strategy were introduced. The strategy was explained in terms of the scatter parameter of the time-to-fouling distribution corresponding to a critical level of fouling, and the risk factor representing the probability of tubes being fouled to a critical level after which a cleaning cycle is needed. In addition, the cost implications of the above mentioned strategy were explained and their impact on heat exchanger maintenance was highlighted.

Sheikh and Al-Bagawi (1999) has performed statistical analysis to characterize the time between cleaning of thermosyphon reboilers in oil industry. The time between cleaning of these heat exchangers has been characterized using statistical distributions. Various probability models are fitted to the time between cleaning data. Based on the coefficient of determination, the best statistical model is identified which can be used in developing an optimal maintenance strategy for such heat exchangers. In addition to operational failure statistics, such as MTTF, standard deviation and median time to failure, it pointed out how the parameters of selected model can be used to simulate the underlying average or median fouling growth pattern of heat exchangers. Such simulated fouling growth curves can provide the clue to adjust the operational parameters such as velocity at a level, which can enhance the average time between these operational failures.

Yeap et. al. (2001) developed an algorithm for simulating fouling behavior in shell and tube heat exchangers based on statistical approach. They reported a model to investigate the interactions between temperature effects, fluid dynamics and fouling. A statistical analysis was applied by Lodge et. al. (2002) to quantify the relative fouling propensities of feed a water matrix which was blended prior to filtration by a UF membrane. The regression analysis indicated that, the surface water fouls the UF membrane more than the ground water by a factor of (0.0292x - 0.00740) / (0.00573x- 0.00154), where x, is the mean trans-membrane pressure(TMP). Hence, for a typical operating mean TMP of 0.32 bar, the surface water was 6.6 times more fouling than the groundwater. The results outlined in this work demonstrated that the method is a viable way of assessing the relative fouling propensities of combined feed waters to a UF membrane.

Hasson et. al. (2006) presented a simple and reliable residence time distribution (RTD) technique for on line detection and diagnosis of scaling and fouling deposits of RO plants. The method was based on determination of flow dispersion intensities from online RTD signals that can be simply measured. The systems investigated spiral wound membranes fouled with either $Mg(OH)_2$ or $CaCO_3$. Analysis of RTD data of fouled membranes showed that an increasing membrane permeability loss is accompanied by a systematic increase in the dispersion coefficient, thus providing an indicator for detecting a fouling event. The effect of fouling on the RTD was studied in a laboratory membrane fouled by a $Mg(OH)_2$ deposit. The dispersion coefficients for the clean membrane (D = 6–10 cm^2/sec) increased to D = 8–27 cm^2/sec in the

presence a fouling layer causing a 14% permeate flow reduction and to D = 12–47 cm^2/sec in the presence a fouling layer causing 36% permeate flow reduction. It was also found that the magnitude of the dispersion coefficient is affected by deposit morphology, thus indicating the possibility for diagnosing the nature of the fouling deposit.

The classical detection methods are based on study of the heat transfer coefficient or the effectiveness, temperature measurements, ultrasonic or electrical measurements and weighing of heat exchanger pipes (Gudmundur et. al., 2007). But to get accurate results, these methods require the system to present successive steady states which is far too restrictive or costly. To enforce compliance with critical pressure and operational criteria, heat exchangers must be cleaned often, according to a regular maintenance schedule. The scheduling of cleaning interventions can be based on the prior knowledge of the time behavior of the thermal resistance deposits in the individual exchanger. As fouling is usually not visible from outside the industrial processing equipment, a direct method of measurement of the fouling developed on the heat transfer surfaces of a heat exchange device is almost impossible. This can only be ascertained and quantified from its effects on various performance parameters of a heat exchanger. But the major drawback of these techniques is mainly due to limited number of sensors which can detect only localized fouling. Besides that though these temperatures can be useful for trending, there are many factors that can affect this calculation including variable process heat loads, different temperature levels in different seasons, and even the accuracy of thermocouples used. Because this method involves subtraction of two large numbers, accurate measurement techniques and equipment are also critical

Coletti and Macchietto (2011) developed a dynamic mathematical model capable of describing tube-side crude oil fouling in shell-and-tube heat exchangers as a function of local conditions throughout the unit. This model was able to devise a procedure to systematically analyze plant data and estimate necessary model parameters using primary plant measurements such as temperatures and flow rates rather than derived fouling resistances. The model was validated with plant measurements and tested for its predictive capabilities against primary quantities that can be directly measured. Based on this model, they concluded that the model can be used with confidence to identify and predict the fouling state of exchangers, assess economic losses due to fouling, support operating decisions such as planning of cleaning schedules and to assist in the design and retrofit of heat exchangers.

The comprehensive review of statistical analysis in thermal systems provides a clue for generating an appropriate fouling growth model. Using the results of best distribution with its parameters, the fouling growth model can be developed from end point fouling. The end point fouling can be obtained from mathematical relationships linking the heat transfer performances. The heat transfer performances take into account the overall heat transfer coefficient and the fouling resistance for estimation of fouling behavior of the shell-and-tube heat exchanger.

2.4 A Review of Wilson Plot Method in Heat Exchangers

The Wilson plot developed by Wilson (1915) constitutes a suitable technique to estimate the heat transfer coefficients and thermal resistances in a shell and tube heat exchanger. It is based on the separation of the overall thermal resistance into the inside convective thermal resistance and the remaining thermal resistances participating in the heat transfer process. the overall thermal resistance of the condensation process in shell and tube condensers (R_{ov}) can be expressed as the sum of the thermal resistances corresponding to external convection (R_o), the external fouling film ($R_{f,o}$), the tube wall (R_t), the internal fouling film ($R_{f,i}$) and the internal convection (R_i).

$$R_{ov} = R_o + R_{f,o} + R_t + R_{f,i} + R_i \quad (2.15)$$

Taking into account the specific conditions of a shell and tube condenser and the equations correlating the overall thermal resistance, Wilson theorized that if the mass flow of the cooling liquid was modified, then the change in the overall thermal resistance would be mainly due to the variation of the in-tube convection coefficient, while the remaining thermal resistances remained nearly constant. For the case of fully developed turbulent liquid flow inside a circular tube, the convection coefficient was found to be proportional to a power of the reduced velocity (v_r) which accounts for the property variations of the fluid and the tube diameter. Further the overall thermal resistance was represented in the original Wilson plot as a linear function of the experimental values of $1/v_r^n$ as shown in Figure 2.1 (Shah, 1990).

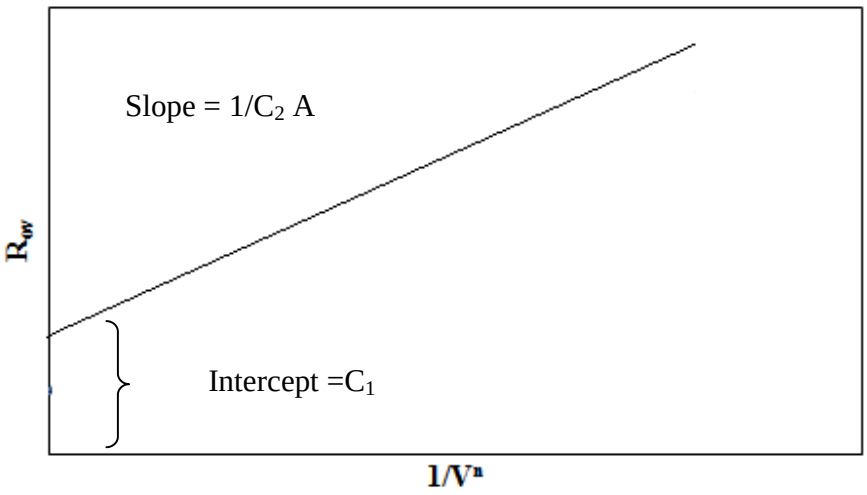

Figure 2.1 Original wilson Plot

Chang et. al., (1997) selected the Wilson plot method for the quantification of the condensing convection coefficients of R-134a and R-22 flowing inside four different extruded aluminum flat tubes and one micro-fin tube. The tube testing was accomplished in a double-tube configuration set-up. In contrast, the micro-fin tube was located inside a shell with circular cross-section. The refrigerant condensation took place inside the tubes and coolant water flowed between the tube and the shell. The convection coefficient for the coolant water was held constant by controlling a steady flow rate of water and a small deviation of the mean water temperature was noticed. In this case, the condensing convection coefficient was varied by changing the quality of the inlet refrigerant; the quality was controlled by means of a pre-condenser. The condensing convection coefficient was considered proportional to a power of the inlet quality with an exponent of –0.8. The paper reported experimental results of the condensing convection coefficients as a function of the quality of inlet refrigerant. The experimental results indicated a variation of convective heat transfer coefficient from 1900 $W/m^2.^oC$ for quality 0.5 to 3000 $W/m^2.^oC$ for quality 1.0 with mass flux 35 kg/m^2.sec and system pressure 1.76 MPa. Within same range of quality, the heat transfer coefficient was within 2000 to 3200 $W/m^2.^oC$ for mass flux 65 kg/m^2.sec.

Kumar et. al. (2001) utilized the modifications in Wilson plot technique to investigate the heat transfer coefficient during condensation of steam and R-134a over single horizontal plain and finned tubes. Using the original Wilson Plot method, general correlation equations were obtained for the analysis of internal forced convection based on Reynold's analogy. These

correlation equations relate the Nusselt number with the Reynolds number and Prandtl number. But some of these equations are susceptible to temperature variations because they incorporate the variability of the fluid properties with temperature. Therefore, modifications of the Wilson plot method were incorporated that assumed a general correlation for the convection coefficient in which the mass flow is varied as a power of the Reynolds number and Prandtl number instead of the fluid velocity. This simple modification of the original Wilson plot method presupposed the existence of a general functional form for the convection coefficient of the fluid whose flow conditions can be varied in the experimental analysis. In these works, the outside tube thermal resistance was taken as a constant and the in-tube convection coefficient was expressed by the general form of the Dittus–Boelter equation. The modified Wilson plot technique was found to underpredict the value of condensing-side heat transfer coefficient in the range of 7.5–15% for the condensation of steam and 13– 25% for the condensation of refrigerants R-12 and R-134a.

Hasim et. al.,(2003) used the original Wilson plot to investigate the heat transfer enhancement by combining ribbed tubes with wire and twisted tape inserts. They used an experimental apparatus that consists of a double pipe heat exchanger with water as the cooling and heating fluids. The convection coefficients inside the enhanced tubes were assumed to be proportional to a power of the fluid velocity with known exponents. Zheng et. al.,(2006) applied the Wilson plot method to analyze the heat transfer processes in a shell and tube flooded evaporator in an ammonia-compression refrigeration system. The study was carried out for plain tubes forming the bundle where the ammonia–lubricant mixture evaporates outside the tubes and a heated water–glycol solution flows inside the tubes. Based on the results of the boiling convection coefficients, a correlation equation was proposed in order to determine the overall heat transfer coefficient and thermal resistance. The correlation was given as

$$\alpha = 1.156 - 16.31 p_r + 206.79 p_r^2 + 1.742 w - 29.21 w^2 \quad (2.16)$$

This correlation equation took into account the effect of reduced pressure (p_r) and mass concentration of lubricant (w) on the non-dimensional heat flux (α). It was also observed that all the experimental data were within a range of $\pm 15\%$ of the correlation results.

Chang and Hsu (2006) applied the modified Wilson plot method to analyze the condensation of R-134a on two horizontal enhanced tubes with internal grooves. The authors

considered the functional form of the Dittus–Boelter equation for the convection coefficient of water flowing inside the tubes and a constant thermal resistance for the condensing fluid

The application of the original Wilson plot method to analyze the performance of six plain and finned-tube bundles forming a shell and tube heat exchanger was reported by Barman and Ghosal (2007). Experiments were conducted for water, lubricating oil and glycerin in the shell side and cooling water inside the tubes. The Wilson plot method was applied to all sets of experimental data and the outside convection coefficient were obtained. Afterwards, in a subsequent analysis the shell-side convection coefficients were correlated in a form resembling the Sieder–Tate correlation equation. Based on this analysis, new exponents for the Reynolds and Prandtl numbers and a multiplier for each one of the tubes bundles were proposed.

Fernandez-Seara et. al., (2007) described a simple experimental apparatus that allows for the measured data required for the application of the Wilson plot method. The test section consisted of a transparent methacrylate enclosure, wherein water vapour generated at the bottom condenses over a test tube cooled by circulating water inside. Once the experimental data was recorded, the original Wilson plot method and modified Wilson plot method were applied. Also, a collection of results gathered with the experimental apparatus consisting of a smooth and a spirally corrugated tube made of stainless steel were reported afterwards by Fernandez-Seara et. al.,(2007).

The Wilson plot method was employed by Fernando et. al. (2008) to investigate the heat transfer on both the shell and tube sides of a heat exchanger. Tests were conducted with varying water flow rates, temperature levels and heat fluxes on both the tube and shell sides at Reynolds numbers of approximately 170–6000 on the tube-side and 1000–5000 on the shell-side, respectively. It was found that the Nusselt numbers agreed with the experimental results within $\pm 5\%$ accuracy. The inverse of the overall heat transfer coefficient (1/U) was plotted versus the inverse of the hot water flow rate to the power of ‘n’ assuming the exponent ‘n’ initially to be 0.8. By the least squares method, the best linear fit to the data was determined. The exponent ‘n’ was then varied until the minimum variance was obtained for the linear fit with the estimated value of ‘n’.With the exponent n =1.25, the minimum variance was obtained and all the data in the Reynolds number range of 2300–6000 followed a straight line.

Rooyen et. al. (2012) investigated the current status and future perspectives of Modified Wilson Plots for enhanced heat transfer experiments. In this study, a modification of the

solution procedure was proposed to take into account the experimental uncertainties of the data and to estimate the error in the final Wilson plot correlation. Furthermore, a new method based on unconstrained minimization was also proposed and compared to the previous correlations. This method attempted to calculate the leading coefficients of the tube-side and annulus-side correlations and the Reynolds number exponent of the annulus side. The developed Wilson plot based on experimental results was having a coefficient of determination 0.922 for falling film data and 0.982 for the tube bundle data.

In process plants incorporating heat exchangers for heat recovery, fouling of heat transfer surfaces hinders correct production activity and increases energy consumption thus giving rise to huge economic losses. As complete elimination of fouling in heat transfer equipments is rarely achieved in practice, cleaning of fouled units is a regular task in the process industries. The performance reduction due to fouling is mitigated by periodic cleaning of the heat exchangers. However, during cleaning, the heat exchanger is out of the heat recovery loop and hence the overall heat recovery goes down. If the rate of fouling can be predicted a priori, cleaning of heat exchangers can be prescheduled to minimize operational disruptions. The scheduling of cleaning interventions on the individual heat exchanger can be based on a prior knowledge of the time behaviour of the thermal resistance of fouling. Also untimely and frequent cleaning will lead to huge economic loss as well as unnecessary shut down of the plant. Hence development of such a prediction model has been the subject of intensive research by several investigators. This present work aims for the development of such a prediction model so that cleaning of a heat exchanger can be prescheduled much earlier than a significant loss in performance of the equipment and minimum operational disruptions.

2.5 A Review of Artificial Intelligence in Thermal Systems

The artificial intelligence techniques such as Artificial Neural Network, Genetic Algorithm and Fuzzy Logic have been successfully applied in many scientific researches and engineering practices related to thermodynamic applications. Among the different soft computing methodologies, the ANN analysis has seen sustained interest in recent years for addressing much wider applications based on thermal properties. ANNs are now unquestionably the leading soft-computing methodologies for the general thermal problems

(Diaz et. al., 2001). It has a powerful ability to recognize accurately the inherent relationship between any set of input and output without a physical model, and yet the ANN results do account for all the physics relating the output to the input. This ability is essentially independent of the complexity of the underlying relation such as nonlinearity, multiple variables and parameters, and noisy and uncertain input and output data. Secondly, the methodology is inherently fault tolerant, due to the large number of processing units in the network undergoing massive parallel data processing. Thirdly, its learning ability gives the methodology the ability to adapt to changes in the parameters.

Artificial neural network (ANN) is an important class of empirical technique to model nonlinear, complex or little understood processes with large input–output data sets. ANN has been successfully used for a number of chemical engineering applications such as inferential measurements and control, fault-diagnosis, process modeling, identification and control. Radhakrishnan et. al., (2007) developed a predictive model using statistical methods which can predict the rate of the fouling and the decrease in heat transfer efficiency in a heat exchanger. A neural network based fouling model was developed using historical plant operating data. The ratio of actual overall heat transfer coefficient under fouled condition to the clean design value of overall heat transfer coefficient was considered as the efficiency of the exchanger. The predicted model was used to develop a preventive maintenance scheduling tool. The successful prediction of the temperatures allowed the prediction of the decrease in heat transfer efficiency for effective preventive maintenance scheduling of the heat exchanger cleaning and process improvement.

Malayeri and Steinhagen (2007) investigated the formation of fouling deposits on heat transfer surfaces by highlighting governing fouling mechanisms and introduced a revolutionary prediction method using radial basis functions. The dominant fouling mechanisms in thermal desalination plants such as crystallisation fouling in form of $CaSO_4$ and $CaCO_3$ deposits and biofouling were studied. Numerical and phenomenological models were developed to predict fouling behavior based on neural network approach. This is due to the fact that neural networks are basically unsupervised methods because they can synthesise without detailed knowledge of the underlying process. This is certainly a benefit for modelling phenomena such as fouling in which the interaction of the dominant variables is not firmly established. The method can also be used for processing very substantial data sets, which is difficult for conventional approaches

such as regression approaches. The network was developed in two phases namely the training or learning phase in which a set of known input-output patterns were presented to the network and the weights were adjusted between the nodes until the desired output was provided. Secondly the generalization phase in which the network was subjected to input patterns that it has not seen before, but whose outputs were known and the performance was monitored. Comparison with the experimental data revealed an average relative error of 14% for the training data and 17% for the learning data. Overall, these preliminary attempts highlighted some important features of artificial neural networks for analysis and prediction of experimental data, which correlated experimental data with the use of neural networks. The resulting networks could predict the objective function significantly better than the empirical correlations available in literature. The resulting networks not only quantitatively predicted objective functions but also captured the underlying mechanism of the processes such as mass transfer control region at lower velocities and reaction control at higher surface temperatures during fouling under subcooled flow boiling conditions.

Wang et. al., (2007) applied Artificial Neural Network for heat transfer analysis of shell-and-tube heat exchangers with segmental baffles or continuous helical baffles. Three heat exchangers were experimentally investigated and limited experimental data was obtained for training and testing neural network configurations. The commonly used Back Propagation (BP) algorithm was used to train and test networks for prediction of the outlet temperature differences in each side and overall heat transfer coefficient. For most of the data, the ANN error was within $\pm 2\%$ while the correlation error was within $\pm 8\%$ of the experimental results. On comparing with empirical correlations, it was recommended that ANN can be used to predict the performances of thermal systems in engineering applications such as modeling of heat exchangers with reasonable accuracy.

Aminian and Shahhosseini (2009) carried out Evaluation of ANN modeling for prediction of crude oil fouling behavior. In this research, artificial neural network (ANN) modeling for predictions of crude oil fouling behavior in preheat exchangers of crude distillation units has been evaluated. Outputs of the ANN model have been compared with appropriate sets of experimental data in order to compute overall mean relative error. This study addressed crude oil fouling by evaluating recently developed threshold fouling models and comparing them with a neural network model. They also estimated the degradation in

output variables of a trained neural network when the weights connecting the input variable to the nodes of the hidden layer were all set to zero.

Moreover, the neural network based heat transfer analysis of heat exchangers has been successfully utilized by many researchers. Tan et. al., (2009) reported the use of ANN models to simulate the thermal performance of a compact, fin-tube heat exchangers with air and water or ethylene glycol anti-freeze mixtures as the working fluids. The neural network was concluded to to be superior over conventional non-linear regression models in capturing the underlying non-linearity in the data as it predicted the overall rate of heat transfer in the exchanger with a high degree of accuracy. An application of artificial neural networks (ANNs) was presented by Peng and Ling (2009) to predict the pressure drop and heat transfer characteristics in the plate-fin heat exchangers (PFHE). A feed-forward neural network based on back propagation algorithm was developed to model the thermal performance of the PFHEs. The ANNs was trained using the experimental data to predict the Colburn factor and friction factor in PFHEs. The predicted values were found to be in good agreement with the actual values from the experiments with mean squared errors less than 1.5% for Colburn factor and 1% for friction factor, respectively.

Vasickaninova et. al., (2011) used neural network as a non-linear process model to predict the future behaviour of the controlled process with distributed parameters. The simulation results provided a confirmation that the neural network based predictive control is a better tool than the classical PID control for tubular heat exchangers. The integrated square error of the NNPC was 8% lower than the PID control while the integrated absolute error was 25% less than PID control method. To overcome the inconveniences due to heat exchanger fouling, Gracia (2012) provided an improved heat exchanger supervision strategy using neural network and rule based technique. This strategy was able to monitor the heat exchanger for fouling condition with ability to diagnose the probable causes of fouling. A repetitive gradient descent algorithm for training the backpropagation neural network was used to minimize the mean square error between the actual output and the desired output. Fouling detection was achieved by processing the information provided by the output of the neural network.

Time-series forecasting is an important area of research and application in thermal systems. Much effort has been devoted over the past several decades to the development and improvement of time series forecasting models (Zainuddin and Pauline, 2012). Wavelet neural

networks (WNNs) have been introduced as an alternative to MLPs that overcome their shortcomings (Amina et. al., 2012). Due to the advantages of WNNs as universal approximators, the fact that they have more compact topology than other neural networks and their fast learning speed owing to the constitution of the localized wavelet activation function in the hidden layer, WNNs had received much attention from other researchers and have been used extensively to solve numerous real world problems such as face recognition, time-series prediction, pattern classification and system identification (Wallhauber et. al., 2012).

The review of literature provides quite valuable information about the ability of artificial neural network (ANN) for time series prediction of complex systems.

2.6 Gaps in Existing Literature

The literature review has introduced the concept of fouling and its key characteristics. This was followed by an extensive outline of the main fouling models and the different techniques used to predict its transient behaviour. Based on the extensive literature review, the following gaps were identified in the context of fouling in heat exchangers.

- The resistance-based models are the most established technique that provides details on the global influence of operating parameters. However there is lacking in a comprehensive model predicting the fouling behaviour.
- There is quite limited literature available regarding the effect of fouling on pressure drop and flow rate in case of a shell and tube heat exchanger. There is a need to identify the interconnections among heat transfer performance under fouling, volume flow rate and pressure drop.
- It is also clear from literature that fouling cannot be quantified directly. It can only be ascertained from the various thermo hydraulic effects depending on operating conditions. The simple form of quantification of fouling is to compare the terminal temperature differences between the hot fluid and the cold fluid known as approach temperature. Although the approach temperature is a suitable tool for trending the

fouling behavior, but there are many factors that affect the accuracy of the calculation which includes variable process load, different temperature levels under different operating conditions and even the accuracy of the temperature measuring thermo-couples. Another method for fouling estimation uses overall heat transfer coefficient and fouling factors considering both shell and tube side data. But this method doesn't distinguish between the fouling developed due to shell side or tube side flow. Also the variations in fluid characteristics under variable operating conditions may affect the accurate calculation of fouling effects. This method incorporates very complex calculation process and the uncertainty in all the parameters involved in the calculation process may contribute significantly towards the inaccuracy of the fouling estimation process. Therefore there is a need of a method to quantify the fouling which can offer most reproducible and consistent results while being easy to calculate by incorporating minimum number of operating variables.

- The fouling monitoring methods in a heat exchanger range from very simple to complex depending on the operating conditions. The commonly used method is to open up at regular time interval and check for fouling or corrosion. But this method is a final report on the success or failure of the monitoring program. This may be an untimely selection of the cleaning program which can be avoided. Also by the time it is implemented, it may be too late and the plant may be running inefficiently which may lead to shut down of the plant. Hence an accurate predictive model indicating the estimation of fouling is necessary for process industries involved with heat exchangers.

Chapter 3

Estimation of Fouling Resistance by Thermal Analysis

This chapter presents an overview of the methodology for calculation of fouling in a shell and tube heat exchanger. Various quantitative and qualitative design aspects and their interaction and interdependence are investigated to obtain the different thermo-hydraulic performance parameters such as overall heat transfer coefficient, pressure drop and fouling resistance. As modeling of fluid flow and heat transfer phenomena in heat exchangers of arbitrary geometry is a complex process, successful modeling of this process relies on quantifying the heat, mass and momentum transport phenomena. The advantages of this methodology include diagnosis of flow, rapid evaluation of novel process route, and energy efficient and low cost design. A multidisciplinary approach of heat exchanger performance evaluation as a component is discussed taking into account the simultaneous consideration of most geometric and process variables dependent on each other.

3.1 Introduction

The theoretical framework for estimation of heat transfer and pressure drop parameters is dependent on the design of a heat exchanger to a great extent. Design is an activity aimed at providing complete descriptions of an engineering system or part of a system. These descriptions represent an unambiguous specification of the system or component structure, size and performance as well as other important characteristics important for subsequent operation. The shell and tube heat exchanger is such a system that finds wide engineering applications including space heating, air conditioning, power production, waste heat recovery and chemical processing. Although the calculation principles underlying the problem to design a heat exchanger are more or less same everywhere, these differences can be addressed by a well-defined design methodology. Besides the performance evaluation of shell-and-tube heat exchangers involves a large number of geometric and operating variables as part of the search for an exchanger geometry that meets the heat duty requirement and a given set of design constraints.

Most of the heat exchanger performance estimation methods employ empirical relations with a cut-and try approach that depends on the judgment and prior experience by extrapolation

from tested units. The primary concern in this chapter is thermal analysis based on analytical approach developed by Taborek (Taborek, 1983) commonly known as Bell-Delaware Method. The estimation of heat transfer performances must consider several factors that influence the shell-side and tube-side heat transfer coefficients that, in turn, determine the overall rate of heat transfer.

- When baffles are provided, the system directs the shell-fluid from axial flow to top-to-bottom flow or side-to-side flow with the effect that the heat transfer coefficient is higher than for undisturbed flow along the axes of the tubes (Serna and Jimenez, 2005).
- Patterns of tube layout influence turbulence and hence heat transfer coefficient. The triangular pitch gives greater turbulence than square pitch. And under comparable conditions of flow and tube size the heat transfer coefficient for triangular pitch are roughly 25% greater than for square pitch.
- The closer the baffle spacing, greater is the number of times the shell-fluid is to change its direction resulting in greater turbulence.
- Shell-side coefficient is also affected by tube size, clearance and fluid-flow characteristics.

3.2 Assumptions for Heat Transfer Analysis

For developing theoretical models that is simple enough for analysis of heat transfer and pressure drop of a shell and tube heat exchanger, a set of assumptions or idealizations have been taken into account (Than et. al., 2008). These assumptions are made for heat transfer problem formulation that includes energy balance, rate equations, boundary conditions and subsequent analysis in an integral form.

- The heat exchanger operates under steady state condition. The flow rates and the fluid temperatures at the inlet and within the exchanger are invariant with respect to time.
- The heat exchanger shell wall is well insulated such that heat transfers either to or from the surroundings is negligible.
- There is no change of phase of both the shell and tube side fluid.
- The temperature of each fluid is uniform over every cross section and there exists no temperature gradient normal to the fluid flow direction.

- The tube-wall thermal resistance is uniformly distributed throughout the exchanger.
- The longitudinal heat conduction in the tube wall is negligible.
- The thermo physical properties of the fluids such as density and specific heat are constant and are characterized at the mean temperature of the inlet and exit terminal.
- The heat transfer surface area is uniformly distributed on both side fluids.
- The temperature variation along any baffle window is small as compared to the overall temperature variation of the shell side fluid.
- The velocity and the temperature at the inlet terminals of the exchanger on both side fluids are uniform over the flow cross-section.
- There occurs no flow stratification, flow bypassing or flow leakage in any of the streams.

3.3 Heat Exchanger Model

In this section, the heat exchange between two fluids using the shell and tube heat-exchanger kind of equipment with the considerations of no phase changes and constant physical properties is discussed. Essentially, the model is based on the Bell-Delaware correlations for the shell-side heat-transfer coefficient and Fanning factor. In the Bell-Delaware method, the shell side heat transfer coefficient and the pressure drop are estimated starting with correlations for flow over ideal tube banks. Then the effects of leakage, bypassing and flow in the window zone are incorporated subsequently through suitable correction factors. The turbulent Sieder-Tate equation is used for the tube-side heat-transfer coefficient. The Blasius equation is used for the tube-side Fanning factor. The heat transfer analysis correlates the heat transfer rate, the heat transfer area, heat capacity rate of each fluid, fluid terminal temperatures and the overall heat transfer coefficient. The two basic relationships that predominantly constitute the entire thermal design are

(i) The energy balance enthalpy rate equation based on first law of thermodynamics given by

$$q = q_i = \dot{m}_j \Delta h \tag{3.1}$$

(ii) The heat transfer rate equation given by

$$q = UA\Delta T_{lm} \tag{3.2}$$

3.3.1 Thermal Circuit Analysis

In steady state, heat transfer from the hot to cold fluid involves three processes such as convection from hot fluid to tube wall, conduction through tube wall and convection from tube wall to cold fluid. Besides the fouling film resulted due to accumulation of unwanted deposits having lower thermal conductivity increases the resistance to heat flow. The added thermal resistance on individual fluid sides for heat conduction through the fouling film is taken into account by fouling factor. The figure 3.2 illustrates the thermal resistance and the thermal circuit for a heat exchanger.

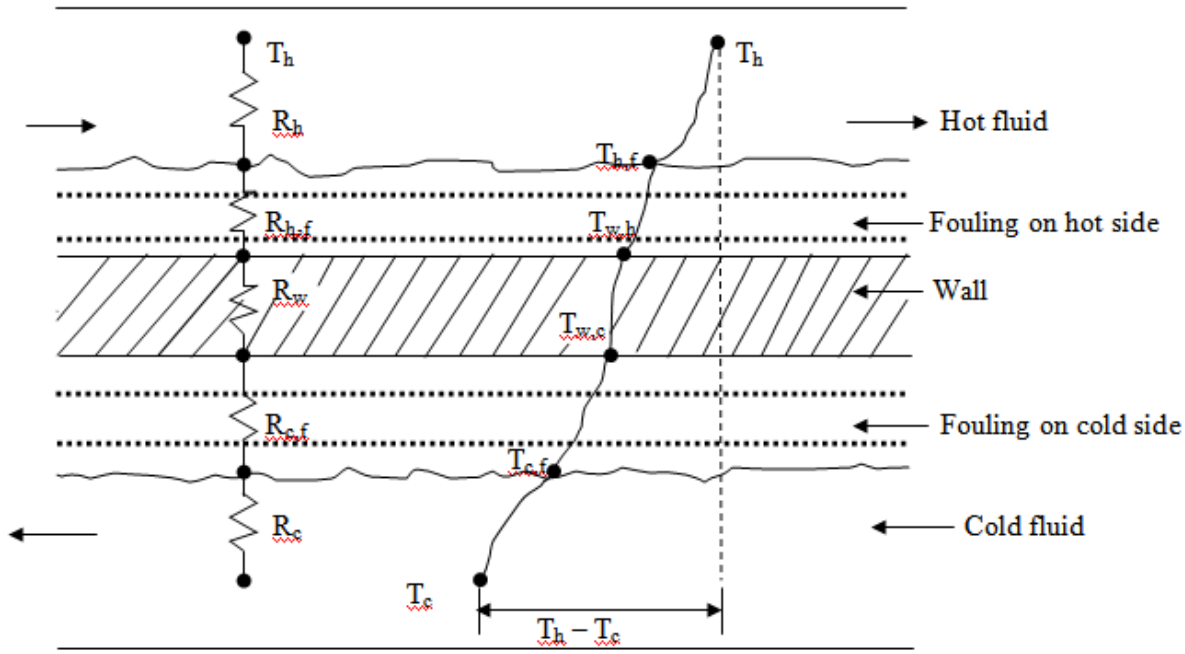

(a)

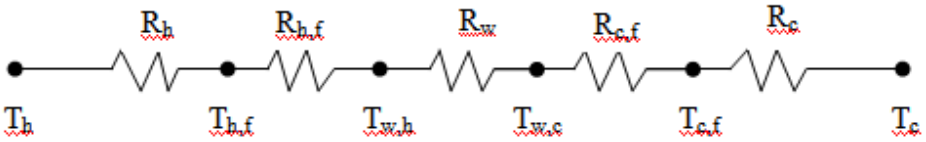

(b)

Figure 3.1 (a) Thermal resistances in a heat exchanger

(b) Thermal circuit for heat exchanger

The heat transfer rate per unit area at any section *dx* can be represented as

$$dq = \frac{T_h - T_{h,f}}{dR_h} = \frac{T_{h,f} - T_{w,h}}{dR_{h,f}} = \frac{T_{w,h} - T_{w,c}}{dR_w} = \frac{T_{w,c} - T_{c,f}}{dR_{c,f}} = \frac{T_{c,f} - T_c}{dR_c} \tag{3.3}$$

Alternatively,

$$dq = \frac{T_h - T_c}{dR_o} = UdA(T_h - T_c) \tag{3.4}$$

where the overall differential thermal resistance dR_o includes the convective resistances of both fluids and the conductive resistance due to tube wall and the conductive resistances due to fouling deposits on both sides of the tube wall.

Hence,

$$dR_o = \frac{1}{UdA} = dR_h + dR_{h,f} + dR_w + dR_{c,f} + dR_c \tag{3.5}$$

$$dR_o = \frac{1}{UdA} = \frac{1}{(hdA)_h} + \frac{1}{(h_f dA)_h} + dR_w + \frac{1}{(h_f dA)_c} + \frac{1}{(hdA)_c} \tag{3.6}$$

It is assumed that the heat transfer surface area is uniformly distributed on each fluid side. This indicates the ratio of differential area on each fluid side to the total area on the respective fluid side remains the same.

Thus,

$$\frac{dA_h}{A_h} = \frac{dA_c}{A_c} = \frac{dA}{A} \tag{3.7}$$

So replacing the differential area by total area, equation (3.6) can be represented as

$$\frac{1}{UA} = \frac{1}{(hA)_h} + \frac{1}{(h_f A)_h} + R_w + \frac{1}{(h_f A)_c} + \frac{1}{(hA)_c} \tag{3.8}$$

In this equation, the U and all the h terms are local. Considering the overall rate equation, the total heat transfer rate can be written as

$$q = U_m A \Delta T_m = U_m A(T_{h,e} - T_{c,e}) = \frac{1}{R_o}(T_{h,e} - T_{c,e}) \tag{3.9}$$

Considering the individual resistances, the heat transfer rate can be expressed as

$$q = \frac{T_h - T_{h,f}}{R_h} = \frac{T_h, f - T_{w,h}}{R_{h,f}} = \frac{T_{w,h} - T_{w,c}}{R_w} = \frac{T_{w,c} - T_{c,f}}{R_{c,f}} = \frac{T_{c,f} - T_c}{R_c}$$

(3.10)

In this equation, the subscript "e" denotes the effective value for the exchanger and all the individual temperatures mean or effective values for respective fluid sides. The overall thermal resistance is the sum of individual resistances in series.

$$R_o = \frac{1}{UA} = R_h + R_{h,f} + R_w + R_{c,f} + R_c$$

(3.11)

The individual resistances can be defined as follows

$$R_h = \frac{1}{(hA)_h}$$

(3.12)

$$R_{h,f} = \frac{1}{(h_f A)_h}$$

(3.13)

$$R_w = \frac{\ln(d_o / d_i)}{2\pi k_w L N_t}$$

(3.14)

$$R_{c,f} = \frac{1}{(h_f A)_c}$$

(3.15)

$$R_c = \frac{1}{(hA)_c}$$

(3.16)

where,

R_h = hot-fluid-side convective resistance

$R_{h,f}$ = hot-fluid-side fouling resistance

R_w = tube-wall thermal resistance

R_c = cold-fluid-side convective resistance

$R_{c,f}$ = cold-fluid-side fouling resistance

h = heat transfer coefficient

h_f = fouling coefficient

η_o = extended surface efficiency

d_o = outside tube diameter

d_i = inside tube diameter

L = effective length of tube

N_t = number of tubes

The extended surface efficiency may be included in the expression for resistance in order to get the most general expression for overall resistance. However for unfinned exchangers both the fin efficiency is considered to be unity.

In actual practice, the overall thermal resistance or the overall heat transfer coefficient are expressed in terms of outside or inside tube surface area.

$$\frac{1}{U_o} = \frac{1}{h_o} + \frac{1}{h_{o,f}} + \frac{d_o \ln(d_o / d_i)}{2k_w} + \frac{d_o}{d_i h_{i,f}} + \frac{d_o}{d_i h_i}$$

(3.17)

$$\frac{1}{U_i} = \frac{d_i}{d_o h_o} + \frac{d_i}{d_o h_{o,f}} + \frac{d_i \ln(d_o / d_i)}{2k_w} + \frac{1}{h_{i,f}} + \frac{1}{h_i}$$

(3.18)

In this equation, the subscripts o and *i* denote the tube outside and inside respectively. The overall thermal resistances $1/U_o$ and $1/U_i$ are the unit overall thermal resistances based on tube outside and inside surface area respectively.

3.3.2 Shell-side Heat Transfer Coefficient

According to the propositions based on Bell-Delaware method, the heat transfer coefficient and pressure losses are calculated from Kern's correlations (Kern, 1950) for flow over an ideal tube bank, in which there are no bypass or leakage streams. The ideal coefficient and pressure losses are then multiplied by suitable correction factors to account for the deviation from the ideal model of the flow inside the shell of the heat exchanger.

For single segmental baffle geometry, the minimum shell side crossflow area(S_m) is

$$S_m = L_{bc}\left[D_s - D_{otl} + \frac{(p_t - d_o)(D_{otl} - d_o)}{p_n} \right]$$

(3.19)

For square pitch tube layout, the tube pitch normal to flow direction is equal to the tube pitch. The number of effective tube rows crossed in one crossflow section between the baffle tips is

$$N_{tcc} = \frac{D_s}{L_{pp}}\left(1 - \frac{2B_c}{100}\right)$$

(3.20)

Similarly the effective number of tube rows crossed in one baffle window is given by

$$N_{tcw} = \frac{0.8}{L_{pp}}\left[\frac{D_s B_c}{100} - \frac{D_s - D_{otl}}{2} \right]$$

(3.21)

The bypass area between the shell and the tube bundle within one baffle (S_b) is calculated as

$$S_b = L_{bc}\left[D_s - D_{otl} + L_{pl} \right]$$

(3.22)

where L_{pl} represents the width of the bypass lane between the tubes. For a pass partition lane normal to the flow direction, L_{pl} is set to be zero while for a partition lane parallel to the flow direction, L_{pl} is assumed to be equal to tube diameter (d_o). For calculation of shell side correction factors, the fraction of crossflow area available for bypass flow (F_{sbp}) plays a vital role.

$$F_{sbp} = \frac{S_b}{S_m}$$

(3.23)

The shell to baffle leakage area (S_{sb}) is a factor for calculating the baffle leakage effect parameters. The diametral clearance (L_{sb}) between the shell diameter and the baffle diameter is given as

$$L_{sb} = 3.1 + 0.004 D_s$$

(3.24)

The shell-to-baffle leakage area within the circle segment occupied by the baffle is calculated as

$$S_{sb} = \pi D_s \frac{L_{bs}}{2}\left(\frac{2\pi - \theta_{ds}}{2\pi}\right)$$

(3.25)

The tube-side baffle leakage area for each baffle (S_{tb}) can be determined by calculating the fraction of total tubes in crossflow.

$$S_{tb} = 0.25\pi d_o \delta_t \left(1 + F_c\right)$$

(3.26)

where,

$$F_c = \frac{1}{\pi}\left[\pi + 2\lambda \sin\left(-\arccos\lambda\right)\right]$$

(3.27)

$$\lambda = 0.5 D_s / D_{otl}$$

(3.28)

The shell side mass velocity is given by

$$G_s = \frac{m_s}{S_m}$$

(3.29)

The shell side Reynolds number is calculated considering the minimum cross-flow area in the shell side flow direction.

$$\mathrm{Re}_s = \frac{d_o G_s}{\mu_s} = \frac{d_o m_s}{\mu_s S_m}$$

(3.30)

The shell-side Prandtle number is expresses as

$$\mathrm{Pr}_s = \frac{\mu_s C_{ps}}{k_s}$$

(3.31)

The heat transfer coefficient for an ideal tube bank is

$$h_o = \frac{j_i C_{ps} G_s (\phi_s)^{0.14}}{(\mathrm{Pr}_s)^{2/3}}$$

(3.32)

where, j_i is the Colburn factor for an ideal tube bank and Φ_s is the viscosity correction factor.

The ideal Colburn factor for the shell-side can be determined from appropriate Bell-Delaware correlations.

$$j_i = a_1 \left(\frac{1.33 d_o}{L_{tp}} \right)^a (\mathrm{Re}_s)^{a_2}$$

(3.33)

$$a = \frac{a_3}{1 + 0.14(\mathrm{Re}_s)^{a_4}}$$

(3.34)

The values of the coefficients are presented in table 3.1.

The viscosity correction factor which accounts for the viscosity gradient at the tube-wall and viscosity at the bulk mean temperature of the fluid is given by

$$\phi_s = \frac{\mu_s}{\mu_w}$$

(3.35)

According to the Bell-Delaware method, the flow fraction for each stream is found out by knowing the corresponding flow areas and the flow resistances. The heat transfer coefficient for ideal tube bank is then modified for the presence of each stream through the correction factors.The actual heat transfer coefficient for shell side is given by

$$h_s = h_o \left(j_c j_l j_b j_r j_s \right)$$

(3.36)

where, h_o is the heat transfer coefficient for ideal tube bank and j_c, j_l, j_b, j_r, j_s are the correction factors for baffle cut, baffle leakage effects, bundle bypass flow, laminar flow and unequal baffle spacing in the inlet and outlet sections respectively.

(i) Baffle cut correction factor (j_c)

The baffle cut correction factor j_c accounts for the non-ideal flow effects due to difference in flow velocity through the window and the crossflow velocity over the bundle. Secondly the flow over the window is partially longitudinal to the tubes, which is less effective than

crossflow. The baffle cut correction factor, j_c is a function of the baffle cut, the outer tube limit diameter and the window flow area.

$$j_c = F_c + 0.54\left(1 - F_c\right)^{0.345}$$

(3.37)

But for baffle cuts in a range of 15% to 45%, the baffle cut correction factor j_c can be expressed as (Mizutani et. al., 2003)

$$j_c = 0.55 + 0.72F_c$$

(3.38)

(ii) Baffle leakage correction factor(j_l)

The flow through the baffle to tube hole gaps and the annular gap between shell and the baffle edge reduce a part of the flow that passes over the tube bundle as crossflow. This causes the reduction in both the heat transfer coefficient and the pressure drop which is accounted in the baffle leakage correction factor (j_l).

$$j_l = \alpha + (1-\alpha)\exp\left(-2.2\frac{S_{sb} + S_{tb}}{S_m}\right)$$

(3.39)

where,

$$\alpha = 0.44\left(1 - \frac{S_{sb}}{S_{sb} + S_{tb}}\right)$$

(3.40)

(iii) Bundle bypass correction factor (j_b)

The Bundle bypass correction factor (j_b) accounts for the the adverse effect of the flow between the inner shell wall and the tube bundle and the bypass lane created by any pass partition lanes in the direction of flow. The bypass correction factor (j_b) is

$$j_b = \exp\left(-0.3833F_{sbp}\right)$$

(3.41)

(iv)Unequal baffle spacing correction factor (j_s)

The unequal baffle spacing correction factor (j_s) accounts for the adverse effect of an inlet baffle spacing (L_{bi}) or the outlet baffle spacing (L_{bo}) larger than the central baffle spacing

(L_{bc}). The value of j_s is determined directly from the effect on the flow velocity and is given by the following expression.

$$j_s = \frac{(N_b - 1)(L_{bi} / L_{bc})^{1-n} + (L_{bo} / L_{bc})^{1-n}}{(N_b - 1) + (L_{bi} / L_{bc}) + (L_{bo} / L_{bc})}$$

(3.42)

where n = 0.6 for turbulent flow and n=1/3 for laminar flow. The number of baffle compartments is determined from the effective tube length and the baffle spacing. However for equispaced baffles no correction is required as j_s=1.0.

(v) Laminar flow correction factor (j_R)

The heat transfer is reduced by the adverse temperature gradient formed in the boundary layer as the flow thermally develops along the flow channel. The laminar flow correction factor j_R accounts for this effect.

$$j_R = \left[\frac{10}{N_c}\right]^{0.18}$$

(3.43)

where N_c is the number of tube rows crossed in one cross-flow section. The laminar flow correction factor is subjected to the limits

$j_R = 0.4 \; for \; \mathrm{Re} \le 100$

$j_R = 1.0 \; for \; \mathrm{Re} > 100$

3.3.3 Tube-side Heat transfer Coefficient

The tube side mass velocity can be expressed as the tube side volumetric flow rate per unit cross-sectional area. It can be expressed as

$$G_t = \frac{4 m_t N_{tp}}{\pi (d_i)^2 \rho_t N_t}$$

(3.44)

The Reynolds number of the flow inside the tube can be calculated considering the mass velocity.

$$\mathrm{Re}_t = \frac{4 m_t N_{tp}}{\pi d_i \mu_t N_t}$$

(3.45)

Similarly Prandtle number can be determined from thermophysical properties of the tube side fluid.

$$\mathrm{Pr}_t = \frac{\mu_t C_{pt}}{k_t}$$

(3.46)

The correlations by Sieder and Tate (1936) for single-phase fluids are used to calculate the tube-side heat transfer coefficient.

$$= 270(\mathrm{Re}_t)^{0.8}(\mathrm{Pr}_t)^{1/3}\left(\frac{\mu_t}{\mu_{tw}}\right)^{0.14} \quad \text{for } \mathrm{Re}_t > 10000$$

(3.47)

Table 3.1 Empirical Coefficients for Colburn factor and friction factor

Tubes pattern	Reynolds number	a_1	a_2	a_3	a_4	b_1	b_2	b_3	b_4
Triangular	10^5-10^4	0.321	-0.388	1.450	0.519	0.372	-0.123	7.00	0.500
	10^4-10^3	0.321	-0.388			0.486	-0.152		
	10^3-10^2	0.593	-0.477			4.570	-0.476		
	10^2-10	1.360	-0.657			45.100	-0.973		
	<10	1.400	-0.667			48.000	-1.000		
Square	10^5-10^4	0.370	-0.395	1.187	0.370	0.391	-0.148	6.30	0.378
	10^4-10^3	0.107	-0.266			0.0815	0.022		
	10^3-10^2	0.408	-0.460			6.0900	-0.602		
	10^2-10	0.900	-0.631			32.100	-0.963		
	<10	0.970	-0.667			35.000	-1.000		

3.4 Experimental Estimation of Fouling Resistance

The objective of this research is to estimate fouling resistances in a laboratory scale shell and tube heat exchanger and determine the effect of fouling on the heat transfer

performances. The formulations based on Bell-Delaware method as discussed in the previous section is utilized to calculate the clean overall heat transfer coefficient and the fouling resistance.

3.4.1 Experimental set-up

Experiments were conducted on a 1-1 shell and tube heat exchanger. The Figure 3.2 shows the sketch of the 1-1 shell and tube heat exchanger, which was used for carrying out the experimentation work. The figure 3.3 shows the complete heat exchanger system including the various measuring instruments used for measurement of different parameters such as temperature and flow rate. The data acquisition unit records the inlet and outlet temperatures of the tube and the shell. The hot water was allowed to flow through the tubes while the cold water in the annular space between the shell and the tubes. The water source was the common tap water. The flow of the two liquids is counter-current in direction.

The heat exchanger consists of parallel tubes fitted in a shell containing baffles along its length. The whole unit is insulated such that there is no heat transfer from the exchanger to the environment. However any loss of heat from the shell side fluid to the surroundings is assumed to be negligible. The baffles ensure turbulent water flow conditions providing efficient heat transfer and simultaneously support the tubes. The outer shell made up of mild steel is having internal diameter 150mm and length 860 including dish ends on both sides. The shell consists of 55 numbers of copper tubes having internal diameter 9.6mm and outer diameter 12mm. The effective tube length is 800mm. The exchanger consists of 4 numbers of single segmental baffles with 22.5% baffle cut.

The geyser used for heating the water is a vertical storage water heater type of geyser having metallic body with outer cover made up of rust proof ABS material. The inner tank is made up of 304 grade stainless steel. It can withstand pressure upto 3.5 kg/cm^2. The geyser is equipped with automatic temperature regulation through thermostat safety devices. The thermostat is set with a cut off at 100^oC. The geyser works with 230v, 50Hz single phase AC supply.

Hot water from the geyser flows through the inner tubes via a rotameter which measures the flow rate. The rotameter consists of a tapered tube, typically made of glass with a

'float'. The float is actually a shaped weight that is pushed up by the drag force of the flow and pulled down by gravity. Drag force for a given fluid and float cross section is a function of flow speed. The rotameter is positioned vertically in the fluid system with the smallest diameter end of the tapered flow tube at the bottom. This is the fluid inlet. The float, typically spherical, is located inside the flow tube, and is engineered so that its diameter is nearly identical to the flow tube's inlet diameter. When the fluid is introduced into the tube, the float is lifted from its initial position at the inlet, allowing the fluid to pass between it and the tube wall. As the float rises, more and more fluid flows by the float because the tapered tube's diameter is increasing. Ultimately, a point is reached where the flow area is large enough to allow the entire volume of the fluid to flow past the float. This flow area is called the annular passage. The float is now stationary at that level within the tube as its weight is being supported by the fluid forces which caused it to rise. This position corresponds to a point on the tube's measurement scale and provides an indication of the fluid's flow rate. The flow tube is made of borosilicate glass and the wetted parts including the float are made of 316 stainless steel. The maximum operating pressure is 8.6 kg/cm^2 for a maximum operating temperature of 93^oC.

Cold water is pumped through the shell by means of a 0.25hp pump which can supply water upto 1900LPH with this head. The attached rotameter measures the cold water flow rate. The inlet and outlet temperatures for both the hot and cold fluid were measured with thermocouples and read from a digital temperature indicator. All the data for a particular combination of hot and cold water flow rate were taken at steady state. At the steady state the inlet and outlet temperatures of both the hot and cold fluids do not undergo any change for a particular flow rate.

To measure the inlet and outlet temperatures of the heat exchanger, Resistance Temperature Detector (RTD) type of temperature transmitters are used. RTD is a device that senses temperature by variation in the resistance of an electrically conductive material. RTDs are the most accurate method of measuring temperature over wide ranges and highly stable over time and temperature cycling. The electrically conductive material used is platinum. The RTD probe consists of a protective sheath which is a closed end stainless steel tube, a sensor element, lead wires and a threaded termination. Although the RTD probe has a protective sheath, it is inserted into a thermowell for added protection from process contamination. The temperature range for both the shell and tube side is from -30^oC to 175^oC. The accuracy of the

temperature transmitter was checked in the laboratory using a mercury thermometer. The temperature transmitters are connected to the control panel for continuous monitoring and data logging.

The calibration of the thermocouples was performed using a mercury thermometer which showed that maximum temperature uncertainty (ΔT) was 0.1^0C. Similarly by calibrating the rotameters, it was determined that the mass of fluid flow uncertainty was ±1%. The flow measuring rotameters were calibrated by using a Doppler flow meter.

3.4.2 Experimental Procedure

The experiments were conducted with normal tap water as the cold fluid while the hot fluid was hard water having hardness within a range of 500 to 550 ppm of NaOH. The geyser used for heating the water was set with a cut-off temperature of 100^oC. The experiments were carried out for 5 to 6 hours on daily basis. For every set of data it was waited until steady state is reached. The experimentation involved four major steps.

(i) Operating Boundaries :

First of all the operating boundaries of the heat exchanger was determined. Then the heat exchanger was operated at various combinations of cold and hot water flow rates ranging from 600LPH to 1200LPH. The inlet temperature of the hot fluid to the tubes was maintained within a range of 40^o C and 70^o C while the cold fluid inlet temperature was maintained at the ambient room temperature. Depending on the operating conditions throughout the experimentation period, cold fluid inlet was varied between 24^oC to 28^oC. Then an operating space was determined by considering hot water flow rates and hot water inlet temperature.

(ii)Tube Side Analysis:

Initial trials were conducted keeping the hot water flow rate constant while varying the cold water flow rates. After each increase in cold water flow rate, it was waited until the flow rates reached steady state.

(iii)Shell Side Analysis:

This time step 2 was repeated except the cold water flow rate was maintained constant and the hot water flow rate was varied.

(iv) Data Duplication:

The procedure of steps (ii) and (iii) were repeated a few times to achieve steady state and to ensure that the data was reproducible. After getting the data corresponding to various flow rates and inlet temperature of the fluids, suitable data reduction method was applied for further analysis.

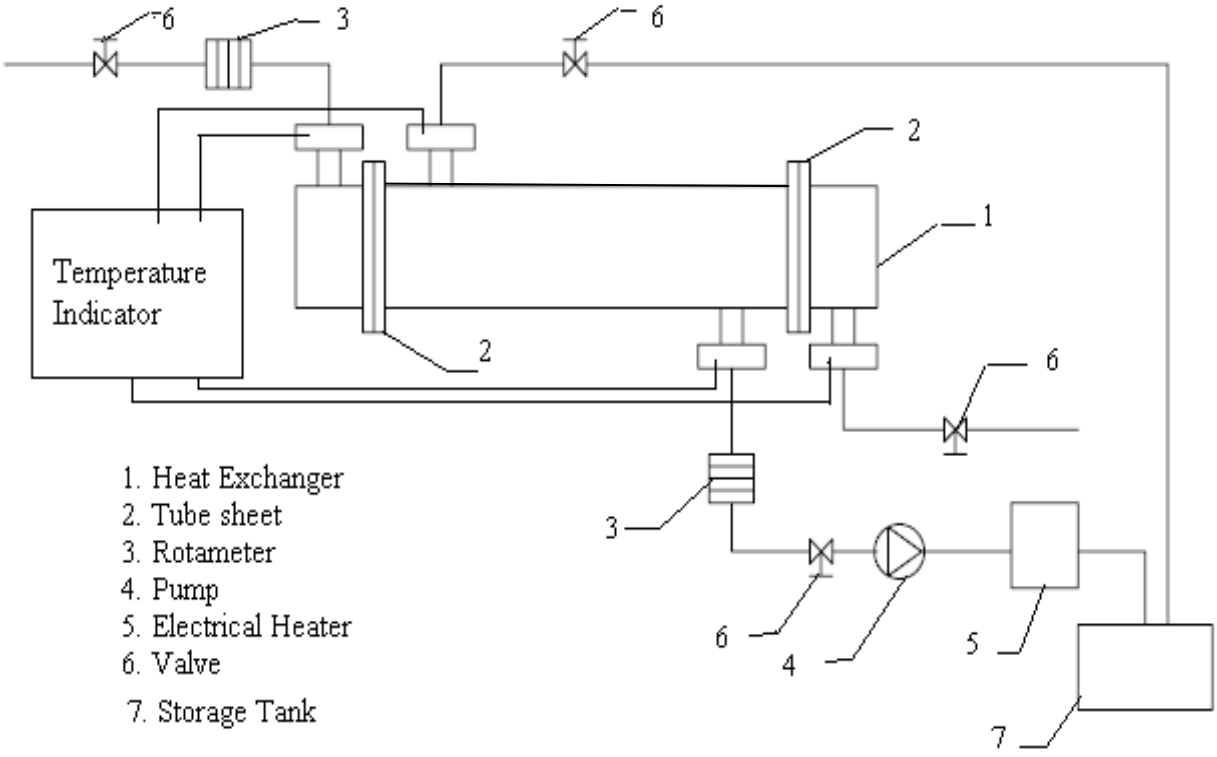

Figure 3.2 : Schematic diagram of experimental set-up

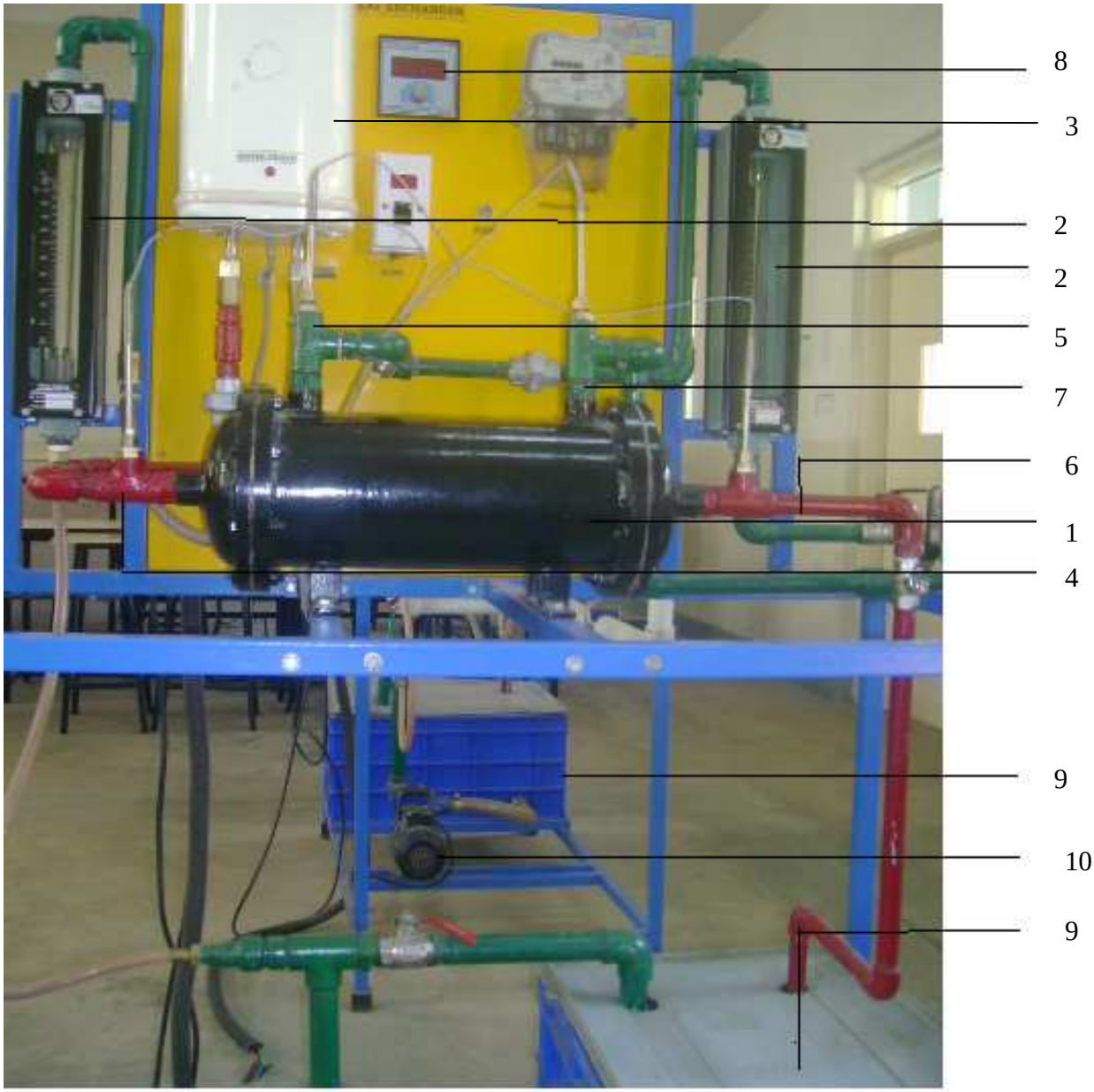

1 Shell & Tube Heat Exchanger
2 Rotameter
3 Heater
4 Hot Water Inlet
5 Cold Water Inlet
6 Hot Water Outlet
7 Cold Water Outlet
8 Temperature Indicator
9 Storage Tank
10 Motor

Figure 3.3 : Shell and Tube Heat Exchanger used for experiments

3.5 Results and Discussion

The experimental results with the above mentioned experimental set up were analyzed using Bell-Delaware method to find out the clean overall heat transfer coefficient. The flow chart of the Bell-Delaware analysis method is shown in Figure 3.4. The input data included the inlet and outlet temperatures, flow rates, properties of both fluids and detailed geometry of the heat exchanger under consideration. This method calculates both the clean and actual heat transfer coefficient and consequently the fouling resistance of the subject heat exchanger.

The samples of operation data including flow rates and temperatures for both shell and tube side are shown in Table 3.2 and A.1 of Appendix A for one fouling cycle. A fouling cycle is considered as the period of operation during which one of the flow rates either the shell or the tube side is maintained constant. The total experimental work is carried out with ten cycles of operation.

Table 3.2 : Samples of Temperature and Flow rates during Cycle 1.

Days	m_t (kg/s)	m_s (kg/s)	$T_{h,in}$ (^oC)	$T_{h,out}$ (^oC)	$T_{c,in}$ (^oC)	$T_{c,out}$ (^oC)
1	0.10958	0.08246	40	34.6	22	28.6
2	0.10958	0.08246	40	34.6	22	28.6
3	0.10958	0.08246	40	34.5	22	28.8
4	0.10958	0.08246	40	34.6	22	28.8
5	0.10958	0.08246	40	34.7	22.1	28.7
6	0.10958	0.08246	40	34.7	22.1	28.8
7	0.10958	0.08246	40	34.7	22.1	28.8

The first set of results shown in table 3.2 pertains to the variation of mass flow rates and temperatures during first cycle. The cold water flow rate was maintained constant at a rate of 600LPH while the hot water flow rate was varied within 450 to 1200 LPH. The thermophysical property such as density was determined at an average temperature for both the hot and the cold fluid. The figure 3.5 shows the variation of temperature differences of both the hot and cold fluid with time for the first fouling cycle. As can be seen, the hot water flowing through the tubes undergo a change of temperature approximately 6^oC higher than the cold fluid flowing through the annular space in the shell.

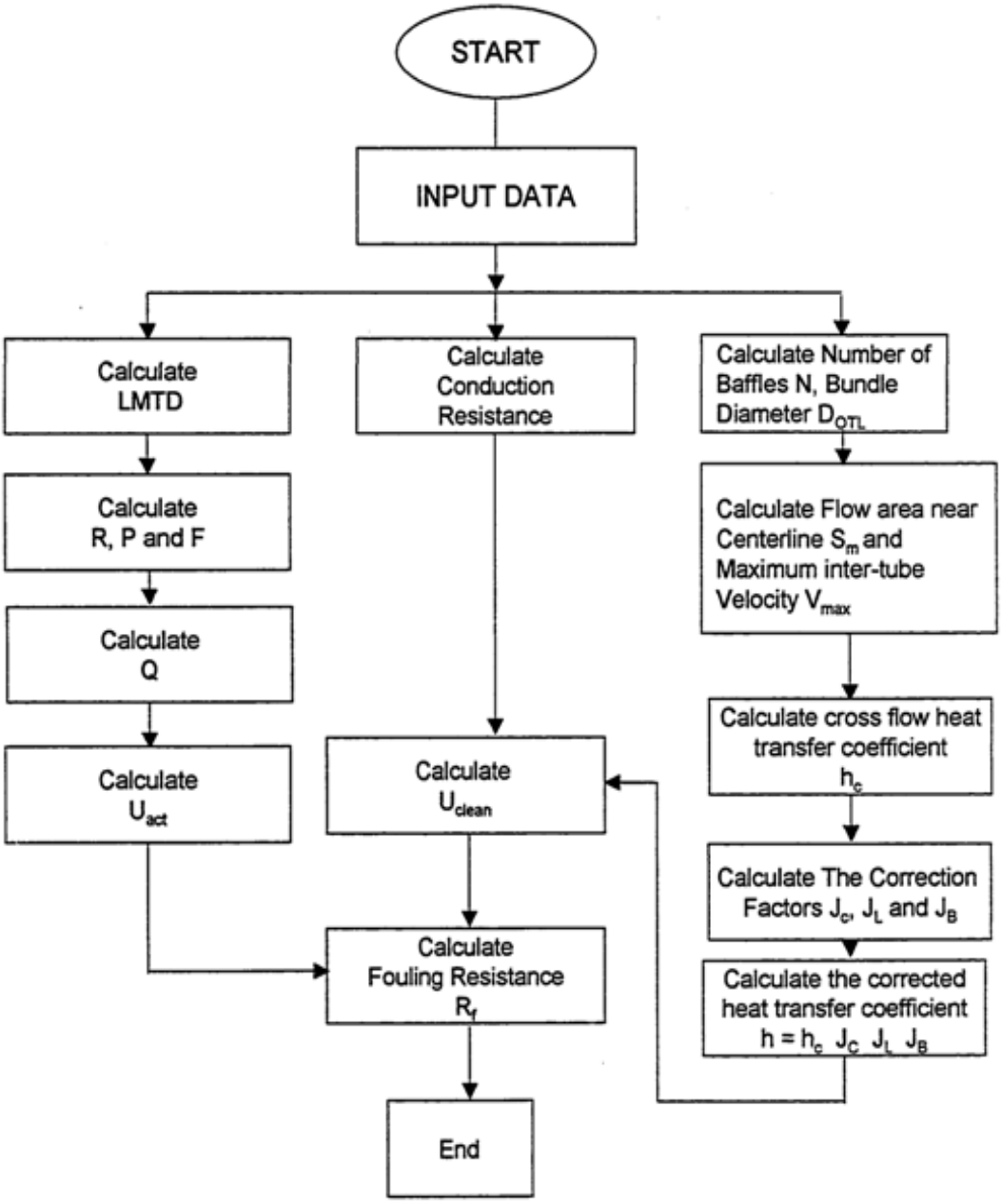

Figure 3.4 : Flow chart for Fouling Resistance Calculation using Bell-Delaware Method

The second set of results pertains to the variation of overall heat transfer coefficients with time. The Bell-Delaware method is used to determine the clean overall heat transfer coefficient. Samples of results corresponding to the specified geometry and operating conditions of the heat exchanger are provided in Table A.2 of Appendix A. The change of cross-flow and the corrected heat transfer coefficients as a function of time for the shell side flow during the same fouling cycle is shown in figure 3.6. The variation in heat transfer coefficients with time during the same fouling cycle exhibits the same trend as that of the flow rates. These heat transfer coefficients are theoretical values corresponding to clean operating conditions and are independent the fouling growth. The corrected heat transfer coefficient is less than the corrected heat transfer coefficient by shell side heat transfer coefficient correction factor (J) which accounts for the baffle configuration, leakage and bypass. These correction factors are dependent on the geometrical construction of the heat exchanger. For the geometrical configuration of the heat exchanger used for experimental work, the heat transfer correction factor was calculated to be 0.88. Based on the calculated values of the heat transfer coefficients, log mean temperature difference, temperature correction factor and heat balance on one of the flow streams, the actual and clean overall heat transfer coefficient as a function of time are calculated and shown in Figure 3.7. It can be observed that the actual overall heat transfer coefficient decreases with time, but the clean overall heat transfer coefficient exhibits the trend of mass flow rate and independent of time. This is expected as the actual heat transfer coefficient is a function of heat transfer rate, inlet & outlet temperatures and heat transfer area while the clean overall heat transfer coefficient is a function of heat exchanger geometry and flow rates which do not change during the fouling cycle. The reduction in actual overall heat transfer coefficient is a clear indication of fouling growth on the heat transfer surfaces.

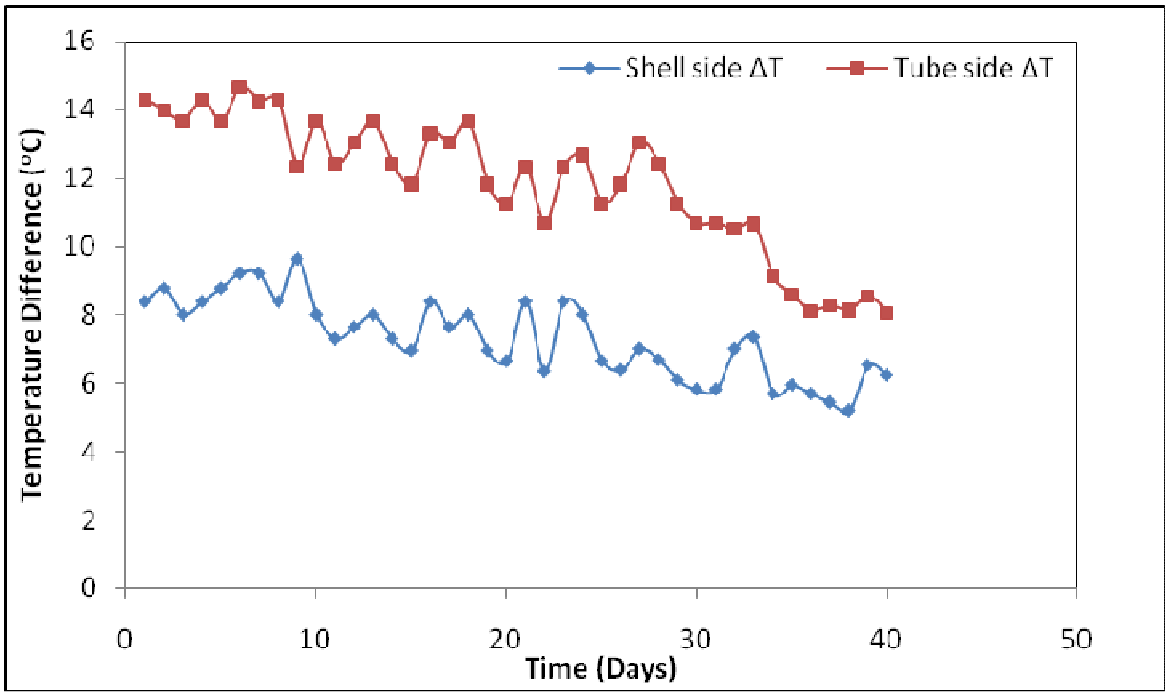

Figure 3.5 Temperature Differences of the hot and cold fluid

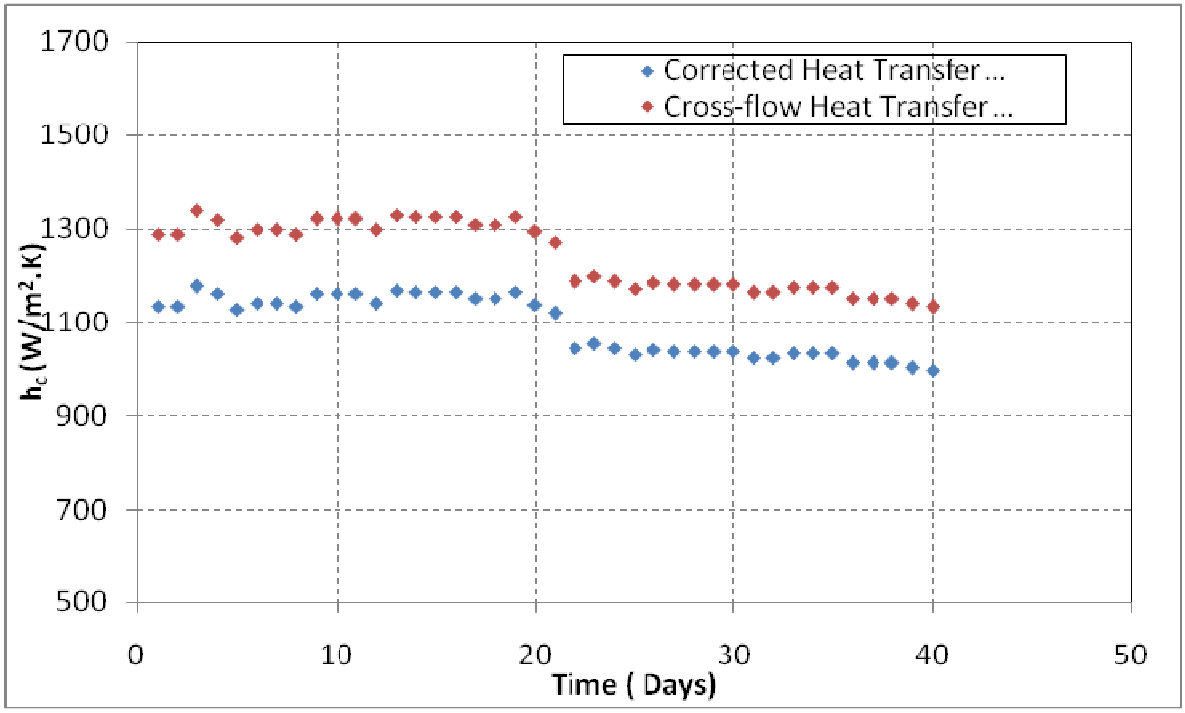

Figure 3.6 Cross-flow and Corrected Heat Transfer Coefficient

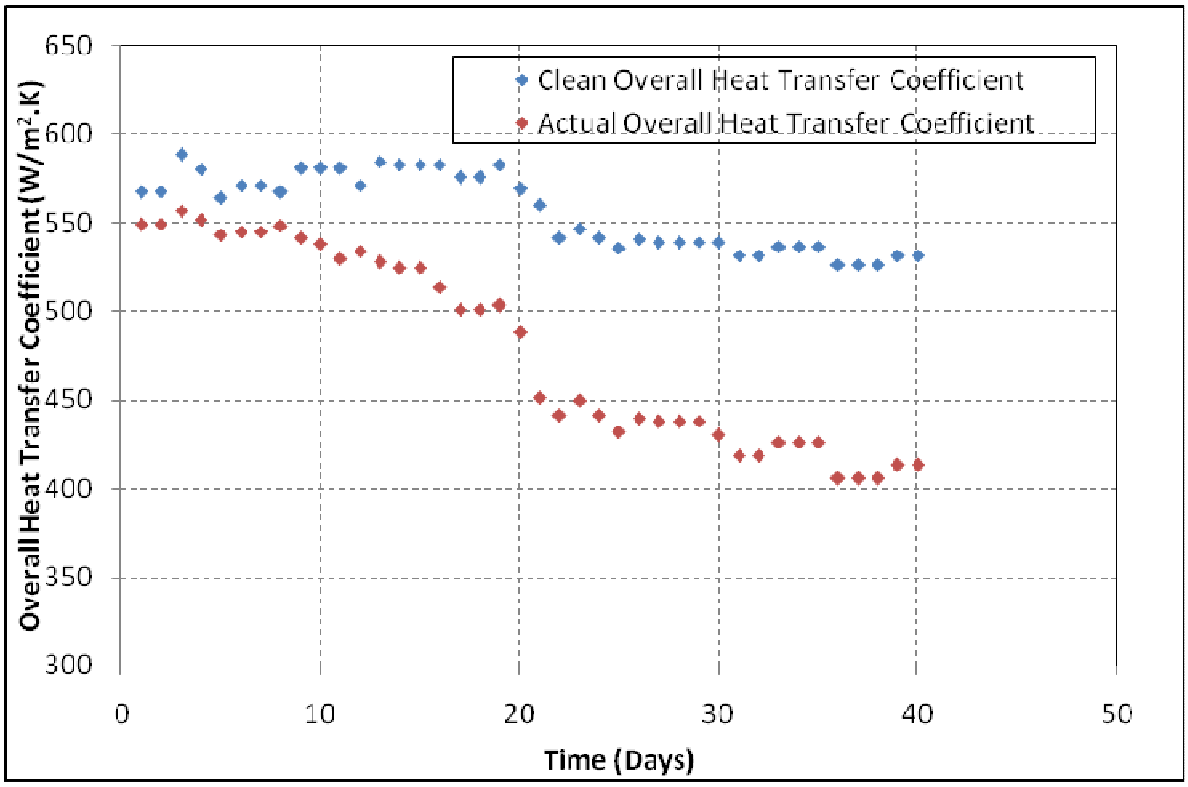

Figure 3.7 Clean and Actual Overall Heat Transfer Coefficient

The third set of results pertains to the variation of fouling growth with time during the same fouling cycle. Figure 3.8 indicates the fouling growth for the first cycle. For the fouling cycle under consideration, the fouling resistance has increased from 0.0987×10^{-3} w/m^2.K to 3.805×10^{-3} W/m^2.K during a period of 40 days. Similar trends are obtained for different fouling cycles for the subjected heat exchanger as shown in Figure 3.9 and Figure 3.10. It is observed that the plots exhibit power law and it will be used further in the statistical analysis. The growth rate of fouling decreases with while the fouling continues to increase. This is attributed to the decrease of deposition rate and increase of mass removal rate as a result of increase in flow rate and consequently the flow velocity.

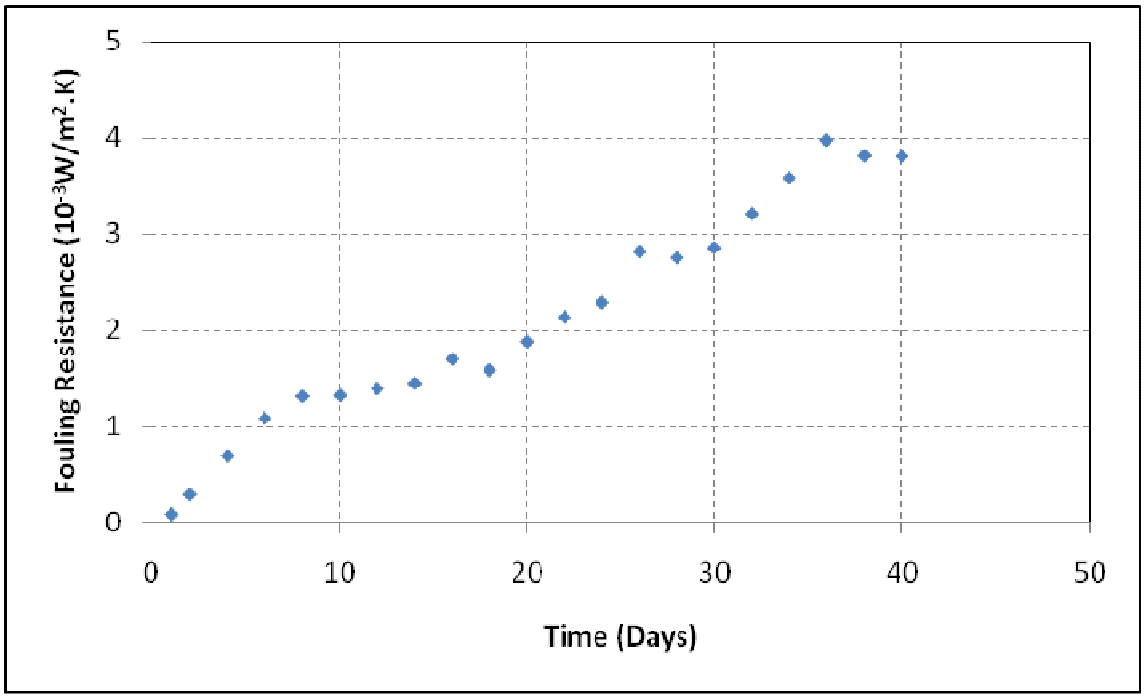

Figure 3.8 Fouling growth versus time for first fouling cycle

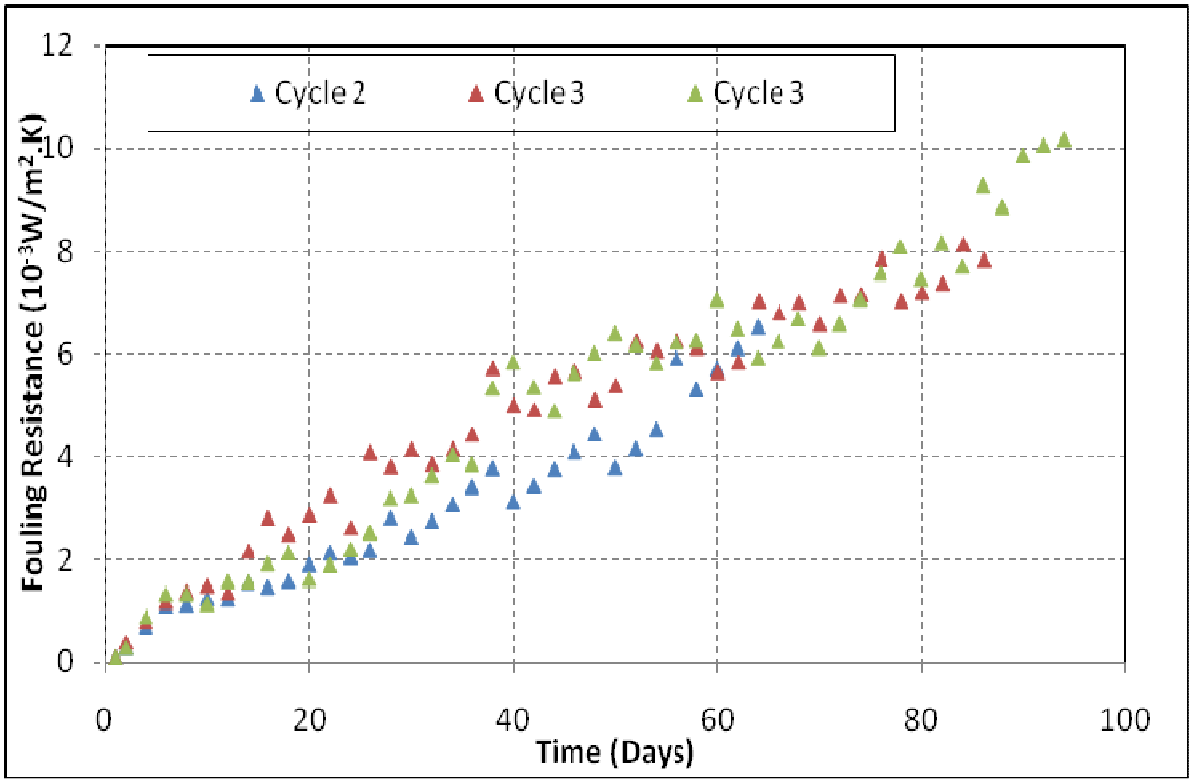

Figure 3.9 Fouling growth versus time for cycles 2, 3 and 4

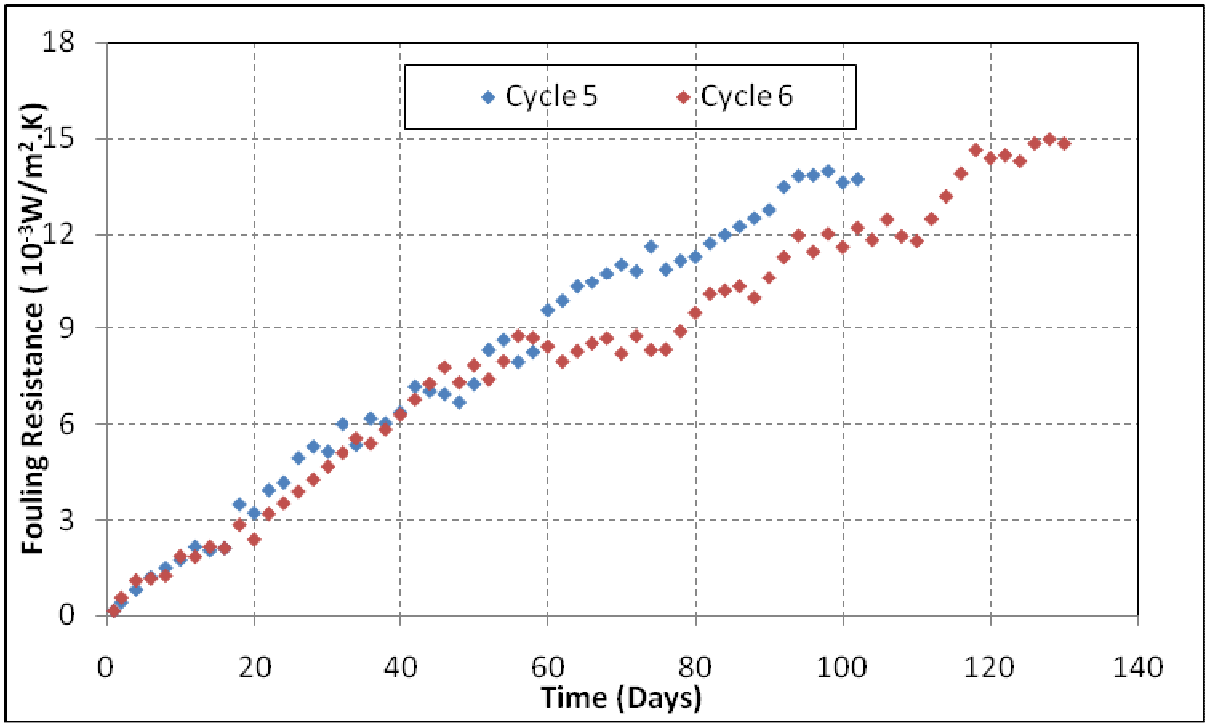

Figure 3.10 Fouling growth versus time for cycles 5 and 6

3.6 Summary

A quantitative estimation has been carried out to estimate the heat transfer performance parameters such as overall heat transfer coefficient and fouling resistance of a shell and tube heat exchanger. Since the calculations of shell side heat transfer coefficient is involved more as compared to the tube side heat transfer coefficient, the well established Bell-Delaware method has been used to carry out the thermal analysis. This method takes into account the complex flow configurations for the shell side flow by incorporating the correction factors. The experimental results obtained by the thermal analysis are further used to develop a statistical model for analysis of fouling growth.

Chapter 4

Fouling Analysis

This chapter describes an integrated approach for quantification of fouling resistance in a shell and tube heat exchanger. The approach combines laboratory scale experiments with statistical analysis to investigate the thermo hydraulic performance due to fouling. The fouling growth model developed by using statistical approach is applied on a single pass shell and tube heat exchanger with water both as the hot and cold fluid. The various performance parameters such overall heat transfer coefficient, fouling resistance and cleanliness factors have been calculated based on the correlations mentioned in the previous chapter and investigated with the results of experimentation. The uncertainty in measurements of mass flow rate and temperature has been taken into consideration for determination of thermal performances of the heat exchanger.

4.1 Introduction

Fouling is a complex phenomenon and its accurate quantification based on current knowledge is quite a difficult task. Several researchers have worked on theoretical modeling of the fouling behavior in different kind of heat exchangers under different operating conditions. The deposits due to fouling on the heat transfer surfaces reduces the heat transfer rate and simultaneously increases the pressure drop across a heat exchanger by increasing flow resistance. The amount of deposits on a heat transfer surface can be quantified using fouling thermal resistance. Measuring the fouling thermal resistance can assist in extracting parameters that could be used for predicting fouling behavior in similar heat exchangers operating at similar conditions. However the estimation depends not only on the physical model employed but also on the correlation method used.

As discussed in chapter 2, fouling is usually classified into six categories depending on the key physical parameters or chemical processes involved in the operating conditions. The fouling mechanism due to each individual type is quite complex and it becomes much more complex when there is a combination of two or more types of fouling mechanisms. However in industrial applications fouling is a combination of two or more mechanisms. In most cases, one mechanism plays the role of a fouling precursor for another mechanism. Among the various types of fouling, crystallization fouling has the most detrimental effect on the industry around

the world as it accounts for more than 35% of the fouling problems in industrial applications (Mwaba et. al., 2006). In general, the type and concentration of mineral salts and operating conditions, such as temperature, pH, pressure, time, flow velocity, radiation, mechanical motions, and impurities, determine the severity of fouling and scale formation. Crystallisation fouling is caused by the crystallisation of a dissolved species from the process solution onto a heat transfer surface. It occurs when the concentration of the dissolved species in the process solution exceeds its solubility limit. The inverse solubility salts that are originally dissolved in process fluid, deposit on heat transfer surfaces as crystallization fouling. The salts like $CaSO_4$, $CaCO_3$, Na_2SO_4, $CaSiO_3$, etc. precipitate on hot surfaces which cause more fouling problems during heat exchange process in aqueous systems (Bansal et. al., 2008).

An analytical description for precise and accurate calculation of overall fouling resistance resulting from complex combinations of different fouling mechanisms is not yet possible, because the formation of deposits is a very complex process, and depends on parameters whose influence can only be roughly estimated. Heat exchanger literature such as TEMA Standards presents data for routine cases in process and thermal engineering applications, but special cases need a real quantification of fouling resistances. The classical detection methods are based on study of the heat transfer coefficient and effectiveness. Such types of investigations are generally carried out by end temperature measurements, ultrasonic or electrical measurements or weighing of heat exchanger pipes (Lalot and Palsson, 2010). But to get accurate results, these methods require the system to present successive steady states which is too difficult to achieve.

This chapter provides a brief description of the statistical distributions and their applicability to the development of a fouling model in case of a laboratory scale shell and tube heat exchanger. Simultaneously the uncertainties in measurements of temperature and mass flow rate have been taken into consideration in order to achieve higher accuracy. The statistical approach has been introduced to develop fouling growth model which can be used for optimal maintenance schedule of the exchanger.

4.2 Statistical Analysis

Much of the research in engineering, basic science and industry are empirical and make extensive use of experimentation. Statistical analysis can greatly increase the efficiency of these experiments and often strengthen the conclusion so obtained (Sheikh and

Al-Bagawi, 1999). In this work a statistical analysis is developed to formulate the fouling model of a shell and tube heat exchanger. This analysis considers various probability distributions for analyzing the fouling data of the heat exchanger. The distribution having highest coefficient of distribution has been considered as the best distribution for development of the fouling growth model.

The probability density function (PDF) is the most important mathematical function in life data analysis. The area under the PDF curve between two defined points on the x-axis gives the probability of an event occurring between those two points. This function can be used to derive other functions that are important to life data analysis, including the unreliability function, the reliability function, the failure rate function etc. This is known as the cumulative distribution function (CDF). In relation to this work, it is the probability that a device or system does not perform its intended function for a given interval of time under specified operating conditions. The Unreliability is identical to the cumulative distribution function (CDF) in probability theory. The CDF measures the cumulative probability of a failure occurring before a certain time. The CDF function returns the probability of a failure occurring before a certain time.

For the time required to reach critical fouling level, the cumulative Distributive Function (CDF) can be given as (Little, 1978)

$$F(t_i) = \frac{i}{N_f + 1} \tag{4.1}$$

where i = 1,2,……., N_f for the i^{th} event of time to reach the critical level of fouling and $F(t_i)$ is the cumulative value of F(t) at $t = t_i$.

The most frequently used function in data analysis and reliability engineering is the reliability function. This function gives the probability of an item operating for a certain period of time without failure. The functions most commonly used in reliability engineering and data analysis, namely the reliability function, failure rate function, mean time function and median life function, can be determined directly from the cumulative distribution function. The reliability function enables the determination of the probability of success of a unit for a specified duration. The CDF function returns the probability of a failure occurring before a certain time. Another useful function is the one that provides the probability of a failure occurring after a certain time. The CDF measures the area under the PDF curve up to a given

time, and the area under the PDF curve is always equal to 1. Given these concepts, subtracting the CDF from 1 would result in the probability of a failure occurring after a given time. This is the widely-used reliability function. Accordingly, the CDF is also known as the unreliability function. Besides, since reliability and unreliability are the probabilities of two mutually exclusive states, the sum of these probabilities is always equal to unity.

Thus the probability of trouble free operation of the exchanger can be expressed in terms of the probability function R(t) defined as

$$R(t) = 1 - F(t) \tag{4.2}$$

Another function that can be derived from the CDF is the failure rate function. The failure rate function also known as the hazard rate function gives the instantaneous failure frequency based on accumulated age. To describe the lifetime distribution of a random variable, it's also possible to use the hazard function, which measures the instantaneous failure rate at time . The hazard function is the risk of failure in a small time interval, given survival at the beginning of the time interval. As a function of time, a hazard function may be increasing, meaning as time increases the rate for failure increases. The hazard function is used in reliability applications to describe the instantaneous failure rate at any point in time. The cumulative hazard function (CHF) also known as the integrated hazard function is the integral of the hazard function. Like the hazard function, the cumulative hazard function is not a probability. However, it is also a measure of risk. The greater the value of CHF, the greater is the risk of failure within a same time span.

The cumulative hazard function in this work represents a degree of cumulative damage to the heat exchanger. Increasing rate of CHF indicates that the heat exchanger surfaces are undergoing ageing type of failure due to fouling deposits. Thus the degree of cumulative damage to the heat exchanger due to ageing failure can be expressed in terms of cumulative hazard function H(t) given by (Kapur and Lamberson, 1977)

$$H(t) = -\ln R(t) \tag{4.3}$$

Several distributions have been postulated to describe the time required to reach the critical level of fouling in a heat exchanger by probability plotting, parameter estimation or distribution model's validation. This work transforms the equation for the CDF to a form that can be plotted as

$$Y = aX + b \tag{4.4}$$

The parameters for various distributions can be found out by the above transformation. The slopes “a” and the intercept “b” of the regression model for various distributions are summarized in table 4.1 (Al-Bagawi, 2002).

Table 4.1 : Distribution models and their transformation

	Probability distribution function	CDF F(t)	X	Y
Normal	$\frac{1}{\sigma\sqrt{2\pi}}\exp\left[-\frac{1}{2}\left(\frac{t-\mu}{\sigma}\right)^2\right]$	$\int_{-\infty}^{t} f(t)dt = \Phi\left(\frac{t-\mu}{\sigma}\right)$	t	$\emptyset^{-1}[F(t)]$
Log-Normal	$\frac{1}{t\sigma'\sqrt{2\pi}}\exp\left[-\frac{1}{2}\left\{\frac{\ln(t)-\mu'}{\sigma'}\right\}^2\right]$	$F(t') = \Phi\left(\frac{t'-\mu'}{\sigma'}\right)$	ln(t)	$\Phi^{-1}[F(t')]$
Exponential	$\lambda e^{-\lambda t} = \frac{1}{\theta}e^{-t/\theta}$	$1 - e^{-\lambda t}$	t	$ln\left[\frac{1}{1-F(t)}\right]$
Weibull	$\frac{m}{\theta}\left(\frac{t}{\theta}\right)^{m-1} exp\left[-\left(\frac{t}{\theta}\right)^m\right]$	$1 - exp\left[-\left(\frac{t}{\theta}\right)^m\right]$	ln(t)	$ln\left[ln\left[\frac{1}{1-F(t)}\right]\right.$

The coefficient of determination (R^2) is used to determine the ability of a model to interpret the data. It can be expressed as

$$R^2 = \frac{\left(\overline{XY} - \overline{X}\,\overline{Y}\right)^2}{\left(\overline{X^2} - \overline{X}^2\right)\left(\overline{Y^2} - \overline{Y}^2\right)} \tag{4.5}$$

where,

$$\overline{X} = \frac{1}{N}\sum_{i=1}^{N} X_i \quad \text{and} \quad \overline{Y} = \frac{1}{N}\sum_{i=1}^{N} Y_i \tag{4.6}$$

In this work the exponential, weibull, normal and log-normal distributions have been considered to find out the best possible distribution. These distribution methods are characterized in terms of mean, variance and confidence limits as follows.

(i) Exponential Distribution :

In probability theory and statistics, the exponential distribution is a family of continuous probability distributions. It describes the time between events in a Poisson process in which events occur continuously and independently at a constant average rate. The mean, variance and confidence limits of exponential distribution are given as

$$\mu_c = \frac{1}{\lambda} = \theta \tag{4.7}$$

$$\sigma^2 = \frac{1}{\lambda^2} = \theta^2 \tag{4.8}$$

$$\theta^{\pm} = \hat{\theta} \exp\left[\pm 1.018 \left| Z_{\alpha/2} \right| N^{-1/2}\right] \tag{4.9}$$

For different confidence limits, the value of $|Z_{\alpha/2}|$ takes different values.

Confidence Limit	80%	90%	95%	99%
$\|Z_{\alpha/2}\|$	1.28	1.648	1.96	2.58

(ii) Weibull distribution :

The Weibull distribution is a continuous probability distribution. The Weibull distribution gives a distribution for which the failure rate is proportional to a power of time. The mean, variance and confidence limits of weibull distribution are given as

$$\mu_c = \theta\left(1+\frac{1}{m}\right)$$

(4.10)

$$\sigma^2 = \theta^2\left[\Gamma\left(1+\frac{2}{m}\right) - \left\{\Gamma\left(1+\frac{1}{m}\right)\right\}^2\right]$$

(4.11)

$$\theta^{\pm} = \hat{\theta} \exp\left[\pm 1.018 \left| Z_{\alpha/2} \right| N^{-1/2}\right]$$

(4.12)

$$m^{\pm} = \hat{m} \exp\left[\pm 1.049 \left| Z_{\alpha/2} \right| N^{-1/2}\right]$$

(4.13)

(iii) Normal Distribution :

The normal or Gaussian distribution is a continuous probability distribution that has a bell-shaped probability density function known as the Gaussian function. The normal distribution is

considered the most prominent probability distribution in statistics. This is due to the fact that the normal distribution is very tractable analytically where a large number of results involving this distribution can be derived in explicit form. Secondly, the normal distribution arises as the outcome of the central limit theorem, which states that under mild conditions the sum of a large number of random variables is distributed approximately normally. The mean, variance of normal distribution are given as

$$\mu_c^{\pm} = \hat{\mu}_c \pm |Z_{\alpha/2}| \frac{\hat{\sigma}}{\sqrt{2N}}$$

(4.14)

$$\sigma^{\pm} = \hat{\sigma} \pm |Z_{\alpha/2}| \frac{\hat{\sigma}}{\sqrt{2(n-1)}}$$

(4.15)

(iv) Lognormal Distribution:

The log-normal distribution is a probability distribution of a random variable whose logarithm is normally distributed. If X is a random variable with a normal distribution, then $Y = \exp(X)$ has a log-normal distribution; likewise, if Y is log-normally distributed, then $X = \log(Y)$ is normally distributed. In a log-normal distribution, the parameters describing mean and variance are given as

$$\mu_c = t_0 \exp\left[\frac{w^2}{2}\right]$$

(4.16)

$$\sigma^2 = t_0^2 \exp(w^2)\left[\exp(w^2) - 1\right]$$

(4.17)

$$t_0^{\pm} = \hat{t}_0 \exp\left[\pm |Z_{\alpha/2}| \hat{w} N^{-1/2}\right]$$

(4.18)

$$w^{\pm} = \hat{w} \pm |Z_{\alpha/2}| \frac{\hat{w}}{\sqrt{2(N-1)}}$$

(4.19)

Using the results of the optimum distribution with its parameters, the fouling growth model can be developed by calculating the critical fouling level from thermal analysis of the

heat exchanger performance. The thermal analysis of a heat exchanger provides a mathematical relationship linking the heat exchanger performance with the extent of fouling. This provided a practical approach of generating appropriate fouling growth curves in order to adjust the operational parameters for optimal cleaning schedule of a heat exchanger.

Depending on the distribution methods, the fouling growth models can be different. For the lognormal distribution, the fouling growth model is given as

$$R_f(t) = R_f(1)t^{\beta}$$

(4.20)

where, $R_f(t)$ is the fouling resistance at any instant of time t (day), $R_f(1)$ is the fouling resistance at the start of operation of the heat exchanger corresponding to clean condition and β is the constant assumed for this model.

Figure 4.1 shows the algorithm for statistical analysis of a heat exchanger subjected to fouling. The input data of the analysis includes the critical level of fouling which can be determined by the operation engineers either from thermal analysis, previous experience or some specific standards.

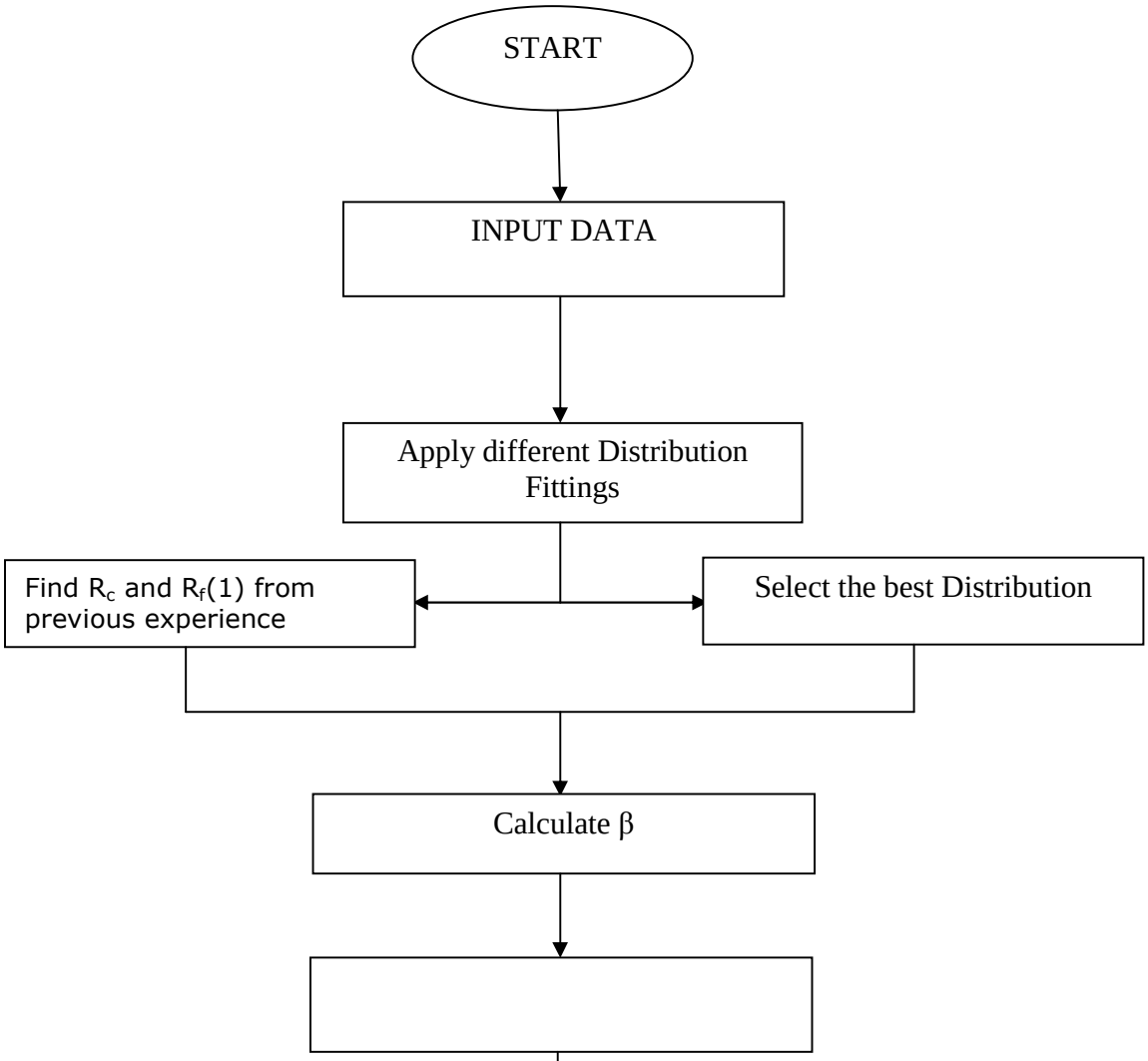

Figure 4.1 Statistical Evaluation of Fouling

4.3 Interpretation of Experimental Data:

Since there occurs no change of phase in any of the liquids and the heat exchanger is operating at a lower range of temperature, specific heat capacity for both the hot and cold water is assumed to be invariant. As the heat duty of the hot and cold fluids are different in all practical cases, three heat duties for the heat exchanger can be determined from each set of test data.

Heat duty for the hot fluid

$$Q_1 = m_1 c_p (T_1 - T_2)$$

(4.21)

Heat duty for the cold fluid

$$Q_2 = m_2 c_p (T_4 - T_3)$$

(4.22)

Hence the mean value of heat duty for both the hot and cold fluids is

$$Q_m = \frac{1}{2}(Q_1 + Q_2)$$

(4.23)

The unsteadiness of each working regime is calculated as a factor of dispersion about the mean heat duty which is defined as

$$\Delta_Q = \frac{\sqrt{(Q_1 - Q_m)^2 + (Q_2 - Q_m)^2}}{Q_m}$$

(4.24)

For analysis of the experimental data only measurements corresponding to steady state were taken into consideration. Therefore the measurements for which Δ_Q was less than 10% were taken into account and other measurements were discarded for further analysis (Milanovic et. al., 2006).

As there exists uncertainties both in temperatures and mass of fluid flow, the exact heat duties can be calculated taking into consideration these uncertainties.

$$Q_{1,\max} = (m_1 + \Delta m_1) c_p (T_1 - T_2 + 2\Delta T)$$

(4.25)

$$Q_{1,\min} = (m_1 - \Delta m_1) c_p (T_1 - T_2 - 2\Delta T)$$

(4.26)

$$Q_{2,\max} = (m_2 + \Delta m_2) c_p (T_4 - T_3 + 2\Delta T)$$

(4.27)

$$Q_{2,\min} = (m_2 - \Delta m_2) c_p (T_4 - T_3 - 2\Delta T)$$

(4.28)

The heat exchanger is a single tube pass shell and tube heat exchanger operating in counter-current flow direction. Considering the uncertainty in measurement of temperature, two mean logarithmic temperature differences can be determined as

$$\mathrm{LMTD}_{\max} = \frac{(T_1 - T_4 + 2\Delta T) - (T_2 - T_3 + 2\Delta T)}{\ln[(T_1 - T_4 + 2\Delta T)/(T_2 - T_3 + 2\Delta T)]}$$

(4.29)

$$\mathrm{LMTD}_{\min} = \frac{(T_1 - T_4 - 2\Delta T) - (T_2 - T_3 - 2\Delta T)}{\ln[(T_1 - T_4 - 2\Delta T)/(T_2 - T_3 - 2\Delta T)]}$$

(4.30)

Due to uncertainty in temperature and mass flow there are two values of heat duty each for the hot and cold fluid. Also there exist two values of LMTD. As overall heat transfer coefficient is a function of heat duty and LMTD, there can be four sets of overall heat transfer coefficients considering uncertainties in temperature and mass flow rate.

$$U_{1,\max} = \frac{Q_{1,\max}}{A \times LMTD_{\min}}$$

(4.31)

$$U_{1,\min} = \frac{Q_{1,\min}}{A \times LMTD_{\max}}$$

(4.32)

$$U_{2,\max} = \frac{Q_{2,\max}}{A \times LMTD_{\min}}$$

(4.33)

$$U_{2,\min} = \frac{Q_{2,\min}}{A \times LMTD_{\max}}$$

(4.34)

The mean overall heat transfer coefficient is calculated as

$$U_m = \frac{1}{4}(U_{1,\max} + U_{1,\min} + U_{2,\max} + U_{2,\min})$$

(4.35)

The unsteadiness of each working regime from the overall heat transfer point of view was taken into account considering the dispersion according to statements of Perry and Green [23]. The dispersion limit for overall heat transfer coefficient was set at 20% so that only the measurements within this limit were taken into consideration (Milanovic et. al., 2006). The dispersion about mean overall heat transfer coefficient was determined as

$$\frac{\Delta U_m}{U_m} = \sqrt{\frac{(U_m - U_{1,\max})^2 + (U_m - U_{1,\min})^2 + (U_m - U_{2,\max})^2 + (U_m - U_{2,\min})^2}{3U_m^2}}$$

(4.36)

The overall thermal resistance due to fouling was calculated according to the following equation

$$R_f = \frac{1}{U_f} - \frac{1}{U_c}$$

(4.37)

The overall heat transfer coefficient for the heat exchanger with clean condition (U_c) is determined as the overall heat transfer coefficient at initiation of the experimentation. Since the variation in inlet temperature of the cold fluid is very less, the clean overall heat transfer coefficient is assumed to be invariant.

4.4 Results and Discussion

The experiments were conducted with the experimental set-up described in section 3.4 of the previous chapter. The experimental data collected with the subjected heat exchanger were analyzed taking into account the uncertainties in temperature and flow measurement. The uncertainties in temperature measurement resulted in one maximum and one minimum value of LMTD corresponding to a single set of experiment. The minimum and maximum LMTD values for the whole experimental results are summarized in Table A.3 of Appendix A. Similarly the uncertainties in the flow measurement resulted in two values of heat duty out of which one is a minimum and the other one is maximum. The heat duty values were calculated with the specific heat values corresponding to the mean temperature of the fluids. The dispersion about mean heat duty for all the experimental results were calculated according to equation 4.24 and are represented in Table A.4 of Appendix A. The maximum dispersion about the mean heat duty was observed to be 6.45% while the mean dispersion about same mean value was 7.57%. Corresponding to the uncertainty in flow measurement, both the hot and the cold side fluids have maximum and minimum values of heat duty. The actual overall heat transfer coefficient is dependent on the heat duty and the LMTD. As the both side heat duties have two different values due to flow uncertainty and LMTD has two different values due to temperature uncertainty, a set four values for overall heat transfer coefficient ($U_{1,\,max}$, $U_{1,min}$, $U_{2,max}$, $U_{2,min}$) has been calculated. The dispersion of the overall heat transfer coefficient about its mean value is determined and summarized in Table A.5 of Appendix A. The maximum dispersion of the experimental data for overall heat transfer coefficient about its mean value was found to be 10.5%. Since this value is well within the maximum limit of 20%, the data is further used for statistical analysis.

Fouling Cycle	Time (Days)	Cumulative Distribution Function F(t)	Reliability R(t)	Cumulative Hazard Function H(t)
1	40	0.091	0.909	0.095
2	64	0.182	0.818	0.201
3	87	0.273	0.727	0.318
4	93	0.364	0.636	0.452

5	102	0.455	0.545	0.606
6	129	0.545	0.455	0.788
7	142	0.636	0.364	1.012
8	145	0.727	0.273	1.299
9	148	0.818	0.182	1.705
10	164	0.909	0.091	2.398

Table 4.2 : Statistical Functions for the fouling cycles

The statistical analysis method is considered in this work for the prediction of fouling in case of the above mentioned shell and tube heat exchanger. The result of the experimental work was analyzed by statistical approach for prediction of the time required to reach critical level of fouling. The whole experimentation work is divided into 10 number of fouling cycles. The results of the statistical analysis are summarized in the Table 4.2 and 4.3.

Table 4.3 : Statistical distributions for fouling cycles

Fouling Cycle	Time (Days)	F(t)	Normal Distribution		Log-normal Distribution		Exponential Distribution		Weibull Distribution	
			X	Y	X	Y	X	Y	X	Y
1	40	0.091	40	-1.54	3.69	-2.12	40	0.1	3.69	-1.54
2	64	0.182	64	-1.16	4.15	-1.66	64	0.22	4.15	-1.16
3	87	0.273	87	-0.69	4.46	-1.17	87	0.36	4.46	-0.69
4	93	0.364	93	-0.44	4.53	-0.84	93	0.54	4.53	-0.44

5	102	0.455	102	-0.12	4.62	-0.46	102	0.77	4.62	-0.12
6	129	0.545	129	0.12	4.85	-0.12	129	0.98	4.85	0.12
7	142	0.636	142	0.44	4.96	0.14	142	1.24	4.96	0.44
8	145	0.727	145	0.69	4.98	0.37	145	1.68	4.98	0.69
9	148	0.818	148	1.16	5.0	0.52	148	2.46	5.0	1.16
10	164	0.909	164	1.54	5.1	0.84	164	3.62	5.1	1.54

The statistical functions are represented in Figure 4.3 which illustrates the fouling behavior and the possible failure of the exchanger for different kinds of statistical distributions. It can be observed that the efficiency of operation of the exchanger reduces with progress of time. Simultaneously the fouling growth increases in a slower rate at the beginning of operation while it improves rapidly after certain period of time.

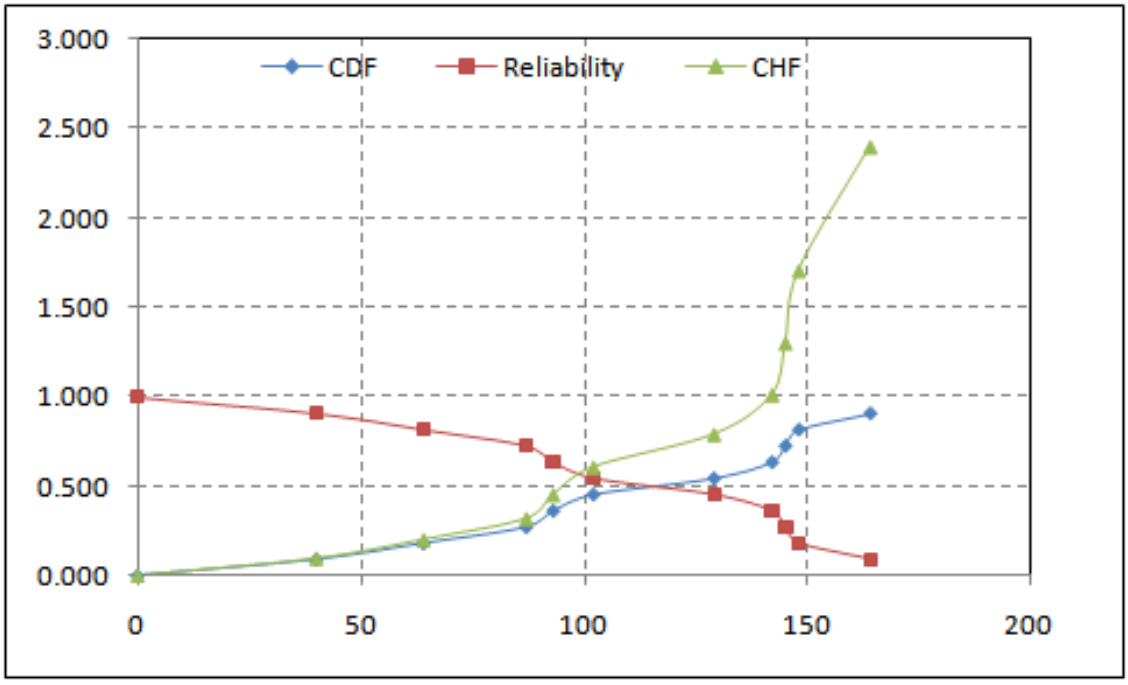

Figure 4.2 Statistical functions for the fouling cycles of heat exchanger

The statistical data for different distributions are illustrated in Figures 4.3 and 4.4. All the distributions are fitted with linear functions and the corresponding fitted equation,

coefficient of determination and the goodness of fit test results are summarized in Table 4.4. The coefficient of distribution for lognormal distribution is highest as compared to the other distributions. As illustrated in the Figure 4.3 and 4.4, the exponential distribution is weakest having lowest coefficient of determination 0.794 while the lognormal distribution is having a highest value of coefficient of distribution equal to 0.967. Hence in this study the lognormal distribution is used as the most suitable distribution for data analysis.

Table 4.4 : straight line fit results of statistical distributions

Distribution	Fitted Linear Equation	Coefficient of Determination (R^2)
Normal	Y=0.026X- 2.323	0.924
Log-Normal	Y= 2.151X- 10.07	0.967
Exponential	Y=0.016X- 0.905	0.794
Weibull	Y=2.327X-11.30	0.921

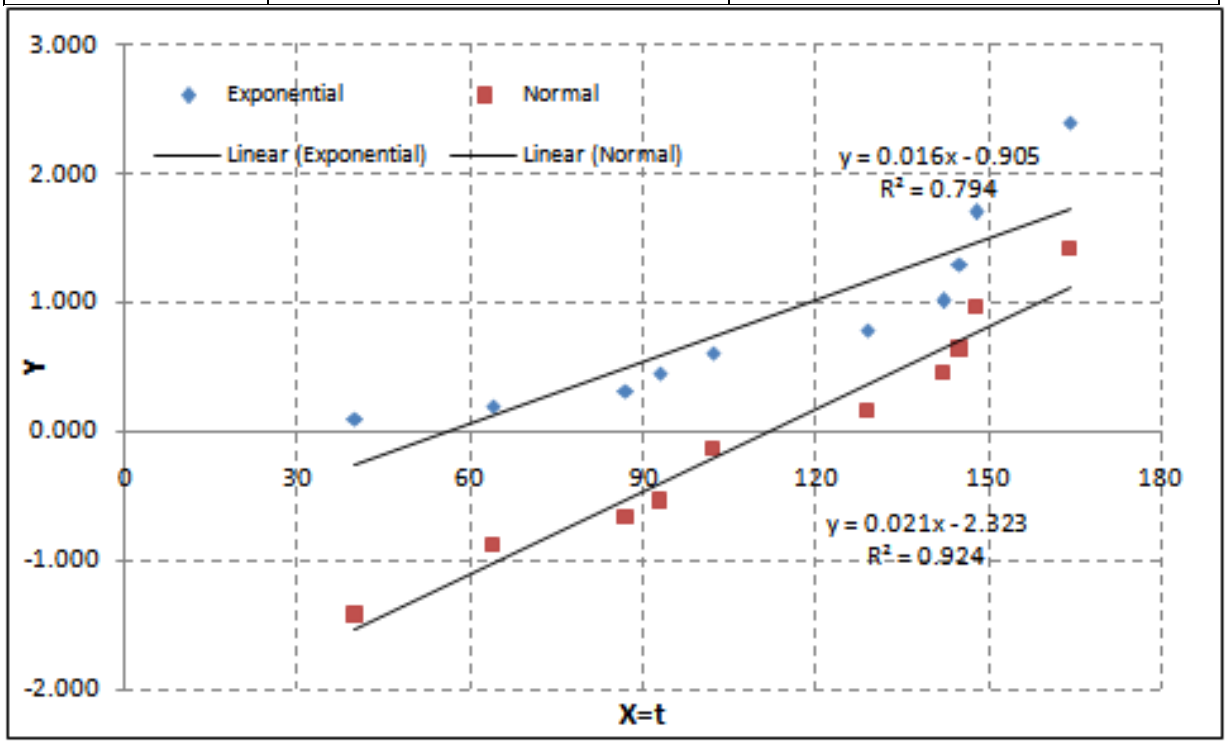

Figure 4.3 : Exponential and Normal distribution for fouling

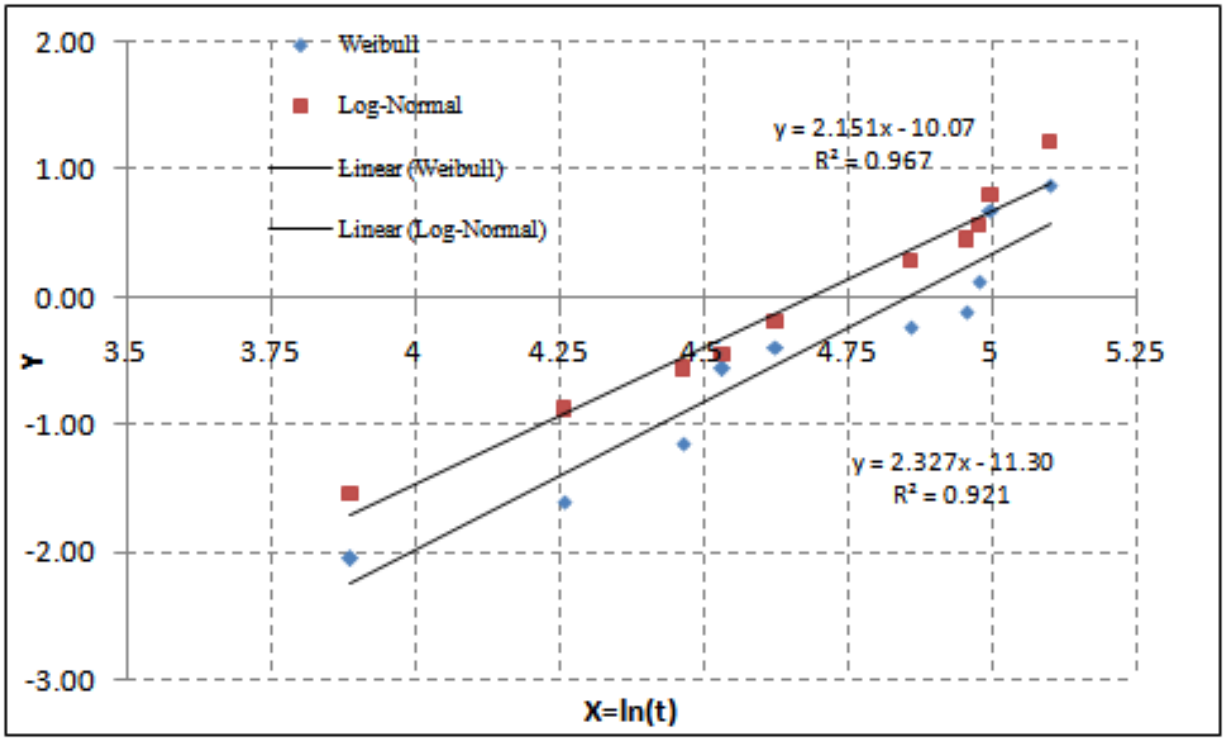

Figure 4.4 : Weibull and Log-normal distribution for fouling

All data taken during the whole period of experimentation is divided into 10 numbers of cycles. In the present work, only six cycles are considered for analysis. The initial value of fouling resistance considering the thermal analysis of six fouling cycles is found to be 0.000186m^2.K/W. The critical level of fouling for any particular heat exchanger can be determined depending on the process requirements and operating conditions. In the present equipment studied, the critical level of fouling is taken to be 0.00125m^2.K/W based on the TEMA correlations. The mean time required to attain the critical level of fouling based on log-normal distribution is found to be 106.4 days.

The log-normal distribution can be expressed as a power law function $R_f(t) = R_f(1)\, t^{\beta}$ which represents the fouling growth in the present work. The average fouling growth using statistical analysis is derived to be

$$R_f(t) = 0.000186t^{0.9206} \quad (4.38)$$

Figure 4.6 indicates the thermal analysis of all the six fouling cycles under consideration and fitted with a single regression line of power equation law. The coefficient of

determination for this distribution is 0.945 which indicates a good accuracy of fitting of the results. The thermal analysis of all the six cycles gives a power distribution law as

$$R_f(t) = 0.000171t^{0.908} \quad (4.39)$$

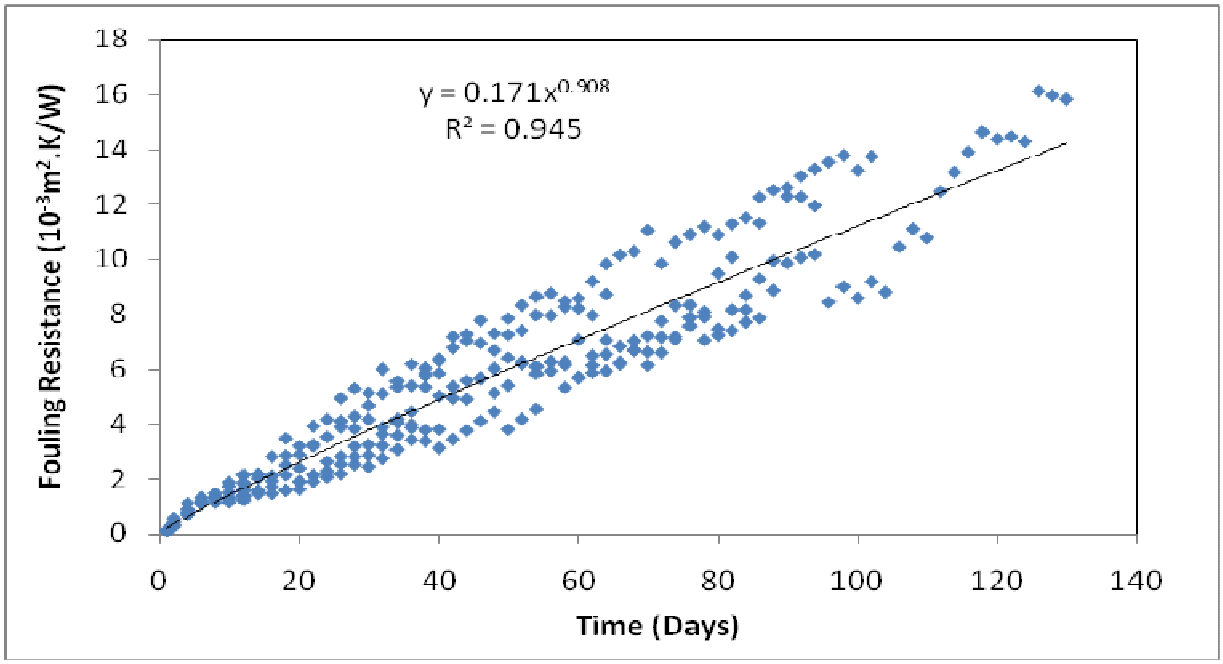

Figure 4.5 Fouling growth results for all cycles

The comparison between the statistical analysis and the thermal analysis is illustrated in the table 5. It indicates a variation of maximum 8.7% in the study of fouling growth over a span of 120 days. Hence the accuracy of statistical approach can considered quite reasonable as compared to the thermal analysis of fouling growth in a heat exchanger. Figure 4.7 illustrates the comparison of results from the present statistical model and those of thermal analysis for the six fouling cycles considered for analysis in this present work.

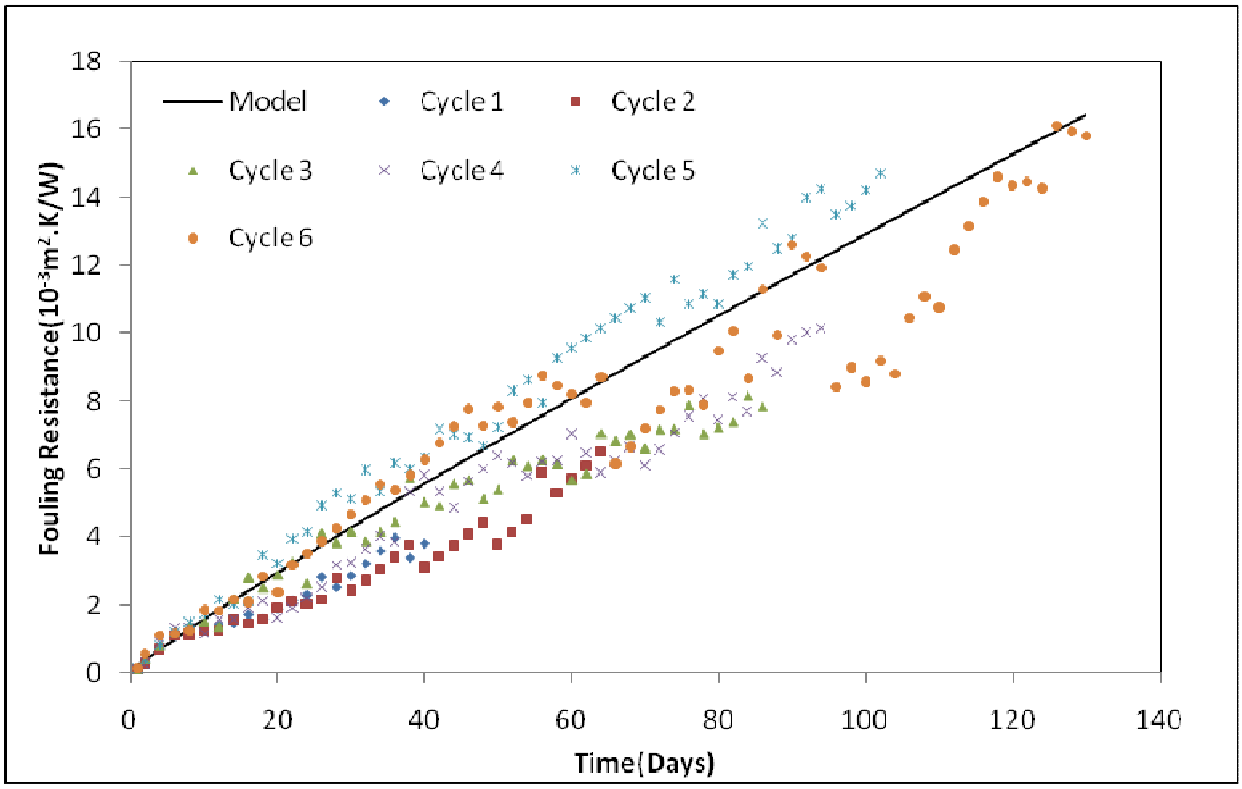

Figure 4.6 : Comparison of fouling growth results with model

Table 4.5 : Comparison of statistical and thermal analysis

Time (Days)	$R_f(t)$ from statistical analysis	$R_f(t)$ from thermal analysis	% Difference
1	0.000186	0.000171	8.77193
10	0.001484	0.001384	7.279523
20	0.002774	0.002596	6.834286

30	0.003998	0.003752	6.574697
40	0.005183	0.004872	6.390898
50	0.006338	0.005966	6.24855
60	0.007471	0.00704	6.132386
70	0.008586	0.008097	6.034269
80	0.009685	0.009141	5.949349
90	0.010771	0.010173	5.874502
100	0.011844	0.011194	5.807593
110	0.012908	0.012206	5.747103

4.5 Summary

In this chapter the statistical analysis is used for investigation of performance of a shell azand tube heat exchanger under fouling condition. The statistical analysis can be used for optimal cleaning schedule in chemical process industries so that the idle time can be reduced to possible minimum and simultaneously the heat exchanger running with poor performance can be avoided. The statistical analysis gives a theoretical framework towards the indication of the extent of fouling on the heat transfer surface which cannot be estimated from the outside of the exchanger body. Hence this can be used for prediction of fouling without opening the exchanger which is very much a complicated process. Thus systematic statistical analysis provides an effective means for prediction of decrease in heat transfer efficiency for effective preventive maintenance scheduling of the heat exchanger cleaning. This can be used for continuous monitoring of a heat exchanger system and improved maintenance scheduling. In further study, the experimental methods such as Wilson plot method and C-Factor method are used for quantification of fouling and its effect on heat transfer performances of a heat exchanger.

Chapter 5

Heat Transfer Performance Analysis using Wilson Plot Method

This chapter describes an integrated approach for investigation of heat transfer performances of a shell and tube heat exchanger using Wilson Plot method and its various

modifications. A theoretical framework for fouling analysis using statistical approach has been discussed in the previous chapter. The Wilson plot method takes into account the theoretical correlations along with experimental observations to study the heat transfer performances of a heat exchanger subjected to fouling. The most significant thermodynamic performance parameter for a heat exchanger is the overall heat transfer coefficient. In this chapter, the overall heat transfer coefficient has been calculated based on the correlations among non-dimensional numbers such as Reynolds number and Prandtle number as described in the previous chapter.

5.1 Introduction

The heat transfer mechanism by convection entails to energy transfer between a solid surface and a moving fluid due to a prescribed temperature difference between the solid surface and the fluid. The estimation of convection coefficients constitutes a crucial issue in designing and sizing any type of heat exchange device. The commonly used method to determine the heat transfer coefficients and hence the overall heat transfer is the Wilson plot method. This chapter presents an overview of the Wilson plot method and its use to determine the relationship between overall heat transfer coefficient and Nusselt number.

The mechanism of heat exchange in heat exchangers is essentially contributed mostly by the process of convection. It is the process of energy transfer between a solid surface and a fluid moving over the surface due to the existence of a temperature difference between the surface and the fluid. This process can be analyzed as a combination of effects due to conduction and fluid motion as presented by Fernandez-Seara et. al.(2007).The analysis of convection problems requires the solution of mass, moment and energy conservation equations taking into consideration the surface geometry and fluid properties. Secondly such problem requires determination of the flow field and the temperature distribution in the fluid. This approach is too much complex and solutions have only been found for simple surface geometries and under several restrictive assumptions.

In actual practice, most of the convective heat transfer processes inherent to heat exchangers usually involve complex geometries and intricate flows so that the analytical solutions are too much complex. Therefore, a more practical and simpler approach has been developed based on Newton’s law of cooling which correlates heat transfer by convection (q),

the surface area (A), average convection coefficient (h) and the temperature difference between the solid surface (T_s) and the fluid (T_f).

$$q = Ah(T_s - T_f) \tag{5.1}$$

For a given flow and surface geometry, the experimental data can be easily obtained by measuring surface area and fluid temperatures. Consequently the convection coefficient can be determined by using equation (5.1). However the major drawback of this methodology lies in the measurement of solid surface temperature as the surface temperature varies along the length of the tube and the fluid flow pattern is altered by the presence of baffles in a heat exchanger. Secondly this becomes much more complex in heat exchangers as the heat transfer surfaces are not accessible. Hence this is one of the most lucrative areas for researchers to find out an alternative methodology to calculate heat transfer coefficients in heat exchangers due to its widespread industrial applications.

The Wilson plot method provides a suitable technique to estimate the heat transfer coefficient in most of the convective heat transfer processes. The Wilson plot is a technique to estimate the film coefficients in several types of heat transfer processes and to obtain general heat transfer correlations. The Wilson plot method and its different modifications provide an outstanding tool for the analysis and design of convection heat transfer processes in research laboratories and practical applications that involve analysis of heat exchangers. This method deals with the determination of convection coefficients based on experimental data and the subsequent formulation of appropriate correlation equations. In the present work, experiments were conducted using a single pass shell and tube heat exchanger to determine the relationship between overall heat transfer coefficient and Nusselt Number. The correlations between the overall heat transfer coefficient and Nusselt Number have been developed both for the tube side and shell side flow based on the Wilson plot method and modified versions of Wilson plot.

The major advantage of Wilson plot method is that it avoids the direct measurement of the temperature of the surface separating the fluids which consequently eliminates the effect of fluid flow disturbances due to presence of baffles and temperature measuring sensors. The input parameters for this method include the physical parameters of the heat exchanger, the fluids flowing through the shell and tubes, the mass flow rates and the temperatures at the inlet and exit of both the shell and tubes. Besides, the Wilson plot method and its modifications develop an indirect tool to generate more accurate correlation equations for convective heat

transfer coefficients in heat exchanging devices. Hence it is an outstanding tool for thermal analysis of heat exchangers and determination of general heat transfer correlations. Simultaneously this method has certain drawbacks. This method cannot be accurately applied to flow regimes other than turbulent flow. Secondly the variations in fluid thermo physical properties are not taken into consideration.

5.2 The Wilson plot Method

This method was originally proposed by Wilson (Wilson, 1915) to evaluate the film coefficients in shell and tube condensers for the case of a vapour condensing outside the tubes by means of a cooling liquid flowing inside the tubes. Taking into account the specific conditions of a shell and tube condenser, Wilson theorized that if the mass flow of the cooling liquid was modified, then the change in the overall thermal resistance would be mainly due to the variation of the in-tube convection coefficient, while the remaining thermal resistances remained nearly constant. The original Wilson plot for a shell and tube condenser is shown in Figure 5.1. Therefore, as indicated in Figure 5.1, the thermal resistances outside of the tubes and the tube wall could be considered constant. In this case, the Wilson plot is obtained considering the Dittus-Boelter correlation as a general functional form for the internal convection heat transfer coefficient. It is based on the separation of the overall thermal resistance into the inside convective thermal resistance and the remaining thermal resistances involved in the heat transfer process. The input data for this method are the physical parameters defining the dimensions of the heat transfer surfaces of the equipment, the fluids flowing in each circuit, the mass flow rates and the temperatures in both inlet and outlet sections. The heat transfer coefficients on each side of the heat transfer surface are dependent on the flow regime. Temperature and mass flow rate are the input parameters varying during the experimentation.

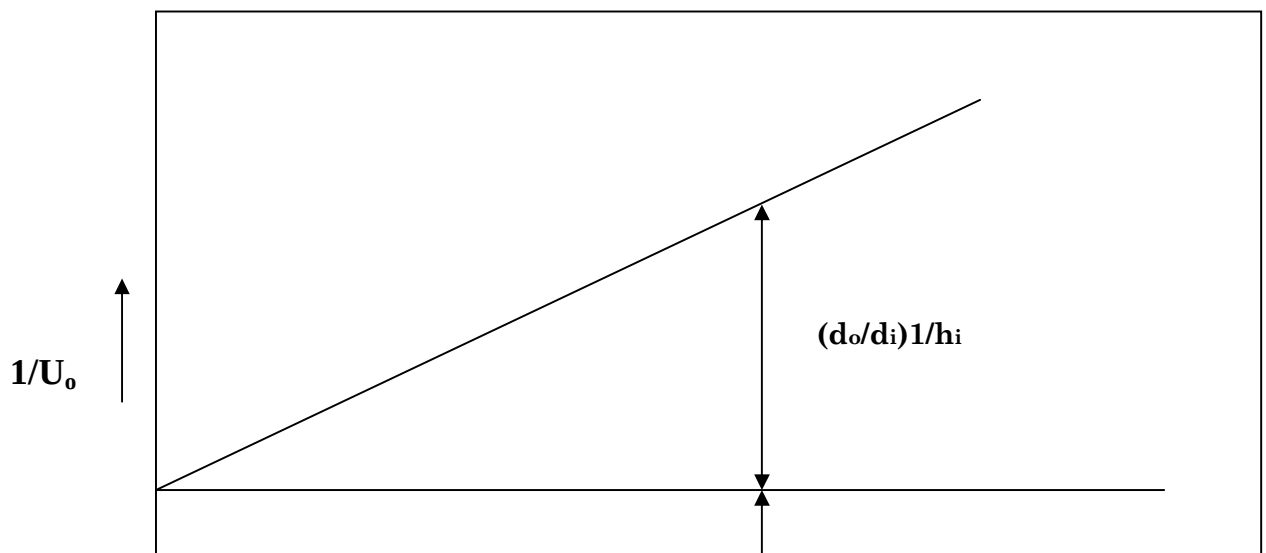

Figure 5.1 Original Wilson Plot with thermal resistances

As discussed previously in chapter 2, the basic principle of heat transfer indicates that the overall thermal resistance is the sum of the thermal resistances in series corresponding to each one of the constituting heat transfer processes. The overall thermal resistance of the heat transfer process in a shell and tube heat exchanger (R_{ov}) can be expressed as the sum of the thermal resistances corresponding to external convection (R_o), the external fouling film ($R_{f,o}$), the tube wall (R_t),the internal fouling film ($R_{f,i}$) and the internal convection (R_i), as presented in the below mentioned equation.

$$R_{ov} = R_o + R_{f,o} + R_t + R_{f,i} + R_i \tag{5.2}$$

The overall thermal resistance can be correlated in terms of overall heat transfer coefficient with respect to inner or outer surface area of the tubes and the corresponding area.

$$R_{ov} = \frac{1}{U_o A_o} = \frac{1}{U_i A_i} \tag{5.3}$$

The individual thermal resistances in each of the heat transfer processes in series from the outer fluid to the inner fluid of the tubes are determined from the equations 3.12 – 3.16 as mentioned in chapter 3.

According to the theoretical framework developed by Wilson, if the mass flow rate of cooling fluid is modified, then the change in overall thermal resistance is mainly due to the variation of the in-tube convection coefficient while the remaining thermal resistances almost

remain constant. Therefore the thermal resistances due to the outsides tubes convection process, the outer and inner fouling films and the tube wall can be considered to be constant. Hence,

$$R_o + R_{f,o} + R_t + R_{f,i} = C_1 \tag{5.4}$$

The film heat transfer coefficient for fully developed turbulent flow inside the circular tubes is proportional to a power of the Reynolds number which accounts for the property variations of the tube-side fluid and the tube diameter. The convection coefficient is determined accoding to the correlation proposed by Dittus-Boelter (Incropera and Dewitt, 2007).

$$h_i = C\,\mathrm{Re}^m\,\mathrm{Pr}^{0.4}\left(\frac{k_i}{d_i}\right) \tag{5.5}$$

However if the effects of fluid flow variation on the properties of the fluid are neglected, then the internal convection coefficient will be proportional to Re^m as the remaining parameters can be expressed as a constant. Consequently the inner convective thermal resistance can be expressed as

$$R_i = C_2\frac{1}{\mathrm{Re}^m} \tag{5.6}$$

Further combining all the thermal resistances, the overall thermal resistance can be obtained as a linear function of Re^m.

$$R_{ov} = C_1 + C_2\frac{1}{\mathrm{Re}^m} \tag{5.7}$$

Thus the overall thermal resistance is represented as a straight line with C_1 as the intercept of the regression line and C_2 as the slope of the straight line. On the other hand, the overall thermal resistance can be determined from the experimental data using energy balance equation.

$$R_{ov} = \frac{LMTD}{q} \tag{5.8}$$

Therefore, if the value of the exponent ‘m’ is assumed, then the experimental values of the overall thermal resistance can be represented as a linear function of the experimental values of $1/\mathrm{Re}^m$. Further the straight line equation that fits the experimental data can be deduced by applying simple linear regression. Consequently the values of the constants C_1 and C_2 can be obtained according to equation (5.7). Once the constants C_1 and C_2 are determined, both the

internal and external convection coefficients and the unknown parameter C can be calculated as follows.

$$h_o = \frac{1}{\left[C_1 - \left(R_{f,o} + R_t + R_{f,i}\right)\right] A_o} \tag{5.9}$$

$$h_i = \frac{\mathrm{Re}^m}{C_2 A_i}$$

(5.10)

$$C = \frac{1}{C_2 \left(\frac{k_i}{d_i}\right) \mathrm{Pr}^{0.4} A_i}$$

(5.11)

The above exposition is the original Wilson plot method (Wilson, 1915). It relies on the fact that, the overall thermal resistance can be extracted from experimental measurements in a reliable manner. As a result of the Wilson plot method, the mean value of the convection coefficient outside the tubes and the convection coefficient inside the tubes as a function of cooling fluid mass flow are obtained. However the exponent of the Reynolds number in the general correlation equation considered for the convection coefficient should be assumed. Wilson assumed the exponent to be 0.8 (Fernandez-Siera et. al., 2005). The assumptions involved in the application of original Wilson plot method is its major drawback which has further been modified by Briggs and Young (Briggs and Young, 1969) and Shah (Shah, 1990). The modifications are widely used in heat transfer analysis of heat exchange equipments.

5.3 Modified Wilson Plot Method

The modified Wilson plot method based on the original Wilson plot method takes into account a second linear equation obtained by applying logarithms to both sides of the equation (5.7) for overall thermal resistance.

$$\ln\left(\frac{1}{R_{ov} - C_1}\right) = \ln\left(\frac{1}{C_2}\right) + m \ln(\mathrm{Re})$$

(5.12)

This modified form of Wilson plot represents a linear relationship between $\ln[1/(R_{ov} - C_1)]$ and $\ln(\mathrm{Re})$ with the intercept between the regression line and the vertical axis as $\ln(1/C_2)$ and slope of the line as m.

The value of exponent 'm' is determined by an iteration procedure. Initially assuming the value of 'm', the values of the constants C_1 and C_2 are obtained. From the energy balance analysis and experimental data, the values of the terms $\ln[1/(R_{ov} - C_1)]$ and $\ln(\mathrm{Re})$ are determined. Then the equation of the straight line that fits the experimental data is obtained by simple linear regression. The slope of the straight line gives the value of 'm' which is compared with the initially assumed value. The modified Wilson plot technique provides the mean value of the tube inside convection coefficient as a function of the cooling fluid flow rate. Subsequently the shell side convection coefficient is obtained which resembles the form of Sieder-Tate correlation given as

$$Nu = C\,\mathrm{Re}^m\,\mathrm{Pr}^n$$

(5.13)

In this chapter, the original Wilson plot method and the modified Wilson plot methods are used to develop a correlation between overall heat transfer coefficient and the Nusselt number both for the shell and tube side flow.

5.4 Experimental estimation of Convection Coefficients

The Wilson plot method gives a reliable solution to heat transfer analysis of a heat exchanger based on experimental data. The experimentation work for this analysis has been carried out in two phases namely the data acquisition and data interpretation.

5.4.1 Data Acquisition

Experiments were conducted on a laboratory scale 1-1 shell and tube heat exchanger as described in the section 3.5 of previous chapter. The experiments were conducted with water both as the hot and the cold fluid. The cold water was allowed to flow through the tubes while the hot water in the annular area between the shell and the tubes. The water source was the common tap water. The flow of the two liquids is counter-current in direction. The experimentation involved the measurement of end terminal temperatures including hot water

inlet, hot water outlet and cold water inlet and cold water outlet temperatures corresponding to various flow rates of both hot and cold water. The geyser used for heating the water was set with a cut-off temperature of 100^{o}C. All the temperature measurements were recorded at steady states corresponding to every flow rate. At the steady state the inlet and outlet temperatures of both the hot and cold fluids do not change for a particular flow rate.

First of all the operating boundaries of the heat exchanger was determined. Then the heat exchanger was operated at various combinations of cold and hot water flow rates ranging from 600 LPH to 1200 LPH. Then an operating space was determined by plotting hot water flow rates versus hot water temperature as shown in figure 5.2. Then the same experimentation procedure as described in section 3.5 was repeated a few times to achieve steady state and to ensure that the data was reproducible.

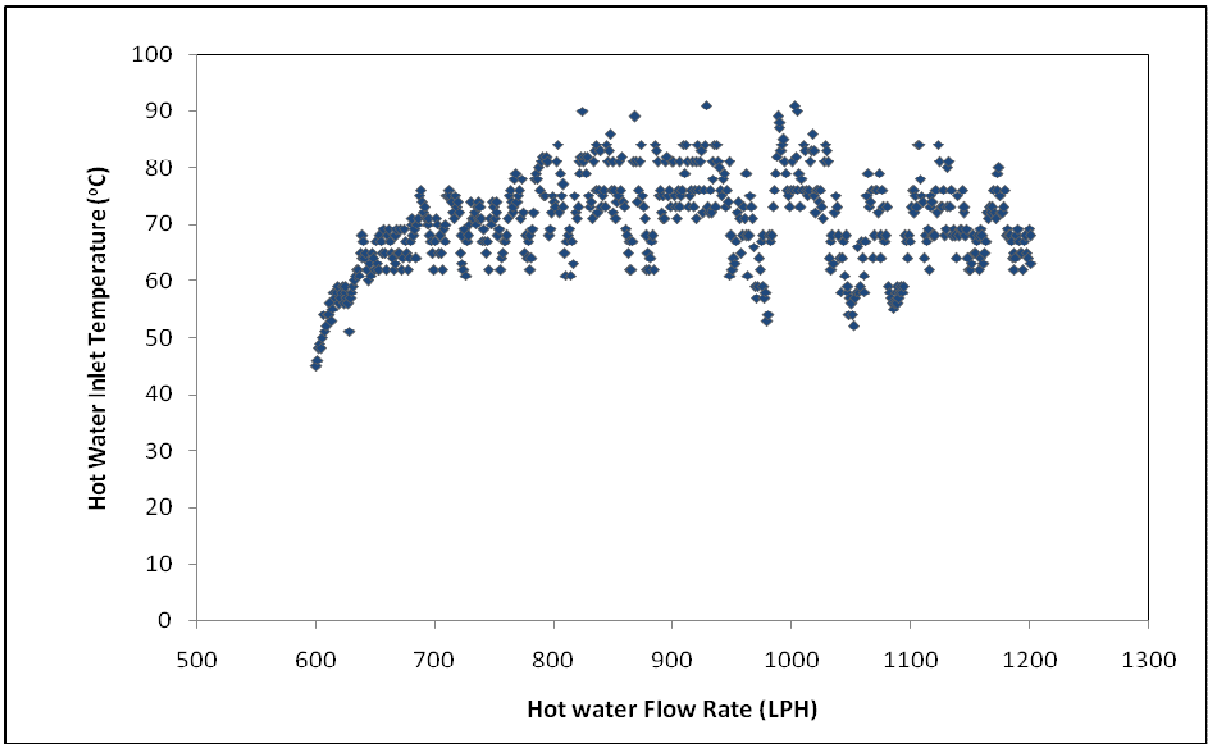

Figure 5.2 : Operating Space for Heat Exchanger

5.4.2 Modelling of Heat Exchanger

Every heat exchanger design should meet the specific heat duty as required in any process industry. Heat duty is the amount of heat exchanged between the hot and the cold fluid during the process of exchange. Heat duty can be calculated as the heat loss by the hot fluid to

the cold fluid by performing energy balance. This can also be expressed as a function of the overall heat transfer coefficient (U).

$$q = UA\Delta T_{lm}$$

(5.14)

where, q is the heat duty, U is the overall heat transfer coefficient, A is the area of heat transfer and ΔT_{lm} is the logarithmic mean temperature difference.

The Reynolds number of the flow inside the tube can then be calculated by the following equations.

$$\mathrm{Re}_t = \frac{\rho_t v_t d_i}{\mu_t}$$

(5.15)

where ρ_t is the tube side fluid density, v_t is the tube side flow velocity, μ_t is tube side fluid viscosity and d_i is the tube inner diameter.

The tube side Prandtle number is calculated to be

$$\mathrm{Pr}_t = \frac{C_{pt}\mu_t}{k_t}$$

(5.16)

where C_{pt} is the specific heat of tube side fluid and k_t is the thermal conductivity coefficient for tube side fluid.

The simplest and most commonly used model of shell side flow is based on Kern's method proposed by Kern (Kern, 2000). But one of the major in-adequacy of kern's method is that it doesn't consider the effect of leakage and bypass streams. Hence results obtained by Kern's method become erroneous and it is quite significant particularly in the calculations of shell side heat transfer co-efficient as suggested by Serna et. al (2007). The shell side flow in almost all the process applications remains within the turbulent region. Besides Dirker and Mayer (Dricker and Mayer, 2005) suggested that baffles in the shell increase the turbulence so that heat transfer coefficient increases. Hence the shell side Nusselt Number considering turbulent flow is calculated as

$$Nu = C\left(\mathrm{Re}\right)^m (\mathrm{Pr})^{0.4}$$

(5.17)

where the constants C and exponent m are to be determined from the experimental data analysis using Wilson plot method. These constants were evaluated for different operating conditions by considering the various design procedures suggested by various researchers (Raghavani et. al., 2003; Serna and Jimenez, 2004; Kukulka and Devgun, 2007).

The models described above are simulated with the experimental data. Simulation is done for various flow rates using water both as hot and cold fluids.

5.5 Results and Discussion:

The operating space for the heat exchanger under consideration is represented in Figure 5.2 which shows the variation of hot water inlet temperature with the flow rate within the operating boundaries. The shell-and-tube heat exchanger has an operating space with an inlet hot water temperature range from 40°C to 100°C. As shown in Figure 5.2, the temperature was most often between 60°C and 80°C. The Wilson plot is used to relate the overall heat transfer coefficient (U) to fluid velocity by a double reciprocal plot. Since Reynolds Number (Re) is primarily dependent on velocity (v), a correlation between U and Nu is derived based on the experimental results. The plot between 1/U versus $1/v^{0.8}$ displays a linear relationship for fully developed turbulent flows. Simultaneously the Wilson plot method is applied considering the Dittus-Boelter equations to develop correlations between overall thermal resistance and the Reynolds number.

5.5.1 Results of Wilson Plot Method

The Dittus-Boelter equation is considered for the experimental analysis using Wilson plot. The exponent for prandtle number has been taken 0.4 while the exponent for Reynolds number is assumed to be 0.8 according to the assumptions of Wilson. The overall thermal resistance is expressed as a function of $Re^{0.8}$ considering the experimental data. Figure 5.3 represents the variation of overall thermal resistance with $Re^{0.8}$. as illustrated in figure 5.3, the experimental data represents a linear relationship between R_{ov} and $Re^{0.8}$. The linear regression

fitting with a regression coefficient 0.990 justifies linear relationship. According to the regression fitting of the experimental data, the overall thermal resistance can be given as

$$R_{ov} = 1.081\,\mathrm{Re}^{-0.8} + 0.0005 \qquad (5.18)$$

From the equation for overall thermal resistance obtained from linear regression fit of the experimental data, the values of the constants are found to be C_1 = 0.0005 and C_2 = 1.081. Consequently the coefficient 'C' of the general correlation is evaluated using equation (5.11). Thus the general correlation for inside convection coefficient is found out to be

$$Nu = 0.0266\,\mathrm{Re}^{0.8}\,\mathrm{Pr}^{0.4} \qquad (5.19)$$

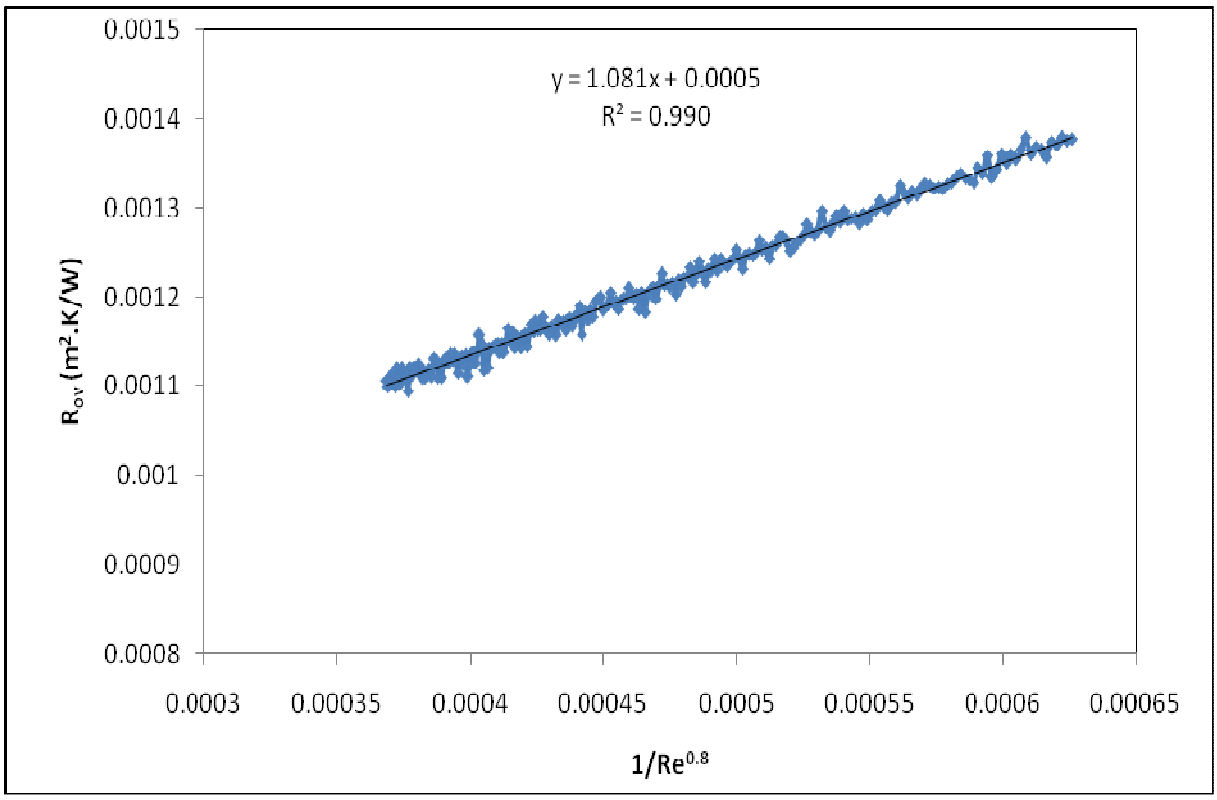

Figure 5.3 : Wilson plot

5.5.2 Results of Modified Wilson Plot Method

The Wilson plot method assumes the exponent of Reynolds number to be 0.8. The modified Wilson plot method uses a modified value of the exponent by applying iteration

procedure as described previously. The value of the exponent of the Reynolds number from the iteration process is obtained to be 0.674. The Figure 5.4 illustrates the variation of overall thermal resistance with $1/Re^{m}$ where 'm' is the modified exponent of Reynolds number. Thus the modified Wilson plot with exponent of Reynolds number m = 0.674 indicates a linear regression line as shown in Figure 5.4. The regression coefficient of 0.99 justifies the suitable fitting of the linear regression line. From the experimental data, the overall thermal resistance can be expressed as

$$R_{ov} = 0.385\,\mathrm{Re}^{-0.674} + 0.0005 \tag{5.20}$$

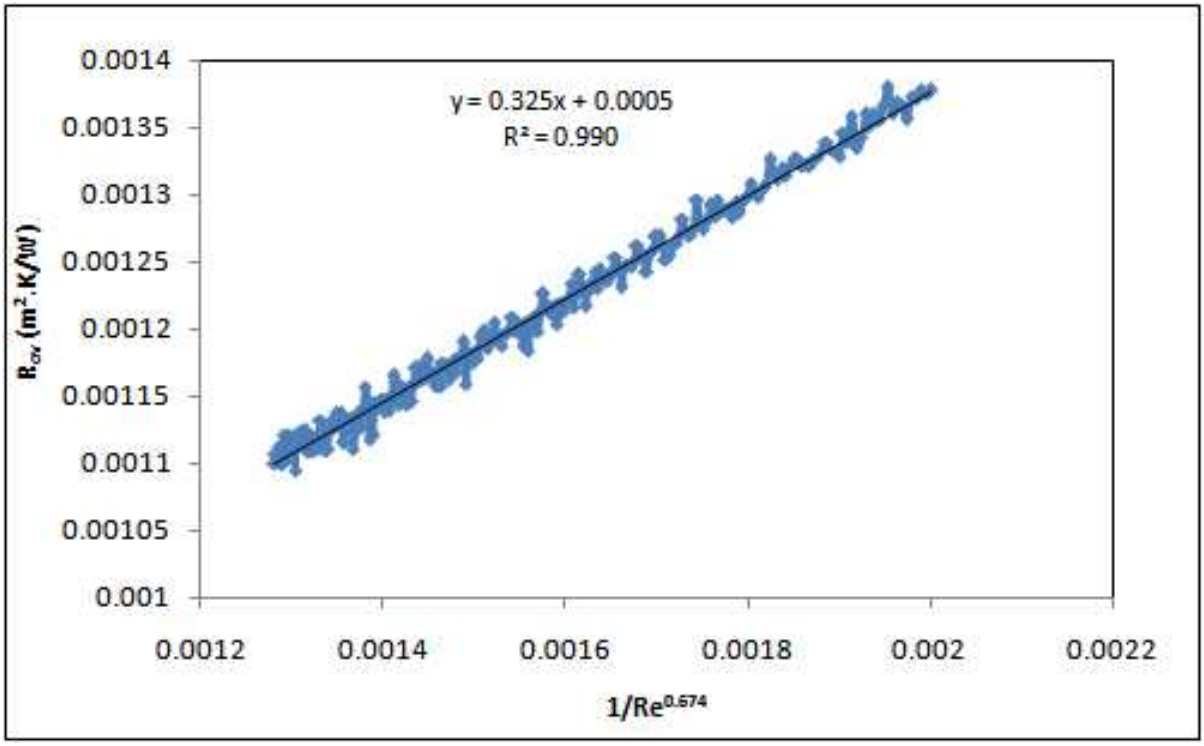

Figure 5.4 : Modified Wilson plot (I)

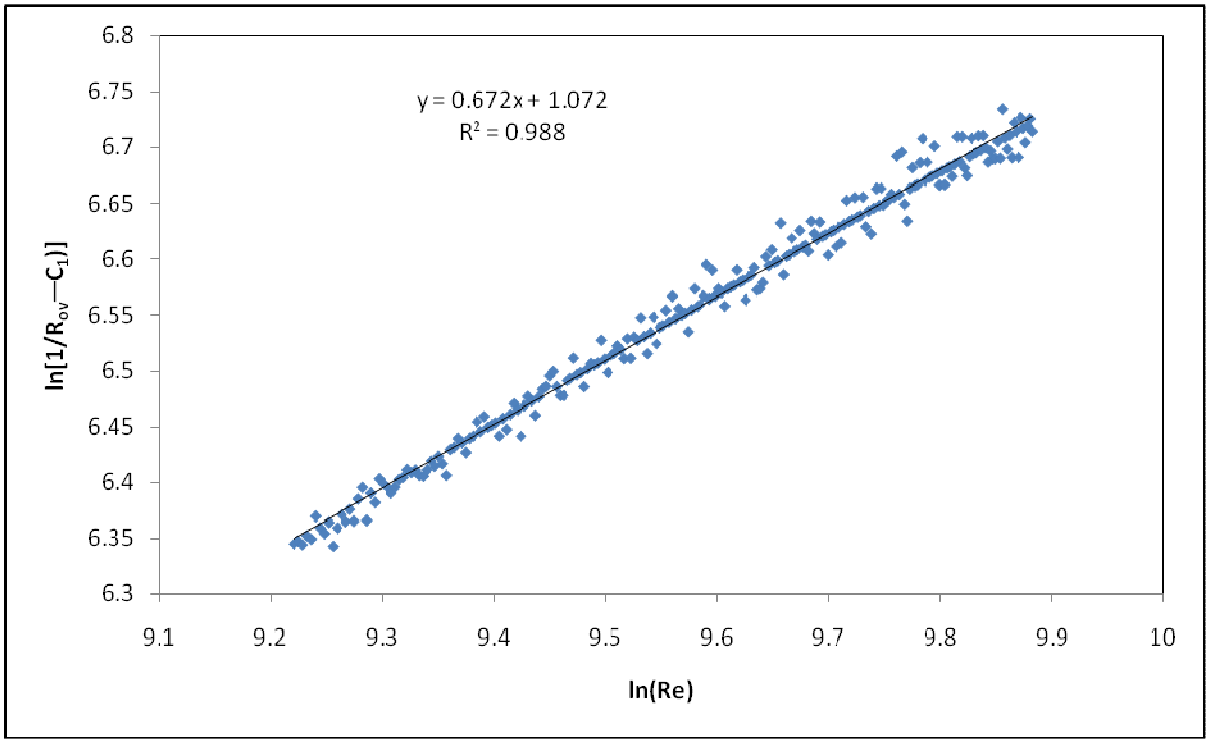

Figure 5.5: Modified wilson plot (II)

It can be observed that the slope of the regression line shown in Figure 5.5 is equal to the exponent of Reynolds number as obtained by the iteration process. Thus by taking into account the experimental data the general correlation for the internal convection coefficient based on modified Wilson plot can be given as

$$Nu = 0.037\,\mathrm{Re}^{0.674}\,\mathrm{Pr}^{0.4} \qquad (5.21)$$

5.5.3 Tube Side Correlations :

For the single pass shell-and-tube heat exchanger, fluid velocity inside the tube ranged from 0.85m/sec to 1.64m/sec. The Reynolds number ranged from 10100 to 19500. The overall heat transfer coefficient (U) is calculated using equation (5.14). By using the Wilson plot method a linear relationship is obtained between 1/U and $1/\mathrm{Re}^{0.8}$ as shown in the Figure 5.6.

Based on the Wilson plot, a double reciprocal plot of U and N_u is plotted. For the operating temperature range of 60°C to 80°C, the changes in Prandtl number and viscosity were

negligible. From the Sieder-Tate equation, it can be concluded that the only significantly changing parameter of Reynolds Number (Re) is the fluid velocity. Therefore, the relationship between 1/U and 1/Nu is also linear as shown in Figure 5.7.

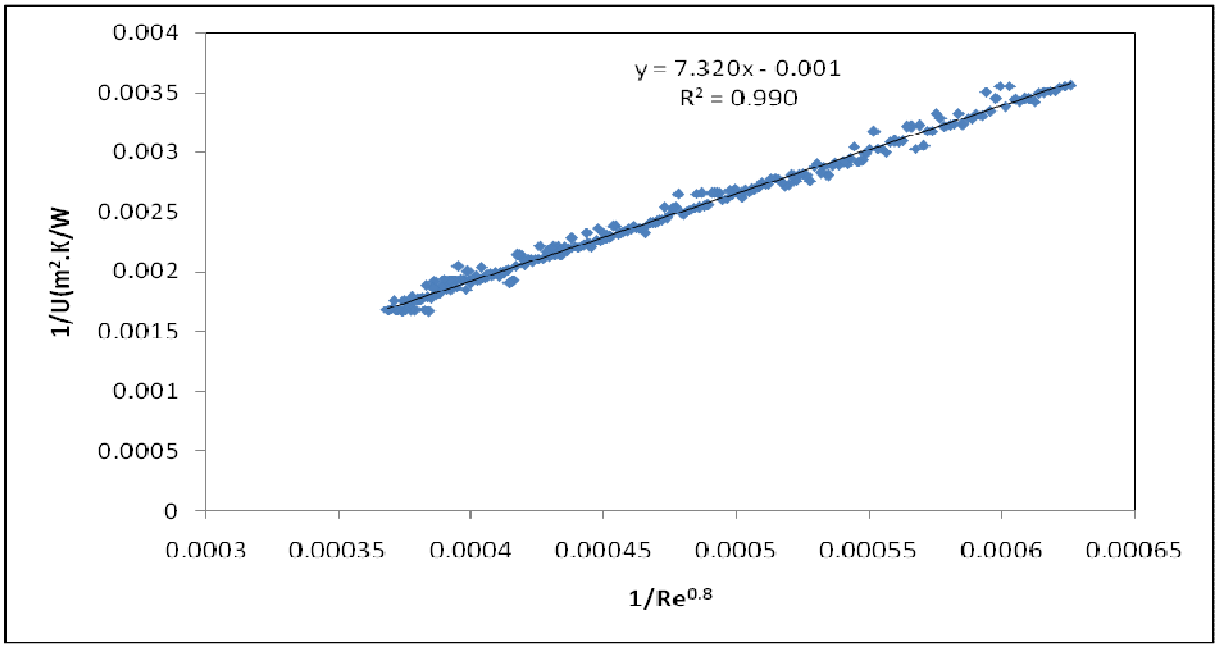

Figure 5.6 : Wilson Plot (Tube side)

As predicted, a linear relationship between the Nusselt number and the overall heat transfer coefficient is observed. Secondly a linear relationship between U and velocity v as predicted by the Wilson plot is observed with experimental results. The coefficient of regression is 0.99 in case of the Wilson plot between U and $Re^{0.8}$ as shown in the figure 5.6 which gives a good resemblance of the experimental results with the prediction.

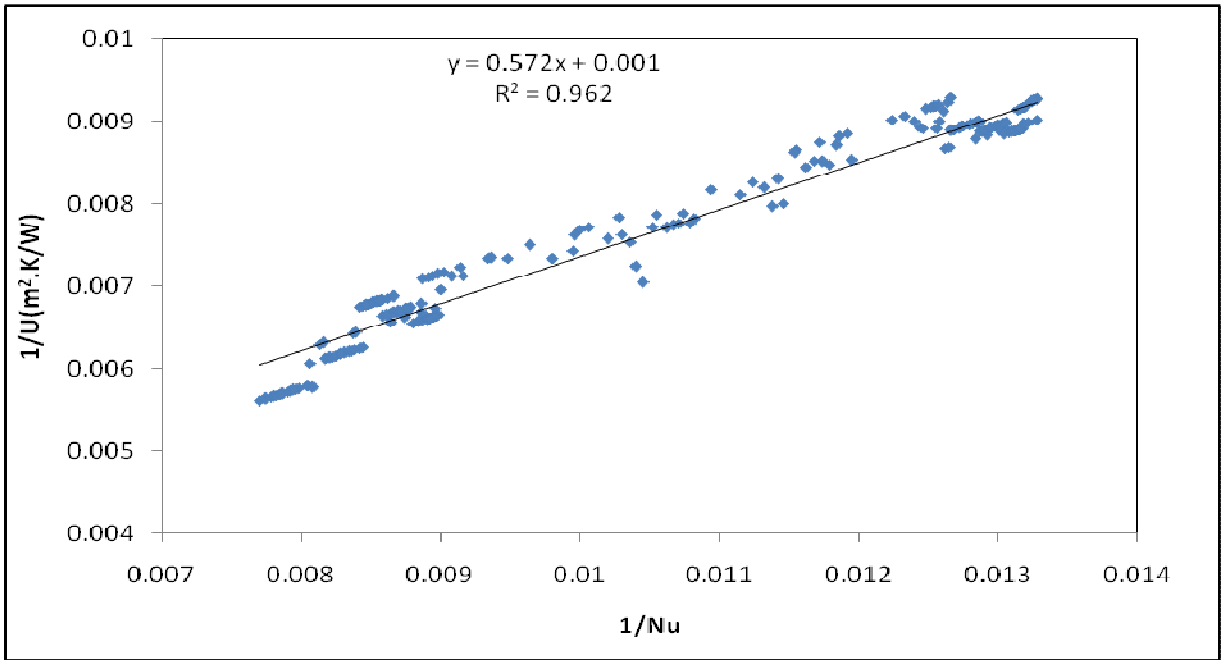

Figure 5.7 : Double Reciprocal Plot of U vs Nu (Tube side)

Similarly the coefficient of regression is 0.96 in the double reciprocal plot of U and Nu. This again satisfies the prediction fairly. By relating velocity to Reynolds number with Nusselt number, a relationship between U and Nusselt number is obtained. From the double reciprocal plot for tube side as shown in Figure 5.7, the overall heat transfer coefficient and Nusselt Number can be related as

$$\frac{1}{U} = 0.5718\frac{1}{Nu} + 0.0016$$

(5.22)

5.5.4 Fouling Performance of the heat Exchanger

The decrease in overall thermal coefficient and consequently the increase on overall thermal resistance is contributed due to the development of fouling layer on heat transfer surfaces of the exchanger. The variation of overall heat transfer coefficient with time is illustrated in Figure 5.8. As discussed in the previous chapter, the critical level of fouling is taken to be 0.00125 m^2.K/W . From the figure 5.6, the critical level of fouling is achieved when the tube side Reynolds number attains a value of around Re = 13260. As illustrated in the Figure 5.5, the overall heat transfer coefficient corresponding to Reynolds number 13260 is

found to be 373.5 W/m^2.K which is 60.25% of the clean design value. This satisfies the criteria of critical fouling condition as in almost all the chemical process industries, the critical overall heat transfer coefficient is considered to be 60 to 65% of the clean overall heat transfer coefficient (Shah, 2003). As indicated in the Figure 5.8, this critical value of overall heat transfer coefficient is attained in 104 days of operation of the exchanger. Similarly, taking into account the modified Wilson plot, the same critical operating condition is attained in 109 days of operation.

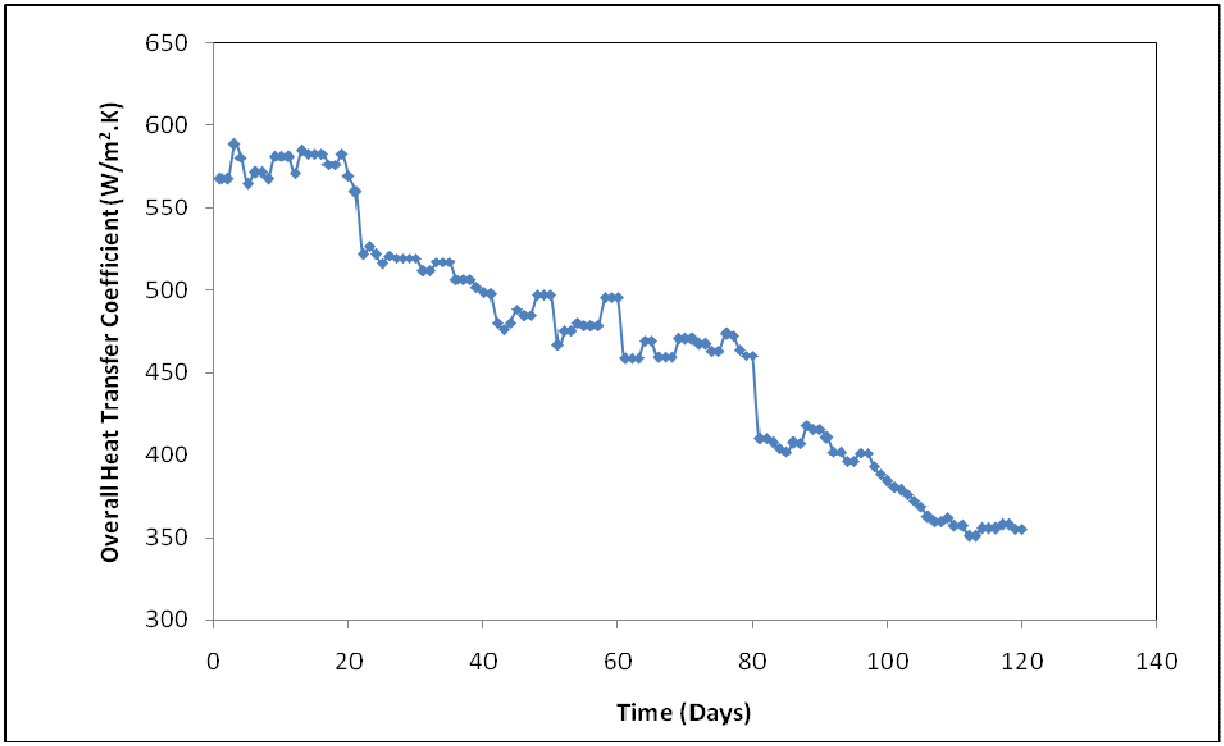

Figure 5.8 : Variation of overall heat transfer coefficient with time

5.5.5 Shell side Correlations :

The Wilson plot method uses the tube side data for investigation of heat transfer performances of a shell and tube heat exchanger. However based on the results of Wilson plot, the correlations for shell side flow can be developed for shell side flow analysis. The variation of overall heat transfer coefficient (U) with velocity for the shell side displays a negative slope because the heat transfer is from the shell side to the tube side. The flow on the shell side is

turbulent. The shell side Reynolds number ranges from 14,000 to 28,800 for square pitch tube arrangements.

Figure 5.9 shows a linear relationship between the overall heat transfer coefficient and the velocity of hot water on the shell side. Since the shell side flow is very much turbulent, the Wilson plot shows a linear relationship between 1/U and $1/v^{0.674}$. The shell side Nusselt number is calculated using Equation (5.17). Since the Nusselt Number (Nu) uses Reynolds Number (Re), the Wilson Plot for the shell side is represented to be a plot between 1/U and $1/v^{0.674}$ .Similar to tube side, the Nusselt number for shell side flow bears a linear relationship with the overall heat transfer coefficient (U). A double reciprocal plot of U and Nu for the shell side illustrated in the Figure 5.10 shows a linear relationship.

Similarly for the shell side the overall heat transfer coefficient and Nusselt Number can be related from the double reciprocal plot as shown in the Figure 5.10. The double reciprocal plot of U and Nu illustrates a linear relationship with a regression coefficient of 0.933 which justifies the experimental results. Thus the overall heat transfer coefficient and the Nusselt number can be correlated as

$$\frac{1}{U} = -0.849\frac{1}{Nu} - 0.002$$

(5.23)

As there is a heat transfer from the tube side to the shell side, there is a loss of heat occurring in case of tube side fluid while there is a gain of heat for the shell side fluid. Due to this, the plot between U and Nu is having a positive slope for the tube side flow and the same plot for shell side fluid is having a negative slope.

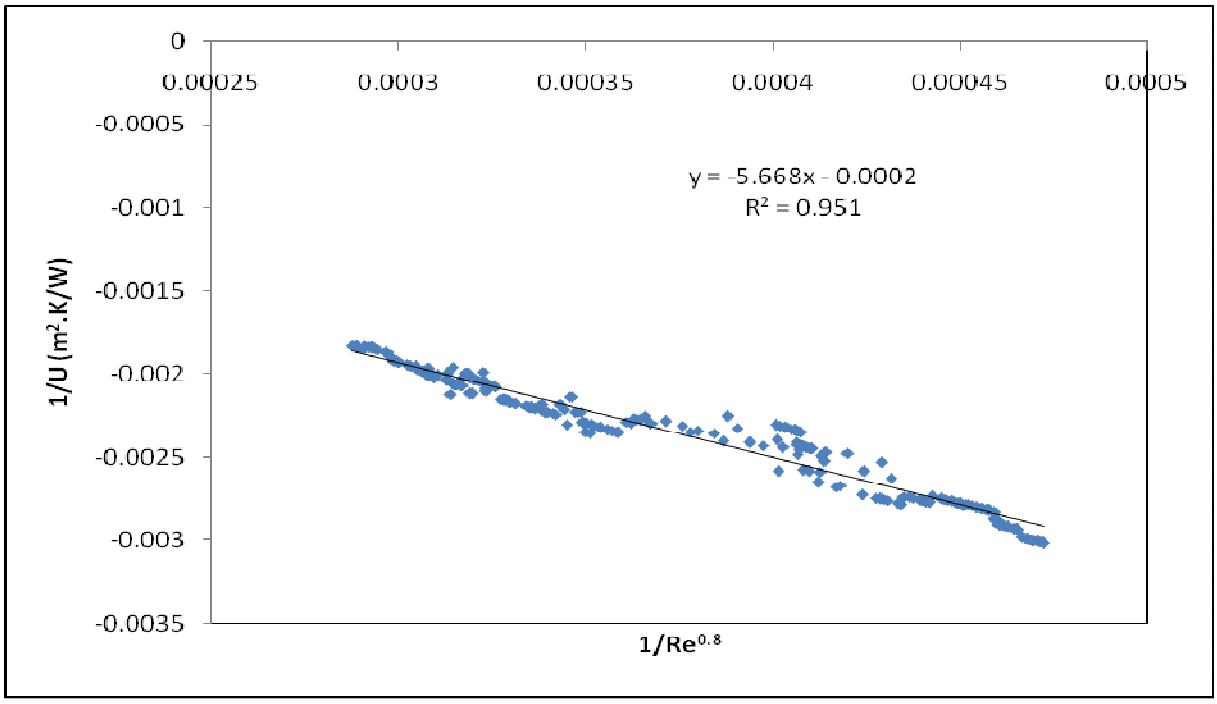

Figure 5.9: Wilson Plot (Shell side)

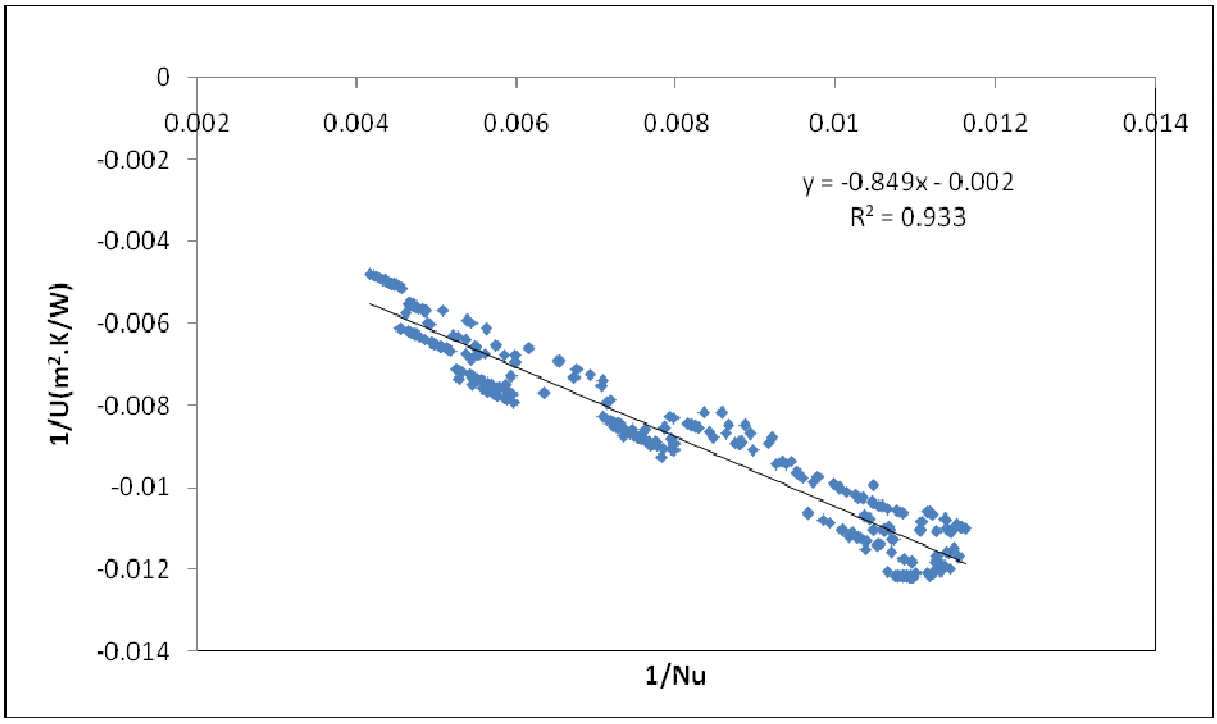

Figure 5.10 : Double Reciprocal Plot of U vs Nu (Shell side)

5.6 Summary

The calculation of convection coefficients constitutes a crucial issue in designing and sizing any type of heat exchange device. This chapter presents an overview of the Wilson plot method and its modifications to obtain correlations for the overall heat transfer coefficient and Nusselt number. This method deals with the determination of convection coefficients based on experimental data and the subsequent formulation of appropriate correlation equations. Based on the experimental results, a correlation between the overall heat transfer coefficient and Nusselt Number is developed both for the tube side and shell side flow by using Wilson plot method. The correlations developed are applicable for turbulent flow both inside the shell and the tubes as the Reynolds number was within a range of 10100 to 19500 on the tube side while it was within a range of 14000 to 28800 on the shell side. Thus the Wilson plot method and the modified version of the Wilson plot method have been used as a tool for the analysis of heat transfer in both the shell and the tubes of a shell and tube heat exchangers.

Chpater 6

An Integrated approach for Monitoring of Fouling by C-Factor Method

The objective of this chapter is to develop a methodology by which the fouling and its thermo-hydraulic effects on a heat exchanger can be quantified easily and accurately. In the previous chapter, the Wilson plot method was used for thermal analysis of overall heat transfer coefficient from the experimental data. This chapter takes into account the pressure drop along with the overall heat transfer coefficient by introducing a novel factor for monitoring of fouling in a shell and tube heat exchanger known as C-factor. The C-factor gives an indication of the extent of fouling on the heat transfer surface which cannot be estimated from the outside of the exchanger body.

6.1 Introduction

The fouling layers deposited on the heat transfer surfaces due to accumulation of unwanted materials such as scale, organic compounds, corrosion products, particulates or other deposits degrade the heat exchanger performance over time as compared with clean conditions at start up. Simultaneously cross sectional flow area reduces due to fouling resulting in increased pressure drop. To enforce compliance with critical pressure and operational criteria, heat exchangers must be cleaned often, according to a regular maintenance schedule (Bott, 1995). However, unnecessary cleaning leads to system downtime and waste of water and chemicals, which increases costs and causes ecological problems. Therefore the cleaning schedule should be optimal so that the exchanger can run for a maximum possible period without hindering the efficiency of the plant. The scheduling of cleaning interventions can be based on the prior knowledge of the time behaviour of the thermal resistance deposits in the individual exchanger (Crittenden et. al., 1987; Crittenden et. al. 1992). This is possible if the operating parameters have been measured and recorded during previous production methods.

Monitoring fouling and the consequent cleaning processes can provide useful information for operational decision- makers in processing plants in order to avoid risk of running the plant with far less efficiency which can further lead to shut down of the plant. Secondly fouling is usually not visible from outside the industrial processing equipment. Hence

a direct method of measurement of the fouling developed on the heat transfer surfaces of a heat exchange device is almost impossible. This can only be ascertained and quantified from its effects on various performance parameters of a heat exchanger (Lalande et. al., 1989). Fouling of a heat exchanger is studied mainly to protect the heat exchanging surface so that an un-interrupted operation of the heat exchanger can be achieved without remarkable degradation in its performance (Lalot, 2006). The objective of this chapter is to alert the user before a significant degradation of the heat exchanger occurs. This gives the indication when the preventive maintenance can be carried out so that the life time of the device can be increased efficiently. As fouling cannot be completely avoided, it can be monitored. Through proper monitoring, problems due to fouling can be detected long before the economics of the process are threatened and necessary remedies can be adopted.

Heat exchanger monitoring methods range from the very simple to the very complex (Teruel et. al., 2005). The simplest form of monitoring has always been to open up exchangers at a turnaround and look for fouling or corrosion. This method is a final report on the success or failure of a program. However, by the time it is implemented, it may be too late. The plant may have been running inefficiently or even have been forced to shut down if there was a problem. This method gives no indication of when or why a problem happened, which makes troubleshooting difficult. Among other methods, the ultrasonic guided wave and acoustic impact methods for pipe fouling detection may be used as a technique for monitoring of fouling (Lohr and Rose, 2003). The fouling monitoring can also be carried out by comparing the terminal temperature differences. This method uses the difference between the hot fluid outlet temperature and the cold fluid outlet temperature as a measure of the fouling (Negrao et. al., 2007). Also the difference between the hot fluid outlet temperature and the cold fluid inlet temperature known as the approach temperature can be used as a valuable tool for fouling measurement of multipass heat exchangers. However the major drawback of these techniques is mainly due to limited number of sensors which can detect only localized fouling. Although these temperatures can be useful for trending, but there are many factors that can affect this calculation including variable process heat loads, different temperature levels in different operating conditions and even the accuracy of thermocouples used.

In practice the most complete and thorough method of measuring heat transfer efficiency and fouling of a heat exchanger uses the overall heat transfer coefficient and fouling

factor. This method uses both the hot and cold side data to determine the overall efficiency of the exchanger in terms of various performance parameters (Zubair et. al., 2000). But unfortunately the thermal analysis does not give clear information regarding the fouling formation as it is too much complex to distinguish between the cold and hot fluid side fouling. Secondly the changes in hot fluid characteristics due to variation in operational conditions make it almost impossible to compare the results meaningfully.

All of these shortcomings lead to the thought of introducing a new parameter that can provide the most reproducible and consistent results while being easy to calculate. The aim of this chapter is to introduce such a factor called the C-factor which can be utilized to predict the fouling formation effectively.

The C-factor concept comes from the equation for flow through an orifice of a fixed size and shape. An orifice plate for measuring the volumetric flow rate uses the Bernoulli's principle which states that there is a relationship between the pressure of the fluid and the velocity of the fluid. When the velocity increases, the pressure decreases and vice versa. A fluid passing though an orifice constriction will experience a drop in pressure across the orifice. This change can be used to measure the flowrate of the fluid. Applying Bernouli's equation to a streamline traveling down the axis of the horizontal tube gives,

$$\Delta P = P_1 - P_2 = \frac{1}{2}\rho\left(v_2^2 - v_1^2\right) \tag{6.1}$$

where 1 is the location upstream of the orifice and 2 is downstream of the orifice. Since the pressure at 1 will be higher than the pressure at 2 for flow moving from 1 to 2, the pressure difference as defined will be a positive quantity. From continuity, the velocities can be replaced by cross-sectional areas of the flow and the volumetric flowrate.

$$V = \sqrt{\frac{2\Delta P}{\rho}} \frac{A_2}{\sqrt{1-\left(\frac{A_2}{A_1}\right)^2}} \tag{6.2}$$

Since the actual flow profile at location 2 downstream of the orifice is quite complex, thereby making the effective value of A_2 uncertain, the flow rate can be expressed in terms of a flow

coefficient (C_f) and the area of orifice (A_o). As a result, the volumetric flow rate for real flows is given by the equation

$$V = C_f A_o \sqrt{\frac{2\Delta P}{\rho}} \tag{6.3}$$

For a particular geometry of the orifice and flow regime, the volumetric flow rate can be expressed in terms of ΔP. Thus

$$V = C\sqrt{\Delta P} \tag{6.4}$$

This equation is applicable for fixed size orifices where "C" is the constant for that orifice. Unfortunately, in cooling water systems of a heat exchanger, the tubes don't always stay clean, so the value of C can change. Back-calculating for C will show if a change in orifice coefficient has taken place. That indicates if fouling has occurred. The C-factor measures both tube plugging in a multiple-tube exchanger and uniform fouling. The value of C-factor decreases as fouling.

6.2 Theoretical Framework for Interpretation of Fouling:

Fouling can be determined by measuring the increase in overall heat transfer resistance, which is the major concern in heat exchangers. The overall heat transfer resistance is the sum of conductive and convective heat transfer resistance. For a clean tube, at time t = 0, the conductive resistance of the deposit is zero so that the convective resistance is equal to the overall heat transfer resistance. At any time, t > 0, the relative contribution of conductive and convective resistance to overall heat transfer resistance will depend on the type of deposit accumulated on the heat transfer surface.

Regardless the type of fouling process the net mass fouling rate is the difference between the foulant deposit rate m_d and the foulant reentrainment rate m_r. hence the mass of foulant deposited on the heat transfer surface over a given period of time can be expressed as

$$\frac{\partial m(s,t)}{\partial t} = m_d(s,t) - m_r(s,t) \tag{6.5}$$

where s denotes the spatial dependence of the mass of foulant. But as the deposition rate is spatially non-uniform and time dependant, equation (6.1) can be reformulated in terms of mass per unit heat transfer area for a uniform spatial distribution of deposit (Brahim et. al., 2003).

$$\frac{dM}{dt} = M_d - M_r \tag{6.6}$$

Furthermore mass per unit heat transfer area considering uniform distribution of fouling along the heat transfer surface can be expressed as

$$M_A = \rho_f \delta_f = \rho_f k_f R_f \tag{6.7}$$

The fouling factor R_f represents the thermal resistance of the foulant layer deposited for a unit area of the heat transfer surface. Consequently fouling rate can be specified as

$$\frac{dM_A}{dt} = \rho_f \frac{d\delta_f}{dt} = \rho_f k_f \frac{dR_f}{dt} \tag{6.8}$$

It is assumed that both the mass density and the thermal conductivity are invariant with time. Hence the equation (6.4) becomes

$$\frac{dR_f}{dt} = R_d - R_r \tag{6.9}$$

where $R_d = M_{A,d} / \rho_f k_f$ represents the fouling resistance rate for deposition while $R_r = M_{A,r} / \rho_f k_f$ represents the fouling resistance rate for removal.

The relationship between overall heat transfer coefficient based on tube outside surface area and thermal resistance for a clean heat exchanger can be defined as

$$\frac{1}{U_c} = \frac{1}{h_{o,c}} + R_w \frac{A_o}{A_w} + \frac{1}{h_i} \frac{A_o}{A_i}$$

(6.10)

Similarly for a fouled heat transfer surface the above relation is defined as

$$\frac{1}{U_f} = \frac{1}{h_{o,f}} + R_f + R_w \frac{A_o}{A_w} + \frac{1}{h_{i,f}} \frac{A_o}{A_i}$$

(6.11)

The model is idealized with the assumptions that $h_{o,c} = h_{o,f}$ and $h_{i,c} = h_{i,f}$ to calculate the overall thermal resistance due to fouling (Shah, 2003).

$$R_f = \frac{1}{U_f} - \frac{1}{U_c}$$

(6.12)

The overall surface area of the heat exchanger "A" is computed from the relation between the differential surface area "dA", the local heat flow dQ and the local temperature difference as (Takemoto et. al., 1999)

$$A = \int_0^A dA = \int_0^Q \frac{dQ}{U(T-t)}$$

(6.13)

So the heat transfer rates for same heat exchanger under fouled and clean condition is

$$Q_f = U_f A \Delta T_{lm}$$

(6.14)

$$Q_c = U_c A \Delta T_{lm}$$

(6.15)

Hence the heat transfer rates can be related with fouling resistance as

$$\frac{Q_c}{Q_f} = U_c R_f + 1$$

(6.16)

Thus the loss of heat transfer due to development of fouling layer is

$$Q_c - Q_f = \frac{U_c R_f}{1 + U_c R_f} Q_c$$

(6.17)

This clearly shows that fouling has a significant impact on the heat transfer performance of a heat exchanger. Thus from fouling point of view the performance index of a heat exchanger can be expressed in another term known as cleanliness factor (CF) which is defined as

$$CF = \frac{U_f}{U_c} = \frac{1}{1 + R_f U_c}$$

(6.18)

The cleanliness factor (CF) can be used as a performance index of a fouled heat exchanger.

Although the C-factor is not designed to be correlated with fouling factor, but it is quite instructive to express the C-factor as a measure of fouling factor. The concept of C-factor comes from the analysis of flow through an orifice. The flow through an orifice of fixed size and shape is expressed as

$$V = C\sqrt{\Delta P}$$

(6.19)

This equation is valid for an orifice of fixed size and C is constant for the orifice. But in almost all practical applications of a heat exchanger, the tubes don't always remain clean. The variation of the flow area due to deposition of fouling layer on its surface causes an obstruction in fluid flow through it for which the value of C constantly changes in an unpredictive manner. Hence to predict the formation of fouling a back calculation of C-factor plays an important role which shows the change in orifice coefficient that has taken place due to fouling. The C-factor measures both tube plugging in a multiple pass shell and tube heat exchanger and uniform fouling. The value of C decreases significantly with the development of fouling layers on the tube surfaces.

As the fouling formation is not uniform over the tube surfaces, an accurate calculation and prediction of actual fouling is too much complex. Hence it is assumed to be uniform fouling over the tube surfaces that gives an approximate analysis of the fouling development by this method of using C-factor. When fouling layers develop on the tube surface, the effective diameter of the tube decreases. For a given flow, the pressure drop increases by the fifth power of the ratio of clean diameter to the fouled diameter (Shah, 2003).

$$\frac{\Delta P_f}{\Delta P_c} = \left(\frac{d_c}{d_f}\right)^5$$

(6.20)

Hence though the fouling layer is a very thin film, it can give a remarkable impact on the functioning of the heat exchanger.

6.3 Experimental Methods

The objective of this work is to find out accurate results on fouling resistances in a shell and tube heat exchanger and determine the effect of fouling on the heat transfer performance.

Experiments were conducted on a 1-1 shell and tube heat exchanger as described earlier in the section 3.5.1. The cold water was allowed to flow through the tubes while the hot water in the annular space between the shell and the tubes in counter-current direction. The attached rotameters were used to measure both the hot and cold water flow rates. The inlet and outlet temperatures for both the hot and cold fluids were measured with thermocouples and read from a digital temperature indicator. The experimental data was taken corresponding to steady state for a particular flow rate when the inlet and outlet temperatures of both the hot and cold fluids remain invariant.

The calibration of the thermocouples was performed using a mercury thermometer which showed that maximum temperature uncertainty was 0.1^0C. Similarly by calibrating the rotameters, it was determined that the mass of fluid flow uncertainty was ±1%. The flow measuring rotameters were calibrated by using a Doppler flow meter.

This chapter introduces the C-factor principle which is quite effective in carrying out the detection of fouling in industrial equipments without much additional instrumentation. Although some special instrumentations are required, but the cost can be justified by the predictive value of this method. Once a critical heat exchanger is identified for the application of C-factor principle, the measurements required for analysis are the flow rate and pressure differential. For measurement of pressure differential a single or differential pressure gauge is mounted on the heat exchanger under consideration. By using small diameter tubes, fluid is tapped into each line and then both are connected to a single or differential pressure gauge to measure the pressure differential. The use of a single or differential pressure gauge is advantageous rather than two separate gauges to measure the pressure diffential.

- As there is only one measurement, therefore no much cumbersome calculations are required.
- Only one instrument needs to be calibrated for better accuracy of the system.
- No correction is required for different elevations.
- A differential pressure gauge can be suitably set up for continuous monitoring.

The accuracy in flow measurement affects the usefulness of the C-factor. The flow is measured by using a rotameter. Once the flow and differential pressure are known, the C-factor can be easily determined by using the mathematical formula.

6.4 Results and Discussion

The experiments were conducted over a time span of 240 days from October 2008 to April 2010. The changes in the four major characteristic temperatures at the inlet and outlet of the heat exchanger at a constant mass flow rate were recorded.

During the initial phase of experimental work, the hot water flow rate was almost constant within a range of 387 to 394.5 kg/hr. This small variation was due to variation of density of water with temperature for constant volumetric flow rate. The inlet temperature of the hot water was maintained at different values between 40^0C to 65^0C with an interval of 5^0C. The difference of the inlet and outlet temperature of the hot water varied from 5.4^0C to 7.2^0C through the experimentation. The cold water flow rate practically maintained constant at about 296.8kg/hr as the variation of density was very small. The cold water inlet temperature was within 22^0C to 26^0C with an increase of about 6.6^0C to 8.6^0C at the outlet.

As mentioned earlier in section 4.3.3, only those experimental run were treated acceptable for which $\Delta_Q \leq 10\%$ and $(\Delta U_m/U_m) \leq 20\%$. Figure 6.1 represents the variation of experimental value of overall heat transfer coefficient with respect to time. The initial value of overall heat transfer coefficient at the start of experimental work was about $U_c(t=0) = U_m(t=0) = 596 W/m^2K$, whereas after 240 days of operation it reduced to around $285 W/m^2K$. The clean overall heat transfer coefficient is the initial value of overall heat transfer coefficient corresponding to t = 0.

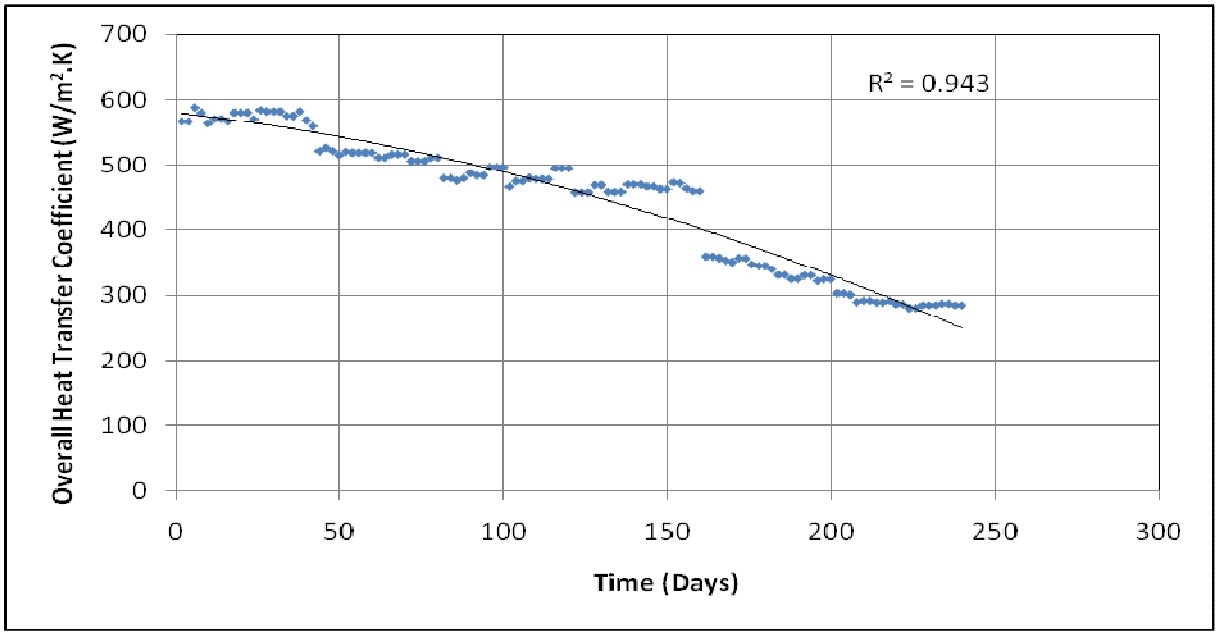

Figure 6.1 : Variation of Overall Heat Transfer Coefficient with Time

Figure 6.2 represents the values of overall fouling resistance as a function of time. During the period of experiments spanning over 240 days, the overall fouling thermal resistance increased from 8.72×10^{-5} to $2\times10^{-3}m^2K/W$ showing an increase of around $1.913\times10^{-3}m^2K/W$. The normal tap water used for this experimental work by chemical analysis was found to have a hardness of around 200-250mg/liter. Since the hardness of water is contributed mostly due to salts of calcium it is assumed that the fouling process is primarily crystallization fouling. Hence a linear behaviour of fouling is assumed. From the figure 6.2 a linear function that describes the dependence of overall fouling resistance with time can be expressed as

$$R = 2\times10^{-5}t - 0.0001 \quad (6.21)$$

The regression coefficient for this curve is 0.9515 which shows a good resemblance of the relation with the experimental results.

The experimental observations for overall heat transfer coefficient and fouling resistance as shown in figure 6.1 and 6.2 indicate unusual patterns near 120days and 160 days from starting of experimental observation. The irregularities in the overall heat transfer coefficient and fouling resistance with time are mostly due to the interruption in the operation of the exchanger. The unusual variations in the fouling correspond to system shut downs, start

ups and other transient operating conditions. Besides trapping of air inside the surface deposits during shut downs may contribute to the sharp variation of fouling resistance with time.

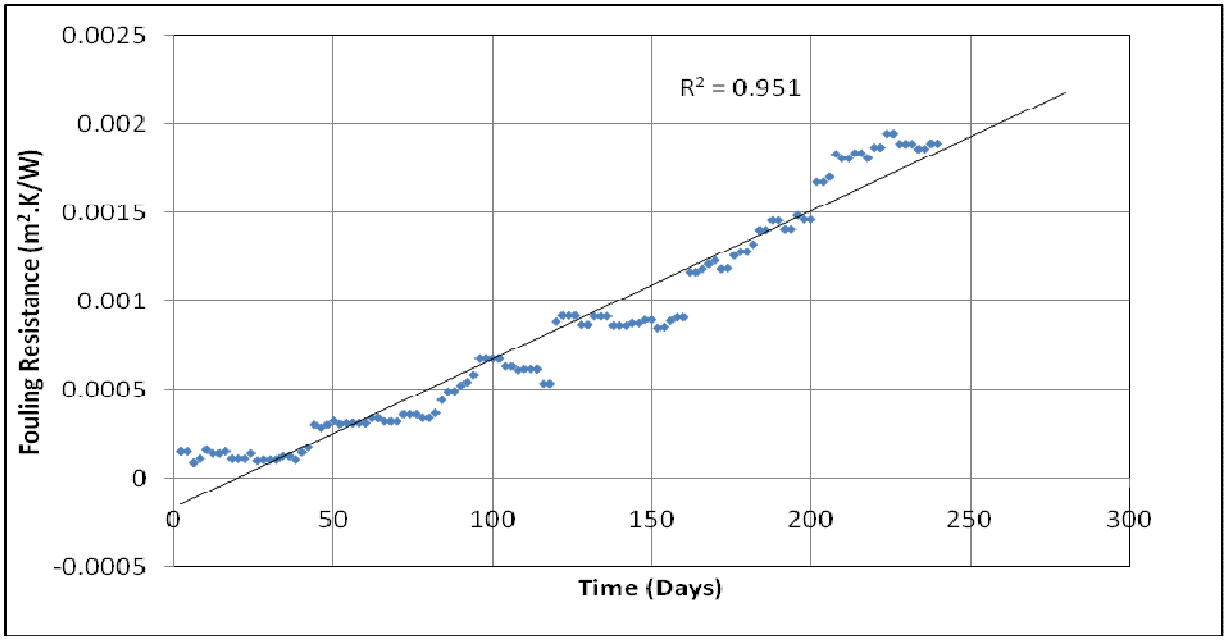

Figure 6.2 : Variation of Overall Fouling Resistance with Time

The observations clearly indicate positive initial value of fouling resistance with time. The minimum value of fouling resistance at the start of observation is 0.00011m^2.K/W. The Figure 6.2 indicates that within the initial periods of observation, the rate of fouling development is very slow and afterwards it increases sharply as compared to initial period. The fitted curve just gives an appearance of negative fouling rate. The correlation between fouling resistance and time indicates a negative value of fouling at the initiation stage. However in actual practice, the fouling resistance at the beginning of operation of a heat exchanger is not negative. It is of very small magnitude and it almost remains constant at the initial phase. The increase in overall heat transfer coefficient at the beginning phase is often considered as negative fouling. Sometimes relatively small amounts of deposit can improve heat transfer, relative to clean surface, and give an appearance of negative fouling rate and negative total fouling amount. Negative fouling is often observed under nucleate-boiling heat-transfer conditions when deposit improves bubble nucleation or forced-convection if the deposit

increases the surface roughness and the surface is no longer hydraulically smooth. After the initial period of surface roughness control, the fouling rate usually becomes strongly positive.

According to TEMA standards (1988), the fouling thermal resistance is 0.53×10^{-3} m^2K/W for hard water having hardness of 200-250mg/l. On comparing the measured data with that of TEMA standards it is observed that TEMA fouling thermal resistance is achieved after 98 days. This indicates that after about 3.5 months of continuous use of a heat exchanger in a process plant where the hardness of water is around 200-250mg/l would fall below its designated heat duty and has to be cleaned for better performance.

The cleanliness factor, CF, is an alternate measurement of relative degradation in exchanger performance. The CF is close to 1.0 for a clean exchanger and decreases over time as the exchanger fouls. Figure 6.3 indicates the cleanliness factor of the heat exchanger at different times of operation. It is observed that the CF value decreases from 0.96 to around 0.45 during the period of observation spanning over 240 days. The CF varies linearly with time of operation with a negative slope.

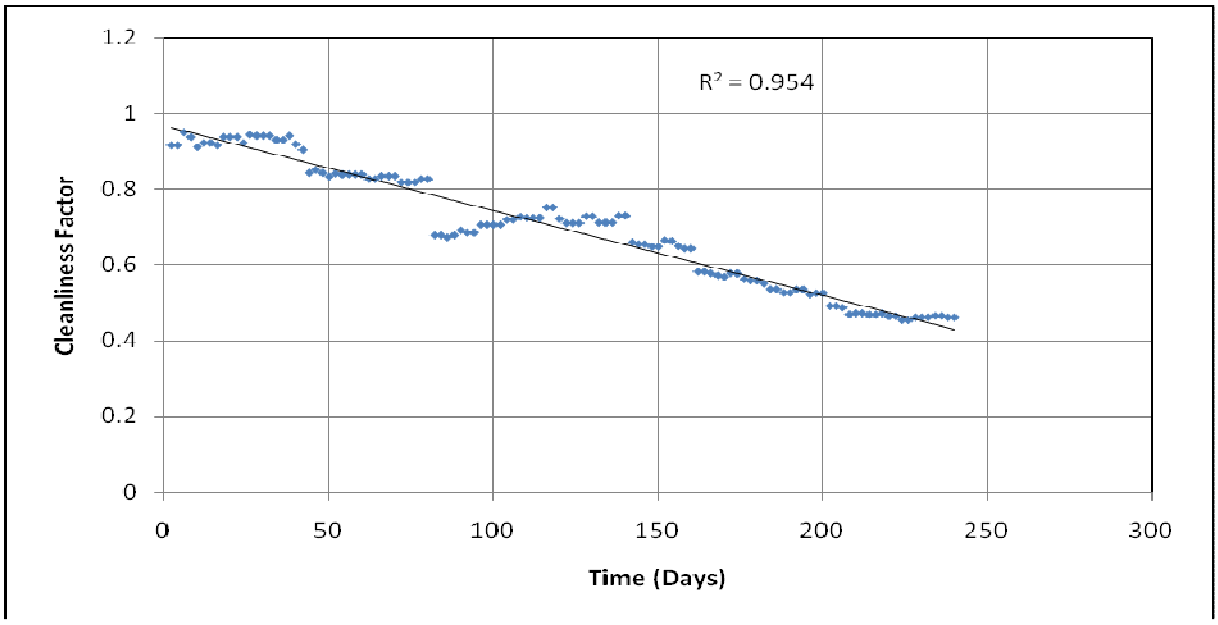

Figure 6.3: Cleanliness Factor as a function of Time

The second phase of the experimental work involved the application of C-Factor for quantification of the fouling effects in the heat exchanger under consideration. The design specifications of the heat exchanger show a flow rate of 2700LPH with a pressure drop of

7.6kPa for the fluid flowing through the tubes. Hence the C-factor corresponding to design specifications is calculated to be

$$C = \frac{V}{\sqrt{\Delta P}} = \frac{2700}{\sqrt{7.6}} = 980$$

(6.22)

First of all pretreatment was done by circulating a cleaning solution of polyphosphate, surfactant, and antifoam to remove light rust, calcium carbonate scale and hydrophobic materials deposited on the tube surface. The temperature was maintained at 60-80°C and the pH was controlled in the range of 5.5-7.0. With this clean exchanger, the maximum value of C-factor was found to be 960.4 which is around 98% of the clean design value. Simultaneously the C-factor value got reduced to 348 during a period of 240 days which is around 36% of the clean design value. Correspondingly, for a flow rate of 600 LPH along the tubes, the pressure drop increased from 0.4 kPa to 3 kPa. The variation of the C-factor during the period of experimentation is illustrated in Figure 6.4. This indicates that there is a significant increase in pressure drop and decrease in flow rate which resulted from the obstruction in passage due to development of fouling layer on

the tube surfaces.

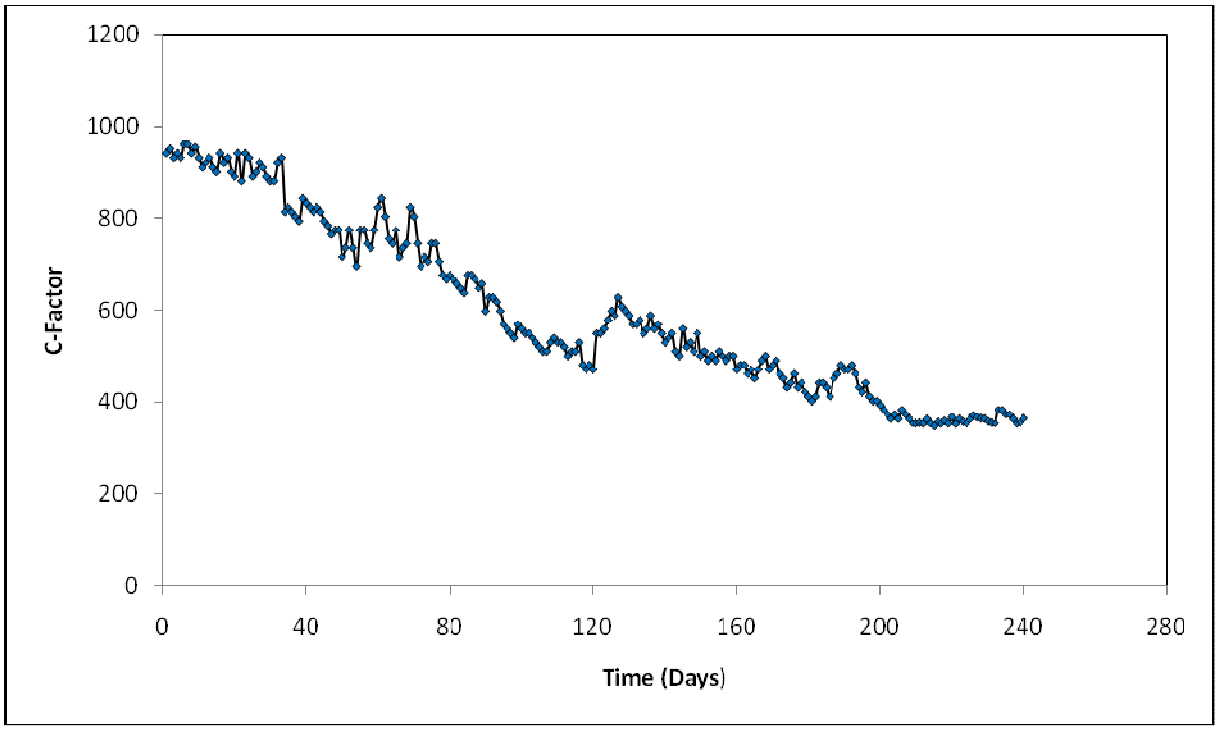

Figure 6.4 : Variation of C-Factor with Time

Considering the heat transfer performances of the exchanger, the C-factor value falls to 490 which is 50% of the clean design value, when the overall heat transfer coefficient attains 60% of the clean design value. Thus 50% of the design C-factor value has been taken to be the critical operating condition. The variation of C-factor indicates that it reaches a value of 490 which is 50% of the clean design value during a period of 114 days from start of operation. However the critical operating condition can be specified depending on the specific requirements and operating conditions of a process industry.

The most widely used and conventional method for study of fouling in a heat exchanger is the investigation of overall heat transfer coefficient and fouling resistance. The Figure 6.5 indicates the fouling behavior of the exchanger with C-factor, overall heat transfer coefficient and fouling resistance. At the beginning stage of experimentation, when the exchanger is under clean condition, the C-factor is around 98% of the clean design value while the overall heat transfer coefficient is around 96% of the clean design value. Simultaneously the fouling resistance was at the lowest value of $0.00056 m^2.K/W$. During the span of the experimental work, the C-factor gets reduced to 350 which is around 36% of the design value. Correspondingly, the overall heat transfer coefficient drops to 280 indicating a drop of 55% of the design value and the fouling resistance increases to $0.0039\ m^2.K/W$. This clearly indicates that C-factor is an indicative parameter for performance estimation of a heat exchanging equipment subjected to fouling.

In a similar manner, it can be shown that the C-factor can be used as an indicative parameter to specify the cleanliness factor and hence the operating condition of a heat exchanger subjected to fouling. As illustrated in Figure 6.6, the C-factor is found to be 882 while the cleanliness factor is approximately 80% of the designed clean value. When the exchanger is fouled, the cleanliness factor drops down to 34% and simultaneously the C-factor reduces to 425 which is around 43% of the designed value. Hence the C-factor can be used as an indicative parameter to specify the cleanliness factor and hence the operating condition of a heat exchanger subjected to fouling.

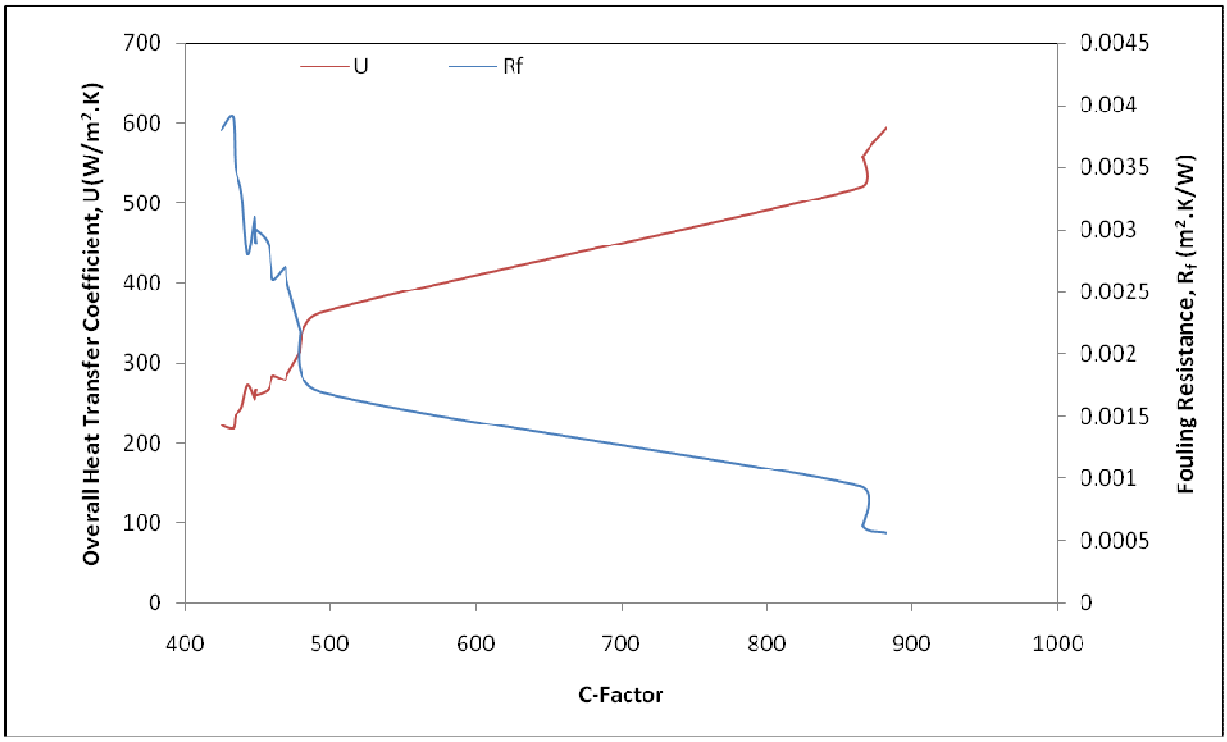

Figure 6.5 : Variation of Overall heat transfer coefficient(U) and Fouling resistance(R_f) with C-Factor

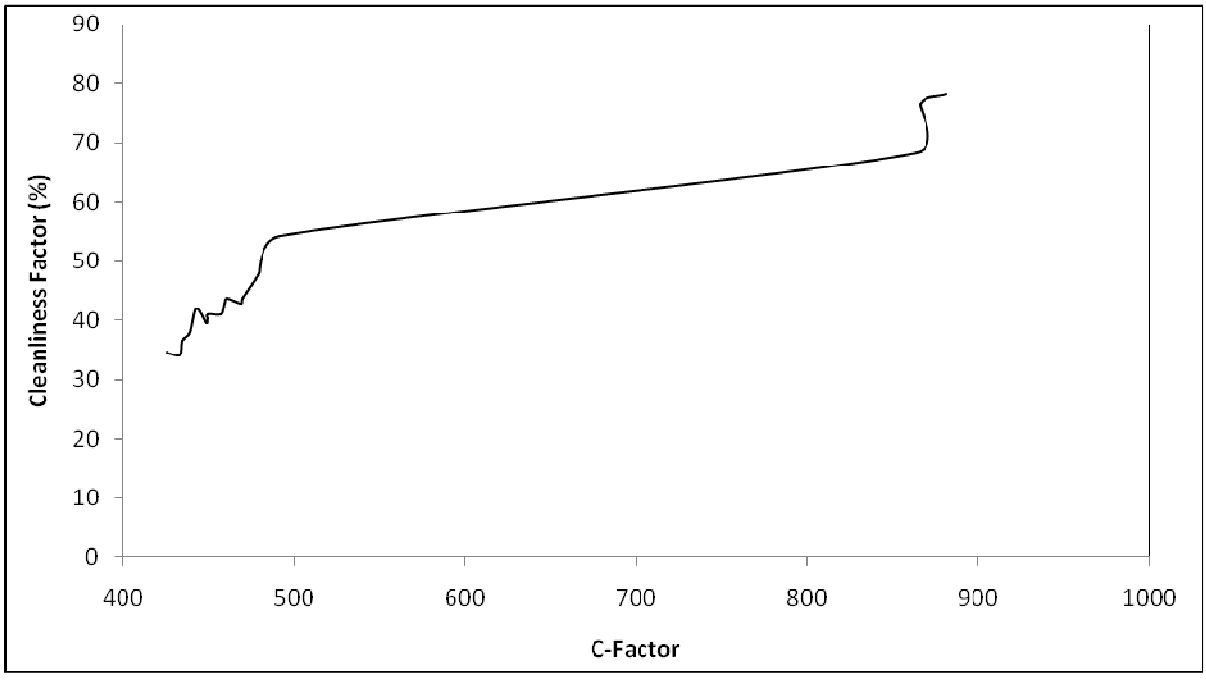

Figure 6.6 : Variation of cleanliness factor (CF) with C-Factor

The C-factor can be correlated to fouling factor by considering a uniformly thick layer of fouling on the tube surface. The fouling behaviour of the exchanger is illustrated in Figure 6.7 and Table 6.1. This indicates the performance of the exchanger corresponding to different values of fouling factor. In general, the expected fouling factor is 0.003 which is considered as dirty value for design calculations in almost all chemical process plants. At this dirty level of fouling, the C-factor got dropped by 45% of the deign value. For a fouling factor value of (f) 0.002, the C-factor dropped by 28% from the designed value. Though this is an exemplary value of the exchanger considered for analysis, but the correlation for any specific exchanger in field application can be calculated by using commercially available packages such as Hextran program.

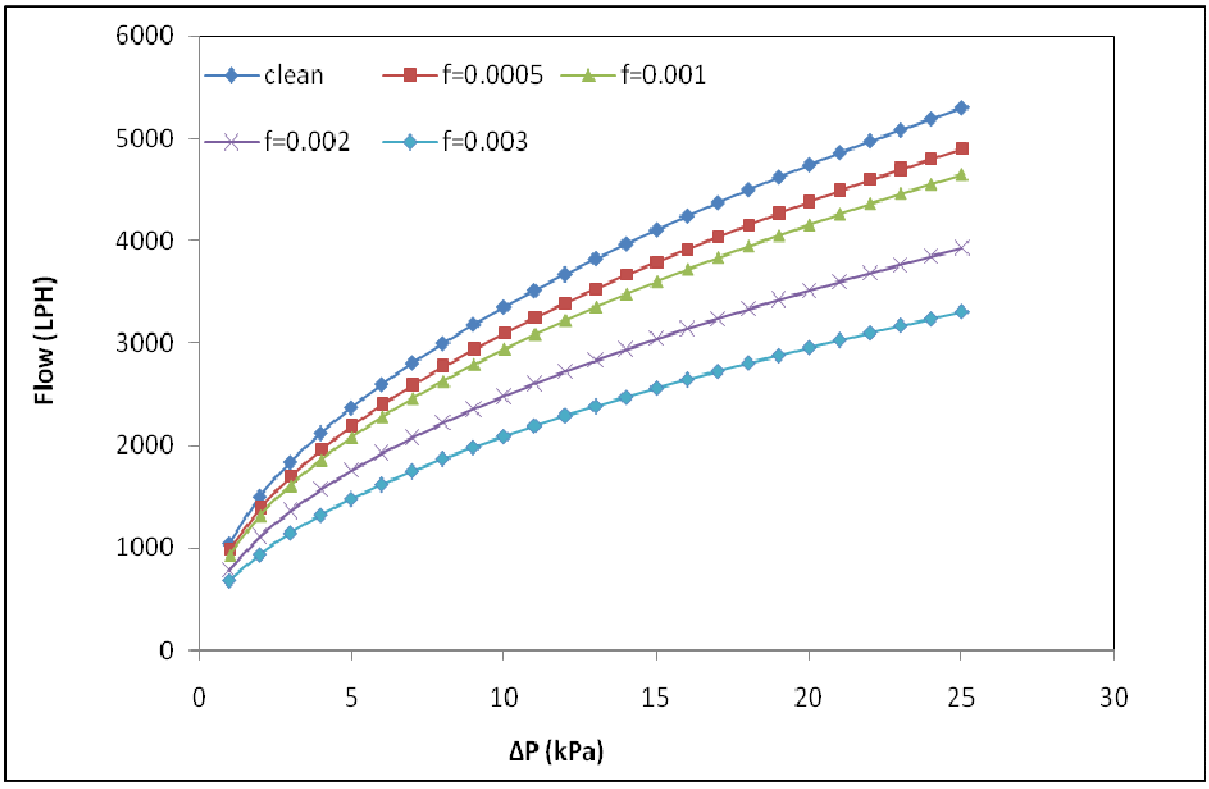

Figure 6.7 : Variation of Flow with Pressure Drop for different fouling factors

Table 6.1 : C-Factor corresponding to fouling factors

	Fouling Factor (f)	C-Factor	C-Dirty/ C-Clean

Clean	0	1040	100%
Design-Clean	0.0005	980	94%
	0.001	930	89%
	0.002	748	72%
Design- Dirty	0.003	572	55%

6.5 Summary

In this chapter the C-Factor is used as an invaluable tool for investigation of heat transfer performance of a shell and tube heat exchanger under fouling condition. The results show that the proposed tool is very effective in detecting the fouling developed and the corresponding degradation in heat transfer efficiency of a heat exchanger. Hence the C-factor can be used for preparing cleaning schedule in chemical process industries so that the idle time can be reduced to possible minimum and simultaneously the heat exchanger running with poor performance can be avoided. The C-factor gives an indication of the extent of fouling on the heat transfer surface which cannot be estimated from the outside of the exchanger body. As compared to other online methods of fouling monitoring, the use of C-factor eliminates the measurement of end temperatures and effect of changes in properties of both hot and cold fluids during operation. Thus systematic calculation of C-factor with accuracy in measurement of flow and pressure drop provides an effective means for prediction of decrease in heat transfer efficiency for effective preventive maintenance scheduling of the heat exchanger. Besides, this analysis uses only two factors namely flow and pressure drop for which neither much more special instrumentation nor cumbersome mathematical calculation is required. This can be used for continuous monitoring of a heat exchanger system and improved maintenance scheduling.

Chapter 7

Fouling Prediction Using Artificial Neural Network Approach

The objective of this chapter is to develop a methodology based on artificial neural network approach for prediction of fouling in a shell and tube heat exchanger, which considers various performance parameters such as outlet temperature differences in each side and the exchanger efficiency. In this chapter, the efficiency of the exchanger is defined in terms of C-factor which is a performance indicative parameter as discussed in the previous chapter. Moreover, the chapter predicts the behavior of a heat exchanger subjected to fouling so that an optimal cleaning schedule can be developed without hindering the operation of a plant involving the exchanger.

7.1 Introduction

Under Heat transfer fouling conditions, unwanted materials deposit on heat transfer surfaces either from inorganic solutions with inverse solubility or organic species. The deposit layer, with low thermal conductivity, decreases the overall heat transfer coefficient which may further lead to significant loss of thermal exchange capacity. Fouling generally behaves as a non-linear and unsteady-state process of an extremely complicated nature. It involves a considerable number of independent variables with poorly understood interaction. Some of these parameters are Surface temperature, Bulk composition and chemistry, Fluid velocity and turbulence, Physical properties of the working fluid, Surface specifications, physical properties of the deposit and Chemical kinetics (Mayaleri and Steinhagen,2007).

Several approaches are presently followed for the prediction of fouling behaviour. These may include

- Tabulated, time-independent fouling resistances such as TEMA tables
- Rules of thumb that approximates 25% overdesign
- Bench scale measurements under accelerated conditions
- Empirical or semi-theoretical correlations based on laboratory experiments
- Numerical simulations such as CFD

However all these methods have significant limitations in accurate prediction of fouling behavior of an exchanger. The application of the TEMA fouling resistances does not consider any effects of operating conditions such as flow velocity, temperature, foulant concentration or flow geometry such as baffles, corrugations on the extent of fouling. Similar conclusions may be drawn for proportional overdesign. Empirical models based on laboratory or pilot plant measurements may be useful as long as the actual fouling process is not significantly different in any major aspect. But extrapolations to different conditions or general predictions are not possible as the physical phenomena underlying fouling are extremely complex. Regression models may be partially theory-based or completely empirical. In both cases, it is not known a priori how many explanatory variables and parameters have to be included in the model for obtaining an optimal regression model. All of these shortcomings led to the development of a model based on artificial neural network, which can effectively predict nonlinear behavior of a heat exchanger with limited experimental data (Haykin, 1999).

The ANN analysis as a new paradigm represents an excellent candidate for the purpose of solving thermal problems which involve a multitude of fundamental disciplines, their interactions and complex geometry. The traditional approach and associated numerical analysis correlate the experimental data with dimensionless groups to develop physical models for performance prediction and design. On the other hand, the ANN analysis deals with time-dependant dynamic thermal phenomena of heat exchangers more accurately than traditional correlated models. Neural networks are basically unsupervised methods because they can synthesise without detailed knowledge of the underlying process. This is certainly a benefit for modelling phenomena such as fouling in which the interaction of the dominant variables is not firmly established. The method can also be used for processing very substantial data sets, which is difficult for conventional approaches such as regression approaches.

The construction of a neural function network in its most basic form involves three entirely different layers. The input layer is made of input nodes. The layer between the input and output layers is known as hidden layer, which may consist of only one or of several sub-layers. It has sufficient nodes, which serves a transformer of weights between the input and output layers. The output layer supplies the response of the network to the activation patterns applied to the input layer. Neural networks are generally developed in two phases, as follows:

- The training or learning phase in which a set of known input-output patterns are

presented to the network. The weights are adjusted between the nodes until the desired output is provided.

- The testing phase in which the network is subjected to input patterns that it has not seen before, but whose outputs are known and the performance is monitored.

Input and output variables in designing the networks can be used in terms of normalised form. In general, the majority of data are used for training of the network, and the remaining part for the testing phase.

7.2 Neural Network Analysis

This chapter addresses one of the objectives of this project, i.e. the application of ANNs to the prediction of steady-state heat transfer performances in heat exchangers. For a given device exchanging heat between two fluids, the heat transfer rate depends on the flow rates and the inlet temperatures of each fluid. Currently, most calculations are done on the basis of manufacturers' data for specific fluids that give the heat transfer rate as a function of the two flow rates and the two inlet temperatures. This is a four-variable function and difficult to represent completely. In principle the functional relation depends on the geometry of the heat exchanger, the materials with which it is made, the surface conditions, the fluids used, etc. It would be advantageous to be able to compress the information in the heat transfer rate function from which it can later be accurately recovered.

The artificial neural network technique offers an alternative approach to the problem of information compression for heat exchangers. It is a procedure that is usually used for predicting the response of a physical system that cannot be easily modeled mathematically. The network is first trained by experimentally obtained input-output sets of data, after which it can be used for further prediction. Once a network is trained using the experimental data; the constants or

parameters of the trained network can then be transferred further to calculate the performance of the heat exchanger under any other flow rate or inlet temperature conditions.

The artificial neural network (ANN) consists of a series of layers, each with a number of nodes. The first and last layers are the input and output layers, respectively. The number of nodes in the input and output layers depend upon the number of input variables and output parameters.

In a fully connected network, all nodes are connected to all nodes of the previous and following layers. A typical structure of an ANN is schematically shown in Figure 7.1. As explained earlier, out of the whole data a major portion is used for training of the network while the rest portion is used for testing the network. It is assumed that the available data consist of M runs. Of these M_1 will be used for training and M_2 for testing purpose. Each run is a single experiment providing a number of values of the physical variables for that run. These variables include the inlet and outlet temperatures, flow rates and heat transfer coefficient and the C-factor.

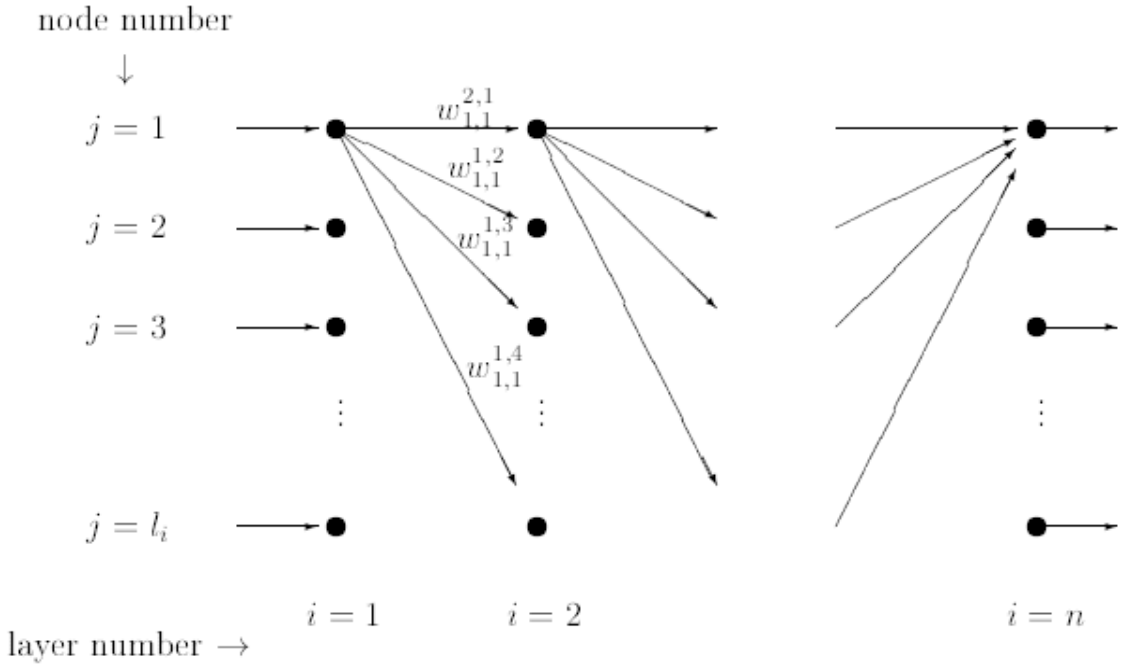

Figure 7.1 : Artificial neural network

7.2.1 Wavelet Neural Network

A wavelet network is a nonlinear regression structure that implements input-output mappings as the superposition of dilated and translated versions of a single function, which is localized both in the space and frequency domains. Such a structure can approximate any square-integrable function to an arbitrary precision, given a sufficiently large number of network elements called “wavelets”. Wavelet Neural Networks (WNNs) has recently attracted great interest, because they are universal approximations which can achieve faster convergence than Radial Basis Function Neural Networks (RBFNN) and are capable to deal with the

problems of “curse of dimensionality”. In addition, WNN are generalized RBFNN. The structure of the WNNs is similar to the RBFNNs, except the radial basis function is replaced with orthonormal basis functions. The efficiency of this type of networks is in learning of the function and its evaluation. Wavelet Neural Networks use a three-layer structure and wavelet activation functions in hidden layer.

The WNNs possesses an unique attribute besides the formation of an orthogonal basis. They are capable of being explicit and can represent the behaviour of a function in several resolutions of input variables. The fundamental concept in the formulation and the design of WNN as basis function is the representation of multi-resolution of functions that use wavelet. This provides the essential frame for completely learning methodology of WNN. The wavelets are a family of functions where each one is defined by one parameter of dilation (A_j) that controls the scaling parameter and one parameter of translation (B_j) which controls the position of a single function called mother wavelet φ(*x*). The position of functions in a space of input data ensure that a WNN can reflect the properties of the function more exactly than the RBFNNs. Considering a set of learning of n-elements, The output of the WNN is given as

$$F(x) = \sum_{j=1}^{m} w_j \cdot \varphi_j \left(\frac{x - B_j}{A_j} \right) \tag{7.1}$$

where *m* is the number of the mother wavelet nodes in the hidden layer, w_j is the weight connecting the *jth* unit of the hidden layer to the output layer unit, φ (*x*) is the wavelet activation function (mother wavelet) of *jth* unit of the hidden layer. In terms of wavelet transformation theory, mother wavelets are given by the following form

$$\varphi = \left| A_j \right|^{-1/2} \varphi \left(\frac{x - B_j}{A_j} \right) \tag{7.2}$$

where $x = \{x_1, x_2,\ldots, x_p\}$, $A_j = \{A_{j1}, A_{j2},\ldots, A_{jp}\}$ and $Bj = \{B_{j1}, B_{j2},\ldots, B_{jp}\}$ are a family of functions generated from one single function φ(*x*) . For the *p* dimensional input space, the mother wavelet can be calculated by the product of *p* single mother wavelets as follows.

$$\varphi(x) = \prod_{i=1}^{p} \varphi(x_i) \tag{7.3}$$

A WNN can be considered as a function approximation which estimates an unknown functional using the following equation

$$y = F(x) + \varepsilon \tag{7.4}$$

where F is the regression function and the error term ε is a zero-mean random variable of disturbance. The localization of the *jth* units of the hidden layer is determined by the scale parameter A_j and the translation parameter B_j. These parameters are modified as well as the weight parameters during the process of training. This flexibility simplifies more reliability towards optimum learning solution. The two parameters A_j, B_j can either be predetermined based upon the wavelet transformation theory or be determined by a learning algorithm. A learning method for a WNN is optimizing the translation B_j which controls the position of a single basis function.

7.2.2 Linear Wavelet Neural Network

The main advantage of wavelet networks over similar architectures such as multi-layer perceptrons and networks of radial basis functions (RBF) is the possibility of optimizing the wavelet network structure by means of efficient deterministic construction algorithms. However, owing to the localized nature of the wavelet basis functions, wavelet networks may not be well-suited to dealing with high-dimensional data. In fact, constructing and storing a wavelet basis of large dimension may be computationally prohibitive (Benveniste et al., 1994). To circumvent this problem, Zhang (1997) proposed a construction technique which takes into account only those wavelets whose support contains at least one modelling sample. However, even by doing so, there remains the problem of providing interpolation over those regions of the input space in which modelling data are not available. Such a problem clearly intensifies with the number of inputs to the network.

This limitation is alleviated by adding a linear term to the basic wavelet network architecture, resulting in a structure termed “linear-wavelet network” (Galvao and Becerra, 2002). Linear regressors can be seen as appropriate complements to wavelets and vice-versa. In fact, linear functions can more easily provide interpolation when the modelling samples are sparse, whereas wavelets can account for nonlinearities in the system to be identified. In the approximation of functions that display only small deviations from linearity, linear regressors may replace a much larger number of wavelets, thus allowing a more parsimonious representation to be obtained.

The model structure of a linear wavelet network with one output y and 'd' inputs {x1, x2, x3……..x_d } has the form

$$y = F_{lin}(x) + F(x) \tag{7.5}$$

where $F_{lin}(x)$ is a linear term and F(x) is implemented by a network of radial wavelets, as indicated in (7.1). Henceforth, a model with the structure given by above equation is termed a "linear-wavelet" network. In problems involving the approximation of a function over a compact subset, the linear-wavelet network has the same approximation capabilities of a standard wavelet network. In fact, linear functions are square-integrable over any compact subset and they can be replaced by a linear combination of wavelets. However, many wavelets may be required to approximate a linear function, specifically in high-dimensional domains, because linear functions are not localized in space. Hence, if a function to be approximated is only mildly nonlinear, the use of a linear term may replace a large number of wavelets, thus leading to a more parsimonious representation.

7.2.3 Local Linear Wavelet Neural Network

Recently, instead of using the common sigmoid activation functions, the wavelet neural network (WNN) employing nonlinear wavelet basis functions named wavelets, which are localized in both the time space and frequency space, has been developed as an alternative approach to nonlinear fitting problem. The key problems in designing of WNN are how to determine architecture of WNN and what learning algorithm can be effectively used for the training of the WNN. These problems are related to determine the optimal architecture of the WNN, to arrange the windows of wavelets, and to find the proper orthogonal or non-orthogonal wavelet basis. Secondly, Curse-of-dimensionality is a mainly unsolved problem in WNN theory which brings some difficulties in applying the WNN to high-dimension problems. In order to address these shortcomings a local linear wavelet neural network is proposed (Chen et. al., 2004), in which the connection weights between the hidden layer units and output units are replaced by a local linear model. The usually used learning algorithm for wavelet neural networks is gradient descent method. The difference of the network with the original wavelet neural network is that the connection weights between the hidden layer and output layer of the original WNN are replaced by a local linear model.

The usually used learning algorithm for local linear wavelet neural networks is gradient descent method. The wavelets in most generalized form can be expressed as

$$\psi = \left\{ \psi_i = |a_i|^{-1/2} \psi\left(\frac{x - B_i}{A_i} \right) : A_i, B_i \in R, i \in Z \right\} \tag{7.6}$$

$$x = (x_1, x_2, \cdots x_n)$$

$$A_i = (A_{i1}, A_{i2}, \cdots A_{in})$$

$$B_i = (B_{i1}, B_{i2}, \cdots B_{in})$$

In terms of wavelet transformation theory, wavelets in the above mentioned form is a family of functions generated from one single function ψ(x) by the operation of dilation and translations. ψ(x), which is localized in both the time space and the frequency space, is called a mother wavelet and the parameters A, B are named the and translation parameters, respectively.

In the standard form of wavelet neural network, **t**he output of a WNN is given by

$$f(x) = \sum_{i=1}^{M} w_i \psi_i(x) = \sum_{i=1}^{M} w_i |A_i|^{-1/2} \psi\left(\frac{x - B_i}{A_i} \right) \tag{7.7}$$

It is obvious that the localization of the i*th* units of the hidden layer is determined by the dialation parameter A_i and the translation parameter B_i. The above wavelet neural network is a kind of basis function neural network in the sense that the wavelets consists of the basis function. The intrinsic feature of the basis function networks is the localized activation of the hidden layer units, so that the connection weights associated with the units can be viewed as locally accurate piecewise constant models whose validity for a given input is indicated by the activation functions. Compared to the multilayer perceptron neural network, this local capacity provides some advantages such as the learning efficiency and the structure transparency.

In order to take advantage of the local capacity of the wavelet basis functions while not having to have too many hidden units, LLWNN has been used as an alternative neural network. The output of LLWNN is given by

$$Y = \sum_{i=1}^{m} (w_{i0} + w_{i1} x_1 + \cdots\cdots + w_{in} x_n) \psi_i(x) \tag{7.8}$$

where, instead of the straight forward weight w_i (piecewise constant model), a linear model

$v_i = w_{i0} + w_{i1}x_1 + \cdots\cdots + w_{in}x_n$ is introduced. The activities of the linear models v_i (i=1,2,--------n) are determined by the associated locally active wavelet functions $\psi_i(x)$ (i= 1,2,-------,n), so that v_i is only locally significant.

For the present study the network uses a local linear wavelet neural network in which the connection weights between the hidden layer units and output units are replaced by a local linear model and the learning algorithm uses a back propagation gradient descent method. The architecture of the proposed model is shown in Fig.ure 7.2.

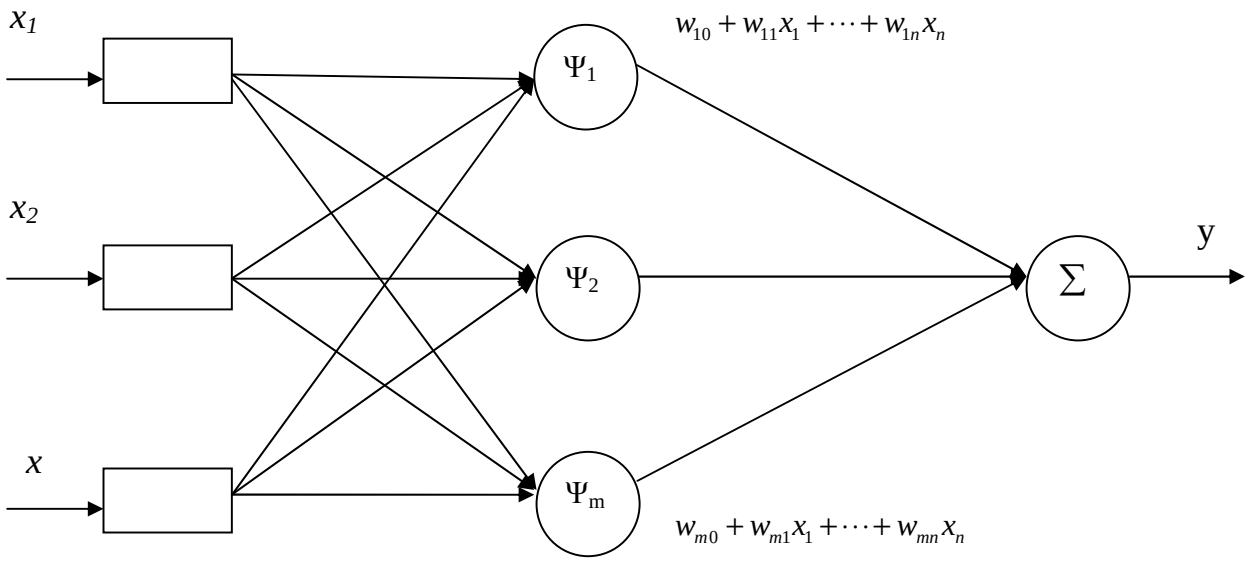

Figure 7.2 : General structure of a Local Linear Wavelet Neural Network

7.2.4 Learning Algorithm

A neural learning algorithm to get all the unknown parameters of network i.e. translation and dilation coefficients, weights may be used for supervised training of an LLWNN. Since the function computed by the LLWNN model is differentiable with respect all the mentioned unknown parameters, a standard back propagation (BP) gradient descent training algorithm can

be used for updating weights, dilation and translation parameters which are randomly initialized at beginning. It is possible to over fit the training data if the training session is not stopped at the right point. The unset of the over fitting can be detected through cross validation

in which the available data set are divided in to training, validation and testing subsets. The training set is used to compute the gradients and update all the unknown parameters of the networks. The error on the validation set is monitored during the training session. In this work, the standard BP gradient descent training algorithm has been adopted and training is based on minimization of

the fouling resistance (E), given as:

$$R = \frac{1}{2}\begin{bmatrix} D - w_{10}\psi_1(x) - w_{11} f_1\psi_1(x) - \cdots - w_{20}\psi_2(x) - w_{21} f_2\psi_2(x) - \cdots \\ \cdots - w_{m0}\psi_m(x) - w_{m1} f_1\psi_m(x) - \cdots - w_{mn} f_n\psi_m(x) \end{bmatrix} \tag{7.9}$$

where D is the desired output.

$$w(k+1) = w(k) + \eta e \frac{\partial R}{\partial w}$$

(7.10)

such that $w_{10}(k+1) = w_{10}(k) + \eta e\psi_1(x)$, $w_{11}(k+1) = w_{11}(k) + \eta e f_1\psi_1(x)$ and so on.

Similarly,

$$\sigma(k+1) = \sigma(k) - \eta e \frac{\partial R}{\partial \sigma}$$

(7.11)

$$c(k+1) = c(k) - \eta e \frac{\partial R}{\partial c}$$

(7.12)

Correspondingly,

$$\sigma_1(k+1) = \sigma_1(k) + \eta e(w_{10} + w_{11} f_1 + \cdots\cdots + w_{1n} f_n)\frac{\partial \psi_1(x)}{\partial \sigma_1}$$

(7.13)

$$c_1(k+1) = c_1(k) + \eta e(w_{10} + w_{11} f_1 + \cdots\cdots + w_{1n} f_n)\frac{\partial \psi_1(x)}{\partial c_1}$$

(7.14)

$$\frac{\partial \psi_1(x)}{\partial \sigma_1} = \frac{-x^4}{\sigma^3} e^{-x^2/\sigma_1^2}$$

(7.15)

$$\frac{\partial \psi_1(x)}{\partial \sigma_1} = \frac{2(x-c_1)^2}{\sigma^3} e^{-\frac{(x-c_1)^2}{\sigma^2}}$$

(7.16)

$$\frac{\partial \psi_1(x)}{\partial c_1} = \frac{4c_1(x)}{\sigma_1^2} e^{-(\frac{x-c_1}{\sigma_1})^2}$$

(7.17)

If fouling resistance at time t (f_t) is to be forecasted, the resistance information of previous day up to "m" days i.e. f_{t-1}, f_{t-2},….,f_{t-m} should be taken as a part of the input of short term resistance forecasting model. The auto co-relation function (ACF) can be used to identify the degree of association between data in the price series separated by different time lags i.e. previous resistance. In order to identify the load influence on resistance, load at any day to be predicted at different lagged days are also included as an exogenous variable in the input set of the forecasting models. The historical hourly data prior to the day whose resistance to be predicted have been considered to build the forecasting model.

7.2.5 Backpropagation

Training of a network consists of changing the weights until the output values converge maximum possible to the known target values. The back propagation methodology is widely used for training a network. This methodology utilizes the principle of propagating the output errors in a backward direction by modifying the weight values.

For a sigmoidal activation function, the error quantified at the output layer is given by

$$\delta_{n,j} = \left(t_j - y_{n,j}\right) y_{n,j}(1-y_{n,j})$$

(7.18)

where t_j is the target output for the node (n,j). Once all the errors corresponding to layer n is determined, then the previous layer (n–1) is considered for determination of error. But unlike the nth layer, there is no target output to compare with the network output. The error for such a layer is defined as

$$\delta_{n-1,j} = (t_j - y_{n,j}) y_{n-1,j}(1-y_{n-1,j}) \sum_{l=1}^{m_n} \delta_{n,l} \omega_{n-1,j}^{n,l}$$

(7.19)

As the errors for all the nodes of the (n-1) th layer is computed, the (n-2)th layer is taken into consideration for computing the errors in a similar manner as that for the (n-1)th layer. Consequently the errors corresponding to all the nodes upto the second layer is computed. After computing all the values of $\delta_{i,j}$, the change in the weights and bias are computed as

$$\Delta\omega_{i-1,k}^{j,j} = \lambda\delta_{i,j}y_{i-1,k}$$

(7.20)

$$\Delta\theta_{i,j} = \lambda\delta_{i,j}$$

(7.21)

where λ is the learning rate that is used to scale down the degree of change made to the connections. For the current network development the learning rate is taken to be λ= 0.4. At the end of one cycle of back propagation, an updated set of weight values are determined by using the above mentioned corrections.

7.2.6 Network Training

Of the total number of runs, a significant number of runs were used for training the network. In this work, out of total 320 runs, 240 runs were considered for network training which constitutes 75% of the total data. Initially arbitrary values were assigned to the weights and biases. Then the backpropagation methodology was applied to this set of training data for adjusting the values of the weights and biases. In order to stop the training of the network, certain criterion should be provided. In this study, the training of the network was terminated when the maximum number of training cycles was reached. The number of cycles can be determined by trial and error method in which it may be changed if the performance of the network is not good enough during training. In this study, the number of training cycles was chosen to be 100,000 after a series of trial tests where the maximum absolute percentage error (MAPE) between the network output and the target output was less than 2%. The maximum absolute percentage error used to assess the prediction accuracy of the developed model of every predicted output was determined as

$$Er = \left|A_e - A_p\right| / A_e$$

(7.22)

where A_e is the target output of the experimental data and A_p is the predicted output of the neural network. The maximum error was determined by the maximum value of the relative errors of the three output variables. During the training process of the network, the performance of the network was evaluated by calculating the root mean square values of the output errors.

$$RMSE = \sqrt{\frac{1}{M}\sum_{i=1}^{M}\left(\frac{A_e - A_P}{A_e}\right)^2}$$

(7.23)

In a similar manner as that of the relative error, the rms error was determined by the maximum value of the rms error of the three output variables.

7.2.7 Network Prediction Accuracy

The developed neural network model was used to predict the efficiency of the exchanger, exit temperatures of both the shell and tube using test data set. The accuracy of prediction can be analysed statically using various information criteria. These information criteria combine some measure of fit to the complexity of a model so that the same criteria can be used for detecting the process drift.

The root mean square deviation (RMSD) or root mean square error (RMSE) is a frequently-used measure of the differences between values predicted by a model or an estimator and the values actually observed from the thing being modeled or estimated. These individual differences are also called residuals and the RMSD serves to aggregate them into a single measure of predictive power. RMSE is given as defined in equation (7.9).

Correct Directional Change (CDC) is a measure of the ability of a network to predict the correct direction of changer in a variable. CDC is defined as (Ramasamy et. al., 2008)

$$CDC(\%) = \frac{1}{N-1}\sum_{t=2}^{N} D_t$$

(7.24)

where, D_t =1, if $D = 1, if\ [y_i(t) - y_i(t-1)] \times [\tilde{y}_i(t) - \tilde{y}_i(t-1)] > 0$

$D_t = 0$, if $[y_i(t) - y_i(t-1)] \times [\tilde{y}_i(t) - \tilde{y}_i(t-1)] < 0$

Besides Coefficient of Determination (R^2) is another statistical parameter that can be considered for accuracy prediction of a network. In statistics, the coefficient of determination (R^2) is used in the context of statistical models whose main purpose is the prediction of future outcomes on the basis of other related information. It is the proportion of variability in a data set that is accounted for by the statistical model. It provides a measure of how well future outcomes are likely to be predicted by the model.

$$R^2 = 1 - \frac{\sum_{t=1}^{N} (y_t - \hat{y}_t)^2}{\sum_{t=1}^{N} (y_t - \bar{y}_t)^2}$$

(7.25)

7.2.8 Network Testing

Testing is the process of verifying the ability of a network to provide accurate output results when the input data that have never been used for training were fed into the trained network. Testing consists of using the network with weights and biases found from the training process and then trying them out with the test data. The performance of the trained network is evaluated by comparing its prediction with the data set used for testing. In this study, out of the total data set consisting of 320 runs, 80 runs were used for testing the developed neural network. The testing errors are computed in terms of maximum absolute percentage error as discussed in the section 7.2.6.

7.3 Physical Model of Heat Exchanger:

The experimental runs were conducted with a single pass shell-and-tube heat exchanger as described in the section 4.3 of the previous chapter. The tube side fluid is normal tap water which functions as cold fluid while the hot fluid passing through the shell is hard water. The hardness of the water flowing through the shell is within a range of 500-550 ppm of NaOH.

7.3.1 Data acquisition

Three major parameters such as mass flow rate, inlet temperature and exit temperature of the tested heat exchanger were collected for both the hot and cold fluids. The data was collected for 320 days on a daily average basis within a period starting from October 2008 to December 2010. In order to accelerate the rate of convergence and avoid the possibility of coupling among different inputs, it is necessary to do this pre-processing work before we input these data to the network. First, the data with distinct errors were discarded. All the data considered in training and testing of the network were taken within a 20% dispersion limit of overall heat transfer coefficient as discussed earlier in section 4.3.3 (Milanovic et. al., 2006). The uncertainties associated with temperature difference, flow rate and pressure drop were 0.1^{o}C, 1% and 8% respectively. Then the data was scaled relative to one another in order to have a balanced importance of important variables having less magnitude and less important variables having higher magnitude. The data were normalized as

$$x_{norm} = \frac{x - x_{\min}}{x_{\max} - x_{\min}} \tag{7.28}$$

As a result of the normalization, the output activity becomes an activity-weighted average of the input weights in which the weights from the most active inputs contribute more on the value of the output activity. This results in novel computational properties which have attracted high attention in the neural network community. In standard WNN, the weights determine how much each hidden node contributes on the output. In NWNN, the activities of the hidden nodes determine which weights contribute more on the output. In Normalized Wavelet Networks, the output weights become the network's output over the partition defined by the hidden nodes. Consequently, a NWNN exhibit excellent generalization properties, to the extent that hidden nodes need to be recruited only for training data at the boundaries of class domains. In NWNN, the output activity is normalized by the total input activity in the hidden layer.

7.3.2 Heat Exchanger Historical Performance

The heat exchanger was cleaned at the beginning of this experimentation. After cleaning, the overall heat transfer coefficient and corresponding C-factor value were around

96% of the clean design value. The present study analyses the data collected during a span of around 2 years from October 2008 to December 2010. The heat transfer coefficient was calculated using the actual log mean temperature difference (LMTD). The heat transfer efficiency was expressed in terms of C-factor which is quite instructive to be expressed as a measure of fouling. The C-factor gives an indication of the extent of fouling on the heat transfer surface which cannot be estimated from the outside of the exchanger body. The C-factor can be expressed in terms of volume flow rate and the pressure drop on the tube side as mentioned in the previous chapter.

$$C = \frac{V}{\sqrt{\Delta P}}$$

The C-factor value for the clean design condition is 980 as discussed in the previous chapter. The efficiency of the exchanger is defined as the ratio of C-factor under fouled condition to the same under design condition. Thus the efficiency is

$$\eta = \frac{(C - factor)_{fouled}}{(C - factor)_{design}}$$

(7.29)

The performance of the heat exchanger is shown in the figure 7.3. As indicated in the figure, the efficiency value reduced from 96% to around 36% during this period of operation. This experimental data is used as input for training the ANN. Similarly Figure 7.4 represents the temperature difference both for the shell and tube side during this period of time. The temperature difference indicates both the shell and tube side inlet and exit temperature differences obtained from the experimental data. As observed in the experimental data, the hot fluid undergoes a reduction in temperature within a range of 5.5^{o}C to 14.2^{o}C while the cold fluid undergoes an increase within a range of 3.5^{o}C to 9.6^{o}C. The flow rates were maintained between 600LPH to 1500LPH during the experimentation process.

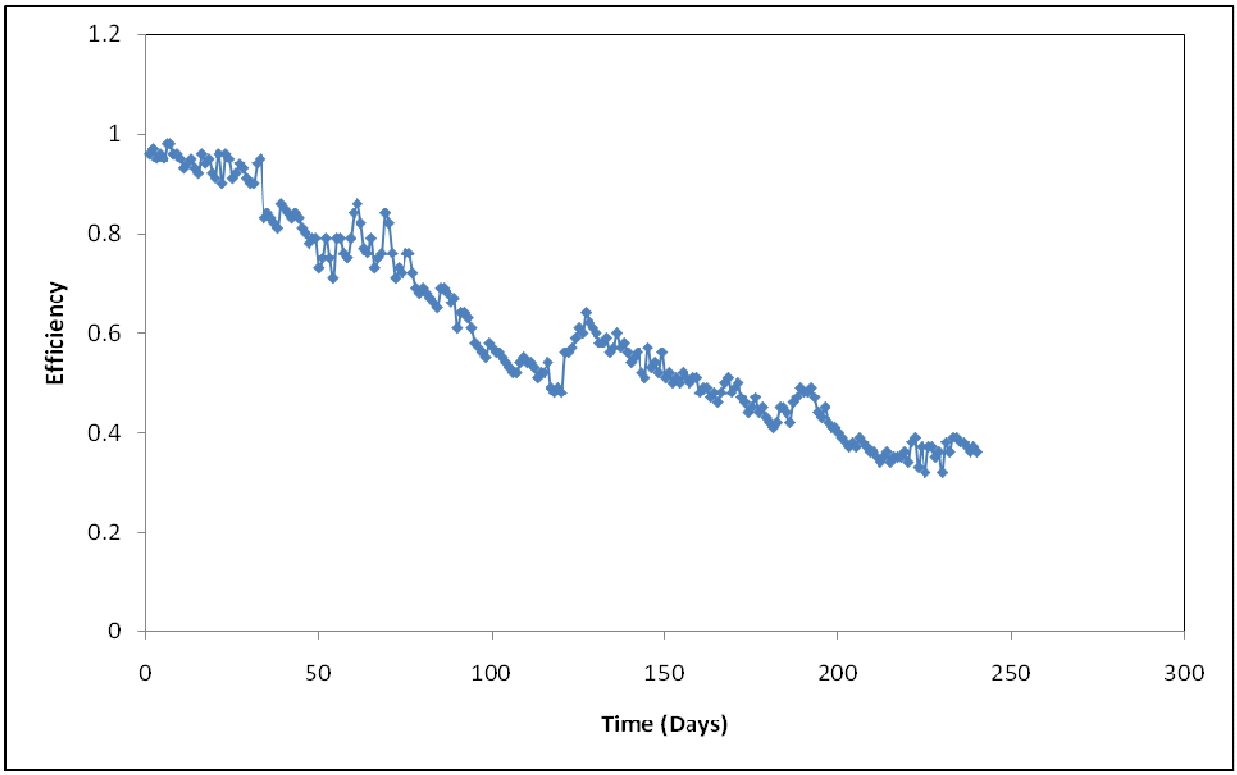

Figure 7.3 : Efficiency of heat exchanger with Time (Days)

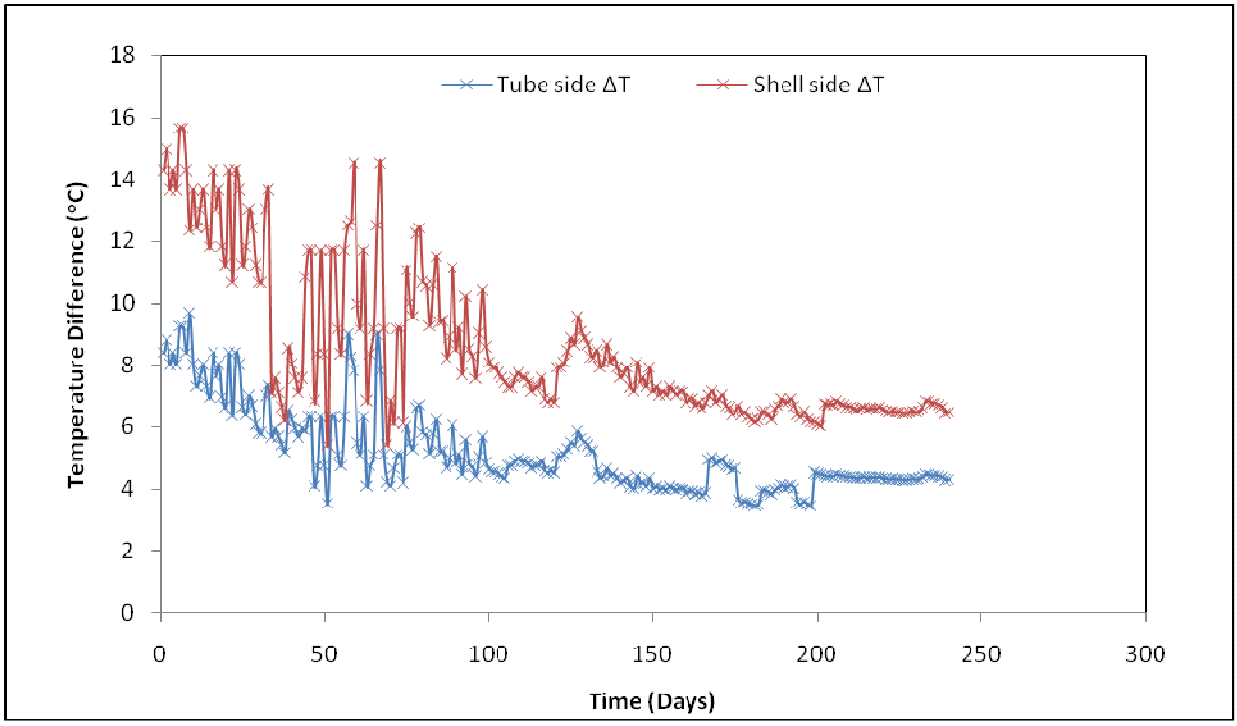

Figure 7.4 : Variation of Temperature difference with Time (Days)

7.4 Results and Discussion :

The experimental set up utilized for the ANN analysis was described in the section 4.3. as already discussed, a total of 320 runs were made out of which 240 runs were used for training while the rest 80 runs were used for testing. The data used for the purpose of training can be selected randomly. However in this study, the data of 240 days from the beginning of experimentation were taken for training while the data corresponding to the last 80 days of operation were considered for testing. The training and testing data for all the three parameters are presented in Appendix A.6 and A.7 of the Appendix A. Also the computer program written in MATLAB to train and test the neural network is presented in Appendix C.

The mean absolute percentage errors were determined for efficiency and temperature diffences on both the tube and shell side fluids. The evolved local linear wavelet neural network was obtained at iteration 6000 with MAPE 1.25% for training data set and MAPE 0.017% for test data set, respectively for the tube side fluid. Figure 7.5 and 7.6 present the errors in case of tube side fluid temperature difference for the training and testing data set respectively. This indicates the prediction accuracy of the developed LLWNN model. The training and testing errors for shell-side temperature difference and efficiency are presented in figures 7.7, 7.8, 7.9 and 7.10. Also the maximum errors for all the three cases have been presented in table 7.1.

Table 7.1 : Maximum errors in training and testing

Parameter	Training Error (MAPE)	Testing Error (MAPE)
Tube-side ΔT	1.25	0.017
Shell-side ΔT	0.064	0.003
Efficiency	0.1	0.064

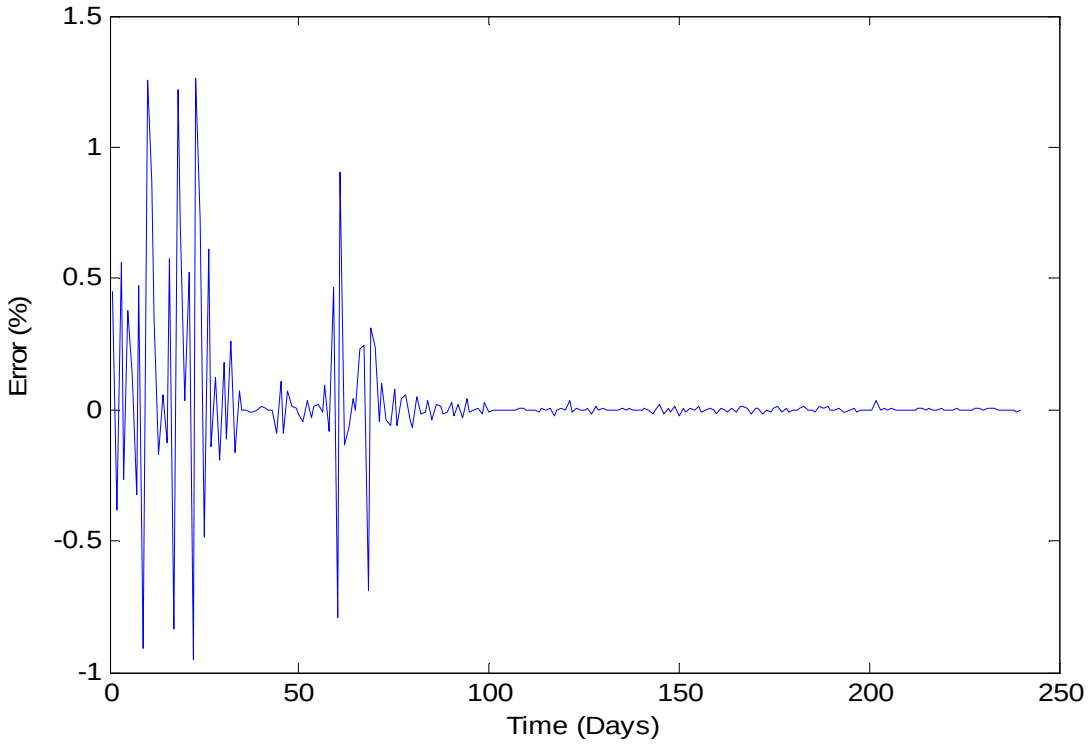

Figure 7.5 : Training error for tube-side temperature difference

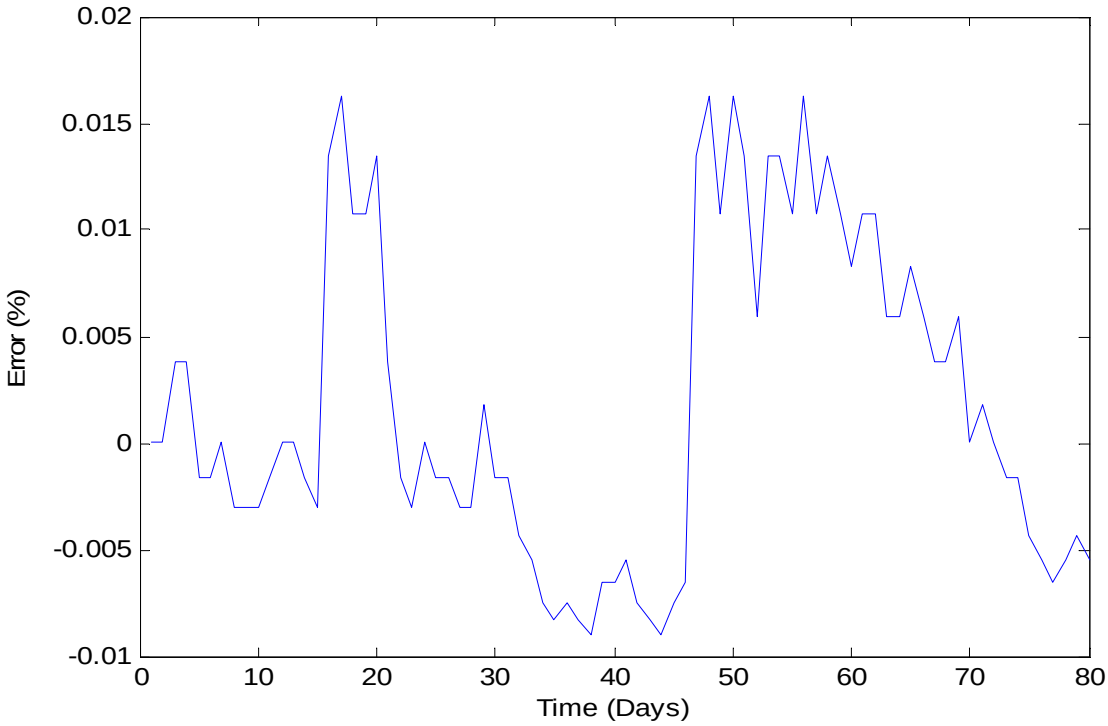

Figure 7.6 : Testing error for tube-side temperature difference

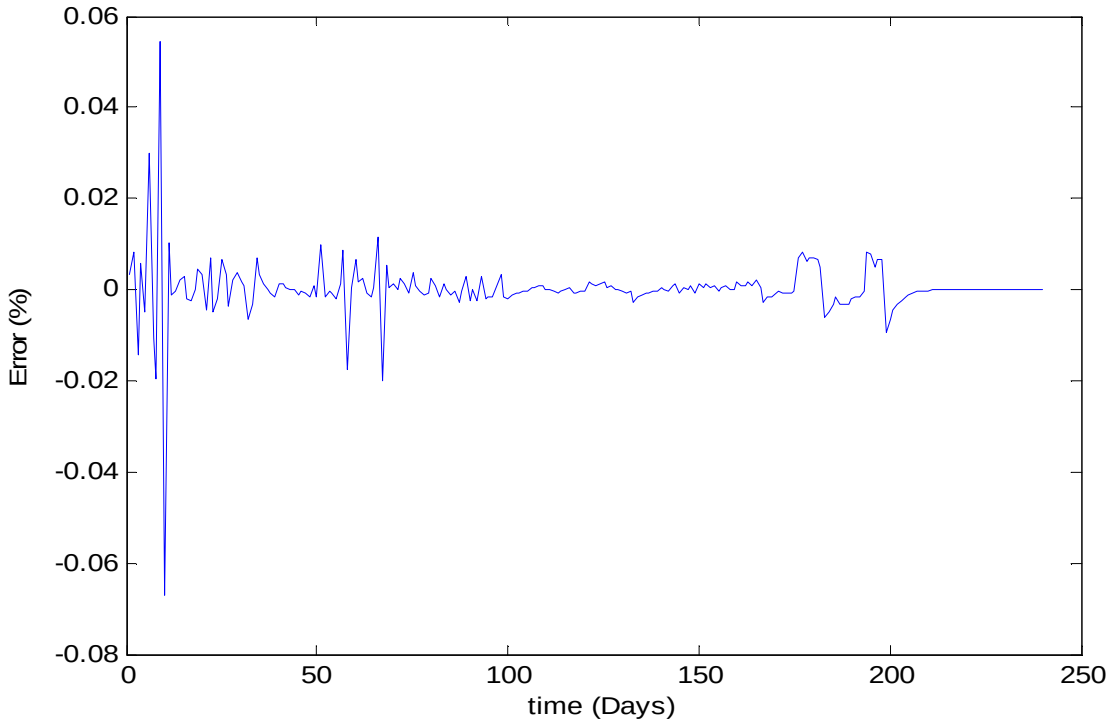

Figure 7.7 : Training error for shell-side temperature difference

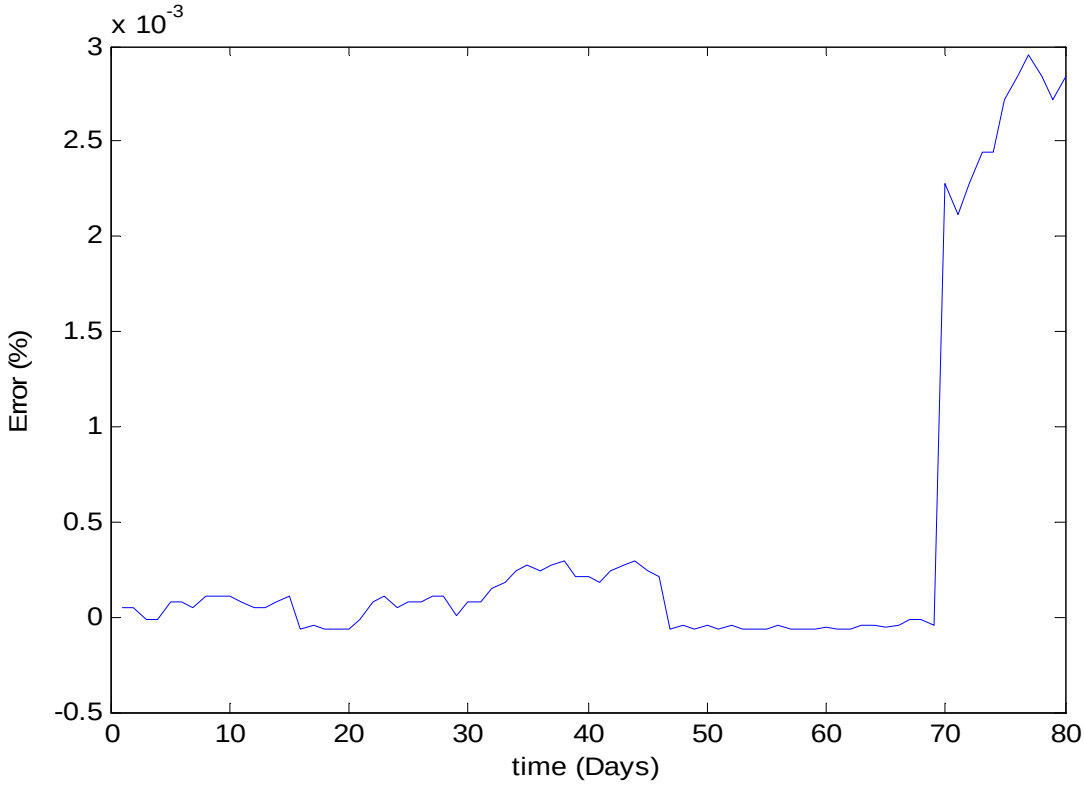

Figure 7.8 : Testing error for shell-side temperature difference

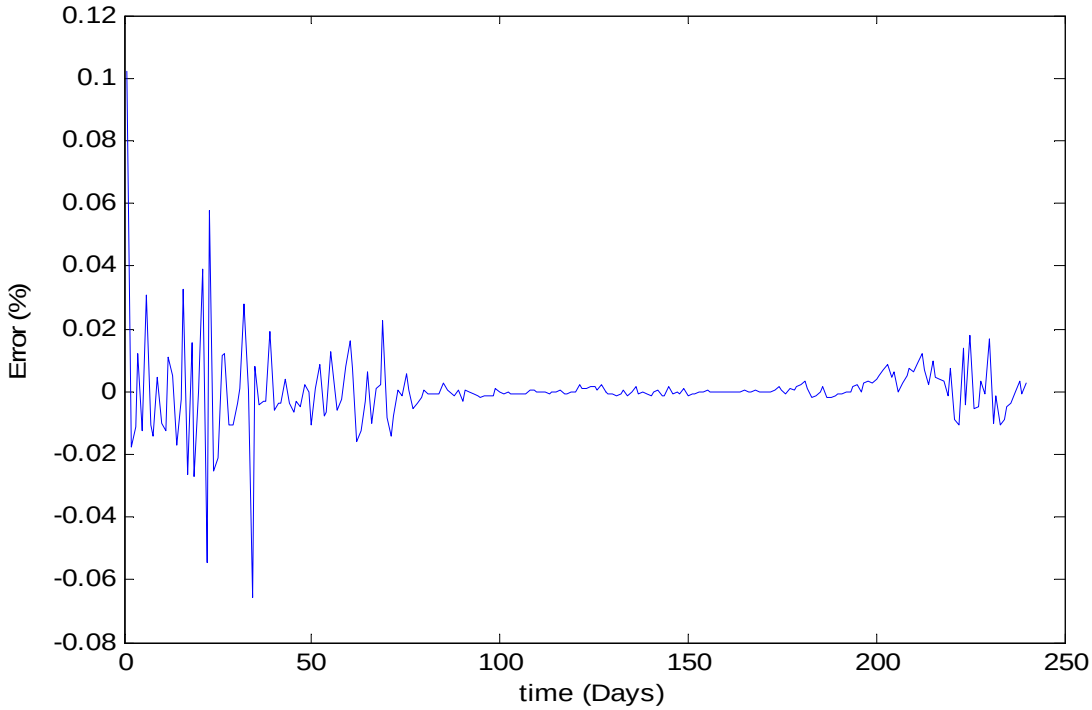

Figure 7.9 : Training error for efficiency

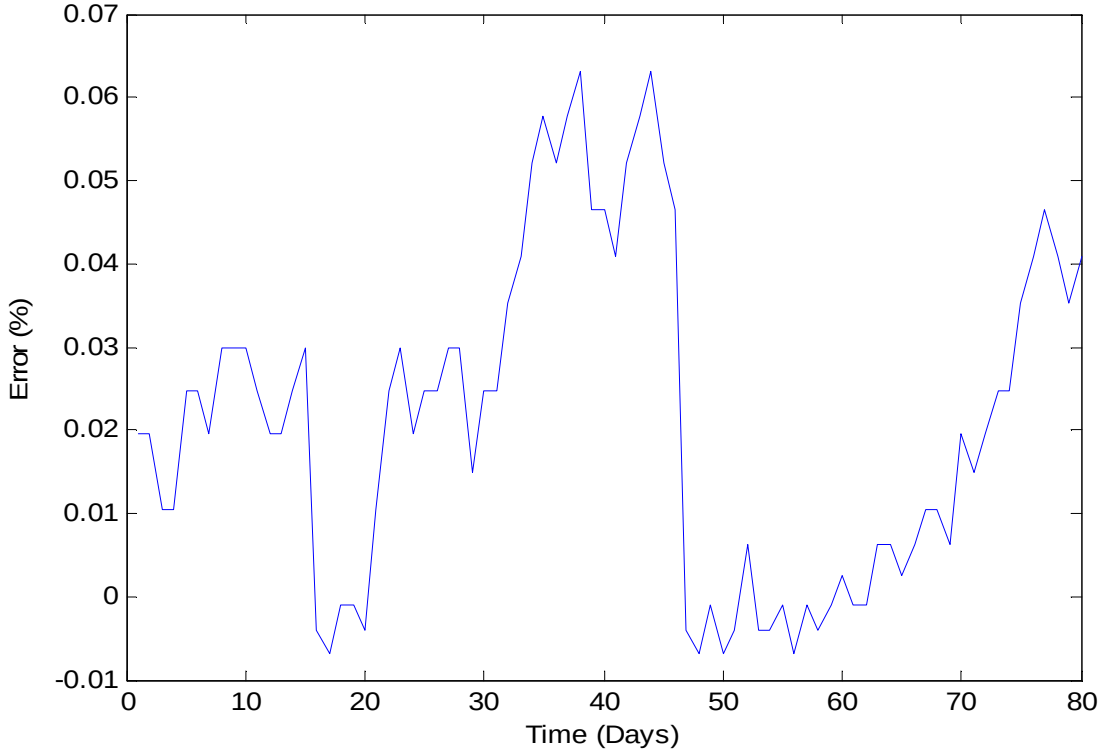

Figure 7.10 : Testing error for efficiency

The predicted temperature difference of the network for shell-side fluid during model development phase is shown in Figure 7.11 and 7.12. Figure 7.11 illustrates the variation of shell-side temperature difference with time during the training phase while figure 7.12 shows a variation of the predicted and actual experimental value of shell-side temperature difference in testing phase. The accuracy of the model in terms of CDC for the training and testing data of shell side fluid were found to be 92.36% and 80.82% respectively. Simultaneously the R^2 value both for training and testing were found to be 0.926 and 0.884 respectively. Similarly for the tube side, the CDC was found to be 91.6% and 84.36% during training and testing. The heat transfer efficiency prediction gives a value CDC equal to 90.42% and 85.14% during training and testing respectively. All the CDC and R^2 values corresponding to three outputs are summarized in Table 7.2. This indicates that the model is reasonably accurate. As models of heat exchangers subjected to fouling detoriate their performance very rapidly, the network should be reliable for longer period of time after training. That's why in this work, the test data was taken during a period just after the training data period. The actual experimental output for shell side outlet temperature difference falls within a range of ±5% of the ANN prediction as shown in Figure 7.11. In general practice, the ANN with error band of ±10% is considered quite well (Yang, 2008). Figure 7.13 shows a comparison of the model prediction and the actual experimental output for shell-side temperature difference. This indicates the suitability of neural network for prediction of an output for an unseen input in case of a heat exchanger.

Table 7.2 : Statistical performances during Training and Testing

Statistical Parameter	Training Analysis			Testing Analysis		
	Shell-side ΔT	Tube-side ΔT	Efficiency	Shell-side ΔT	Tube-side ΔT	Efficiency
CDC	92.36%	91.6%	90.42%	80.82%	84.36%	85.14%
R^2	0.926	0.964	0.947	0.884	0.916	0.906

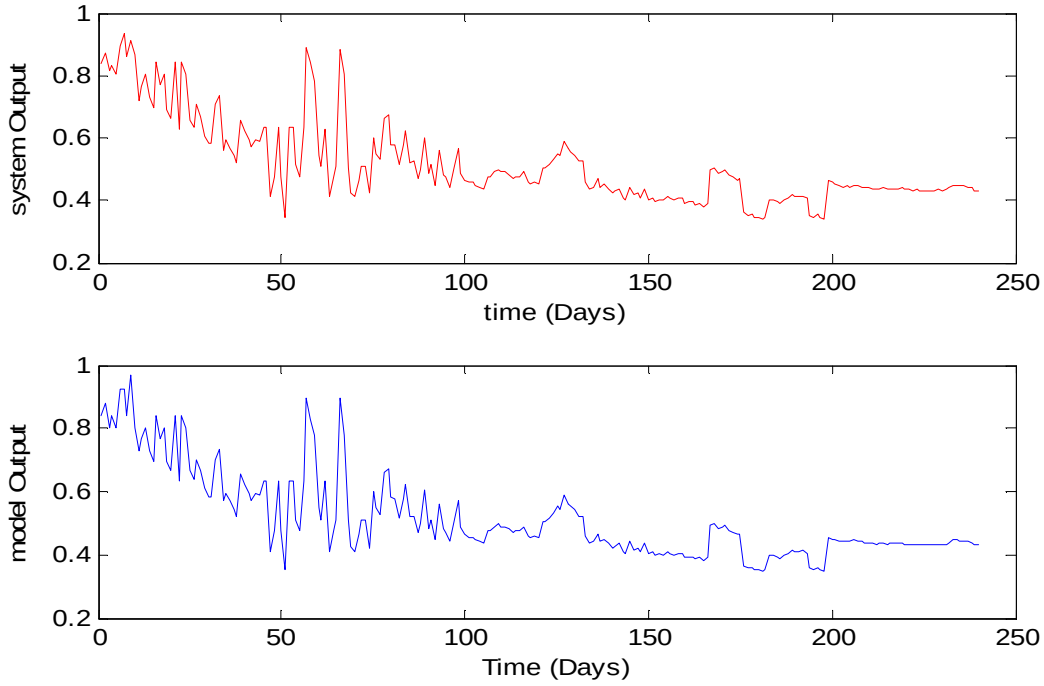

Figure 7.11 : Model output and system output for of shell-side ΔT in Training phase

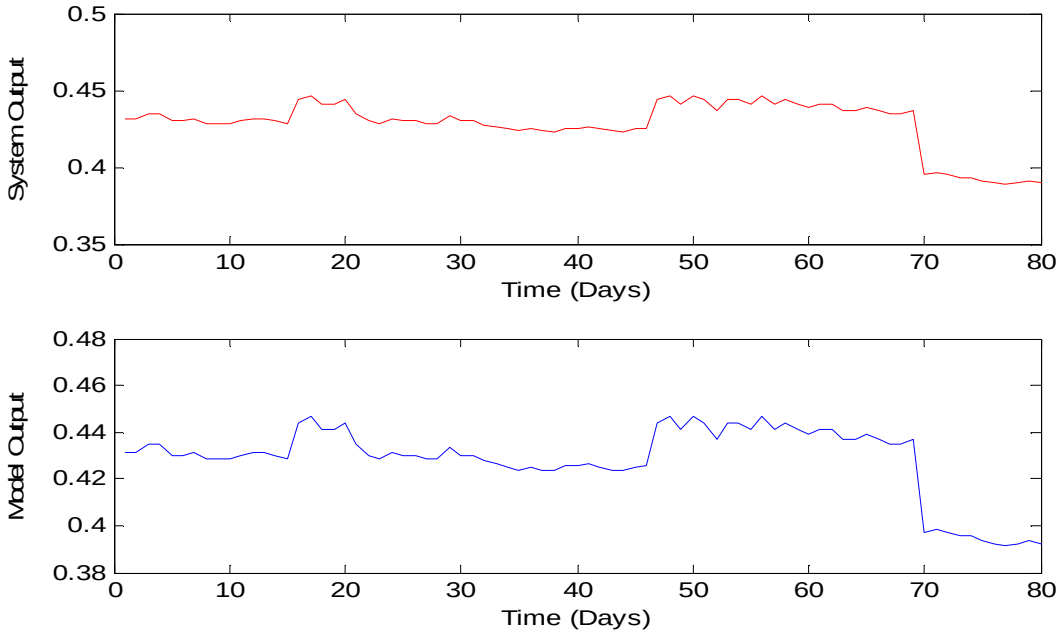

Figure 7.12 : Model output and system output for of shell-side ΔT in Testing phase

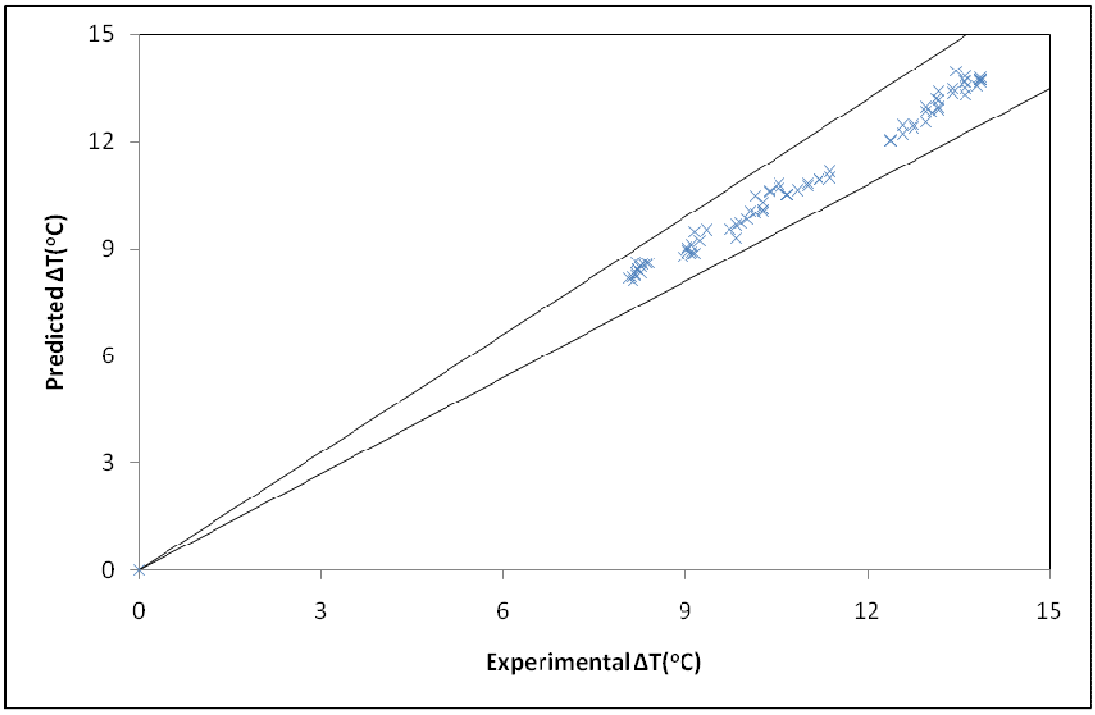

Figure 7.13 : Comparison of Predicted and experimental ΔT (^{0}C) for shell-side fluid

The drift analysis was done by analyzing the data collected after the training period. During this period, the output results for tube-side temperature difference and heat exchanger efficiency were predicted by simulating the original developed model and compared with the actual experimental results. As shown in Figure 7.14, the variation of predicted and output experimental results with time for shell-side temperature difference indicates that there is a drift in the process for which the performance of the model has detoriated. The detoriation is due to fouling deposits on the heat transfer surface. The normalized actual experimental data and the model data of the LLWNN for the testing phase is illustrated in Figure 7.15. However it can observed that the experimental observations of the tube side temperature difference lies within a range of ±10% of the predicted value as shown in Figure 7.16.

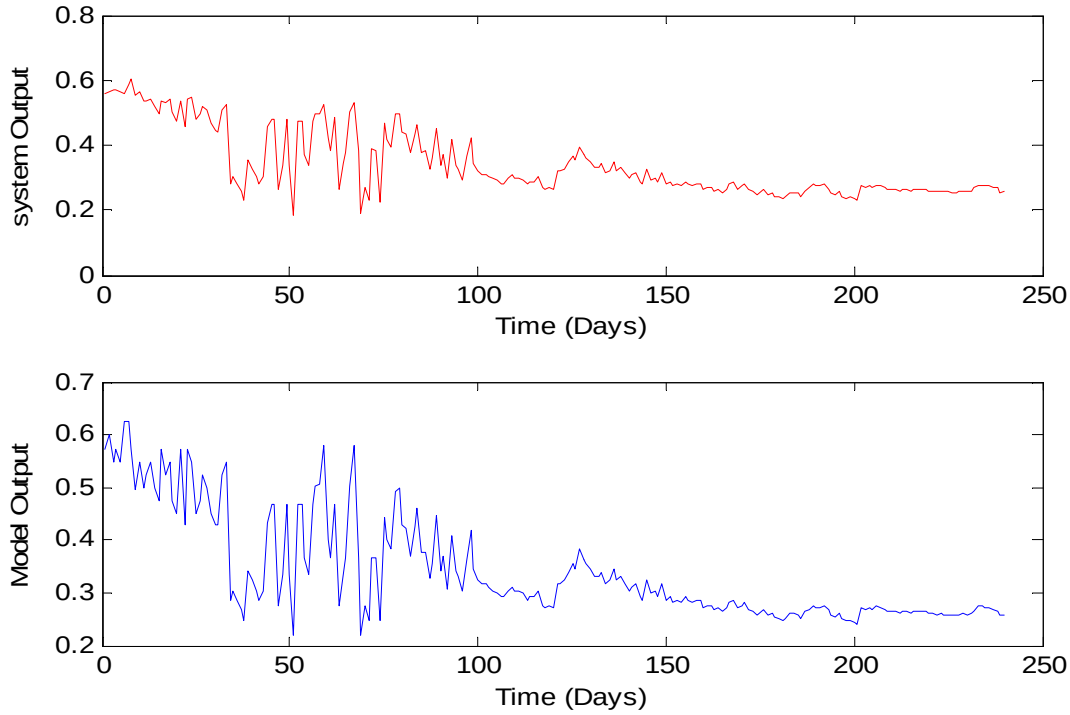

Figure 7.14 : Model output and system output of tube-side ΔT in Training phase

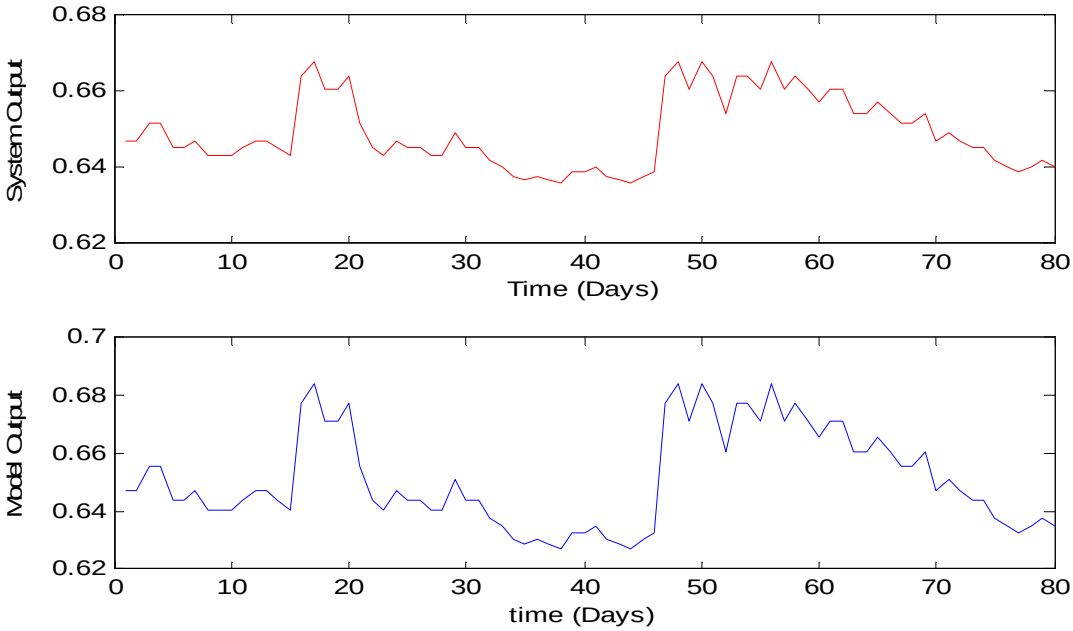

Figure 7.15: Model output and system output of tube-side ΔT in Testing phase

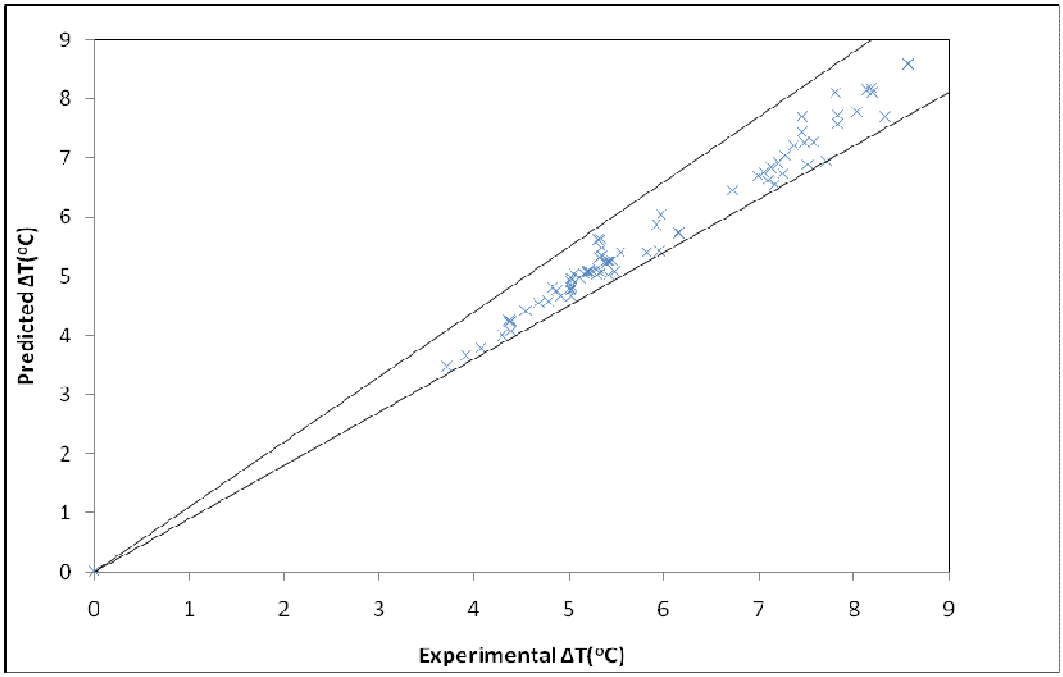

Figure 7.16 : Comparision of Predicted and experimental ΔT (^{0}C) for tube-side fluid

The efficiency expressed in terms of the parameter C-factor of the exchanger is illustrated in Figures 7. 17 and 7.18. Figure 7.17 shows the normalized actual experimental data and the output data of LLWNN for the training phase while Figure 7.18 illustrates the same for testing phase of the heat transfer efficiency. These results indicate a close resemblance of the predicted value with the actual value. The actual efficiency falls below the predicted value within a range of ±10% of the predicted value as shown in Figure 7.19. Hence this model can be considered as a suitable model for prediction of various performance parameters of the exchanger considered. During the test period, the R^2 and CDC values are 0.916 and 84.36% respectively for the tube outlet temperature. The same parameters are 0.884 and 80.82% for tube side while 0.906 and 85.14% for the heat transfer efficiency respectively. The various statistical performance parameters as summarized in Table 7.2 indicate a decrease in CDC and R^2 during testing as compared to training phase. These may be contributed due to the fact that the assumptions considered in deriving correlations are not quite valid for real problem and the uncertainties associated with experimental measurement. As observed in the results, the precision of ANN is much better as compared to simplified correlations. But some limitations

should be considered for neural networks as they do not provide any information about physical phenomena.

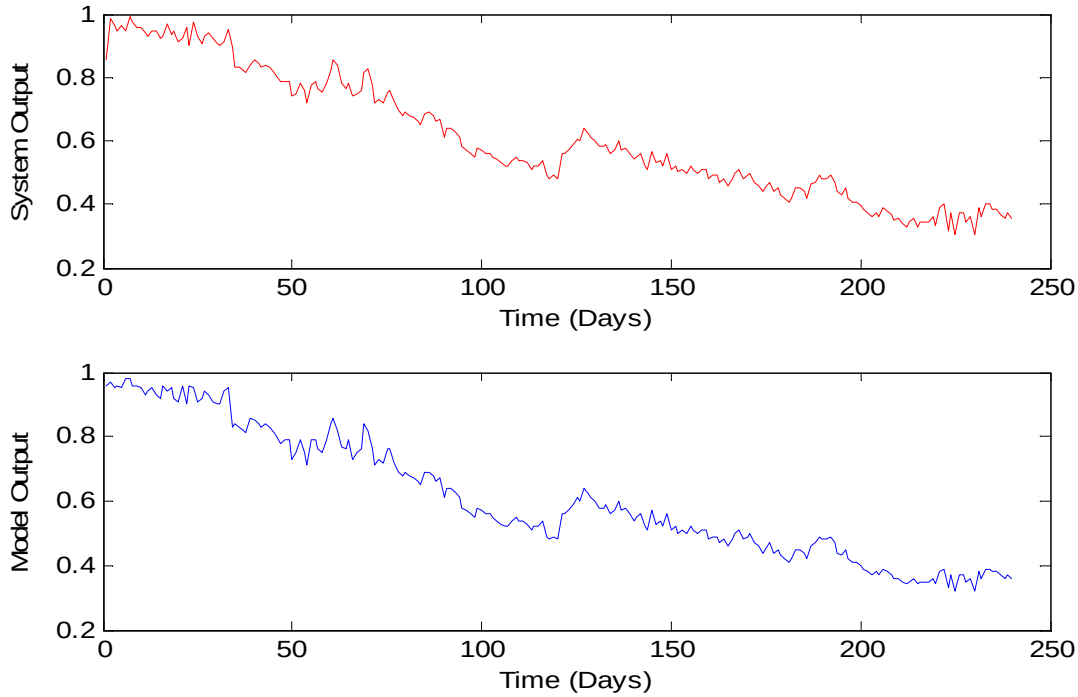

Figure 7.17: Model output and system output of efficiency in Training phase

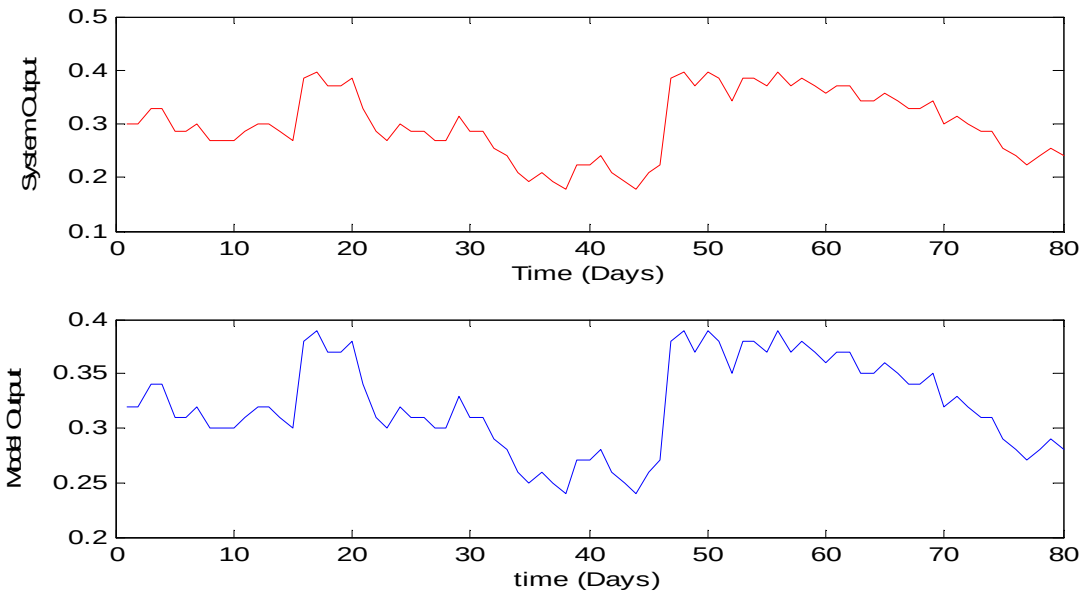

Figure 7.18: Model output and system output of efficiency in Testing phase

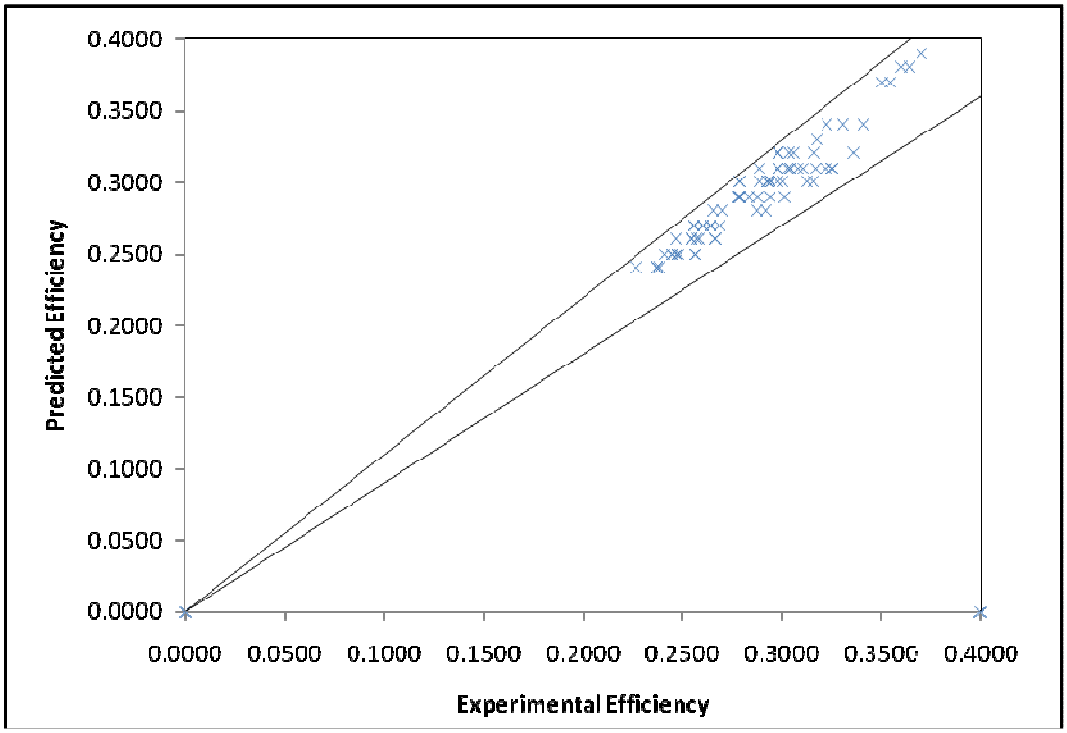

Figure 7.19 : Comparision of predicted and actual efficiency

The objective of the fouling prediction model is to provide a priori picture about the fouling behavior of the exchanger over the next period of operation. However to improve the model accuracy in spite of process drifts, the network may be modified as a recurrent network. When the process undergoes any change due to operational changes, the model has to be changed this can be solved by adaptive retaining of the network to take into account the new process conditions. However this remains as a future scope of the current work to develop an adaptive network in order to improve the model accuracy under process drift conditions.

7.5 Summary

Modeling of heat exchanger fouling using previous data of a shell and tube heat exchanger has been found to be a very useful methodology to predict and consequently improve the overall performance of a process plant involved with such systems. A local linear wavelet neural network based model has been developed to predict the temperature differences

on both the tube and shell side and the heat exchanger efficiency. The characteristic of the network is that the straightforward weight is replaced by a local linear model. The working process of the proposed network can be viewed as to decompose the complex, nonlinear system into a set of locally active submodels, then smoothly integrate those submodels by their associated wavelet basis functions. The proposed LLWNN experiments demonstrate that only a few of wavelet basis functions is needed for a given approximation or prediction problem with sufficient accuracy. This is because the local linear models provide more power than a constant weight. Moreover, the dilation and translation parameters of LLWNN are randomly generated and optimized without predetermination. The closeness of the predicted results with that of the actual experimental results and higher accuracy indicate that LLWNN can be used as a suitable tool for simulation of heat exchangers subjected to fouling in industrial applications. This may be successfully used for effective preventive maintenance scheduling and cleaning of a heat exchanger.

Chapter 8

Conclusion and Scope for Future Work

8.1 Conclusions

This work has presented a detailed investigation for estimation of heat transfer performances of a heat exchanger due to fouling. The goal of this work is to provide a new tool that can be used as an alternative to conventional techniques for analyzing fouling in heat exchanger systems that in general are too complex. The following are the significant conclusions emerging out of this work.

In the formulation presented in this work, the equations of the Bell-Delaware method have been simplified to expressions, with a similar mathematical form as those based on the Kern correlations. Thus, the proposed method has the advantage of offering a more realistic picture of the actual shell side flow pattern, with minimal complexity. The Bell-Delaware model provides a detailed, reliable and simplified method to determine heat transfer coefficients on both the shell and tube side of a shell and tube heat exchanger.

The statistical analysis is used to present a simple probabilistic approach to characterize various fouling models that are commonly encountered in industrial processes. The models investigated are normal, log-normal, exponential and weibull. These random fouling growth models are then used to investigate the thermal effectiveness, overall thermal resistance and overall heat-transfer coefficient of a shell-and-tube heat exchanger. Knowledge of these distributions and the methods to determine their parameters is useful for devising appropriate maintenance and cleaning schedules in a probabilistic framework. Although the analysis presented in this work is applicable to shell-and-tube heat exchangers, the procedure can easily be modified to include other types of heat exchanger such as double pipe, plate-and-frame and other compact heat exchangers. Hence it can be concluded that statistical analysis is a significant tool for predicting the average time required to reach critical level of fouling in a heat exchanger. By utilizing the fouling growth laws and the time required to reach critical level of fouling, appropriate heat exchanger maintenance policies can be developed.

For design and analysis of heat exchangers, it is necessary to evaluate the average heat transfer coefficients for one or both fluid side surfaces. If the heat transfer coefficients are to be determined for both fluid sides of a heat exchanger or for the case when the thermal resistances on both fluid sides are of the same order of magnitude, the Wilson plot method appears to be very useful to determine an accurate heat transfer correlation. The main idea of Wilson plot method is to split the overall thermal resistance into individual thermal resistances. In order to obtain the overall thermal resistance, inlet and outlet flow rates and temperatures on both sides of the heat exchanger and heat transfer rate were measured. Afterwards a precise energy balance of the heat exchanger was carried out and suitable statistical procedure of data analysis was applied. When the modified Wilson plot method was applied, the linear regression is used as a statistical procedure. Due to the fact that only linear regression is used to estimate the unknowns, the number of unknowns cannot be greater than 2 in the modified Wilson method. One of the modifications of Wilson method, which allows us to estimate 3 unknown parameters is based on the double use of the linear regression scheme connected with an iterative procedure. Thus the Wilson plot method and its modifications furnish an indirect tool to develop accurate correlation equation equations for heat transfer analysis of heat exchange devices.

The major outcome of this work is the development of C-factor for estimation of fouling effects on the performance of a heat exchanger. As compared to the conventional methods using overall heat transfer coefficient, this method involves minimum number of parameters to predict the operating status of a heat exchanger. Simultaneously it has been observed that the C-factor gives a clear indication of the degradation of performance due to fouling in heat exchangers. Although it is not related to fouling factor, but it can be used as an instructive parameter to give information about heat transfer performances such as overall heat transfer coefficient, cleanliness factor and overall thermal resistance. Besides the method eliminates the use of correlations which can lead to minimization of errors in analyzing effect of fouling and its quantification. The method takes into account the experimental values of flow rate and pressure drop across the tubes. This eliminates the effect of complexity in geometric configuration of the exchanger. As compared to the Wilson plot method and its modifications, this method takes into consideration no assumptions, which signifies the generality of this

method. Thus this method can find broad application in process industries involving heat exchange equipments to formulate an accurate maintenance schedule so that process efficiency is not hampered and unnecessary cleaning is avoided. Fouling in heat exchangers cannot be eliminated completely, but it can be monitored suitably to obtain the highest possible outcome of a process plant using heat exchangers. The C-factor can be regarded as a parameter for complete monitoring of fouling in heat exchangers.

The experimental outcomes of the heat exchanger under consideration have been used in three different methods to obtain average time required to reach critical fouling obtained. The operating conditions corresponding to critical fouling is dependent on specific process requirement and can be defined by individual specification. As mentioned in literature, the critical fouling is considered to be attained when the overall heat transfer coefficient falls to 60% -65% of the clean design value. In this work, the critical level of fouling is considered to be attained when the overall heat transfer coefficient falls to 60% of the clean design value. The statistical analysis for the heat exchanger under consideration predicts an average time of 106.4 days to attain critical fouling condition. The Wilson plot and its modifications indicate that the same condition is obtained in a period of 104 days of operation. The C-factor method indicates 114 days of operation required to attain the same condition of fouling. The statistical analysis considered in this work takes into account the log-normal distribution with a regression coefficient of R^2=0.945. As the Wilson plot method is based on certain assumptions, it deviates to some extent from the most accurate analysis. Among all these three methods, the C-factor method provides the most accurate results and with minimum complexity involved in the process of estimation of fouling and its effects. Unlike the statistical analysis, the C-factor method eliminates the incorporation of empirical correlations which is too much cumbersome to calculate fouling effects. Similarly this method avoids the assumptions required for Wilson plot method which gives a more generalized and accurate result. A comparison the time required to attain critical fouling is illustrated in table 8.1. As indicated in table 8.1, the statistical analysis and Wilson plot method deviate by 6.6% and 8.7% respectively from the C-factor method. This indicates that the C-factor method can be utilized to avoid undue cleaning prematurely before critical fouling level is reached. This can reduce both cost and un-necessary idle time of a heat exchanger under operation. Thus C-factor method is considered the most

significant tool for predicting the fouling behavior of a heat exchanger by using neural network approach.

Methods	Thermal Analysis (B-D Method)	Statistical analysis Method	Wilson Plot Method	Modified Wilson Plot Method	C-Factor Method
Time to reach critical fouling (Days)	98	106.4	104	109	114

Table 8.1 : Time required to reach critical fouling by various methods

The application of artificial neural network provides a clear picture regarding the fouling behavior of the heat exchanger under consideration. The accuracy of prediction is tested in terms of various errors during the testing analysis of the experimental data which fall outside the scope of the experimental data used for training the network. The neural network approach takes into account the efficiency of the exchanger in terms of the C-factor which is one of the most significant instructive parameter of heat exchanger performance. Considering the closeness of the predicted output with that of the experimental output, local linear wavelet neural network can be used as a predictive tool for fouling behavior of a heat exchanger.

8.2 Scope for Future Work

The present work considers the investigation of fouling behavior of a heat exchanger using water both as the hot and cold fluid. Also both the fluids were considered to be in single phase during the whole period of operation. The further study related to this work can be recommended as follows.

- The fouling analysis can be further carried out for exchangers involving different fluids on shell and tubes such as liquid and gas.
- The phase change of liquids during the operation can be taken up to provide more detailed information for processes involving higher variation of temperatures.
- In order to obtain realistic results, experiments with industrial fluids should be performed at similar conditions as those prevailing in the actual heat exchangers.

- The effective cleaning methodologies and especially self cleaning methodologies should be investigated which can lead to longer operation of a heat exchanger with reduced fouling growth on heat transfer surfaces.

References

1. Al-Bagawi, J.J. (2002) Fouling Analysis and its Mitigation in Heat Exchangers, PhD Thesis, King Fahd University of Petroleum and Minerals, Dhahran, Saudi Arabia.
2. Aminian J.and Shahhosseini, S. (2009) Neuro-based formulation to predict fouling threshold in crude preheaters, International Communications in Heat and Mass Transfer, 36 (5), 525-531.
3. Amina, M., Kodogiannis, V.S., Petrounias, I.P., Ligouras, J.N. and Nychas, G.J.E. (2012) Identification of the listeria monocytogenes survival curves in UHT whole milk utilizing local linear wavelet neural network, 39, 1435 – 1450.
4. Antar, M.A. and Zubair, S.M. (2007) The impact of fouling on performance evaluation of multizone feed-water heaters, Applied Thermal Engineering, 27, 2505 – 2513.
5. Bansal, B, Chen, X. D., Muller-Steinhagen, H.(2008) Analysis of classical deposition rate law for crystallisation fouling, Chemical Engineering and Processing, 47, 1201 – 1210.
6. Bansal, B.,Chen, X.D. and Muller-Steinhagen, H. (2008) Analysis of classical deposition rate law for crystallisation fouling, Chemical Engineering and Processing, 47,1201-1210.
7. Barman , J. and Ghosal, A.K. (2007) Performance analysis of finned tube and unbaffled shell and tube heat exchangers, International Journal of Thermal Sciences, 46 (12), 1311 – 1317.
8. Benveniste, A., Juditsky A., Delyon B., Zhang Q. and Glorennec P.Y. (1994) Wavelets in identification, Proceedings of 10th IFAC Symposium of System Identification, Copenhagen, pp. 27–48.
9. Bott, T. R.(1995) Fouling of heat exchangers, Elsevier, New York.

10. Bouris, D., Konstantinidis, E., Balabani S., Castigila, D. Bergeles, G. (2005) Design of novel, intensified heat exchanger for reduced fouling, 48(18), International Journal of Heat and Mass Transfer, 3817 – 3832.
11. Brahim, F., Augustin, W. and Bohnet, M. (2003) Numerical simulation of fouling process, International Journal of Thermal Sciences, 42, 323 – 334.
12. Chang, Y.J. and Hsu, C.T. (2006) Single-tube performance of condensation of R-134a on horizontal enhanced tubes, ASHRAE Transactions, 102, 821–829.
13. Chang, Y.P., Tsai, R. and Hwang, J.W. (1997) Condensing heat transfer characteristics of an aluminum flat tube, Applied Thermal Engineering, 17, 1055–1065.
14. Chaudagne, D. (1992) Fouling costs in the field of heat exchange equipment in the French market, fouling mechanisms, theoretical and practical aspects, in: Proceedings of the Eurotherm Seminar No. 23, Grenoble, France, 21–28.
15. Coletti, F. and Macchieto, S. (2009) Predicting refinery energy losses due to fouling in heat exchangers, Computer aided Chemical Engineering, 27, 219 – 224.
16. Coletti, F. and Macchietto, S. (2011) A Dynamic, Distributed Model of Shell-and-Tube Heat Exchangers Undergoing Crude Oil Fouling, Industrial and Engineering Chemistry Research, 50 (8), 4515–4533.
17. Costa, A.L.H. and Querioz, E.M. (2008) Design optimization of shell and tube heat exchangers, Applied Thermal Engineering, 28, 1798 – 1805.
18. Crittenden, B. and Kolaczkowski, S. (1979) Mass transfer and chemical kinetics in hydrocarbon fouling. Proceedings of the Conference on Fouling Science or Art, London, 169-187.
19. Crittenden, B.D., Kolaczkowski S.T. and Hout, S.A. (1987) Modelling hydrocarbon fouling. Trans. Chem. Part A, 65, 171-179.
20. Crittenden, B. D., Kolaczkowski, S. T. and Downey, I. L. (1992) Fouling of crude oil preheat exchangers, Chemical Engineering Research and Design, 70, 547–557.
21. Crittenden, B.D., Kolaczkowski S.T. and Phillips, D.Z. (2009) Crude oil fouling in a pilot-scale parallel tube apparatus, Heat Transfer Engineering, 30 (10-11), 777-785
22. Diaz, G., Sen, M., Yang, K.T. and McClain, R.L. (1999) Simulation of heat exchanger performance by arti_cial neural networks, International Journal of HVAC&R Research, 5(3), 195-208.

23. Diaz, G., Sen, M., Yang, K.T. and McClain, R.T. (2001)Adaptive neuro-control of heat exchangers, ASME Journal of Heat Transfer, 123, 417– 612.
24. Diaz, G., Sen, M., Yang, K.T., McClain, R.L. (2001) Dynamic prediction and control of heat exchangers using artificial neural networks, International Journal of Heat and Mass Transfer, 44, 1671 – 1679.
25. Dirker,J. and Meyer, J.P. (2005) Convective heat transfer coefficients in concentric annuli, Heat Transfer Engineering, 26, 38–44.
26. Duffuaa, S.O. and Budair**,** M.O. (1994) Scale removal from heat-exchangers: Using energy utilization as a schedule criterion, Applied Energy, 47 (10), 77 – 85.
27. Dutta, B.K. (2005) Heat transfer principles and applications, Prentice hall of India Private limited, New Delhi, India.
28. Ebert, W.A. and C.B. Panchal, 1995. Analysis of Exxon Crude-Oil Slip Stream Coking Data. In: Fouling Mitigation of Industrial Exchange Equipment, Paschal, C.B. and W.C. Kuru *et al*. (Eds.). Begell House, New York, pp: 451-460.
29. Epstein, N. (1983) Thinking about Heat Transfer Fouling: A 5x5 matrix, Heat Transfer Engineering, 4(1), 43-56.
30. Epstein, N. (1994) A model of the initial chemical reaction fouling rate for flow within a heated tube and its verification, Proceedings of 10th International Heat Transfer Conference, 4, 225-229.
31. ESDU (1988) Fouling in cooling water systems, ESDU Data Item No. 88024, ESDU
32. ESDU (2000) Heat Exchanger fouling in the preheat train of a crude oil distillation unit, ESDU Data Item No. 00016, ESDU International Plc, London, 2000.
33. ESDU (2003) Fouling in cooling systems using sea water, ESDU Data Item No. 03004, ESDU International Plc, London.
34. ESDU (2007) Fouling in cooling systems using fresh water, ESDU Data Item No. 07006, ESDU International Plc, London.
35. Fernandez-Siera, J., Uhia, F.J., Sieres J. and Campo, A. (2005) Experimental apparatus for measuring heat transfer coefficients by the Wilson plot method, European Journal of Physics, 26, 1- 11.

36. Fernandez-Siera, J., Uhia, F.J., Sieres J. and Campo, A. (2007) general review of the Wilson Plot Method and its modifications to determine convection coefficients in heat exchange devices, Applied Thermal Enggineering, 27, 2745 – 2757.
37. Fernando, P., Palm, B., Ameel, T., Per, L. and Granryd, E. (2008) A minichannel aluminium tube heat exchanger- PartI: Evaluation of single phase heat transfer coefficients by the Wilson plot method, international Journal of Refrigeration, 31, 669 – 680.
38. Galvao, R.K.H. and Becerra, V.M. (2002) Linear-wavelet models applied to the identification of a two-link manipulator, Proceedings of 21st IASTED International Conference on Modelling, Identification and Control, Innsbruck, pp. 479–484.
39. Garrett-Price, B.A., Smith, S.A., Watts, R.L., Knudsen, J.G., Marner, W.J.,Suitor, J.W. (1985) Costs of Fouling, Fouling of Heat Exchangers- Characteristics, Costs, Prevention, Control, and Removal, Noyes Publications, Park Ridge.
40. Gracia, R.F. (2012) Improving heat exchanger supervision using neural networks and rule based techniques, Expert Systems with Applications, 39, 3012 – 3021.
41. Gudmundur, R.J., Lalot, S., Palsson, O.P. and Desmet, B. (2007) Use of extended kalman filtering in detecting fouling in heat exchangers, International journal of Heat and Mass Transfer, 50, 2643 – 2655.
42. Hasim, F., Yoshida, M. and Miyashita, H. (2003) Compound heat transfer enhancement by a combination of a helically ribbed tube with twisted tape inserts, Journal of Chemical Engineering of Japan,36, 1116–1122.
43. Hasson, D., Drak, A., Komlos, C., Yang, Q. and Semiat, R. (2007) Detection of fouling on RO modules by residence time distribution analysis, Desalination, 204, 132 – 144.
44. Haykin, S.S. (1999) Neural networks: a comprehensive foundation, 2nd edition, Prentice Hall, London, UK.
45. Hewitt, G.F., Shires, G. L. and Bott, T. R. (1994) Process Heat Transfer, CRC Press. International Plc, London.
46. Kakac, S. and Liu, H (2002), Heat exchangers: selection, rating, and thermal design, 2nd edition, CRC Press, Boca Raton, FL.
47. Kapur, K. C. and Lamberson, L.R. (1977) Reliability in engineering design, John Wiley and sons, New York, 1977.

48. Kern, D.Q. (1950) Process Heat Transfer; McGraw-Hill, New York.
49. Kern, D.Q. and Seaton, R.E. (1959) A theoretical analysis of thermal surface fouling, Britsh Chemical Engineering, 4, 258-262
50. Kukulka, D.J. and Devgun, M. (2007) Fluid temperature and velocity effect on fouling, Applied Thermal Engineering, 27, 2732–2744.
51. Kumar, R., Varma, H.K., Agrawal, K.N. and Mohanty, B. (2001) A comprehensive study of modified Wilson plot technique to determine the heat transfer coefficient during condensation of steam and R-134a over single horizontal plain and finned tubes, Heat Transfer Engineering, 22, 3-12.
52. Kuosa, M., Kaikko, J. and Koskelainen, E. (2007) The impact of heat exchanger fouling on the optimum operation and maintenance of stirling engine, Applied Thermal Engineering, 27 (10), 1671 – 1676.
53. Kuppan, T. (2000) Heat Exchanger Design Handbook, Marcel Dekker Inc., New York.
54. Lalande, M., Rene, F. and Tissier, J P. (1989) Fouling and its control in heat exchangers in dairy industry, Biofouling, 1, 233-250.
55. Lalot, S. (2006) On-line detection of fouling in a water circulating temperature controller (WCTC) used in injection moulding Part 1: Principles. Applied Thermal Engineering,26, 1087-1094.
56. Lalot, S. and Palsson, H. (2010) Detection of fouling in a cross-flow heat exchanger using neural network based technique, International Journal of Thermal Sciences, 49, 675 – 679.
57. Little, R.E. (1978) Probability and Statistics for Engineer, Matrix Publishers, New York.
58. Lodge, B.N., Judd, S.J. and Smith, A. J. (2002) A statistical method for quantifying the different fouling effects of three combined water sources on an ultrafiltration membrane, Deslaination, 142, 143 – 149.
59. Lohr, K. R. and Rose, J. L. (2003) ultrasonic guided wave and acoustic impact methods for pipe fouling detection, Journal of food engineering, 56, 315- 324.
60. Malayeri, M.R. and Müller-Steinhagen, H. (2007) An overview of fouling mechanisms, prediction and mitigation strategies for thermal desalination plants, Eleventh International Water Technology Conference, Egypt, 299- 314.

61. Medardo , S.G., Jose, M.P., Agustin, J.C. and Arturo, J.G. (2007) Feasible design space for shell and tube heat exchanger using Bell-Delaware method, Industrial and Engineering Chemistry Research, 46, 143-145.
62. Melo, L.F., Bott, T.R., Bernardo, C.A. (1988) Fouling Science and Technology, Springer.
63. Milanovic, P., Jacimovic, B. and Genic, S. (2006) experimental measurement of fouling resistance in the heat exchanger of a geothermal heating system, Geothermics, 35, 79-86.
64. Mizutani, F.T., Pessoa, F.L.P., Queiroz, E.M., Hauan, S. and Grossmann, I.E. (2003) Mathematical programming model for heat exchanger network synthesis including detailed heat exchanger design, Industrial and Engineering Chemistry Research, 42, 4009 – 4018.
65. Muller-Steinhagen, H.(2000) Heat Exchanger Fouling: Mitigation and cleaning Technologies, Publico publications, Germany.
66. Mullin, J.W. (2001) Crystallization, Butterworth-Henmann Publications, Oxford.
67. Mwaba, M.G. (2003) Analysis of Heat Exchanger Fouling in Cane Sugar Industry, PhD Thesis, Eindhoven University of Technology, Eindhoven, The Netherlands.
68. Mwaba, M.G.,Golriz, M.R.and Gu, J. (2006) A semi-emirical correlation for crystallization fouling on heat exchanger surfaces, Applied Thermal Engineering, 26, 440-447.
69. Nasr, M.R. and Givi, M.M. (2006) Modeling of crude oil fouling in preheat exchangers of refinery distillation units, Applied Thermal Engineering, 26, 1572-1577
70. Negrao, C. O. R., Tonin, P. C. and Madi, M.(2007) Supervision of the thermal performance of heat exchanger trains, Applied Thermal Engineering, 27, 347–357.
71. Nesta, J. and Bennett, C. A. (2005) Fouling Mitigation by Design, ECI Symposium Series, Volume RP2: Proceedings of 6th International Conference on Heat Exchanger Fouling and Cleaning - Challenges and Opportunities, Engineering Conferences International, Kloster Irsee, Germany.
72. Pacheco-Vega, A., Diaz, G., Sen, M., Yang, K.T. and McClain, R.T. (2001) Heat rate predictions in humid air–water heat exchangers using correlations and neural networks, ASME Journal of Heat Transfer, 123, 348 – 354.

73. Panchal, C.B., Kuru, W.C., Liao, C.F., Ebert W.A. and Palen, J.W. (1997) Threshold conditions for crude oil fouling. Proceedings of the Understanding Heat Exchanger Fouling and its Mitigation, May 11-16, Pascoli, Italy, 273-273.
74. Peng, H. and Ling, X. (2009) Neural network analysis of thermal characteristics on plate-fin heat exchangers with limited experimental data, Applied Thermal Engineering, 29 (5-6) , 2251 – 2256.
75. Pilavachi, P.A. and Isdale, J.D. (1993) European community R&D strategy in the field of heat exchanger fouling: Projects, Heat Recovery Systems and CHP, 13 (2), 133 – 138.
76. Polley, G.T., Wilson, D.I., Yeap B.L. and Pugh, S.J. (2002) Evaluation of laboratory crude oil threshold fouling data for application to refinery preheat trains, Applied Thermal Engineering, 22, 777-788.
77. Pritchard, A.M. (1988) The Economics of Fouling, Fouling Science and Technology, vol. 145, NATO ASI Series, Series E: Applied Sciences, 31–45.
78. Quan, Z., Chen, Y.C. and ChongFang M. (2008) Heat mass transfer model of fouling process of calcium carbonate on heat transfer surface, Science in China Series E: technological Sciences, 51(7), 882 – 889.
79. Radhakrishnan, V.R., Ramasamy, M., Zabiri, H., Thanh, V.D., Tahir, N.M., Mukhtar, H., Hamdi, M.R. and Ramli, N. (2007) Heat exchanger fouling model and preventive maintenance scheduling tool, Applied Thermal Engineering, 27, 2791 – 2802.
80. Ramasamy, M., Shahid, A. and Zabiri, H. (2008) Drift analysis on neural network model of heat exchanger fouling, Journal of Engineering Science and Technology, 3(1), 40 – 47.
81. Ravagnani, M.A.S.S., Silva, A.P. and Andrade, A.L. (2003) Detailed Equipment Design in Heat Exchanger Networks Synthesis and Optimization, Applied Thermal Engineering, 23,141–151.
82. Rooyen, E. V., Christians, M. and Thome, J.R. (2012) Modified Wilson plots for enhanced heat transfer experiments : current status and future perspectives, Heat Transfer Engineering, 33 (4-5), 342 – 355.

83. Ruckstein, E. and Prieve, D. C. (1973) Rate of Deposition of Brownian particles under the action of London and double layer forces, Journal of Chemical Society, 69, 1522 – 1536.
84. Saleh, Z.S., Sheikholeslami R. and Watkinson, A.P. (2005) Fouling characteristics of a light Australian crude oil, Heat Transfer Engineering, 26, 15-22.
85. Serna, M. and Jimenez, A. (2004) An Efficient Method for the Design of Shell and Tube Heat Exchangers, Heat Transfer Engineering, 25, 5–16.
86. Serna, M. and Jimenez, A. (2005) A compact formulation of the Bell-Delaware method for heat exchanger design and optimization, Chemical Engineering Research and Design, 83 (5), 539 – 550.
87. Serna, M.G., Jose, M.P., Agustın, J.C. and Gutierrez, A.J. (2007) Feasible Design Space for Shell-and-Tube Heat Exchangers Using the Bell-Delaware Method, Industrial Engineering & Chemistry Research, 46,143-155.
88. Shah, R.K. (1990) Assessment of modified wilson plot techniques for obtaining heat exchanger design data, 9th International Heat Transfer Conference, 51-56
89. Shah, R.K. and Sekulic, D.P. (2003) Fundamentals of Heat Exchanger Design, John Wiley and Sons, New York.
90. Sheikh, A. K. and Al-Bagawi, J. J. (1999) statistical characterization of time between cleaning of thermosyphon reboilers in oil industry, proceedings of International conference on mitigation of heat exchanger fouling and its economic and environmental implications, Canada, 301 – 313.
91. Sheikh, A.K., Zubair, S.M, Haq, M. U. and Budair, M. O. (1996) Reliability-Based maintenance Strategies for Heat Exchangers Subject to Fouling, Journal of Energy Resource Technology, 118(4), 306 – 312.
92. Sieder, E.N. and Tate, G.E. (1936) Heat transfer and pressure drop of liquids in tubes. Industrial & Engineering Chemistry, 28, 1429-1435.
93. Sinnott, R.K.(1996) Coulson & Richardson's Chemical Engineering - Chemical Engineering Design, revised 2nd ed., Vol. 6., Butterworth-Heinemann, Oxford, U.K.
94. Somerscales, E.F.C. (1981) Fouling of Heat Transfer Equipment, Hemisphere Publishing Corporation.

95. Steinhagen, R., M¨uller-Steinhagen, H., Maani, K. (1993) Problems and costs due to heat exchanger fouling in New Zealand industries, Heat Transfer Engineering, 14 (1), 19–30.
96. Steinhagen H.M., Mayaleri, M.R. and Watkinson, A.P. (2011) Heat Exchanger Fouling : Mitigation and cleaning strategies, Heat Transfer Engineering, 32 (304), 189 – 196.
97. Taborek, J., Ritter, R. B. and Palen J. W. (1972) Fouling: The Major Unresolved Problem in Heat Transfer, Chemical Engineering Progress, 68(2), 59-67.
98. Taborek, J. (1983) Heat Exchanger Design Handbook,Hemisphere Publications, New York.
99. Takemoto, T., Crittenden, B. D. and Kolaczkowski, S. T. (1999) Interpretation of fouling data in industrial shell and tube heat exchangers, Trans IChemE, Part A, 769-778.
100. Tan, C.K., Ward, J., Wilcox, S.J. and Payne, R. (2009) Artificial neural network modelling of the thermal performance of a compact heat exchanger, Applied Thermal Engineering, 29(17-18), 3609-3617 .
101. TEMA (2007) Standards of the Tubular Exchanger Manufactures Association, 9th ed., New York.
102. Teruel, E., Cortes, C., diez, L. I. and Arauzo, I. (2005) monitoring and prediction of fouling in coal-fired utility boilers using neural networks, Chemical Engineering Science, 60, 5035 – 5048.
103. Than, S.T.M., Lin, K.A. and Mon, M.S. (2008) Heat Exchanger Design, World Academy of Science, Engineering and Technology, 46, 604 – 611.
104. Thome, J.R. (2004) Wolverine tube Heat Transfer Data Book III, Wolverine Tube Inc., Lausanne.
105. Van, B. (2001) gas side fouling in heat recovery boilers, PhD Thesis, Eindhoven University of Technology, Eindhoven, the Netherlands.
106. Vasickaninova, A., Bakasova, M., Meszaros, A. and Klemes, J.J. (2011) Neural network predictive control of a heat exchanger, Applied Thermal Engineering, 31 (13), 2094 – 2100.
107. Wallhauber, E., Hussein, M.A. and Becker, T. (2012) Detection methods of fouling in heat exchangers in the food industry, Food Control, 27(1), 1-10.

108. Wang, Q.W., Xie, G.N., Zeng, M. and Luo, L.Q. (2007) heat transfer analysis for shell and tube heat exchangers with experimental data by neural network approach, Applied Thermal Engineering, 27 (5 -6), 1096 – 1104.

109. Watkinson, A.P. and N. Epstein (1969) Gas oil fouling in sensible heat exchanger. CEP Symposium Series, 65, 84-90.

110. Watkinson, A.P. (1988) Critical review of organic fluid fouling, Final report – Contract 73212402, Argonne National Laboratory.

111. Wilson, E.E. (1915) A basis for rational design of heat transfer apparatus, ASME journal of Heat Transfer, 37, 47 – 70.

112. Wright, S., Andrews, G. and Sabir, H. (2009) A review of heat exchanger fouling in the context of air-craft air-conditioning systems and the potential for electrostatic filtering, Applied Thermal Engineering, 29(13), 2596 – 2609.

113. Yeap, B.L., Hewitt, G.F., Wilson D.I.and Pugh, S.J. (2001) Simulating the Fouling Behaviour in Shell-and-Tube Heat Exchangers, Proceedings of the 4th International Conference on Heat Exchanger Fouling Fundamental Approaches and Technical Solutions, Davos, Switzerland, 275 – 283.

114. Yuehui, C., Bo, Y. and Jiwen Dong (2006), Time series prediction using a local linear wavelet neural network, Applied soft computing, 69 (4-6), 449 – 465.

115. Zainuddin, Z. and Pauline, O. (2011), Modified wavelet neural network in function approximation and its application in prediction of time series pollution data, Applied Soft Computing, 11, 4866 – 4874.

116. Zhang, Q. (1997) Using wavelet network in nonparametric estimation, IEEE Transactions on Neural Network, 8(2), 227–236.

117. Zhenhua, Q., Chen, Y. and Chongfang, M.A.(2008) Experimental study of fouling on heat transfer surfaces during forced convective heat transfer, Chinese Journal of Chemical Engineering, 16 (4), 535 – 540.

118. Zheng, X.J., Jin, G.P., Chyu, M.C. and Ayub, Z.H. (2006) Boiling of ammonia lubricant mixture on a horizontal tube in a flooded evaporator with inlet vapor quality, Experimental Thermal and Fluid Sciences, 30, 223–231.

119. Zhi-Ming, X.U., Zhong-Bin, Z. and Shan-Rang, Y. (2007) Costs due to Utility fouling in China, Proceedings of 7th International Conference on Heat Exchanger Fouling and Cleaning – Challenges and Oppertunities, 113 – 118.

120. Zubair, S.M., Sheikh, A.K., Budair, M.O. and Badar, M.A. (1997) A Maintenance Strategy for Heat Transfer Equipment Subject to Fouling: A Probabilistic Approach, Journal of Heat Transfer, 119 (3), 575 – 580.

121. Zubair, S. M., Sheikh, A. K., Budair, M. O. and Younas, M. (1999) A Maintenance Strategy for heat transfer equipment subjected to Fouling, Research Project , KFUPM.

122. Zubair, S. M., Sheikh, A. K., Younas, M. and Budair, M. O. (2000) A risk based heat exchanger analysis subject to fouling. Part I- Performance evaluation, Energy, 25, 427 – 443.

Appendix A

Data and Sample Results for the Heat Exchanger

Table A.1 : Samples of Operation Data

Day	m_t (kg/s)	m_s (kg/s)	$T_{h,in}$ (^oC)	$T_{h,out}$ (^oC)	$T_{c,in}$ (^oC)	$T_{c,out}$ (^oC)
1	0.10958	0.08246	40	34.6	22	28.6
2	0.10958	0.08246	40	34.6	22	28.6
3	0.10958	0.08246	40	34.5	22	28.8
4	0.10958	0.08246	40	34.6	22	28.8
5	0.10958	0.08246	40	34.7	22.1	28.7
6	0.10958	0.08246	40	34.7	22.1	28.8
7	0.10958	0.08246	40	34.7	22.1	28.8
8	0.10958	0.08246	40	34.7	22.3	28.8
9	0.10958	0.08246	40	34.7	22.3	29
10	0.10958	0.08246	40	34.7	22.3	29
11	0.10958	0.08246	40	34.7	22.3	29
12	0.10958	0.08246	40	34.8	22.4	29
13	0.10958	0.08246	40	34.8	22.4	29.2
14	0.10958	0.08246	40	34.8	22.5	29.2
15	0.10958	0.08246	40	34.8	22.5	29.2
16	0.10958	0.08246	40	34.8	22.5	29.2
17	0.10958	0.08246	40	34.8	22.5	29.1
18	0.10958	0.08246	40	34.8	22.5	29.1
19	0.10958	0.08246	40	34.8	22.5	29.2
20	0.10958	0.08246	40	34.9	22.8	29.2
21	0.10903	0.08246	45	38.4	22.8	30.9
22	0.10903	0.08246	45	38.6	22.8	30.4
23	0.10903	0.08246	45	38.6	22.8	30.5
24	0.10903	0.08246	45	38.6	22.8	30.4
25	0.10903	0.08246	45	38.7	22.8	30.4
26	0.10903	0.08246	45	38.7	22.8	30.5
27	0.10903	0.08246	45	38.7	22.9	30.5
28	0.10903	0.08246	45	38.7	22.9	30.5
29	0.10903	0.08246	45	38.7	22.9	30.5
30	0.10903	0.08246	45	38.7	22.9	30.5

Table A.1 : Samples of Operation Data (Contd.)

Day	m_t (kg/s)	m_s (kg/s)	$T_{h,in}$ (^oC)	$T_{h,out}$ (^oC)	$T_{c,in}$ (^oC)	$T_{c,out}$ (^oC)
31	0.10903	0.08246	45	38.8	23	30.5
32	0.10903	0.08246	45	38.8	23	30.5
33	0.10903	0.08246	45	38.8	23	30.6
34	0.10903	0.08246	45	38.8	23	30.6
35	0.10903	0.08246	45	38.8	23	30.6
36	0.10903	0.08246	45	39	23.2	30.7
37	0.10903	0.08246	45	39	23.2	30.7
38	0.10903	0.08246	45	39	23.2	30.7
39	0.10903	0.08246	45	39	23.2	30.8
40	0.10903	0.08246	45	39	23.2	30.8
41	0.10878	0.08246	50	43.7	23.5	31.6
42	0.10878	0.08246	50	43.7	23.5	31.6
43	0.10878	0.08246	50	43.7	23.5	31.5
44	0.10878	0.08246	50	43.7	23.5	31.6
45	0.10878	0.08246	50	43.6	23.5	31.7
46	0.10878	0.08246	50	43.6	23.5	31.6
47	0.10878	0.08246	50	43.6	23.5	31.6
48	0.10878	0.08246	50	43.4	23.5	31.7
49	0.10878	0.08246	50	43.4	23.5	31.7
50	0.10878	0.08246	50	43.4	23.5	31.7
51	0.10878	0.08246	50	43.4	23.5	31.7
52	0.10878	0.08246	50	43.3	23.5	31.8
53	0.10878	0.08246	50	43.3	23.5	31.8
54	0.10878	0.08246	50	43.2	23.5	31.8
55	0.10878	0.08246	50	43.2	23.6	31.8
56	0.10878	0.08246	50	43.2	23.6	31.8
57	0.10878	0.08246	50	43.2	23.6	31.8
58	0.10878	0.08246	50	43	23.6	32
59	0.10878	0.08246	50	43	23.6	32
60	0.10878	0.08246	50	43	23.6	32

Table A.1 : Samples of Operation Data (Contd.)

Day	m_t (kg/s)	m_s (kg/s)	$T_{h,in}$ (^oC)	$T_{h,out}$ (^oC)	$T_{c,in}$ (^oC)	$T_{c,out}$ (^oC)
61	0.10841	0.08246	55	46.7	23.8	33.5
62	0.10841	0.08246	55	46.7	23.8	33.5
63	0.10841	0.08246	55	46.7	23.8	33.5
64	0.10841	0.08246	55	46.5	23.8	33.6
65	0.10841	0.08246	55	46.5	23.8	33.6
66	0.10841	0.08246	55	46.7	24	33.6
67	0.10841	0.08246	55	46.7	24	33.6
68	0.10841	0.08246	55	46.7	24	33.6
69	0.10841	0.08246	55	46.5	24	33.7
70	0.10841	0.08246	55	46.5	24	33.7
71	0.10841	0.08246	55	46.5	24	33.7
72	0.10841	0.08246	55	46.6	24.2	33.8
73	0.10841	0.08246	55	46.6	24.2	33.8
74	0.10841	0.08246	55	46.7	24.2	33.8
75	0.10841	0.08246	55	46.7	24.2	33.8
76	0.10841	0.08246	55	46.5	24.3	33.9
77	0.10841	0.08246	55	46.5	24.4	33.9
78	0.10841	0.08246	55	46.7	24.4	33.9
79	0.10841	0.08246	55	46.8	24.4	33.9
80	0.10841	0.08246	55	46.8	24.4	33.9
81	0.10792	0.08246	60	52.1	24.5	33.8
82	0.10792	0.08246	60	52.1	24.5	33.8
83	0.10792	0.08246	60	52.1	24.5	33.7
84	0.10792	0.08246	60	52.3	24.5	33.8
85	0.10792	0.08246	60	52.3	24.5	33.7
86	0.10792	0.08246	60	52.1	24.5	33.7
87	0.10792	0.08246	60	52.2	24.5	33.8
88	0.10792	0.08246	60	52.3	24.8	33.7
89	0.10792	0.08246	60	52.3	24.8	33.6
90	0.10792	0.08246	60	52.3	24.8	33.6

Table A.1 : Samples of Operation Data (Contd.)

Day	m_t (kg/s)	m_s (kg/s)	$T_{h,in}$ (^oC)	$T_{h,out}$ (^oC)	$T_{c,in}$ (^oC)	$T_{c,out}$ (^oC)
91	0.10792	0.08246	60	52.3	24.8	33.4
92	0.10792	0.08246	60	52.6	25	33.5
93	0.10792	0.08246	60	52.6	25	33.5
94	0.10792	0.08246	60	52.8	25	33.5
95	0.10792	0.08246	60	52.8	25	33.5
96	0.10792	0.08246	60	52.7	25	33.6
97	0.10792	0.08246	60	52.7	25	33.6
98	0.10792	0.08246	60	52.9	25.2	33.6
99	0.10792	0.08246	60	52.9	25.2	33.7
100	0.10792	0.08246	60	52.9	25.2	33.7
101	0.10749	0.08246	65	57.2	25.5	34.5
102	0.10749	0.08246	65	57.2	25.5	34.5
103	0.10749	0.08246	65	57.3	25.5	34.5
104	0.10749	0.08246	65	57.5	25.5	34.2
105	0.10749	0.08246	65	57.5	25.5	34.3
106	0.10749	0.08246	65	57.5	25.5	34.3
107	0.10749	0.08246	65	57.6	25.5	34.3
108	0.10749	0.08246	65	57.6	25.5	34.3
109	0.10749	0.08246	65	57.5	25.7	34.4
110	0.10749	0.08246	65	57.7	25.7	34.4
111	0.10749	0.08246	65	57.7	25.7	34.4
112	0.10749	0.08246	65	57.9	25.8	34.4
113	0.10749	0.08246	65	57.9	25.8	34.4
114	0.10749	0.08246	65	57.8	25.8	34.5
115	0.10749	0.08246	65	57.8	25.8	34.5
116	0.10749	0.08246	65	57.8	25.8	34.5
117	0.10749	0.08246	65	57.7	26	34.6
118	0.10749	0.08246	65	57.7	26	34.6
119	0.10749	0.08246	65	57.8	26	34.6
120	0.10749	0.08246	65	57.8	26	34.6

Table A.2 Samples of Results using Bell-Delaware Method

Day	Re_s	h_c	j_c	j_L	j_B	h_s
1	14358	1289.42	1.04	0.88	0.96	1134.69
2	14374	1289.42	1.04	0.88	0.96	1134.69
3	14406	1337.52	1.04	0.88	0.96	1177.01
4	14426	1319.55	1.04	0.88	0.96	1161.21
5	14462	1282.54	1.04	0.88	0.96	1128.64
6	14499	1297.59	1.04	0.88	0.96	1141.88
7	14519	1297.59	1.04	0.88	0.96	1141.88
8	14523	1289.19	1.04	0.88	0.96	1134.49
9	14560	1319.85	1.04	0.88	0.96	1161.47
10	14577	1319.85	1.04	0.88	0.96	1161.47
11	14585	1319.85	1.04	0.88	0.96	1161.47
12	14630	1297.50	1.04	0.88	0.96	1141.80
13	14641	1328.58	1.04	0.88	0.96	1169.15
14	14666	1324.38	1.04	0.88	0.96	1165.45
15	14730	1324.38	1.04	0.88	0.96	1165.45
16	14751	1324.38	1.04	0.88	0.96	1165.45
17	14793	1308.73	1.04	0.88	0.96	1151.68
18	14812	1308.73	1.04	0.88	0.96	1151.68
19	14827	1324.38	1.04	0.88	0.96	1165.45
20	14831	1293.08	1.04	0.88	0.96	1137.91
21	14848	1272.20	1.04	0.88	0.96	1119.53
22	14859	1186.05	1.04	0.88	0.96	1043.73
23	14872	1197.49	1.04	0.88	0.96	1053.79
24	14878	1186.05	1.04	0.88	0.96	1043.73
25	14942	1172.54	1.04	0.88	0.96	1031.83
26	14955	1183.90	1.04	0.88	0.96	1041.83
27	14968	1180.30	1.04	0.88	0.96	1038.66
28	15007	1180.30	1.04	0.88	0.96	1038.66
29	15029	1180.30	1.04	0.88	0.96	1038.66
30	15068	1180.30	1.04	0.88	0.96	1038.66

Table A.2 Samples of Results using Bell-Delaware Method (Contd.)

Day	Re_t	h_t	R_k	U_c	U_a	R_f
1	10100	994.37	0.000051	620.48	567.34	0.000151
2	10140	993.68	0.000051	618.62	567.34	0.000151
3	10180	991.65	0.000051	612.44	588.51	8.72E-05
4	10220	988.24	0.000051	614.26	580.60	0.00011
5	10260	976.82	0.000051	622.32	564.32	0.00016
6	10300	984.46	0.000051	618.73	570.94	0.00014
7	10340	983.14	0.000051	617.87	570.94	0.00014
8	10380	972.19	0.000051	620.22	567.24	0.000151
9	10420	976.10	0.000051	613.54	580.73	0.00011
10	10460	964.96	0.000051	613.92	580.73	0.00011
11	10500	972.52	0.000051	612.88	580.73	0.00011
12	10540	969.50	0.000051	617.42	570.90	0.00014
13	10580	976.70	0.000051	612.76	584.58	9.86E-05
14	10620	964.74	0.000051	612.94	582.73	0.000104
15	10660	959.24	0.000051	613.27	582.73	0.000104
16	10700	965.43	0.000051	613.06	582.73	0.000104
17	10740	954.27	0.000051	616.53	575.84	0.000125
18	10780	952.50	0.000051	617.12	575.84	0.000125
19	10820	952.30	0.000051	612.44	582.73	0.000104
20	10860	958.62	0.000051	606.36	568.96	0.000146
21	10900	951.32	0.000051	604.72	559.77	0.000174
22	10940	948.02	0.000051	602.35	521.86	0.000304
23	10980	956.33	0.000051	612.44	526.90	0.000286
24	11020	945.29	0.000051	610.63	521.86	0.000304
25	11060	944.38	0.000051	604.66	515.92	0.000326
26	11100	942.65	0.000051	602.14	520.92	0.000308
27	11140	942.61	0.000051	600.73	519.33	0.000314
28	11180	952.26	0.000051	602.31	519.33	0.000314
29	11220	939.62	0.000051	600.43	519.33	0.000314
30	11260	938.36	0.000051	603.39	519.33	0.000314

Table A.2 Samples of Results using Bell-Delaware Method (Contd.)

Day	Re_s	h_c	j_c	j_L	j_B	h_s
31	15120	1163.10	1.04	0.88	0.96	1023.53
32	15160	1163.10	1.04	0.88	0.96	1023.53
33	15186	1174.51	1.04	0.88	0.96	1033.57
34	15229	1174.51	1.04	0.88	0.96	1033.57
35	15249	1174.51	1.04	0.88	0.96	1033.57
36	15266	1151.37	1.04	0.88	0.96	1013.21
37	15284	1151.37	1.04	0.88	0.96	1013.21
38	15320	1151.37	1.04	0.88	0.96	1013.21
39	15356	1140.11	1.04	0.88	0.96	1003.30
40	15397	1133.29	1.04	0.88	0.96	997.30
41	15429	1131.68	1.04	0.88	0.96	995.88
42	15449	1090.77	1.04	0.88	0.96	959.88
43	15474	1082.43	1.04	0.88	0.96	952.54
44	15573	1090.77	1.04	0.88	0.96	959.88
45	15608	1109.30	1.04	0.88	0.96	976.18
46	15617	1100.86	1.04	0.88	0.96	968.76
47	15650	1100.86	1.04	0.88	0.96	968.76
48	15666	1129.75	1.04	0.88	0.96	994.18
49	15706	1129.75	1.04	0.88	0.96	994.18
50	15720	1129.75	1.04	0.88	0.96	994.18
51	15801	1061.56	1.04	0.88	0.96	934.18
52	15848	1080.49	1.04	0.88	0.96	950.83
53	15916	1080.49	1.04	0.88	0.96	950.83
54	15954	1090.90	1.04	0.88	0.96	959.99
55	15988	1087.61	1.04	0.88	0.96	957.10
56	16076	1087.61	1.04	0.88	0.96	957.10
57	16115	1087.61	1.04	0.88	0.96	957.10
58	16169	1126.35	1.04	0.88	0.96	991.19
59	16199	1126.35	1.04	0.88	0.96	991.19
60	16209	1126.35	1.04	0.88	0.96	991.19

Table A.2 Samples of Results using Bell-Delaware Method (Contd.)

Day	Re_t	h_t	R_k	U_c	U_a	R_f
31	11300	938.24	0.000051	598.44	511.76	0.000342
32	11340	938.15	0.000051	596.75	511.76	0.000342
33	11380	946.42	0.000051	599.82	516.78	0.000323
34	11420	943.05	0.000051	602.36	516.78	0.000323
35	11460	935.16	0.000051	598.12	516.78	0.000323
36	11500	933.48	0.000051	594.33	506.60	0.000362
37	11540	932.18	0.000051	598.16	506.60	0.000362
38	11580	932.02	0.000051	590.63	506.60	0.000362
39	11620	931.64	0.000051	606.44	511.65	0.000342
40	11660	930.57	0.000051	598.32	511.65	0.000342
41	11700	930.11	0.000051	614.26	419.94	0.000769
42	11740	930.02	0.000051	613.92	419.94	0.000769
43	11780	922.31	0.000051	606.77	416.27	0.00079
44	11820	928.46	0.000051	612.39	419.94	0.000769
45	11860	924.24	0.000051	587.04	428.09	0.000724
46	11900	926.21	0.000051	594.62	424.38	0.000744
47	11940	925.20	0.000051	612.37	424.38	0.000744
48	11980	924.94	0.000051	616.07	437.09	0.000676
49	12020	924.87	0.000051	622.14	437.09	0.000676
50	12060	914.45	0.000051	624.32	437.09	0.000676
51	12100	918.12	0.000051	626.69	437.09	0.000676
52	12140	923.44	0.000051	608.42	445.42	0.000633
53	12180	922.28	0.000051	598.16	445.42	0.000633
54	12220	922.15	0.000051	628.08	450.00	0.00061
55	12260	921.81	0.000051	632.14	448.55	0.000617
56	12300	921.40	0.000051	622.66	448.55	0.000617
57	12340	920.68	0.000051	627.44	448.55	0.000617
58	12380	920.44	0.000051	620.32	465.59	0.000536
59	12420	919.44	0.000051	617.22	465.59	0.000536
60	12460	919.10	0.000051	608.16	465.59	0.000536

Table A.2 Samples of Results using Bell-Delaware Method (Contd.)

Day	Re_s	h_c	j_c	j_L	j_B	h_s
61	16264	1041.53	1.04	0.88	0.96	916.55
62	16426	1041.53	1.04	0.88	0.96	916.55
63	16438	1041.53	1.04	0.88	0.96	916.55
64	16632	1067.03	1.04	0.88	0.96	938.99
65	16737	1067.03	1.04	0.88	0.96	938.99
66	16779	1043.49	1.04	0.88	0.96	918.27
67	16928	1043.49	1.04	0.88	0.96	918.27
68	16950	1043.49	1.04	0.88	0.96	918.27
69	16993	1069.18	1.04	0.88	0.96	940.88
70	17004	1069.18	1.04	0.88	0.96	940.88
71	17017	1069.18	1.04	0.88	0.96	940.88
72	17118	1062.19	1.04	0.88	0.96	934.72
73	17127	1062.19	1.04	0.88	0.96	934.72
74	17140	1053.05	1.04	0.88	0.96	926.69
75	17146	1053.05	1.04	0.88	0.96	926.69
76	17157	1076.32	1.04	0.88	0.96	947.16
77	17168	1073.58	1.04	0.88	0.96	944.75
78	17207	1055.13	1.04	0.88	0.96	928.51
79	17229	1045.97	1.04	0.88	0.96	920.45
80	17237	1045.97	1.04	0.88	0.96	920.45
81	17259	932.47	1.04	0.88	0.96	820.58
82	17268	932.47	1.04	0.88	0.96	820.58
83	17268	926.77	1.04	0.88	0.96	815.56
84	17273	918.63	1.04	0.88	0.96	808.39
85	17284	912.96	1.04	0.88	0.96	803.41
86	17296	926.77	1.04	0.88	0.96	815.56
87	17301	925.54	1.04	0.88	0.96	814.47
88	17312	950.30	1.04	0.88	0.96	836.26
89	17324	944.65	1.04	0.88	0.96	831.29
90	17329	944.65	1.04	0.88	0.96	831.29

Table A.2 Samples of Results using Bell-Delaware Method (Contd.)

Day	Re_t	h_t	R_k	U_c	U_a	R_f
61	12500	917.97	0.000051	606.79	458.27	0.00057
62	12540	917.87	0.000051	622.57	458.27	0.00057
63	12580	917.69	0.000051	630.16	458.27	0.00057
64	12620	917.34	0.000051	632.5	469.49	0.000518
65	12660	921.07	0.000051	614.68	469.49	0.000518
66	12700	917.00	0.000051	612.44	459.14	0.000566
67	12740	916.85	0.000051	598.98	459.14	0.000566
68	12780	916.39	0.000051	617.76	459.14	0.000566
69	12820	914.25	0.000051	609.43	470.44	0.000514
70	12860	914.23	0.000051	625.42	470.44	0.000514
71	12900	906.77	0.000051	633.12	470.44	0.000514
72	12940	903.41	0.000051	627.73	467.36	0.000528
73	12980	913.20	0.000051	619.8	467.36	0.000528
74	13020	911.93	0.000051	611.94	463.34	0.000546
75	13060	910.63	0.000051	624.64	463.34	0.000546
76	13100	910.27	0.000051	598.46	473.58	0.0005
77	13140	904.85	0.000051	614.57	472.37	0.000505
78	13180	907.40	0.000051	588.3	464.26	0.000542
79	13220	907.30	0.000051	628.66	460.23	0.000561
80	13260	907.14	0.000051	621.75	460.23	0.000561
81	13300	905.20	0.000051	618.45	360.29	0.001164
82	13340	904.40	0.000051	627.37	360.29	0.001164
83	13380	904.06	0.000051	618.97	357.78	0.001183
84	13420	903.52	0.000051	614.49	354.20	0.001211
85	13460	912.14	0.000051	620.8	351.70	0.001231
86	13500	918.01	0.000051	624.54	357.78	0.001183
87	13540	911.73	0.000051	608.48	357.24	0.001187
88	13580	901.13	0.000051	592.88	348.13	0.00126
89	13620	899.15	0.000051	598.58	345.65	0.001281
90	13660	897.74	0.000051	630.42	345.65	0.001281

Table A.2 Samples of Results using Bell-Delaware Method (Contd.)

Day	Re_s	h_c	j_c	j_L	j_B	h_s
91	17335	933.42	1.04	0.88	0.96	821.41
92	17340	913.04	1.04	0.88	0.96	803.48
93	17355	913.04	1.04	0.88	0.96	803.48
94	17374	899.50	1.04	0.88	0.96	791.56
95	17414	899.50	1.04	0.88	0.96	791.56
96	17488	911.80	1.04	0.88	0.96	802.39
97	17533	911.80	1.04	0.88	0.96	802.39
98	17574	892.67	1.04	0.88	0.96	785.55
99	17602	882.29	1.04	0.88	0.96	776.42
100	17620	873.20	1.04	0.88	0.96	768.42
101	17637	866.15	1.04	0.88	0.96	762.21
102	17824	861.60	1.04	0.88	0.96	758.21
103	18033	855.81	1.04	0.88	0.96	753.12
104	18215	846.23	1.04	0.88	0.96	744.68
105	18370	837.24	1.04	0.88	0.96	736.77
106	18432	823.60	1.04	0.88	0.96	724.77
107	18590	817.91	1.04	0.88	0.96	719.76
108	18848	817.91	1.04	0.88	0.96	719.76
109	18980	823.19	1.04	0.88	0.96	724.41
110	19113	811.76	1.04	0.88	0.96	714.35
111	19384	811.76	1.04	0.88	0.96	714.35
112	19655	797.84	1.04	0.88	0.96	702.10
113	19690	797.84	1.04	0.88	0.96	702.10
114	19768	808.15	1.04	0.88	0.96	711.17
115	19861	808.15	1.04	0.88	0.96	711.17
116	19969	808.15	1.04	0.88	0.96	711.17
117	20012	813.39	1.04	0.88	0.96	715.79
118	20107	813.39	1.04	0.88	0.96	715.79
119	20255	807.66	1.04	0.88	0.96	710.74
120	20359	807.66	1.04	0.88	0.96	710.74

Table A.2 Samples of Results using Bell-Delaware Method (Contd.)

Day	Re_t	h_t	R_k	U_c	U_a	R_f
91	13700	906.96	0.000051	622.16	340.71	0.001323
92	13740	896.29	0.000051	618.38	331.74	0.001402
93	13780	895.37	0.000051	612.82	331.74	0.001402
94	13820	894.01	0.000051	619.08	325.78	0.001458
95	13860	893.43	0.000051	627.65	325.78	0.001458
96	13900	902.74	0.000051	614.26	331.19	0.001407
97	13940	891.47	0.000051	604.86	331.19	0.001407
98	13980	890.80	0.000051	616.94	322.77	0.001486
99	14020	890.60	0.000051	598.44	325.21	0.001463
100	14060	897.53	0.000051	596.79	325.21	0.001463
101	14100	886.65	0.000051	614.08	304.10	0.001676
102	14140	896.62	0.000051	623.74	304.10	0.001676
103	14180	894.14	0.000051	619.42	301.56	0.001704
104	14220	882.67	0.000051	626.55	290.34	0.001832
105	14260	881.32	0.000051	608.97	292.39	0.001808
106	14300	880.09	0.000051	618.46	292.39	0.001808
107	14340	878.65	0.000051	616.88	289.88	0.001838
108	14380	878.28	0.000051	624.53	289.88	0.001838
109	14420	887.94	0.000051	608.96	292.20	0.00181
110	14460	877.38	0.000051	617.74	287.18	0.00187
111	14500	882.55	0.000051	625.18	287.18	0.00187
112	14540	875.62	0.000051	620.83	281.05	0.001946
113	14580	878.94	0.000051	612.65	281.05	0.001946
114	14620	874.76	0.000051	627.38	285.58	0.00189
115	14660	874.55	0.000051	611.69	285.58	0.00189
116	14700	873.42	0.000051	615.48	285.58	0.00189
117	14740	872.94	0.000051	622.12	287.89	0.001862
118	14780	870.70	0.000051	628.08	287.89	0.001862
119	14820	876.16	0.000051	620.94	285.37	0.001892
120	14860	862.90	0.000051	616.78	285.37	0.001892

Table A.3 : Minimum and Maximum LMTD

T_1	T_2	T_3	T_4	$T_2-T_3-2\Delta T$	$T_1-T_4-2\Delta T$	$LMTD_{min}$	$T_1-T_4+2\Delta T$	$T_2-T_3-2\Delta T$	$LMTD_{max}$
40	34.6	22	28.6	11.2	12.4	11.790	11.6	12.8	12.190
40	34.6	22	28.6	11.2	12.4	11.790	11.6	12.8	12.190
40	34.5	22	28.8	11	12.3	11.638	11.4	12.7	12.038
40	34.6	22	28.8	11	12.4	11.686	11.4	12.8	12.086
40	34.7	22.1	28.7	11.1	12.4	11.738	11.5	12.8	12.138
40	34.7	22.1	28.8	11	12.4	11.686	11.4	12.8	12.086
40	34.7	22.1	28.8	11	12.4	11.686	11.4	12.8	12.086
40	34.7	22.3	28.8	11	12.2	11.590	11.4	12.6	11.990
40	34.7	22.3	29	10.8	12.2	11.486	11.2	12.6	11.886
40	34.7	22.3	29	10.8	12.2	11.486	11.2	12.6	11.886
40	34.7	22.3	29	10.8	12.2	11.486	11.2	12.6	11.886
40	34.8	22.4	29	10.8	12.2	11.486	11.2	12.6	11.886
40	34.8	22.4	29.2	10.6	12.2	11.381	11	12.6	11.782
40	34.8	22.5	29.2	10.6	12.1	11.333	11	12.5	11.734
40	34.8	22.5	29.2	10.6	12.1	11.333	11	12.5	11.734
40	34.8	22.5	29.2	10.6	12.1	11.333	11	12.5	11.734
40	34.8	22.5	29.1	10.7	12.1	11.386	11.1	12.5	11.786
40	34.8	22.5	29.1	10.7	12.1	11.386	11.1	12.5	11.786
40	34.8	22.5	29.2	10.6	12.1	11.333	11	12.5	11.734
40	34.9	22.8	29.2	10.6	11.9	11.237	11	12.3	11.638
45	38.4	22.8	30.9	13.9	15.4	14.637	14.3	15.8	15.038
45	38.6	22.8	30.4	14.4	15.6	14.992	14.8	16	15.392
45	38.6	22.8	30.5	14.3	15.6	14.941	14.7	16	15.341
45	38.6	22.8	30.4	14.4	15.6	14.992	14.8	16	15.392
45	38.7	22.8	30.4	14.4	15.7	15.041	14.8	16.1	15.441
45	38.7	22.8	30.5	14.3	15.7	14.989	14.7	16.1	15.389
45	38.7	22.9	30.5	14.3	15.6	14.941	14.7	16	15.341
45	38.7	22.9	30.5	14.3	15.6	14.941	14.7	16	15.341
45	38.7	22.9	30.5	14.3	15.6	14.941	14.7	16	15.341

Table A.3 : Minimum and Maximum LMTD (Contd.)

T_1	T_2	T_3	T_4	$T_2-T_3-2\Delta T$	$T_1-T_4-2\Delta T$	$LMTD_{min}$	$T_1-T_4+2\Delta T$	$T_2-T_3-2\Delta T$	$LMTD_{max}$
45	38.7	22.9	30.5	14.3	15.6	14.941	14.7	16	15.341
45	38.8	23	30.5	14.3	15.6	14.941	14.7	16	15.341
45	38.8	23	30.5	14.3	15.6	14.941	14.7	16	15.341
45	38.8	23	30.6	14.2	15.6	14.889	14.6	16	15.289
45	38.8	23	30.6	14.2	15.6	14.889	14.6	16	15.289
45	38.8	23	30.6	14.2	15.6	14.889	14.6	16	15.289
45	39	23.2	30.7	14.1	15.6	14.837	14.5	16	15.238
45	39	23.2	30.7	14.1	15.6	14.837	14.5	16	15.238
45	39	23.2	30.7	14.1	15.6	14.837	14.5	16	15.238
45	39	23.2	30.8	14	15.6	14.786	14.4	16	15.186
45	39	23.2	30.8	14	15.6	14.786	14.4	16	15.186
50	43.7	23.5	31.6	18.2	20	19.086	18.6	20.4	19.486
50	43.7	23.5	31.6	18.2	20	19.086	18.6	20.4	19.486
50	43.7	23.5	31.5	18.3	20	19.137	18.7	20.4	19.538
50	43.7	23.5	31.6	18.2	20	19.086	18.6	20.4	19.486
50	43.6	23.5	31.7	18.1	19.9	18.986	18.5	20.3	19.386
50	43.6	23.5	31.6	18.2	19.9	19.037	18.6	20.3	19.438
50	43.6	23.5	31.6	18.2	19.9	19.037	18.6	20.3	19.438
50	43.4	23.5	31.7	18.1	19.7	18.889	18.5	20.1	19.289
50	43.4	23.5	31.7	18.1	19.7	18.889	18.5	20.1	19.289
50	43.4	23.5	31.7	18.1	19.7	18.889	18.5	20.1	19.289
50	43.4	23.5	31.7	18.1	19.7	18.889	18.5	20.1	19.289
50	43.3	23.5	31.8	18	19.6	18.789	18.4	20	19.189
50	43.3	23.5	31.8	18	19.6	18.789	18.4	20	19.189
50	43.2	23.5	31.8	18	19.5	18.740	18.4	19.9	19.140
50	43.2	23.6	31.8	18	19.4	18.691	18.4	19.8	19.091
50	43.2	23.6	31.8	18	19.4	18.691	18.4	19.8	19.091
50	43.2	23.6	31.8	18	19.4	18.691	18.4	19.8	19.091
50	43	23.6	32	17.8	19.2	18.491	18.2	19.6	18.891

Table A.3 : Minimum and Maximum LMTD (Contd.)

T_1	T_2	T_3	T_4	$T_2-T_3-2\Delta T$	$T_1-T_4-2\Delta T$	$LMTD_{min}$	$T_1-T_4+2\Delta T$	$T_2-T_3-2\Delta T$	$LMTD_{max}$
50	43	23.6	32	17.8	19.2	18.491	18.2	19.6	18.891
55	46.7	23.8	33.5	21.3	22.7	21.993	21.7	23.1	22.393
55	46.7	23.8	33.5	21.3	22.7	21.993	21.7	23.1	22.393
55	46.7	23.8	33.5	21.3	22.7	21.993	21.7	23.1	22.393
55	46.5	23.8	33.6	21.2	22.5	21.844	21.6	22.9	22.244
55	46.5	23.8	33.6	21.2	22.5	21.844	21.6	22.9	22.244
55	46.7	24	33.6	21.2	22.5	21.844	21.6	22.9	22.244
55	46.7	24	33.6	21.2	22.5	21.844	21.6	22.9	22.244
55	46.7	24	33.6	21.2	22.5	21.844	21.6	22.9	22.244
55	46.5	24	33.7	21.1	22.3	21.694	21.5	22.7	22.095
55	46.5	24	33.7	21.1	22.3	21.694	21.5	22.7	22.095
55	46.5	24	33.7	21.1	22.3	21.694	21.5	22.7	22.095
55	46.6	24.2	33.8	21	22.2	21.594	21.4	22.6	21.995
55	46.6	24.2	33.8	21	22.2	21.594	21.4	22.6	21.995
55	46.7	24.2	33.8	21	22.3	21.643	21.4	22.7	22.044
55	46.7	24.2	33.8	21	22.3	21.643	21.4	22.7	22.044
55	46.5	24.3	33.9	20.9	22	21.445	21.3	22.4	21.845
55	46.5	24.4	33.9	20.9	21.9	21.396	21.3	22.3	21.796
55	46.7	24.4	33.9	20.9	22.1	21.494	21.3	22.5	21.895
55	46.8	24.4	33.9	20.9	22.2	21.543	21.3	22.6	21.944
55	46.8	24.4	33.9	20.9	22.2	21.543	21.3	22.6	21.944
60	52.1	24.5	33.8	26	27.4	26.694	26.4	27.8	27.094
60	52.1	24.5	33.8	26	27.4	26.694	26.4	27.8	27.094
60	52.1	24.5	33.7	26.1	27.4	26.745	26.5	27.8	27.145
60	52.3	24.5	33.8	26	27.6	26.792	26.4	28	27.192
60	52.3	24.5	33.7	26.1	27.6	26.843	26.5	28	27.243
60	52.1	24.5	33.7	26.1	27.4	26.745	26.5	27.8	27.145
60	52.2	24.5	33.8	26	27.5	26.743	26.4	27.9	27.143
60	52.3	24.8	33.7	26.1	27.3	26.696	26.5	27.7	27.096

Table A.3 : Minimum and Maximum LMTD (Contd.)

T_1	T_2	T_3	T_4	$T_2-T_3-2\Delta T$	$T_1-T_4-2\Delta T$	$LMTD_{min}$	$T_1-T_4+2\Delta T$	$T_2-T_3-2\Delta T$	$LMTD_{max}$
60	52.3	24.8	33.6	26.2	27.3	26.746	26.6	27.7	27.146
60	52.3	24.8	33.4	26.4	27.3	26.847	26.8	27.7	27.248
60	52.6	25	33.5	26.3	27.4	26.846	26.7	27.8	27.246
60	52.6	25	33.5	26.3	27.4	26.846	26.7	27.8	27.246
60	52.8	25	33.5	26.3	27.6	26.945	26.7	28	27.345
60	52.8	25	33.5	26.3	27.6	26.945	26.7	28	27.345
60	52.7	25	33.6	26.2	27.5	26.845	26.6	27.9	27.245
60	52.7	25	33.6	26.2	27.5	26.845	26.6	27.9	27.245
60	52.9	25.2	33.6	26.2	27.5	26.845	26.6	27.9	27.245
60	52.9	25.2	33.7	26.1	27.5	26.794	26.5	27.9	27.194
60	52.9	25.2	33.7	26.1	27.5	26.794	26.5	27.9	27.194
65	57.2	25.5	34.5	30.3	31.5	30.896	30.7	31.9	31.296
65	57.2	25.5	34.5	30.3	31.5	30.896	30.7	31.9	31.296
65	57.3	25.5	34.5	30.3	31.6	30.945	30.7	32	31.346
65	57.5	25.5	34.2	30.6	31.8	31.196	31	32.2	31.596
65	57.5	25.5	34.3	30.5	31.8	31.145	30.9	32.2	31.546
65	57.5	25.5	34.3	30.5	31.8	31.145	30.9	32.2	31.546
65	57.6	25.5	34.3	30.5	31.9	31.195	30.9	32.3	31.595
65	57.6	25.5	34.3	30.5	31.9	31.195	30.9	32.3	31.595
65	57.5	25.7	34.4	30.4	31.6	30.996	30.8	32	31.396
65	57.7	25.7	34.4	30.4	31.8	31.095	30.8	32.2	31.495
65	57.7	25.7	34.4	30.4	31.8	31.095	30.8	32.2	31.495
65	57.9	25.8	34.4	30.4	31.9	31.144	30.8	32.3	31.544
65	57.9	25.8	34.4	30.4	31.9	31.144	30.8	32.3	31.544
65	57.8	25.8	34.5	30.3	31.8	31.044	30.7	32.2	31.444
65	57.8	25.8	34.5	30.3	31.8	31.044	30.7	32.2	31.444
65	57.8	25.8	34.5	30.3	31.8	31.044	30.7	32.2	31.444
65	57.7	26	34.6	30.2	31.5	30.845	30.6	31.9	31.245
65	57.7	26	34.6	30.2	31.5	30.845	30.6	31.9	31.245

Table A.4 Dispersion factor about mean heat duty

Day	**Q_1**	**Q_2**	**Q_m**	$\sqrt{(Q_1 - Q_m)^2 + (Q_2 - Q_m)^2}$	**Δ_Q**
1	2.477	2.278	2.378	0.019750481	0.059107
2	2.477	2.278	2.378	0.019750481	0.059107
3	2.523	2.347	2.435	0.015414275	0.050985
4	2.477	2.347	2.412	0.008412306	0.038023
5	2.431	2.278	2.355	0.011685781	0.045908
6	2.431	2.313	2.372	0.007004334	0.035284
7	2.431	2.313	2.372	0.007004334	0.035284
8	2.431	2.244	2.337	0.017558815	0.05669
9	2.431	2.313	2.372	0.007004334	0.035284
10	2.431	2.313	2.372	0.007004334	0.035284
11	2.431	2.313	2.372	0.007004334	0.035284
12	2.385	2.278	2.332	0.005725219	0.032449
13	2.385	2.347	2.366	0.000720783	0.011346
14	2.385	2.313	2.349	0.002627207	0.02182
15	2.385	2.313	2.349	0.002627207	0.02182
16	2.385	2.313	2.349	0.002627207	0.02182
17	2.385	2.278	2.332	0.005725219	0.032449
18	2.385	2.278	2.332	0.005725219	0.032449
19	2.385	2.313	2.349	0.002627207	0.02182
20	2.339	2.209	2.274	0.008472713	0.040472
21	3.012	2.796	2.904	0.023344212	0.052611
22	2.921	2.623	2.772	0.044221844	0.075857
23	2.921	2.658	2.789	0.034551751	0.066638
24	2.921	2.623	2.772	0.044221844	0.075857
25	2.875	2.623	2.749	0.03169061	0.064749
26	2.875	2.658	2.767	0.023595933	0.055523
27	2.875	2.623	2.749	0.03169061	0.064749
28	2.875	2.623	2.749	0.03169061	0.064749
29	2.875	2.623	2.749	0.03169061	0.064749

Table A.4 Dispersion factor about mean heat duty (Contd.)

Day	**Q_1**	**Q_2**	**Q_m**	$\sqrt{(Q_1 - Q_m)^2 + (Q_2 - Q_m)^2}$	**Δ_Q**
30	2.875	2.623	2.749	0.03169061	0.044749
31	2.830	2.589	2.709	0.028953105	0.042805
32	2.830	2.589	2.709	0.028953105	0.042805
33	2.830	2.623	2.727	0.021242255	0.053455
34	2.830	2.623	2.727	0.021242255	0.053455
35	2.830	2.623	2.727	0.021242255	0.053455
36	2.738	2.589	2.664	0.0111542	0.03965
37	2.738	2.589	2.664	0.0111542	0.03965
38	2.738	2.589	2.664	0.0111542	0.03965
39	2.738	2.623	2.681	0.00659418	0.03029
40	2.738	2.623	2.681	0.00659418	0.03029
41	2.869	2.796	2.832	0.002639324	0.018138
42	2.869	2.796	2.832	0.002639324	0.018138
43	2.869	2.762	2.815	0.0057431	0.02692
44	2.869	2.796	2.832	0.002639324	0.018138
45	2.914	2.831	2.872	0.003500354	0.020597
46	2.914	2.796	2.855	0.006984393	0.029271
47	2.914	2.796	2.855	0.006984393	0.029271
48	3.005	2.831	2.918	0.015267182	0.042345
49	3.005	2.831	2.918	0.015267182	0.042345
50	3.005	2.831	2.918	0.015267182	0.042345
51	3.005	2.831	2.918	0.015267182	0.042345
52	3.051	2.865	2.958	0.017252789	0.044405
53	3.051	2.865	2.958	0.017252789	0.044405
54	3.096	2.865	2.981	0.026748013	0.054868
55	3.096	2.831	2.963	0.035327867	0.043424
56	3.096	2.831	2.963	0.035327867	0.033424
57	3.096	2.831	2.963	0.035327867	0.043424
58	3.187	2.900	3.044	0.041426887	0.0466875
59	3.187	2.900	3.044	0.041426887	0.036875

Table A.4 Dispersion factor about mean heat duty (Contd.)

Day	**Q_1**	**Q_2**	**Q_m**	$\sqrt{(Q_1 - Q_m)^2 + (Q_2 - Q_m)^2}$	**Δ_Q**
60	3.187	2.900	3.044	0.041426887	0.036875
61	3.767	3.348	3.557	0.08744358	0.028323
62	3.767	3.348	3.557	0.08744358	0.043123
63	3.767	3.348	3.557	0.08744358	0.043123
64	3.857	3.383	3.620	0.112545038	0.029267
65	3.857	3.383	3.620	0.112545038	0.019267
66	3.767	3.314	3.540	0.102475211	0.029423
67	3.767	3.314	3.540	0.102475211	0.030423
68	3.767	3.314	3.540	0.102475211	0.029023
69	3.857	3.348	3.603	0.129518091	0.019889
70	3.857	3.348	3.603	0.129518091	0.019889
71	3.857	3.348	3.603	0.129518091	0.021889
72	3.812	3.314	3.563	0.12404928	0.019854
73	3.812	3.314	3.563	0.12404928	0.019854
74	3.767	3.314	3.540	0.102475211	0.029023
75	3.767	3.314	3.540	0.102475211	0.030423
76	3.857	3.314	3.586	0.147682732	0.071727
77	3.857	3.279	3.568	0.16703896	0.014536
78	3.767	3.279	3.523	0.118698431	0.037795
79	3.721	3.279	3.500	0.097617241	0.049261
80	3.721	3.279	3.500	0.097617241	0.030261
81	3.569	3.210	3.390	0.064238439	0.027475
82	3.569	3.176	3.372	0.077207248	0.028396
83	3.569	3.210	3.390	0.064238439	0.027475
84	3.478	3.038	3.258	0.097101988	0.029544
85	3.478	3.038	3.258	0.097101988	0.019624
86	3.569	3.176	3.372	0.077207248	0.0182396
87	3.524	3.210	3.367	0.04906679	0.064579
88	3.478	3.072	3.275	0.082485579	0.028767
89	3.478	3.038	3.258	0.097101988	0.064564

Table A.4 Dispersion factor about mean heat duty (Contd.)

Day	Q_1	Q_2	Q_m	$\sqrt{(Q_1 - Q_m)^2 + (Q_2 - Q_m)^2}$	Δ_Q
90	3.478	3.038	3.258	0.097101988	0.056144
91	3.478	2.969	3.224	0.129909568	0.011812
92	3.343	2.934	3.139	0.08352692	0.042085
93	3.343	2.934	3.139	0.08352692	0.032465
94	3.253	2.934	3.093	0.05068112	0.022777
95	3.253	2.934	3.093	0.05068112	0.027239
96	3.298	2.969	3.133	0.054130009	0.017426
97	3.298	2.969	3.133	0.054130009	0.019256
98	3.207	2.900	3.053	0.047345749	0.027126
99	3.207	2.934	3.071	0.037319244	0.06291
100	3.207	2.934	3.071	0.037319244	0.06291
101	3.509	3.107	3.308	0.081094393	0.06083
102	3.509	3.107	3.308	0.081094393	0.052013
103	3.464	3.107	3.286	0.063986617	0.027689
104	3.374	3.003	3.189	0.068933767	0.042335
105	3.374	3.038	3.206	0.056712335	0.04278
106	3.374	3.038	3.206	0.056712335	0.04278
107	3.329	3.038	3.184	0.042571452	0.06451
108	3.329	3.038	3.184	0.042571452	0.06451
109	3.374	3.003	3.189	0.068933767	0.02335
110	3.285	3.003	3.144	0.039570115	0.03274
111	3.285	3.003	3.144	0.039570115	0.03274
112	3.195	2.969	3.082	0.02550449	0.051824
113	3.195	2.969	3.082	0.02550449	0.051824
114	3.240	3.003	3.121	0.027924874	0.053537
115	3.240	3.003	3.121	0.027924874	0.053537
116	3.240	3.003	3.121	0.027924874	0.053537
117	3.285	2.969	3.127	0.049876859	0.027143
118	3.285	2.969	3.127	0.049876859	0.027143
119	3.240	2.969	3.104	0.036678479	0.061698
120	3.240	2.969	3.104	0.036678479	0.061698

Table A.5 : Dispersion factor about mean overall heat transfer Coefficient

Days	$Q_{1,max}$	$Q_{1,min}$	$Q_{2,max}$	$Q_{2,min}$	$LMTD_{max}$	$LMTD_{min}$
1	2.594	2.361	2.371	2.187	12.190	11.790
2	2.594	2.361	2.371	2.187	12.190	11.790
3	2.641	2.407	2.441	2.255	12.038	11.638
4	2.594	2.361	2.441	2.255	12.086	11.686
5	2.548	2.316	2.371	2.187	12.138	11.738
6	2.548	2.316	2.406	2.221	12.086	11.686
7	2.548	2.316	2.406	2.221	12.086	11.686
8	2.548	2.316	2.336	2.153	11.990	11.590
9	2.548	2.316	2.406	2.221	11.886	11.486
10	2.548	2.316	2.406	2.221	11.886	11.486
11	2.548	2.316	2.406	2.221	11.886	11.486
12	2.502	2.271	2.371	2.187	11.886	11.486
13	2.502	2.271	2.441	2.255	11.782	11.381
14	2.502	2.271	2.406	2.221	11.734	11.333
15	2.502	2.271	2.406	2.221	11.734	11.333
16	2.502	2.271	2.406	2.221	11.734	11.333
17	2.502	2.271	2.371	2.187	11.786	11.386
18	2.502	2.271	2.371	2.187	11.786	11.386
19	2.502	2.271	2.406	2.221	11.734	11.333
20	2.455	2.225	2.301	2.119	11.638	11.237
21	3.134	2.892	2.894	2.700	15.038	14.637
22	3.042	2.801	2.719	2.529	15.392	14.992
23	3.042	2.801	2.754	2.563	15.341	14.941
24	3.042	2.801	2.719	2.529	15.392	14.992
25	2.996	2.756	2.719	2.529	15.441	15.041
26	2.996	2.756	2.754	2.563	15.389	14.989
27	2.996	2.756	2.719	2.529	15.341	14.941
28	2.996	2.756	2.719	2.529	15.341	14.941
29	2.996	2.756	2.719	2.529	15.341	14.941
30	2.996	2.756	2.719	2.529	15.341	14.941

Table A.5 Dispersion factor about mean overall heat transfer coefficient (Contd.)

Days	U1,max	U1,min	U2,max	U2,min	Um	ΔUm/Um
1	628.740	553.475	574.537	512.626	567.345	0.08518769
2	628.740	553.475	574.537	512.626	567.345	0.08518769
3	648.322	571.235	599.156	535.314	588.507	0.08101177
4	634.325	558.223	596.688	533.180	580.604	0.07634583
5	620.239	545.146	577.073	514.812	564.318	0.07996006
6	622.997	547.488	588.164	525.102	570.938	0.07606333
7	622.997	547.488	588.164	525.102	570.938	0.07606333
8	628.178	551.894	575.865	513.041	567.245	0.08491865
9	633.859	556.710	598.418	533.947	580.734	0.07637131
10	633.859	556.710	598.418	533.947	580.734	0.07637131
11	633.859	556.710	598.418	533.947	580.734	0.07637131
12	622.334	545.794	589.746	525.733	570.902	0.07615678
13	628.049	550.629	612.666	546.964	584.577	0.07153427
14	630.698	552.875	606.461	540.875	582.727	0.0735264
15	630.698	552.875	606.461	540.875	582.727	0.0735264
16	630.698	552.875	606.461	540.875	582.727	0.0735264
17	627.807	550.431	594.932	530.198	575.842	0.07631676
18	627.807	550.431	594.932	530.198	575.842	0.07631676
19	630.698	552.875	606.461	540.875	582.727	0.0735264
20	624.306	546.293	585.048	520.172	568.955	0.08000552
21	611.838	549.417	564.855	512.957	559.767	0.07319096
22	579.789	519.984	518.265	469.419	521.864	0.08656362
23	581.784	521.726	526.716	477.357	526.895	0.08121663
24	579.789	519.984	518.265	469.419	521.864	0.08656362
25	569.157	509.984	516.588	467.940	515.917	0.08048018
26	571.114	511.691	525.010	475.850	520.916	0.07560011
27	572.969	513.311	520.048	470.992	519.330	0.08055574
28	572.969	513.311	520.048	470.992	519.330	0.08055574
29	572.969	513.311	520.048	470.992	519.330	0.08055574
30	572.969	513.311	520.048	470.992	519.330	0.08055574

Table A.5 Dispersion factor about mean overall heat transfer coefficient (Contd.)

Days	$Q_{1,max}$	$Q_{1,min}$	$Q_{2,max}$	$Q_{2,min}$	$LMTD_{max}$	$LMTD_{min}$
31	2.950	2.711	2.685	2.495	15.341	14.941
32	2.950	2.711	2.685	2.495	15.341	14.941
33	2.950	2.711	2.719	2.529	15.289	14.889
34	2.950	2.711	2.719	2.529	15.289	14.889
35	2.950	2.711	2.719	2.529	15.289	14.889
36	2.858	2.621	2.685	2.495	15.238	14.837
37	2.858	2.621	2.685	2.495	15.238	14.837
38	2.858	2.621	2.685	2.495	15.238	14.837
39	2.858	2.621	2.719	2.529	15.186	14.786
40	2.858	2.621	2.719	2.529	15.186	14.786
41	2.989	2.750	2.894	2.700	19.486	19.086
42	2.989	2.750	2.894	2.700	19.486	19.086
43	2.989	2.750	2.859	2.666	19.538	19.137
44	2.989	2.750	2.894	2.700	19.486	19.086
45	3.035	2.795	2.929	2.734	19.386	18.986
46	3.035	2.795	2.894	2.700	19.438	19.037
47	3.035	2.795	2.894	2.700	19.438	19.037
48	3.127	2.885	2.929	2.734	19.289	18.889
49	3.127	2.885	2.929	2.734	19.289	18.889
50	3.127	2.885	2.929	2.734	19.289	18.889
51	3.127	2.885	2.929	2.734	19.289	18.889
52	3.173	2.930	2.963	2.768	19.189	18.789
53	3.173	2.930	2.963	2.768	19.189	18.789
54	3.219	2.975	2.963	2.768	19.140	18.740
55	3.219	2.975	2.929	2.734	19.091	18.691
56	3.219	2.975	2.929	2.734	19.091	18.691
57	3.219	2.975	2.929	2.734	19.091	18.691
58	3.311	3.065	2.998	2.802	18.891	18.491
59	3.311	3.065	2.998	2.802	18.891	18.491
60	3.311	3.065	2.998	2.802	18.891	18.491

Table A.5 Dispersion factor about mean overall heat transfer coefficient (Contd.)

Days	$U_{1,max}$	$U_{1,min}$	$U_{2,max}$	$U_{2,min}$	U_m	$\Delta U_m/U_m$
31	564.154	504.896	513.381	464.627	511.765	0.07990366
32	564.154	504.896	513.381	464.627	511.765	0.07990366
33	566.107	506.597	521.849	472.578	516.783	0.07508036
34	566.107	506.597	521.849	472.578	516.783	0.07508036
35	566.107	506.597	521.849	472.578	516.783	0.07508036
36	550.326	491.369	516.952	467.771	506.605	0.06987052
37	550.326	491.369	516.952	467.771	506.605	0.06987052
38	550.326	491.369	516.952	467.771	506.605	0.06987052
39	552.254	493.043	525.500	475.795	511.648	0.06649309
40	552.254	493.043	525.500	475.795	511.648	0.06649309
41	447.511	403.199	433.194	395.851	419.939	0.05827104
42	447.511	403.199	433.194	395.851	419.939	0.05827104
43	446.305	402.135	426.822	389.809	416.268	0.06066948
44	447.511	403.199	433.194	395.851	419.939	0.05827104
45	456.791	411.924	440.724	402.931	428.092	0.05844029
46	455.553	410.832	434.298	396.839	424.381	0.06102644
47	455.553	410.832	434.298	396.839	424.381	0.06102644
48	473.051	427.353	442.989	404.960	437.088	0.06545038
49	473.051	427.353	442.989	404.960	437.088	0.06545038
50	473.051	427.353	442.989	404.960	437.088	0.06545038
51	473.051	427.353	442.989	404.960	437.088	0.06545038
52	482.564	436.294	450.650	412.160	445.417	0.06605025
53	482.564	436.294	450.650	412.160	445.417	0.06605025
54	490.829	444.133	451.820	413.208	449.997	0.07095391
55	492.109	445.267	447.669	409.149	448.548	0.07572747
56	492.109	445.267	447.669	409.149	448.548	0.07572747
57	492.109	445.267	447.669	409.149	448.548	0.07572747
58	511.646	463.619	463.287	423.819	465.593	0.07719273
59	511.646	463.619	463.287	423.819	465.593	0.07719273
60	511.646	463.619	463.287	423.819	465.593	0.07719273

Table A.5 Dispersion factor about mean overall heat transfer coefficient (Contd.)

Days	$Q_{1,max}$	$Q_{1,min}$	$Q_{2,max}$	$Q_{2,min}$	$LMTD_{max}$	$LMTD_{min}$
61	3.896	3.639	3.452	3.247	22.393	21.993
62	3.896	3.639	3.452	3.247	22.393	21.993
63	3.896	3.639	3.452	3.247	22.393	21.993
64	3.988	3.729	3.486	3.281	22.244	21.844
65	3.988	3.729	3.486	3.281	22.244	21.844
66	3.896	3.639	3.417	3.212	22.244	21.844
67	3.896	3.639	3.417	3.212	22.244	21.844
68	3.896	3.639	3.417	3.212	22.244	21.844
69	3.988	3.729	3.452	3.247	22.095	21.694
70	3.988	3.729	3.452	3.247	22.095	21.694
71	3.988	3.729	3.452	3.247	22.095	21.694
72	3.942	3.684	3.417	3.212	21.995	21.594
73	3.942	3.684	3.417	3.212	21.995	21.594
74	3.896	3.639	3.417	3.212	22.044	21.643
75	3.896	3.639	3.417	3.212	22.044	21.643
76	3.988	3.729	3.417	3.212	21.845	21.445
77	3.988	3.729	3.382	3.178	21.796	21.396
78	3.896	3.639	3.382	3.178	21.895	21.494
79	3.850	3.594	3.382	3.178	21.944	21.543
80	3.850	3.594	3.382	3.178	21.944	21.543
81	3.696	3.444	3.312	3.110	27.094	26.694
82	3.696	3.444	3.312	3.110	27.094	26.694
83	3.696	3.444	3.277	3.076	27.145	26.745
84	3.604	3.354	3.312	3.110	27.192	26.792
85	3.604	3.354	3.277	3.076	27.243	26.843
86	3.696	3.444	3.277	3.076	27.145	26.745
87	3.650	3.399	3.312	3.110	27.143	26.743
88	3.604	3.354	3.173	2.973	27.096	26.696
89	3.604	3.354	3.138	2.939	27.146	26.746
90	3.604	3.354	3.138	2.939	27.146	26.746

Table A.5 Dispersion factor about mean overall heat transfer coefficient (Contd.)

Days	U1,max	U1,min	U2,max	U2,min	Um	ΔUm/Um
61	506.133	464.317	448.410	414.235	458.274	0.08322271
62	506.133	464.317	448.410	414.235	458.274	0.08322271
63	506.133	464.317	448.410	414.235	458.274	0.08322271
64	521.576	478.969	456.030	421.400	469.494	0.0894971
65	521.576	478.969	456.030	421.400	469.494	0.0894971
66	509.586	467.428	446.909	412.621	459.136	0.08826585
67	509.586	467.428	446.909	412.621	459.136	0.08826585
68	509.586	467.428	446.909	412.621	459.136	0.08826585
69	525.161	482.201	454.572	419.825	470.440	0.09463693
70	525.161	482.201	454.572	419.825	470.440	0.09463693
71	525.161	482.201	454.572	419.825	470.440	0.09463693
72	521.529	478.558	452.065	417.295	467.362	0.09408169
73	521.529	478.558	452.065	417.295	467.362	0.09408169
74	514.296	471.670	451.040	416.366	463.343	0.08831857
75	514.296	471.670	451.040	416.366	463.343	0.08831857
76	531.262	487.702	455.208	420.144	473.579	0.09993501
77	532.484	488.803	451.599	416.613	472.375	0.10531025
78	517.863	474.882	449.534	414.742	464.255	0.09351924
79	510.606	467.970	448.510	413.814	460.225	0.08771942
80	510.606	467.970	448.510	413.814	460.225	0.08771942
81	395.562	363.139	354.510	327.943	360.289	0.07738322
82	395.562	363.139	354.510	327.943	360.289	0.07738322
83	394.810	362.459	350.111	323.732	357.778	0.08245979
84	384.381	352.430	353.211	326.759	354.195	0.06657293
85	383.651	351.770	348.829	322.564	351.704	0.07114032
86	394.810	362.459	350.111	323.732	357.778	0.08245979
87	389.961	357.774	353.859	327.350	357.236	0.07183813
88	385.771	353.686	339.562	313.510	348.132	0.086488
89	385.040	353.025	335.194	309.327	345.647	0.09201506
90	385.040	353.025	335.194	309.327	345.647	0.09201506

Table A.5 Dispersion factor about mean overall heat transfer coefficient (Contd.)

Days	$\mathbf{Q_{1,max}}$	$\mathbf{Q_{1,min}}$	$\mathbf{Q_{2,max}}$	$\mathbf{Q_{2,min}}$	$\mathbf{LMTD_{max}}$	$\mathbf{LMTD_{min}}$
91	3.604	3.354	3.068	2.871	27.248	26.847
92	3.468	3.220	3.033	2.836	27.246	26.846
93	3.468	3.220	3.033	2.836	27.246	26.846
94	3.376	3.131	3.033	2.836	27.345	26.945
95	3.376	3.131	3.033	2.836	27.345	26.945
96	3.422	3.175	3.068	2.871	27.245	26.845
97	3.422	3.175	3.068	2.871	27.245	26.845
98	3.331	3.086	2.998	2.802	27.245	26.845
99	3.331	3.086	3.033	2.836	27.194	26.794
100	3.331	3.086	3.033	2.836	27.194	26.794
101	3.635	3.385	3.208	3.007	31.296	30.896
102	3.635	3.385	3.208	3.007	31.296	30.896
103	3.590	3.341	3.208	3.007	31.346	30.945
104	3.499	3.252	3.103	2.905	31.596	31.196
105	3.499	3.252	3.138	2.939	31.546	31.145
106	3.499	3.252	3.138	2.939	31.546	31.145
107	3.454	3.207	3.138	2.939	31.595	31.195
108	3.454	3.207	3.138	2.939	31.595	31.195
109	3.499	3.252	3.103	2.905	31.396	30.996
110	3.408	3.163	3.103	2.905	31.495	31.095
111	3.408	3.163	3.103	2.905	31.495	31.095
112	3.317	3.073	3.068	2.871	31.544	31.144
113	3.317	3.073	3.068	2.871	31.544	31.144
114	3.363	3.118	3.103	2.905	31.444	31.044
115	3.363	3.118	3.103	2.905	31.444	31.044
116	3.363	3.118	3.103	2.905	31.444	31.044
117	3.408	3.163	3.068	2.871	31.245	30.845
118	3.408	3.163	3.068	2.871	31.245	30.845
119	3.363	3.118	3.068	2.871	31.295	30.895
120	3.363	3.118	3.068	2.871	31.295	30.895

Table A.5 Dispersion factor about mean overall heat transfer coefficient (Contd.)

Days	$U_{1,max}$	$U_{1,min}$	$U_{2,max}$	$U_{2,min}$	U_m	$\Delta U_m/U_m$
91	383.588	351.714	326.509	301.011	340.705	0.10359424
92	369.038	337.660	322.814	297.441	331.738	0.09013575
93	369.038	337.660	322.814	297.441	331.738	0.09013575
94	358.013	327.098	321.633	296.369	325.778	0.07771292
95	358.013	327.098	321.633	296.369	325.778	0.07771292
96	364.202	332.988	326.542	301.041	331.194	0.07841938
97	364.202	332.988	326.542	301.041	331.194	0.07841938
98	354.490	323.608	319.121	293.873	322.773	0.07704435
99	355.163	324.213	323.444	298.013	325.209	0.07191654
100	355.163	324.213	323.444	298.013	325.209	0.07191654
101	336.191	309.056	296.620	274.550	304.104	0.08455496
102	336.191	309.056	296.620	274.550	304.104	0.08455496
103	331.460	304.509	296.147	274.118	301.558	0.0785913
104	320.472	294.037	284.188	262.672	290.342	0.08258831
105	320.993	294.509	287.848	266.189	292.385	0.07723136
106	320.993	294.509	287.848	266.189	292.385	0.07723136
107	316.324	290.022	287.394	265.774	289.878	0.07144032
108	316.324	290.022	287.394	265.774	289.878	0.07144032
109	322.540	295.910	286.022	264.346	292.204	0.08261575
110	313.166	286.902	285.115	263.518	287.175	0.07078126
111	313.166	286.902	285.115	263.518	287.175	0.07078126
112	304.333	278.385	281.465	260.011	281.049	0.06470177
113	304.333	278.385	281.465	260.011	281.049	0.06470177
114	309.496	283.318	285.581	263.943	285.585	0.0653599
115	309.496	283.318	285.581	263.943	285.585	0.0653599
116	309.496	283.318	285.581	263.943	285.585	0.0653599
117	315.697	289.191	284.190	262.496	287.893	0.07592886
118	315.697	289.191	284.190	262.496	287.893	0.07592886
119	310.991	284.669	283.736	262.082	285.370	0.07014063
120	310.991	284.669	283.736	262.082	285.370	0.07014063

Table A.6: Training Data for Neural Network

Days	ΔT-shell	ΔT-tube	Efficiency	Days	ΔT-shell	ΔT-tube	Efficiency
1	8.4	14.3	0.96	31	5.8	10.7	0.9
2	8.8	15.0	0.97	32	7.0	13.0	0.94
3	8.0	13.7	0.95	33	7.4	13.7	0.95
4	8.4	14.3	0.96	34	5.7	7.1	0.83
5	8.0	13.7	0.95	35	6.0	7.6	0.84
6	9.2	15.7	0.98	36	5.7	7.1	0.83
7	9.2	15.7	0.98	37	5.4	6.7	0.82
8	8.4	14.3	0.96	38	5.2	6.2	0.81
9	9.7	12.3	0.96	39	6.5	8.6	0.86
10	8.0	13.7	0.95	40	6.2	8.1	0.85
11	7.3	12.4	0.93	41	6.0	7.6	0.84
12	7.7	13.0	0.94	42	5.7	7.1	0.83
13	8.0	13.7	0.95	43	6.0	7.6	0.84
14	7.3	12.4	0.93	44	5.9	10.8	0.83
15	7.0	11.8	0.92	45	6.3	11.7	0.81
16	8.4	14.3	0.96	46	6.3	11.7	0.8
17	7.7	13.0	0.94	47	4.1	6.9	0.78
18	8.0	13.7	0.95	48	4.8	8.4	0.79
19	7.0	11.8	0.92	49	6.3	11.7	0.79
20	6.7	11.3	0.91	50	4.8	8.4	0.73
21	8.4	14.3	0.96	51	3.5	5.4	0.75
22	6.4	10.7	0.9	52	6.3	11.7	0.79
23	8.4	14.3	0.96	53	6.3	11.7	0.75
24	8.0	13.7	0.95	54	5.1	9.2	0.71
25	6.7	11.3	0.91	55	4.8	8.4	0.79
26	6.4	11.8	0.92	56	6.3	11.7	0.79
27	7.0	13.0	0.94	57	9.0	12.5	0.76
28	6.7	12.4	0.93	58	8.3	12.7	0.75
29	6.1	11.3	0.91	59	7.8	14.5	0.79
30	5.8	10.7	0.9	60	5.5	10.0	0.84

Table A.6 Training Data for Neural Network (Contd.)

Days	ΔT-shell	ΔT-tube	Efficiency	Days	ΔT-shell	ΔT-tube	Efficiency
61	5.1	9.2	0.86	91	5.1	9.2	0.64
62	6.3	11.7	0.82	92	4.5	7.7	0.64
63	4.1	6.9	0.77	93	5.6	10.2	0.63
64	4.8	8.4	0.76	94	4.8	8.5	0.61
65	5.1	9.2	0.79	95	4.7	8.3	0.58
66	9.0	12.5	0.73	96	4.4	7.6	0.57
67	7.8	14.5	0.75	97	5.1	9.0	0.56
68	5.1	9.2	0.76	98	5.7	10.4	0.55
69	4.2	5.4	0.84	99	4.9	8.6	0.58
70	4.1	6.9	0.82	100	4.6	8.1	0.57
71	4.7	6.1	0.76	101	4.6	7.9	0.56
72	5.1	9.2	0.71	102	4.6	7.9	0.56
73	5.1	9.2	0.73	103	4.5	7.8	0.55
74	4.2	6.1	0.72	104	4.4	7.6	0.54
75	6.0	11.1	0.76	105	4.4	7.4	0.53
76	5.5	10.0	0.76	106	4.8	7.3	0.52
77	5.3	9.6	0.72	107	4.8	7.3	0.52
78	6.6	12.3	0.69	108	4.9	7.6	0.54
79	6.7	12.4	0.68	109	5.0	7.8	0.55
80	5.8	10.7	0.69	110	4.9	7.6	0.54
81	5.8	10.6	0.68	111	4.9	7.6	0.54
82	5.2	9.3	0.67	112	4.8	7.4	0.53
83	5.8	10.6	0.66	113	4.7	7.2	0.51
84	6.2	11.5	0.65	114	4.8	7.3	0.52
85	5.2	9.4	0.69	115	4.8	7.3	0.52
86	5.2	9.4	0.69	116	4.9	7.6	0.54
87	4.7	8.2	0.68	117	4.6	6.9	0.49
88	5.0	8.9	0.66	118	4.5	6.8	0.48
89	6.1	11.2	0.67	119	4.6	6.9	0.49
90	4.8	8.5	0.61	120	4.5	6.8	0.48

Table A.6 Training Data for Neural Network (Contd.)

Days	ΔT-shell	ΔT-tube	Efficiency	Days	ΔT-shell	ΔT-tube	Efficiency
121	5.1	7.9	0.56	151	4.1	7.3	0.52
122	5.1	7.9	0.56	152	4.0	7.0	0.5
123	5.1	8.1	0.57	153	4.0	7.2	0.51
124	5.3	8.5	0.59	154	4.0	7.0	0.5
125	5.5	8.9	0.61	155	4.1	7.3	0.52
126	5.4	8.7	0.6	156	4.0	7.2	0.51
127	5.9	9.6	0.64	157	4.0	7.0	0.5
128	5.6	9.1	0.62	158	4.0	7.2	0.51
129	5.5	8.9	0.61	159	4.0	7.2	0.51
130	5.4	8.7	0.6	160	3.9	6.8	0.48
131	5.2	8.3	0.58	161	3.9	6.9	0.49
132	5.2	8.3	0.58	162	3.9	6.9	0.49
133	4.6	8.5	0.59	163	3.9	6.7	0.47
134	4.4	7.9	0.56	164	3.9	6.8	0.48
135	4.4	8.1	0.57	165	3.8	6.6	0.46
136	4.7	8.7	0.6	166	3.9	6.8	0.48
137	4.4	8.1	0.57	167	4.9	7.0	0.5
138	4.5	8.3	0.58	168	5.0	7.2	0.51
139	4.4	7.9	0.56	169	4.8	6.8	0.48
140	4.2	7.6	0.54	170	4.9	6.9	0.49
141	4.3	7.8	0.55	171	4.9	7.0	0.5
142	4.4	7.9	0.56	172	4.8	6.7	0.47
143	4.1	7.3	0.52	173	4.7	6.6	0.46
144	4.0	7.2	0.51	174	4.6	6.4	0.44
145	4.4	8.1	0.57	175	4.7	6.5	0.45
146	4.2	7.4	0.53	176	3.7	6.7	0.47
147	4.2	7.6	0.54	177	3.6	6.4	0.44
148	4.1	7.3	0.52	178	3.6	6.5	0.45
149	4.4	7.9	0.56	179	3.5	6.3	0.43
150	4.0	7.2	0.51	180	3.5	6.2	0.42

Table A.6 Training Data for Neural Network (Contd.)

Days	ΔT-shell	ΔT-tube	Efficiency	Days	ΔT-shell	ΔT-tube	Efficiency
181	3.5	6.2	0.41	211	4.4	6.6	0.35
182	3.5	6.2	0.42	212	4.3	6.6	0.34
183	4.0	6.5	0.45	213	4.4	6.6	0.35
184	4.0	6.5	0.45	214	4.4	6.7	0.36
185	3.9	6.4	0.44	215	4.3	6.6	0.34
186	3.9	6.2	0.42	216	4.4	6.6	0.35
187	4.0	6.6	0.46	217	4.4	6.6	0.35
188	4.0	6.7	0.47	218	4.4	6.6	0.35
189	4.1	6.9	0.49	219	4.4	6.7	0.36
190	4.1	6.8	0.48	220	4.3	6.6	0.34
191	4.1	6.8	0.48	221	4.3	6.5	0.38
192	4.1	6.9	0.49	222	4.3	6.5	0.39
193	4.0	6.7	0.47	223	4.3	6.5	0.33
194	3.6	6.4	0.44	224	4.3	6.5	0.37
195	3.5	6.3	0.43	225	4.3	6.5	0.32
196	3.6	6.5	0.45	226	4.3	6.4	0.37
197	3.5	6.2	0.42	227	4.3	6.4	0.37
198	3.5	6.2	0.41	228	4.3	6.5	0.35
199	4.5	6.2	0.41	229	4.3	6.5	0.36
200	4.5	6.1	0.4	230	4.3	6.5	0.32
201	4.5	6.0	0.39	231	4.3	6.5	0.38
202	4.4	6.8	0.38	232	4.4	6.7	0.36
203	4.4	6.7	0.37	233	4.5	6.8	0.39
204	4.4	6.8	0.38	234	4.5	6.8	0.39
205	4.4	6.7	0.37	235	4.4	6.8	0.38
206	4.5	6.8	0.39	236	4.4	6.8	0.38
207	4.4	6.8	0.38	237	4.4	6.7	0.37
208	4.4	6.7	0.37	238	4.4	6.7	0.36
209	4.4	6.7	0.36	239	4.3	6.4	0.37
210	4.4	6.7	0.36	240	4.3	6.5	0.36

Table A.7: Testing Data for Neural Network

Days	ΔT-shell	ΔT-tube	Efficiency	Days	ΔT-shell	ΔT-tube	Efficiency
241	4.3	6.5	0.32	281	4.3	6.3	0.28
242	4.3	6.5	0.32	282	4.2	6.3	0.26
243	4.3	6.6	0.34	283	4.2	6.3	0.25
244	4.3	6.6	0.34	284	4.2	6.3	0.24
245	4.3	6.4	0.31	285	4.2	6.3	0.26
246	4.3	6.4	0.31	286	4.3	6.3	0.27
247	4.3	6.5	0.32	287	4.4	6.8	0.38
248	4.3	6.4	0.3	288	4.5	6.8	0.39
249	4.3	6.4	0.3	289	4.4	6.7	0.37
250	4.3	6.4	0.3	290	4.5	6.8	0.39
251	4.3	6.4	0.31	291	4.4	6.8	0.38
252	4.3	6.5	0.32	292	4.4	6.6	0.35
253	4.3	6.5	0.32	293	4.4	6.8	0.38
254	4.3	6.4	0.31	294	4.4	6.8	0.38
255	4.3	6.4	0.3	295	4.4	6.7	0.37
256	4.4	6.8	0.38	296	4.5	6.8	0.39
257	4.5	6.8	0.39	297	4.4	6.7	0.37
258	4.4	6.7	0.37	298	4.4	6.8	0.38
259	4.4	6.7	0.37	299	4.4	6.7	0.37
260	4.4	6.8	0.38	300	4.4	6.7	0.36
261	4.3	6.6	0.34	301	4.4	6.7	0.37
262	4.3	6.4	0.31	302	4.4	6.7	0.37
263	4.3	6.4	0.3	303	4.4	6.6	0.35
264	4.3	6.5	0.32	304	4.4	6.6	0.35
265	4.3	6.4	0.31	305	4.4	6.7	0.36
266	4.3	6.4	0.31	306	4.4	6.6	0.35
267	4.3	6.4	0.3	307	4.3	6.6	0.34
268	4.3	6.4	0.3	308	4.3	6.6	0.34
269	4.3	6.5	0.33	309	4.4	6.6	0.35
270	4.3	6.4	0.31	310	4.0	6.5	0.32
271	4.3	6.4	0.31	311	4.0	6.5	0.33
272	4.3	6.4	0.29	312	4.0	6.5	0.32
273	4.3	6.3	0.28	313	4.0	6.4	0.31
274	4.2	6.3	0.26	314	4.0	6.4	0.31
275	4.2	6.3	0.25	315	3.9	6.4	0.29
276	4.2	6.3	0.26	316	3.9	6.3	0.28
277	4.2	6.3	0.25	317	3.9	6.3	0.27
278	4.2	6.3	0.24	318	3.9	6.3	0.28
279	4.3	6.3	0.27	319	3.9	6.4	0.29
280	4.3	6.3	0.27	320	3.9	6.3	0.28

Appendix B

General Models of Fouling

The purpose of any fouling model is to assist the designer to make an assessment of the impact of fouling on heat exchanger performance under certain operating condition. Ideally the mathematical interpretation for any fouling model is based on the rate equation of foulant deposit.The rate of build up of foulant deposit on a heat transfer surface is the difference between the rates of deposition and removal. Mathematically this can be expressed as

$$\frac{dm}{dt} = \phi_d - \phi_r \tag{B1}$$

where m is the mass of deposit per unit area, Φ_d and Φ_r are deposit and removal mass flow rates per unit area of surface respectively.

(I) General Model of Fouling

The simplest model for fouling analysis in a heat exchanger is the linear dependant model as shown in figure 1.4. If the induction period is ignored, then the model can be expressed as

$$x_f = \frac{dx}{dt} t \tag{B2}$$

If the induction period (t_i) is taken into account, then the model would have the form

$$x_f = \frac{dx_f}{dt}(t - t_i) \tag{B3}$$

In terms of fouling resistance, the above equation can be expressed as

$$R_{ft} = \frac{dR_f}{dt}(t - t_i) \tag{B4}$$

Where R_{ft} is the fouling thermal resistance at time t. it can be expressed in terms of fouling thickness (x_{ft}) as

$$R_{ft} = \frac{x_{ft}}{\lambda_f} \tag{B5}$$

However in both forms of the model, $\frac{dx_f}{dt}$ or $\frac{dR_f}{dt}$ can be determined only from experimental work.

(II) Asymptotic Fouling

The asymptotic fouling is the most commonly observed fouling phenomenon in industrial applications. The simplest model for mathematical interpretation of the asymptotic fouling was put forward by Kern and Seaton (1959).

$$R_{ft} = R_{f\infty}\left(1 - e^{\beta t}\right) \tag{B6}$$

wKhere R_{ft} is the fouling thermal resistance at time 't', $R_{f\infty}$ is the fouling resistance at infinite time and β is a constant dependent on system properties. The fouling resistance at infinite time $R_{f\infty}$ is the asymptotic value of fouling resistance. The actual values of the constants $R_{f\infty}$ and β depend upon type of fouling and operating conditions which can be determined only from experimental observations. In a modified form of the fouling rate equation (A1), Kern and Seaton provided the modified model as

$$\frac{dx_f}{dt} = K_1 c' M - K_2 \tau x_{ft} \tag{B7}$$

where,

$K_1c'M$ is the rate of deposition term similar to a first order reaction and K_2x_{ft} is the rate of removal term.

K_1 and K_2 are constants

c' is the foulant concentration

M is the mass flow rate

X_{ft} is the foulant layer thickness at time t

τ is the shearing stress.

The thickness of fouling layer is very much less as compared to the tube diameter. Assuming c' and M to constants for a steady state flow heat exchanger, equation (A7) can be integrated to

$$x_f = \frac{K_1 c' M}{K_2 \tau}\left(1 - e^{-K_2 \tau t}\right) \tag{B8}$$

This equation is similar to equation (A6) with $\frac{K_1 c' M}{K_2 \tau}$ equivalent to $R_{f\infty}$ and $K_2\tau$ equivalent to β.

The initial rate of deposition and the asymptotic fouling resistance can be obtained by putting the boundary conditions.

$$\frac{dx_f}{dt} = 0 \text{ when } x = 0$$

Hence,

$$\left(\frac{dx_f}{dt}\right)_{t=0} = K_1 c' M \tag{B9}$$

$K_1 c' M$ is a constant for a fixed set of operating conditions.

The asymptotic fouling thickness is

$$x_{f\infty} = \frac{K_1 c' M}{K_2 \tau} \tag{B10}$$

The asymptotic fouling thickness is also a constant for a fixed set of operating conditions.

Further Kern and Seaton modified the model using Blasius relationship in order to make allowance for the change in flow area caused by deposition process.

Thus,

$$f = \frac{\tau}{\rho u^2} = K_f \, \mathrm{Re}^{-0.25} \tag{B11}$$

$$\Delta P = \frac{2\tau l}{d_i \rho g} \tag{B12}$$

Where, K_f is the Blasius constant, d_i inner tube diameter and l is the tube length in the flow direction. Under turbulent flow conditions,

$$x_{f\infty} = \frac{2K_1 c'}{K_2}\left[\frac{\pi^2 g \rho l^4 M^3}{K_f \left(\Delta P_\infty\right)^4}\right] \tag{B13}$$

The asymptotic value of fouling thickness at a different set of operating conditions can be obtained as

$$\frac{x_{f\infty 1}}{x_{f\infty 2}} = \left[\frac{l_2}{l_1}\right]^{0.8}\left[\frac{\Delta P_{\infty 1}}{\Delta P_{\infty 2}}\right]^{0.8}\left[\frac{M_2}{M_1}\right]^{0.6} \tag{B14}$$

The subscripts 1 and 2 refer to two different set of operating conditions.

However a generalized equation for asymptotic fouling has been proposed by Konak (1973) on the basis of driving force. The driving force is the difference between asymptotic fouling resistance and fouling resistance at any time ‘t’.

$$\frac{dR_{ft}}{dt} = K\left(R_{f\infty} - R_{ft}\right)^n \tag{B15}$$

(III)Falling Rate Fouling

The numerical model for falling rate fouling was proposed by Epstein (1988). According to this model,

$$\frac{dR_f}{dt} = Cq^n \tag{B16}$$

where C is a constant and q is the heat flux.

For constant surface coefficient of heat transfer (α), the heat flux is given as

$$q = U_f \Delta T = \frac{\Delta T}{R_c + R_f} \tag{B17}$$

Assuming constant overall temperature difference,

$$\frac{dR_f}{dt} = \frac{C}{\left(R_c + R_f\right)^n} \tag{B18}$$

On integrating,

$$\left(R_c + R_f\right)^{n+1} - R_c^{n+1} = C(n-1)t \tag{B19}$$

This yields a non-asymptotic fouling rate curve.

Appendix C

Local Linear Wavelet Neural Network Codes in MATLAB

```
clear all
close all
clc
A = xlsread('test_data.xls');
b = xlsread('tra_data.xls');
P_data=[];
max_output=max(A);
min_output=min(A);
max_input=max(b);
min_input=min(b);
disp(max_output);
disp(min_output);
disp(max_input);
disp(min_input);
%-------------------------------------------------------------------------------%
P_data=(b(:,1)-0)./(100-0);
% P_data=(output_data(:,1)-min_output)/(max_output-min_output);
%P_data=log(output_data);
disp(P_data);
maxiter=3000;
eta=0.2; %%Learning rate
y_pred=[];
er=[];
w=rand(7,8)-0.5;%*(0.5-0.002);  %%initialize weight matrix
si=[];
mul=[];
ub=1.5;
lb=0.01;
sigma=rand(7,1)*(ub-lb);
sigma1=sigma(1,1);
sigma2=sigma(2,1);
sigma3=sigma(3,1);
sigma4=sigma(4,1);
```

```
34. sigma5=sigma(5,1);
35. sigma6=sigma(6,1);
36. sigma7=sigma(7,1);
37. for iter=1:maxiter
38. R=0;
39. y_pred=[];
40. er=[];
41. si=[];
42. mul=[];
43. j=1;
44. %--------------------------------------------------------------------------%
45. for k=1:240
46. p1=P_data(k,1);
47. p2=P_data(k,1);
48. p3=P_data(k,1);
49. p4=P_data(k,1);
50. p5=P_data(k,1);
51. p6=P_data(k,1);
52. p7=P_data(k,1);
53. %--------------------------------------------------------------------------%
54. x=0;
55. %*************    Mexican Hat Wavelet  *********************%
56. x=sqrt(p1^2+p2^2+p3^2+p4^2+p5^2+p6^2+p7^2);
57. si1=(-x^2/2)*exp(-x^2/sigma1^2);
58. si2=(-x^2/2)*exp(-x^2/sigma2^2);
59. si3=(-x^2/2)*exp(-x^2/sigma3^2);
60. si4=(-x^2/2)*exp(-x^2/sigma4^2);
61. si5=(-x^2/2)*exp(-x^2/sigma5^2);
62. si6=(-x^2/2)*exp(-x^2/sigma6^2);
63. si7=(-x^2/2)*exp(-x^2/sigma7^2);
64. si=[si1;si2;si3;si4;si5;si6;si7];
65. %--------------------------------------------------------------------------%
66. y1=si1*(w(1,1)+w(1,2)*p1+w(1,3)*p2+w(1,4)*p3+w(1,5)*p4+w(1,6)*p5+w(1,7)*p6+w(1,8)*p7);
67. y2=si2*(w(2,1)+w(2,2)*p1+w(2,3)*p2+w(2,4)*p3+w(2,5)*p4+w(2,6)*p5+w(2,7)*p6+w(2,8)*p7);
68. y3=si3*(w(3,1)+w(3,2)*p1+w(3,3)*p2+w(3,4)*p3+w(3,5)*p4+w(3,6)*p5+w(3,7)*p6+w(3,8)*p7);
69. y4=si4*(w(4,1)+w(4,2)*p1+w(4,3)*p2+w(4,4)*p3+w(4,5)*p4+w(4,6)*p5+w(4,7)*p6+w(4,8)*p7);
70. y5=si5*(w(5,1)+w(5,2)*p1+w(5,3)*p2+w(5,4)*p3+w(5,5)*p4+w(5,6)*p5+w(5,7)*p6+w(5,8)*p7);
```

```
y6=si6*(w(6,1)+w(6,2)*p1+w(6,3)*p2+w(6,4)*p3+w(6,5)*p4+w(6,6)*p5+w(6,7)*p6+w(6,8)*p7);
y7=si7*(w(7,1)+w(7,2)*p1+w(7,3)*p2+w(7,4)*p3+w(7,5)*p4+w(7,6)*p5+w(7,7)*p6+w(7,8)*p7);
%
%
%
%-------------------------------------------------------------------------%
y_pred(j,1)=y1+y2+y3+y4+y5+y6+y7; %predicted output
disp(y_pred);
er(j,1)=P_data(k,1)-y_pred(j,1);%error ccalculation
R=R+(er(j,1)*er(j,1));
%----------  weight updation for input--------------------------
%  for i=1:7
%
%       w(i,1)=w(i,1)+eta*er(j,1)*si(i,1);
%       w(i,2)=w(i,2)+eta*er(j,1)*p1*si(i,1);
%       w(i,3)=w(i,3)+eta*er(j,1)*p2*si(i,1);
%       w(i,4)=w(i,4)+eta*er(j,1)*p3*si(i,1);
%       w(i,5)=w(i,5)+eta*er(j,1)*p4*si(i,1);
%       w(i,6)=w(i,6)+eta*er(j,1)*p5*si(i,1);
%       w(i,7)=w(i,7)+eta*er(j,1)*p6*si(i,1);
%       w(i,8)=w(i,8)+eta*er(j,1)*p7*si(i,1);
%  end
%


% ----------------sigma updation  ---------------------
del1=(-x^4/(sigma1^3))*exp(-x^2/sigma1^2);
del2=(-x^4/(sigma2^3))*exp(-x^2/sigma2^2);
del3=(-x^4/(sigma3^3))*exp(-x^2/sigma3^2);
del4=(-x^4/(sigma4^3))*exp(-x^2/sigma4^2);
del5=(-x^4/(sigma5^3))*exp(-x^2/sigma5^2);
del6=(-x^4/(sigma6^3))*exp(-x^2/sigma6^2);
del7=(-x^4/(sigma7^3))*exp(-x^2/sigma7^2);
for n=1:7
mul(n,1)=w(n,1)+p1*w(n,2)+p2*w(n,3)+p3*w(n,4)+p4*w(n,5)+p5*w(n,6)+p6*w(n,7)+p7*w(n,8);
end
sigma1=sigma1+eta*er(j,1)*del1*(mul(1,1)) ;
sigma2=sigma2+eta*er(j,1)*del2*(mul(2,1)) ;
```

```
107.sigma3=sigma3+eta*er(j,1)*del3*(mul(3,1)) ;
108.sigma4=sigma4+eta*er(j,1)*del4*(mul(4,1)) ;
109.sigma5=sigma5+eta*er(j,1)*del5*(mul(5,1)) ;
110.sigma6=sigma6+eta*er(j,1)*del6*(mul(6,1)) ;
111.sigma7=sigma7+eta*er(j,1)*del7*(mul(7,1)) ;
112.%----------  weight updation for output-------------------------
113.for i=1:7

114.w(i,1)=w(i,1)+eta*er(j,1)*si(i,1);
115.w(i,2)=w(i,2)+eta*er(j,1)*p1*si(i,1);
116.w(i,3)=w(i,3)+eta*er(j,1)*p2*si(i,1);
117.w(i,4)=w(i,4)+eta*er(j,1)*p3*si(i,1);
118.w(i,5)=w(i,5)+eta*er(j,1)*p4*si(i,1);
119.w(i,6)=w(i,6)+eta*er(j,1)*p5*si(i,1);
120.w(i,7)=w(i,7)+eta*er(j,1)*p6*si(i,1);
121.w(i,8)=w(i,8)+eta*er(j,1)*p7*si(i,1);
122.end
123.j=j+1;
124.end
125.RMSE=sqrt(R/(j-1));
126.err(iter)=RMSE;
127.end
128.trn_d=P_data(1:240,1);
129.v=[];
130.aa=[];
131.v=w;  %%initialize weight matrix

132.sigma_up=[sigma1;sigma2;sigma3;sigma4;sigma5;sigma6;sigma7];

133.%----------testing--------------------%
134.sigma11=sigma_up(1,1);
135.sigma22=sigma_up(2,1);
136.sigma33=sigma_up(3,1);
137.sigma44=sigma_up(4,1);
138.sigma55=sigma_up(5,1);
139.sigma66=sigma_up(6,1);
140.sigma77=sigma_up(7,1);
```

```
si_t=[];
data_p=[];
data_p1=[];
data_p1=A(:,1);
%disp(data_p1);
p_max=max(data_p1);
p_min=min(data_p1);
data_p=(data_p1(:,1)-0)./(100-0) ;
%   data_p=data_p1;
sq=0;
n=1;
for kk=1:80
%        si=[];
p1=data_p(kk,1);
p2=data_p(kk,1);
p3=data_p(kk,1);
p4=data_p(kk,1);
p5=data_p(kk,1);
p6=data_p(kk,1);
p7=data_p(kk,1);
%%%%%%%%%%%%%%%%%%%%%%%%%%%%%%%
x=sqrt(p1^2+p2^2+p3^2+p4^2+p5^2+p6^2+p7^2);
%si=-x^/2*exp(-(x^2/sigma^2));
s1=(-x^2/2)*exp(-x^2/sigma11^2);
s2=(-x^2/2)*exp(-x^2/sigma22^2);
s3=(-x^2/2)*exp(-x^2/sigma33^2);
s4=(-x^2/2)*exp(-x^2/sigma44^2);
s5=(-x^2/2)*exp(-x^2/sigma55^2);
s6=(-x^2/2)*exp(-x^2/sigma66^2);
s7=(-x^2/2)*exp(-x^2/sigma77^2);
si_t=[s1;s2;s3;s4;s5;s6;s7];
%--------------------------------------------------------------------%
y1=s1*(v(1,1)+v(1,2)*p1+v(1,3)*p2+v(1,4)*p3+v(1,5)*p4+v(1,6)*p5+v(1,7)*p6+v(1,8)*p7);
y2=s2*(v(2,1)+v(2,2)*p1+v(2,3)*p2+v(2,4)*p3+v(2,5)*p4+v(2,6)*p5+v(2,7)*p6+v(2,8)*p7);
y3=s3*(v(3,1)+v(3,2)*p1+v(3,3)*p2+v(3,4)*p3+v(3,5)*p4+v(3,6)*p5+v(3,7)*p6+v(3,8)*p7);
y4=s4*(v(4,1)+v(4,2)*p1+v(4,3)*p2+v(4,4)*p3+v(4,5)*p4+v(4,6)*p5+v(4,7)*p6+v(4,8)*p7);
y5=s5*(v(5,1)+v(5,2)*p1+v(5,3)*p2+v(5,4)*p3+v(5,5)*p4+v(5,6)*p5+v(5,7)*p6+v(5,8)*p7);
```

```
178.y6=s6*(v(6,1)+v(6,2)*p1+v(6,3)*p2+v(6,4)*p3+v(6,5)*p4+v(6,6)*p5+v(6,7)*p6+v(6,8)*p7);
179.y7=s7*(v(7,1)+v(7,2)*p1+v(7,3)*p2+v(7,4)*p3+v(7,5)*p4+v(7,6)*p5+v(7,7)*p6+v(7,8)*p7);
180.%-------------------------------------------------------------------------%
181.y_test(n,1)=y1+y2+y3+y4+y5+y6+y7; %predicted output
182.er1(n,1)=data_p(kk,1)-y_test(n,1);
183.sq=sq+(er1(n,1)*er1(n,1));
184.n=n+1;%error ccalculation
185.end
186.%    RMSE1=sqrt(sq/n-1);
187.test_d=data_p(:,1);
188.for i=1:80
189.yy(i,1)=abs(y_test(i,1)-test_d(i,1))/test_d(i,1);
190.end
191.xy=sum(yy);
192.MAPE=xy*(100/168);
193.figure(1);
194.clf;
195.subplot(2,1,1);
196.plot(y_pred,'r');
197.subplot(2,1,2);
198.plot(trn_d,'b');
199.figure(2);
200.clf;
201.plot(er);
202.figure(3);
203.clf;
204.subplot(2,1,1);
205.plot(y_test,'r');
206.subplot(2,1,2);
207.plot(test_d,'b');
208.figure(4);
209.clf;
210.plot(er1);
211.end
```

Publications Based on Present Work

1. Dillip Kumar Mohanty & Pravin M. Singru (2011) Use of C-factor for monitoring of fouling in a shell and tube heat exchanger, Energy, 36 (5), 2899-2904.

2. Dillip Kumar Mohanty & Pravin M. Singru (2011) Experimental Measurement of Heat Transfer Coefficient of A Shell and Tube Heat Exchanger by Wilson Plot Method, International Journal of Microscale and Nanoscale Thermal and Fluid Transport Phenomena, 2(2), 121-135.
3. Dillip Kumar Mohanty & Pravin M. Singru (2012) Numerical Method for heat transfer and fouling analysis of a shell and tube heat exchanger using statistical analysis, Korean Journal of Chemical Engineering, 29(9), 1144 – 1150.
4. Dillip Kumar Mohanty & Pravin M. Singru (2013) Effect of Fouling on the Heat Transfer Performances of a Shell and Tube Heat Exchanger, International Conference on Energy Resources and Technologies for Sustainable Development, Bengal Engineering and Science University, Kolkata, India. (Accepted).

Brief Biography of Candidate

Dillip Kumar Mohanty is currently serving as Lecturer in department of mechanical Engineering at Birla Institute of Technology and Science, Pilani-K.K.Birla Goa campus, Goa, India. He received B.Tech degree in Mechanical Engineering from Indira Gandhi Institute of Technology, sarang of Utkal University, Bhubaneswar, Orissa. He completed Post Graduate Diploma in Plastics Engineering from Central Institute of Plastics Engineering and Technology, Ahmedabad. After that he joined JIET, Cuttack, Orissa as a Lecturer. In the year 2004, he received M. Tech. (Master of Technology) degree in Applied Mechanics from IIT, Delhi, India. After completing his M.Tech., he joined Synergy Institute of Technology as an Assistant Professor in Department of Mechanical Engineering. He joined BITS-Pilani KK Birla Goa campus as Assistant lecturer in Department of Mechanical Engineering in the year 2006. He registered for Ph.D program in the year 2008.

He has ten years of teaching experience in various institutes. He has taught several courses in JIET, Synergy Institute of Engineering and Technology and BITS Pilani K K Biral Goa Campus since 1999. He was also actively involved in setting up the department labs and developing the infrastructure of the institute. He has published papers in various international journals of repute to present his work.

Brief Biography of Supervisor

Dr. P. M. Singru is working as an Assistant Professor in Mechanical Engineering Department at BITS-Pilani,K.K.Birla Goa Campus, Goa, India. He received his Master of Technology from Indian Institute of Technology, Kharagpur, India and his PhD Degree from Visvesvaraya National Institute of Technology, Nagpur, India. He is involved in teaching and research since last 20 years. He has been the head of the Mechanical Engineering Department of BITS- Pilani, K K Birla Goa Campus for last six years. He has published a number of papers in various international and national journals and conferences. He has guided a large number undergraduate and postgraduate projects and one PhD thesis. Along with the current thesis, he is the supervisor of another three thesis works. His research contributions are in the field of heat transfer, MEMS and optimization.